Water Resources Availability and Hydropower Production under Current and Future Climate Scenarios: The Case of Jhelum River Basin, Pakistan.

POLITECNICO DI TORINO

Ph.D. in Engineering for Natural and Built Environment

Water Resources Availability and Hydropower Production under Current and Future Climate Scenarios: The Case of Jhelum River Basin, Pakistan

Muhammad Azmat

Matr. 189979

Supervisors

Prof. Francesco Laio

Prof. Davide Poggi

Ph.D. Dissertation

February 2015

Muhammad Azmat

Email: muhammad.azmat@polito.it; azmatwrm@yahoo.com

Politecnico Di Torino

Department of Environment, Land and Infrastructure Engineering

Corso Duca degli Abruzzi, 24 – 10129 Torino, Italy

ACKNOWLEDGEMENTS

It is with great emotion that I address my thanks to all institutions and people who supported me during the completion of this research: without their help and encouragement, this doctoral thesis would never have happened.

I express my thanks to **Prof. Fulvio BOANO, Prof. Alberto VIGLIONE** and **Prof. Gianni PEDRIZZETTI**, who accepted to assess my Ph.D. dissertation in spite of their professional engagements.

I want to thank especially:

- **My family**, particularly my father (late) who never forgot me in their prayers and encourage me at every step of life for higher education;
- **Higher Education Commission (HEC) of Pakistan** to award me a scholarship during the three years of this thesis;
- **Water and Power Development Authority (WAPDA) and Pakistan Meteorological Department (PMD)**, for their exchange of the valuable hydrological and climate data to complete my research;
- **Francesco Laio** and **Davide Poggi**, my advisor, whose encouragement, guidance and support from the initial to the final level enabled me to develop an understanding of the subject. I am highly impressed by his broad vision and kindness. Despite his quite busy schedule, he never refused to have discussions;
- **All my friends and colleagues**, especially Muhammad Adnan Shahid, Muhammad Uzair Qamar, Latif Anjum, Rao Arslan, Sajjad Ahmed, Anna Botto, Stephano Fontan, Muhammad Yaseen, Imran Serwar and Laura bardini, who encouraged me during all the difficult moments of my thesis;

Lastly, I offer my regards and blessings to all of those who supported me in any respect during the completion of my thesis.

Muhammad Azmat

Table of Contents

Abstract **1**

General Introduction **2**

Chapter 1 ..... **9**

General Study Area **9**

1.1 Jhelum River Basin (Mangla Watershed) 9

1.2 Hydrological Regime of the Mangla Basin 12

1.3 Water Resources Management in Mangla Basin 15

1.4 Description of the Dam and Canal Network 17

Chapter 2 ..... **22**

Data Collection and Preliminary Analysis **22**

2.1 Brief Introduction and Background 22

2.2 Description of Data Sets 23

2.2.1 Hydrological and Climate Data 23

2.2.2 Satellite Data 26

A. ASTER GDEM 26

B. MODIS Snow Cover 27

C. TRMM Precipitation 30

D. APHRODITE Precipitation Data 31

2.3 Preliminary Analysis 32

2.3.1 Time series analysis 32

2.3.2 Flow Duration Curve Analysis 40

2.4 Analysis of Snow Cover Dynamics and Hydrological Regime of the Mangla Basin 45

2.4.1 Analysis 45

2.4.2 Climatological Variation Analysis 47

2.4.3 Hydrological behaviour of Jhelum River Basin 52

2.4.4 Cryosphere Dynamics in the Jhelum River Basin..... 55
2.4.5 Correlation between Change in Cryosphere Climate Variables and Stream Flow in the Mangla Basin..... 58
2.5 Conclusion..... 62
Chapter 3 65
Application of Hydrological Models..... 65
3.1 Brief Introduction and Background..... 65
3.2 Description of Hydrological Modelling System (HEC-HMS)... 67
3.3 Description of Snowmelt Runoff Model (SRM)..... 69
3.4 Model Accuracy Criteria 70
3.5 Comparison of Hydrological Models 71
3.5.1 Application of HEC-HMS..... 71
3.5.2 Model Calibration and Validation (HEC-HMS)..... 74
3.5.3 Application of Snowmelt Runoff Model..... 87
3.5.4 Comparison of SRM with HEC-HMS 90
3.6 Calibration of HEC-HMS over Different Time Windows 97
3.6.1 Single Year..... 97
3.6.2 Three Year..... 104
3.6.3 Six Year..... 108
3.7 Water Resources Availability at Mangla Reservoir 109
3.8 Conclusions 112
Chapter 4 114
Climate Change Analysis and its Impact on Sustainability of Water Resources at Mangla Dam..... 114
4.1 Brief Introduction and Background..... 114
4.2 Description of Statistical Downscaling..... 116
4.2.1 Overview Downscaling Models..... 117
A. SDSM..... 117

B. Smooth Support Vector Machine (SSVM) 119
4.2.2 Predictors Data 120
4.3 Application of Downscaling Methods (SDSM and SSVM) 122
4.4 Statistical Downscaling of Climate Variables (Temperature and Precipitation) 124
4.5 Future Climate Scenarios 133
4.6 Hydrological Model Calibration and Validation 139
4.7 Future Water Availability 145
4.8 Some Additional Climate Change Analysis by Using SRM 153
4.9 Conclusion 157
Chapter 5 159
Reservoir Operations and Hydropower Generation: Under Current and Future Scenarios 159
5.1 Brief Introduction and Background 159
5.2 Reservoir Operation and Available Power Calculations 160
5.3 Impact of Water Resources on Dam Management 162
5.4 Impact of Water Resources on Micro-hydropower Production 166
5.5 Operational Pattern of Mangla Dam under Climate Change Scenarios 167
5.6 Impact of Climate Change on Hydropower Generation 169
5.7 Hydropower Production from Future Outflows of the Bong Canal 173
5.8 Micro-hydropower Production at UJC under Climate Change Scenarios 173
5.9 Future Water Supply and Demand: Post Mangla Raising 175
5.10 Conclusion 178
Chapter 6 180
Testing of Kinetic Turbine 180
6.1 Brief Introduction 180

6.2 Experimental Work for Micro-hydropower Generation 180
6.3 Results 185
A. Experiment Results 185
B. Energy Generation at UJC Canal by Using Experimental Data 191
6.4 Conclusions 192
General Conclusion 195
References 201
Appendices 209
Appendix A 209
Appendix B 221

Abstract

An agro-based country, Pakistan is largely dependent on the Indus basin irrigation system (IBIS), one of the largest irrigation networks in the world, mainly contributed by snow- and glacier-melt runoff from Indus River and its tributaries. A significant proportion of water in the Jhelum River is contributed by its snow- and glacier-fed sub-catchments situated in the Himalayan and Pir Panjal ranges along with monsoon rainfall from low-altitude regions. This study presents the change in snow cover dynamics and its impact on the hydrological behaviour of the catchment, water availability under climate change scenarios in high-altitude scarcely gauged (transboundary nature) catchment and subsequently its impact on hydropower generation at Mangla Dam and downstream canal system through operational management of the Mangla Reservoir.

The remotely sensed data products such as MODIS snow cover, TRMM and APHRODITE are utilized, moreover, the climate change investigations are carried out by starting from the different scenarios for climate change as provided by the Intergovernmental Panel for Climate Change (IPCC), and their implementation in climate models known as Global Circulation Models (GCMs), downscaling techniques, and finally Hydrological modeling. The impact of climate change on hydropower generation at Mangla Dam and downstream canal system is computed by the utilization of hydrological outcomes under current and future water resources availability.

The outcomes of this study will not only help to solve several complex problems related to practical designing and management issues of water resources and hydropower crises of Pakistan but also for future proposed studies.

General Introduction

Human sustainability is totally depends upon water on earth. Exponential growth in the world's population and unrestrained water resource consumption threatens the temporal and spatial availability of freshwater resources globally. This intimidation is worse in developing countries such as Pakistan, where large proportion of the population practices agriculture. Pakistan (Fig. 1), a country with the sixth largest population (175 million) in the world (United Nations 2010), has an economy that is highly dependent on agriculture. Nearly, more than 60% of the total population living in rural areas is directly or indirectly dependent on agriculture for their livelihood. Moreover, the raw material generated from this sector is also useful for domestic agro-based industries, such as leather, sugar and textiles. Hence, the importance of the agricultural sector to the people of Pakistan and the well-being of the country's economic growth cannot be overstated. Pakistan is divided into arid and semi-arid regions and the contribution of rainfall in the irrigation of agricultural lands is very minimal. Due to one of the greatest human civilizations, which flourished along the Indus River banks, during the nineteenth (19^{th}) century, wide range irrigation technologies were introduced which dramatically turned the low-level balance of human and water. The Indus Basin Irrigation System became the largest contiguous irrigation canal network in the world. This irrigation system is mainly provided by the Indus River and its two eastern tributaries—the Jhelum and Chenab (Fig. 2). The Indus River catchment is a transboundary nature river catchment, situated in four countries (Pakistan, China, Afghanistan and India) with the major proportion in Pakistan. Since the catchments of all the major Indus River tributaries (Jhelum and Chanab) are transboundary river basins, a number of issues exist in these basins. Therefore, Pakistan faced several challenges due to water-related issues with India during the 1950s.

The Indus Basin Treaty was signed by India and Pakistan in 1960, brokered by the World Bank. This treaty provides rights to Pakistan to use the waters of the Indus, Chanab and Jhelum Rivers. According to this treaty, the waters of the Beas, Ravi, and Sutlej Rivers were deprived for the irrigation of agricultural lands of the Punjab (Fig. 1) (the major contributor in the agriculture sector of Pakistan).

The major complications in the water resource management of transboundary river basin is that the important data on river flows, sources of water, and water used and demand is either missing or not available. The riparian countries located at downstream depend upon the upstream neighbouring countries for data collection and sharing. if it does not happen, the situation can be more sever for downstream countries because they cannot make themselves ready to overcome the droughts and floods or hydropower generation issues (Zawahri 2008). This could be worse in case of developing countries such as Pakistan, where the Indus River and its tributaries are an example. Precipitation data is an essential constituent of the hydrological cycle it is therefore, the water management studies cannot be carried out in scarcely gauged catchments. In the case of the Indus Basin, approximately less than four (4) precipitation gauges are available for an area of nearly 10,000 km^2, which is inadequate for large basin-scale investigations and transboundary nature of the catchment make this worse due unavailability of any type of ground data.

Additionally, due to the discrepancy between the locations of Pakistan's main water sources (western rivers) and the major irrigated agricultural lands in the east (Punjab), two major storage structures, the Tarbela Dam (2nd largest by volume) and the Mangla Dam (9th largest by volume) were constructed in 1961 and 1974, respectively. The Mangla and Tarbela Dams

were constructed on the main stream of the Indus and Jhelum Rivers (one of the major tributaries of the Indus River) (Figs. 1 and 2). Mangla is the first controlled structure on the River Jhelum and most of the annual Jhelum River influx stored at Mangla is derived from the mixed runoff generated from rainfall and snowmelt in the Himalayan and Pir Panjal ranges. The stored water of Mangla Reservoir is then delivered to the downstream irrigated agricultural lands through a network of barrages, canals and small watercourses. The sustainability of Pakistan's economy and food security is largely dependent upon these water resources of the northern regions and their management. Any alteration in the availability of these water resources due to socio-economic factors, climate variability and international policies will have a severe impact on food security and the environment in Pakistan. Therefore it is very important to study the hydrometeorological, snow cover dynamics (cryosphere) and the hydrologic regime of the Jhelum River Basin (Mangla watershed) under climate change for better water management.

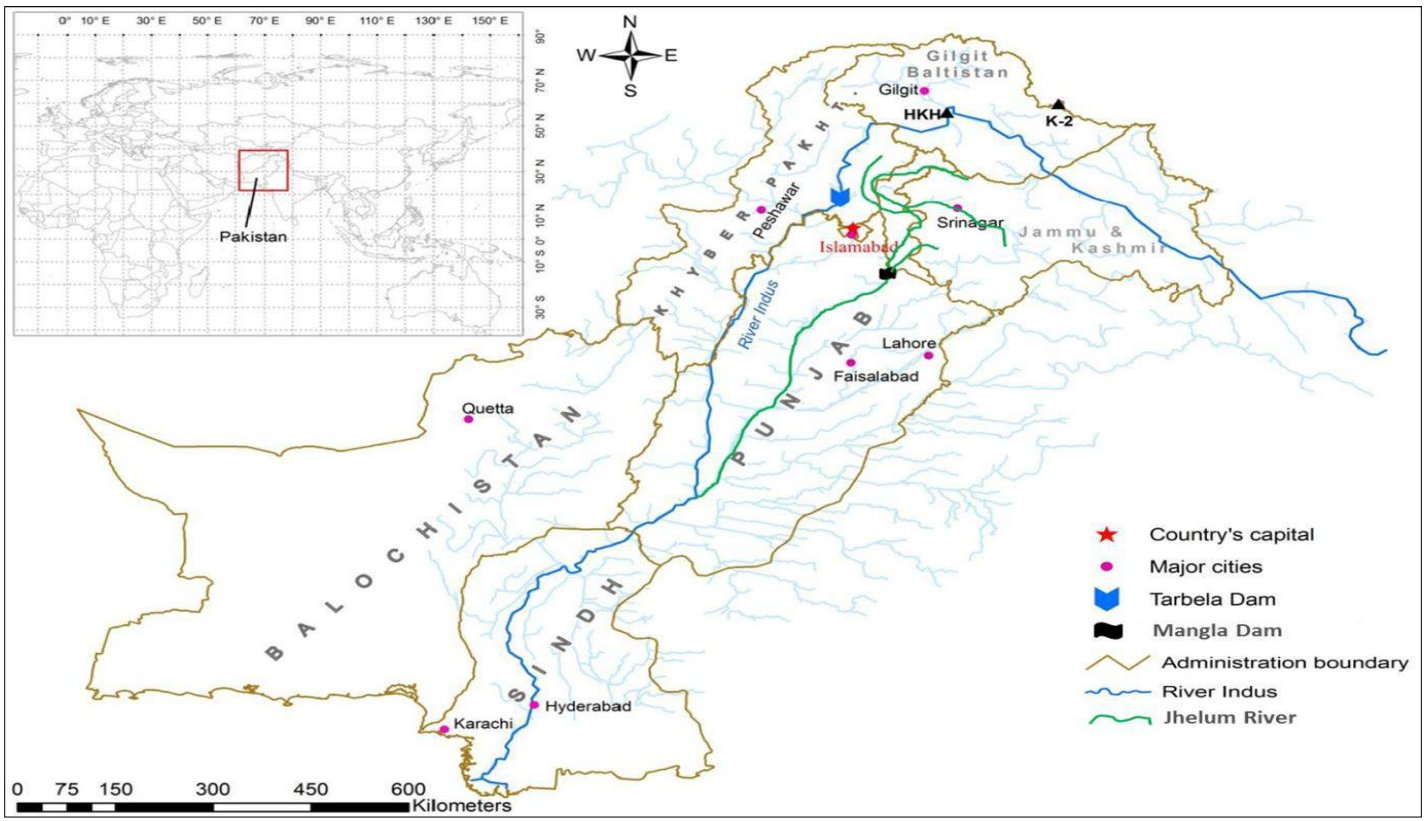

Fig. 1: A map of Pakistan showing provincial/administration boundary lines. Five provinces (Punjab, Sindh, Balochistan, Khyber Pakhtunkhwah and Gilgit Baltistan) are shown with their major cities. (*Source: Tahir et al. (2011)*)

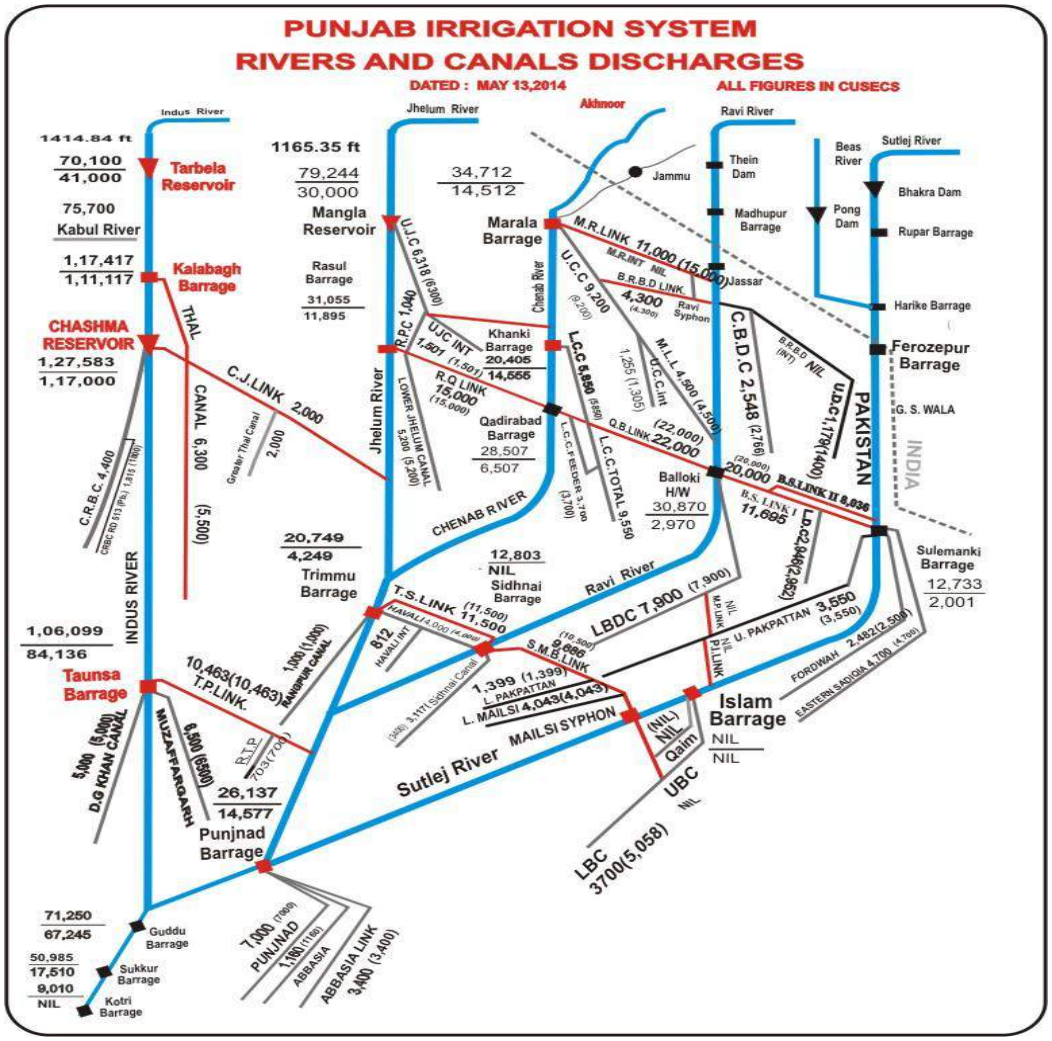

Fig. 2: Schematic diagram of the Indus River System in Pakistan with its major tributaries (*Source: WAPDA*).

Objectives of Our Study

This study is mainly focused on the following objectives:

- Snow cover dynamics and the impact of climate change on the cryosphere (snow and ice) and the hydrological regime in the Jhelum River Basin at Mangla Dam;

- Estimation of water resources availability at Mangla Dam by the application of hydrological models (HEC-HMS and Snowmelt Runoff Model);
- Impact of climate change to downscale climate variable by using the downscaling models and then estimate water availability using the most suitable hydrological model for the Jhelum River Basin;
- Impact of water resources on reservoir operations and micro-hydropower generation at the downstream canal system (theoretical and experimental based).

To achieve the aforementioned objectives, we start with a preliminary analysis (trend analysis) of the available gauge hydro-meteorological data and also with MODIS snow cover (MOD10A2) to estimate the variation in the snow cover of the study area. The hydrological and climate data are treated and discussed for better understanding of the hydrological regime of the area. Selection of the appropriate model was made to estimate water availability at Mangla Dam from two different models (HEC-HMS and snowmelt runoff (SRM)). The MODIS satellite snow cover and the climate (precipitation and temperature) and hydrological data of the ground stations were used in both models. Rainfall data is an important input in rainfall-runoff models, so the Tropical Rainfall Measuring Mission (TRMM) and APROIDITE precipitation product is used for the ungauged sub-catchments.

Moreover, the statistical downscaling model (SDSM) and smooth support vector machine (SSVM) was used to downscale climate variables (precipitation and temperature) to use as input of selected hydrological model for climate change analysis.

An overview of water availability and hydropower generation at Mangla Dam and at the downstream canal system under current and future climate change scenarios was studied. Also, there is a brief analysis of existing and future water demand according to water resources availability.

Chapter 1

General Study Area

This chapter includes the background and characteristics of the study area (Jhelum River Basin). The general characteristics and a global digital elevation model of Jhelum River Basin are presented in section 1.1, followed by a description of the hydrological regime of the catchment in section 1.2. Water resources management in Mangla Basin is illustrated in section 1.3 and this chapter ends with a brief description of the dam and canal networks downstream of the Mangla catchment.

1.1 Jhelum River Basin (Mangla Watershed)

The Jhelum River is a major eastern tributary of the Indus River. It originates from the north-western part of Pir Panjal and receives a significant part of its flow from different tributaries draining the southern slopes of the Greater Himalayan range. It receives flows from alluvial lands in the Kashmir Valley and courses through the Wular Lake. Nearly 130 km downstream of Wular Lake, one of the major tributaries, the Neelum River (Kishan Ganga), joins the Jhelum River at Muzafferabad and also the Kunhar River falls into the Jhelum River 8 km downstream of the Muzafferabad. Two other important tributaries, the Poonch and Kanshi Rivers, join the Jhelum River at Mangla Reservoir. The Poonch River drains the southern slopes of the Pir Panjal range, while the Kanshi River rises from eroded lowland regions, directly joining the Jhelum River in Mangla Lake.

The Jhelum River catchment area situated upstream of the Mangla Dam is called the Mangla watershed (Fig. 1.1). The location and shape file of the

Mangla Basin is extracted from the Advanced Spaceborne Thermal Emission and Reflection Radiometer (ASTER) global digital elevation model (GDEM) with 24.18 m × 24.18 m grid resolution. The watershed area is shown in Fig. 1.1, along with the location of Mangla Dam, mountainous ranges and sub-catchments of different tributaries of the Jhelum River. The geographical location of Mangla Dam is 33.142083 °N and 73.645015 °E. The total catchment area of the Mangla Basin is approximately 33,867 km^2, estimated using GDEM with integration by the ArcGIS tool, in this study. This is a transboundary catchment like other rivers in Pakistan (Indus, Chanab, Bias and Ravi) with 56% (18,966 km^2) of its area situated in India, which makes data collection very difficult due to socio-political issues between the two countries. Such issues of concern also affect other rivers of Pakistan and many other river catchments in the world (Cheema and Bastiaanssen 2012).

Approximately 1.5% (508 km^2) of the total study area is covered by perennial glaciers and nearly 63% of the catchment is covered by seasonal snow cover during the winter months (October–March). The hypsometric curve of the Mangla catchment and the percentage area under different altitudinal zones (1000 m difference between two zones) are estimated from ASTER GDEM and presented in Fig. 1.2. The Mangla catchment has a mean elevation of 2194 m (17,441 km^2 of the total) with almost 23.5% of the area (11,006 km^2) lying above 3000 m elevation (Fig. 1.2). Approximately 25% of the Mangla catchment area is above the altitude where the maximum snow accumulation occurs. A brief description of the hydrological regime and the change in snow cover dynamics in Mangla Basin is given in the next sections. As discussed, it is a transboundary catchment, meaning that data collection for the part of the catchment situated in India is even more difficult, which makes it a sparsely gauged catchment. Furthermore,

precipitation and temperature data records are available only below 2800 m, which also contributes to making it a very scarcely gauged catchment area.

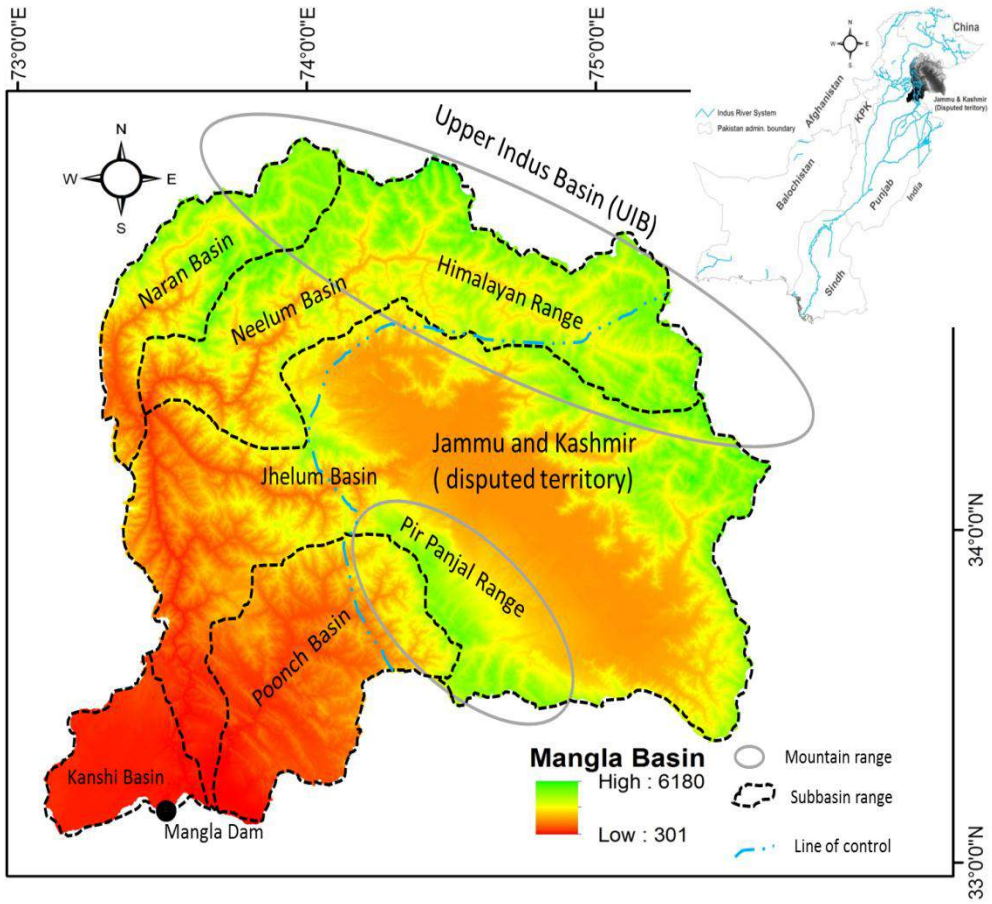

Fig. 1.1: ASTER Global digital elevation model (GDEM) of Jhelum River Basin and the location of Mangla Dam.

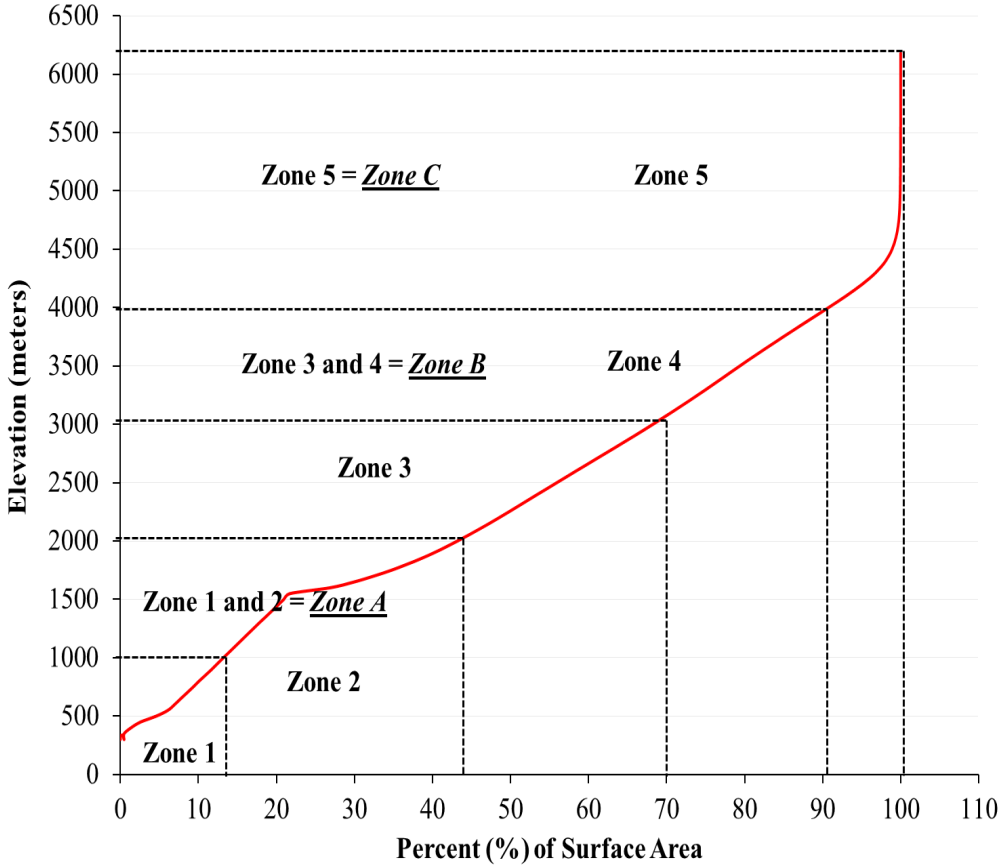

Fig. 1.2: Hypsometric curve of the Mangla Basin showing the area distribution in five and three different elevation zones (Zones 1 and 2= Zone-A, Zones 3 and 4=Zone-B, Zone 5= Zone-C).

1.2 Hydrological Regime of the Mangla Basin

The inflows of the Jhelum River are measured at Mangla Dam with a mean annual flow of 794 m^3/s (standard deviation= 667 m^3/s) (Fig. 1.3), estimated from previous flow records (1995–2010) for Mangla Dam (data provided by the Surface Water Hydrology Project, SWHP). The hydrological behaviour of this catchment is slightly peculiar because of the precipitation behaviour over different stations of the catchment. The eastern Himalayan climate chronicles are altered from the Upper Indus Basin (UIB) (Fowler and Archer

2006; Young and Hewitt 1990). Most of the UIB (90%) is not affected by monsoon rainfall during the summer season because the basin is in the rain shadow of the Himalayas (Immerzeel et al. 2009), while Jhelum Basin is mostly affected by the monsoon rainfall. There are two sources of precipitation in the Mangla Basin: the Western Disturbances and monsoon precipitation. The former take place from December to March and the latter from June to September (Bookhagen and Burbank 2006; Lang and Barros 2004). These both rainfall patterns and abrupt change in elevation make hydrology of this catchment peculiar. The annual precipitation varies from 683 to 1600 mm at Srinagar and Gharidopata, respectively, then again declines towards the southern part to 873 mm at Mangla. The range of annual precipitation totals varies from 70% of the average to a maximum of 135% of the average (Archer and Fowler 2008). A dual rainfall distribution pattern exists in the Jhelum Basin. In the southern part is a bimodal distribution of rainfall with peaks in spring, particularly in March, and maximum peaks during the summer monsoon, specifically during July, and with minima in May and November. Conversely, in northern and western parts of the basin, a single rainfall peak occurs at Naran during spring and at Srinagar while during summer very lower rainfall peaks occurs. However, in the whole Mangla Basin, over the period of 1961–2010, about 38% and 62% of total mean annual rainfall occurred during the winter and summer seasons, respectively.

The low intensity winter and spring rainfall is a primary source of water in the Mangla Basin brought by westerly circulations. The altitude range varies from 300 to 5180 m within the basin, including some parts of the eastern Himalayan range (Fig. 1.1) and as a consequence the climatic condition varies largely within the catchment. The Mangla Basin can be divided into

two hydrological regimes: a) high-altitude catchments (e.g. Kunhar and Neelum Basin) with summer runoff derived mainly from the snow and glacier melt, with concurrent energy input in the form of temperature and with an overlapping small proportion of rainfall-runoff; b) low elevation (foothills) sub-basins that have a runoff regime generated by the existing summer or winter rainfall. In Mangla Basin, the streamflows are a combination of rapid runoff generated by rainfall in the low altitude part of the basin and slow runoff generated by snow and glacier melt from the high altitude part of the basin. Mangla inflows are dominated by the snow and glacier melt runoff contribution during the spring and summer months, along with monsoon rainfall-runoff (Archer and Fowler 2008). The spring and summer flows are essential and the primary source of the irrigation of the whole Mangla Basin.

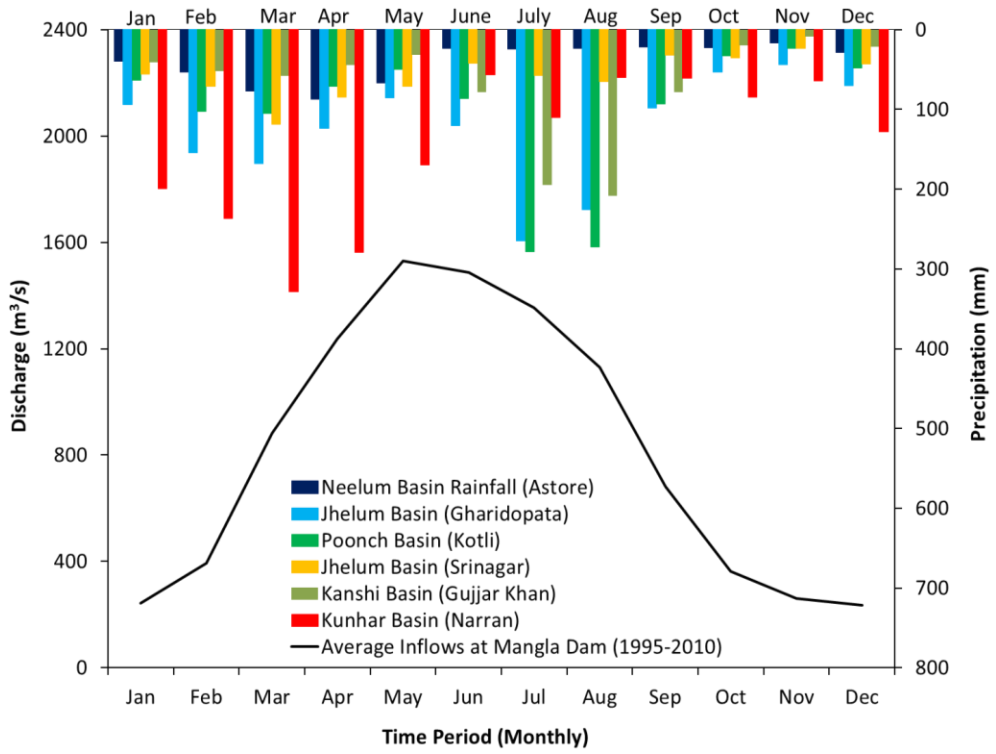

Fig. 1.3: Mean monthly discharge (1995–2010 of Jhelum River at Mangla Dam (estimated from the data available in this study) and mean monthly precipitation in Astore, Gharidopata, Kotli, Srinagar Gujjar Khan and Naran.

1.3 Water Resources Management in Mangla Basin

Mangla Dam is the only storage structure constructed across the Jhelum River. It is a multipurpose structure, constructed from 1961 to 1967, which improved Pakistan's agriculture by increasing the irrigation command area and the cultivable land of Punjab (Province of Pakistan). The total cultivable area increased by 20% after the construction of the Mangla and Tarbela Dams (on the Indus River) and these two reservoirs satisfy nearly one third of the electricity demand of the country (Archer et al. 2010). Almost 6 million hectares of the country's agricultural land are irrigated by the Mangla Reservoir alone (Archer and Fowler 2008). It also plays a vital role in

reducing flood peaks over many flood events by storing the greater part of the water. Unfortunately, the recent reservoir storage capacity has been insufficient to meet the water demands for food, domestic use and energy, due to significant increase in the country's population. Furthermore, a significant decrease in the initial storage capacities of the dams due to sedimentation is making the situation even more severe. The initial gross capacity of Mangla Reservoir has already decreased by 20% due to sedimentation, as per a hydrographic survey over the year 2005 (Haq and Abbas 2007).

Moreover, the decrease in storage capacity results in an increased flood risk in the downstream areas. A recent example was the devastating floods in Pakistan in 2010, 2012 and now in 2014, which affected one third of the country's surface area (Fig. 1.4) and 2.5 million people directly or indirectly (BBC 2010). This flood was caused by a combination of climate factors and the lack of national decisions on water use. July and August 2010 were already the second hottest months on record (NOAA 2010), which led to high runoff from snow and glacier melt, whereas the above average monsoon rainfall (July–August) in Pakistan made the situation worse for rivers and dams that were already filled to capacity.

It is therefore important to study the impacts of climate change on the snow cover, glaciers and hydrological regime of Mangla Basin and to simulate the discharge under future climate change scenarios to sustain the water resources management.

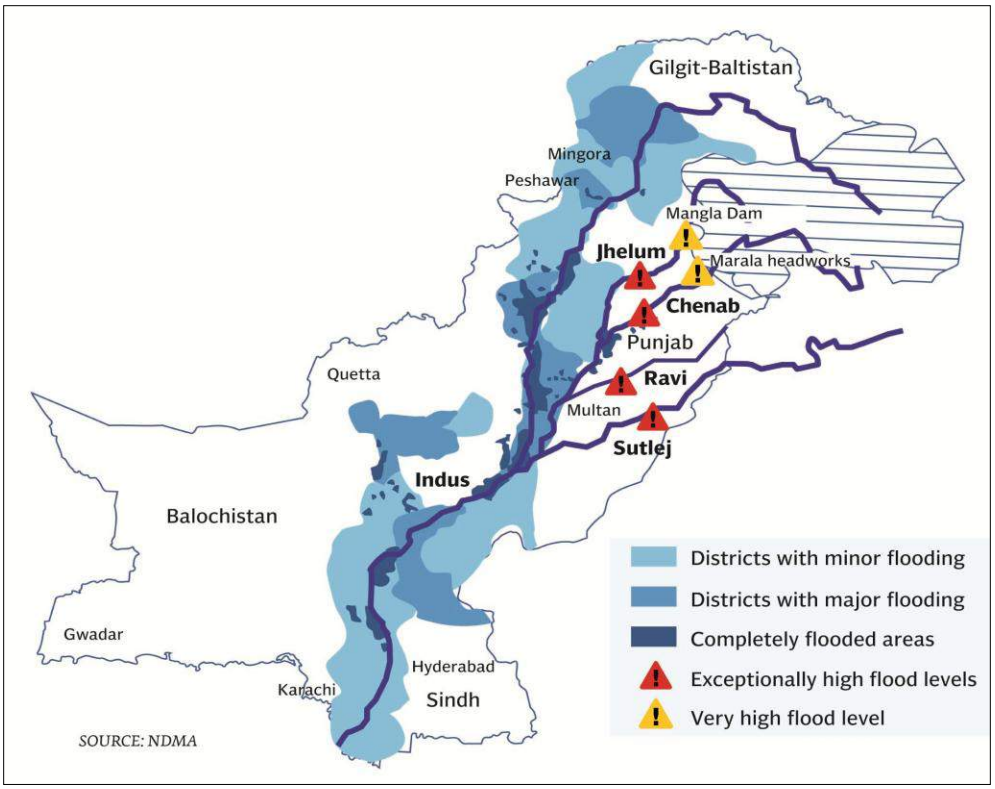

Fig. 1.4: Map showing the flood-affected areas of Pakistan in 2014 and the track of the flood wave along the Indus River (*source: National Disaster Management Agency*).

1.4 Description of the Dam and Canal Network

The reservoir was constructed primarily to store the water of the Jhelum River and its tributaries, for irrigation. The secondary function of the Mangla Reservoir is to generate hydroelectrical power from the artificial head of the reservoir based on the available storage in the reservoir. The initial gross storage capacity of the dam is 7.25 km^3 and the dead storage is 0.663 km^3, as reported by Haq and Abbas (2007). Two spillways (main and emergency) are functioning at Mangla Dam. The main spillway is a submerged orifice type

with 9 radial gates, 10.97 × 12.20 meter each, and has a maximum capacity of 28,600 m^3/s, while the emergency spillway is a weir type with an erodible bund and a maximum capacity of 6500 m^3/s. As discussed in section 1.3, the storage capacity of the reservoir has decreased due to sedimentation, as presented in Table 1.1.

Table 1.1: Loss of storage capacity due to sedimentation (*source: (Haq and Abbas 2007)*.

Reservoir Capacity	**Original (BCM)**	**Year 2005 (BCM)**	**Reduction %**
Gross Storage	7.259	5.768	20.54
Live Storage	6.593	5.605	14.98
Dead Storage	0.666	0.163	75.56

Table 1.2: Some salient features of Mangla Dam and its components (*source: WAPDA*).

Salient Features of Mangla Dam	**Un-raised**
Water surface area at conservation level (km^2)	259
Catastrophic flood level (m)	375
Maximum conservation level (m)	367
Minimum operation level (m)	317
Gross storage (km^3)	7.25
Live storage (km^3)	6.58
Mean annual flow (km^3)	28.61
Maximum height (m)	139
Power generation (MW)	1000
Bong Canal capacity (m^3/sec)	1386
Bong Escape capacity (m^3/sec)	1219

The Mangla Dam is situated on a western tributary of Pakistan, while the major agricultural lands are situated in the east of the country. Therefore, an irrigation canal network called the Indus Basin Irrigation System (IBIS) was

established by the Pakistan Government to supply water towards the east. Since the Mangla Dam is the second largest reservoir in the country (the first largest after raising), the IBIS is also largely dependent on Mangla Reservoir. Power generation is a secondary function of the dam, so the water used for hydropower generation is supplied to the downstream canal system through a power canal named the Bong Canal, which is the only route for outflows other than the spillway. The average annual and design discharge capacities of Bong Canal are 713 and 1386 m^3/s, respectively. The water is shifted to the power house through five steel-lined tunnels towards the Mangla powerhouse and each tunnel is designed to feed two generating units which can generate 100 MW each. The total installed capacity of the Mangla Dam is 1000 MW. Each tunnel, having a design capacity of 277.2 m^3/s, then diverts water into the Bong Canal. The water of the Bong Canal diverts again into the Jhelum River (design capacity 1028 m^3/s) after feeding the Upper Jhelum Canal (UJC) intake. Mangla Dam supplies water to several districts of the Punjab through the UJC and some other canals (Lower Jhelum Canal (LJC), Rasool Qadirabad Link Canal (RBC)), not directly off-taking from the reservoir. The Upper Jhelum Canal (UJC) provides irrigation to downstream areas with average and design discharge of 216 and 358 m^3/s, respectively. It also feeds the Khanki head work at River Chanab with 72 m^3/s as an average and 176 m^3/s as a design discharge (Punjab Irrigation and Power Department (PIPD)). The total agricultural command area of the UJC is approximately 28,000 hectares (Hussain 2005). Several small distributaries take water from the UJC, including two main canals named the Gujrat Branch Canal and Rasool Power Canal, with design discharges of 43.57 and 99.10 m^3/s, respectively. Fig. 1.5 shows a schematic diagram of the UJC network, with the design flow capacities of the different distributaries. The LJC and RBC

are not directly off-taking from Mangla Dam, but their discharge is totally dependent upon the hydrology of the Mangla Basin and operational management of Manga Reservoir. Both canals supply water with 156 and 538 m^3/s design discharge for irrigation, and also divert water into Chanab River (Fig. 1.5) to satisfy the irrigation requirements of southern Punjab through different irrigation canals, as illustrated in Fig. 2 given in the General Introduction.

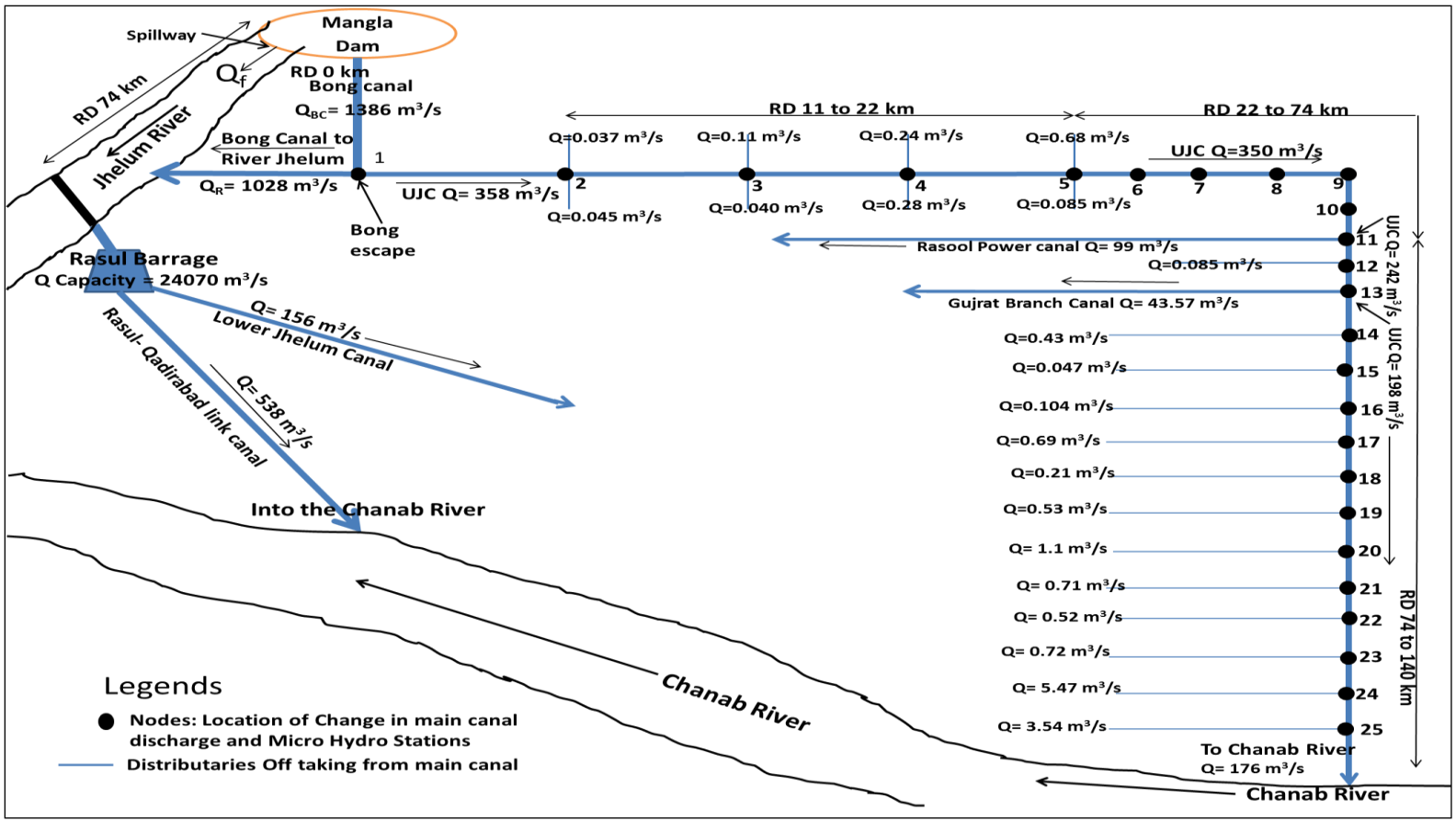

Fig 1.5: Schematic diagram of the canal system downstream of Mangla Dam and design discharges.

Chapter 2

Data Collection and Preliminary Analysis

2.1 Brief Introduction and Background

The agriculture-based economy of Pakistan is dependent on the irrigation water supplied by the Indus River and its tributaries through the Indus Basin Irrigation System (IBIS). The Jhelum River is a major tributary of the Indus River and contributes substantially to the IBIS through Mangla Dam. The maximum Jhelum River flows at Mangla are contributed by its sub-basins situated in the Himalayan and Pir Panjal ranges (Fig. 2.1). Two tributaries of the Jhelum River are mainly snow-fed, but monsoon rainfall also makes a slight contribution. These two tributaries (sub-catchments) are the Neelum (Kishanganga) and Kunhar Rivers, both of which drain the southern slopes of the Himalayas and contribute on average 39% and 11% of the total annual flow of Jhelum River, respectively (De Scally 1994), and both sub-basins are covered by snow during winter. Moreover, the management of Mangla Reservoir largely depends upon this proportion, particularly over the early summer season. Therefore, the preliminary analysis for better understanding of the hydrological behaviour in each sub-catchment or at stations within the catchment is tremendously important. The flow duration curve and time series analysis provide important information about different regions of the Mangla catchment. Furthermore, to the best of our knowledge, no comprehensive study of the snow and ice processes or their consequences for the hydrological behaviour has been carried out so far in most regions of

these high altitude mountain ranges of the Jhelum River catchment. The most active hydrological areas, which generate the greatest amount of water for the Mangla Basin, are ungauged or scarcely gauged, particularly at elevations greater than 3000 m. Hydrometeorological studies are essential in this hydrologically vigorous area at altitudes greater than 3000 m, where the greatest amount of precipitation falls in solid form. Remote sensing tools are a suitable approach to investigate cryosphere dynamics efficiently in these inaccessible highlands. An understanding of cryosphere dynamics and its impact on the hydrological behaviour of the sub-basins of Mangla catchment is vital for better water resources management in Pakistan. In this section, the investigation focuses on studying the snow cover dynamics in Mangla catchment by using a freely available remote sensing snow cover data product and the climate and hydrological gauge data of stations located within or close to the catchment border (at different elevations). Moreover, the precipitation data plays a tremendously important role for the hydrological analysis. During the last decade, the use of remote sensing precipitation data has been considered the most reliable source for estimating the hydrological regime in ungauged or scarcely gauged catchments in high altitude mountainous areas.

2.2 Description of Data Sets

2.2.1 Hydrological and Climate Data

Generally, the collection of streamflow and climate data (precipitation and temperature) is carried out by the Surface Water Hydrology Project of the Water and Power Development Authority (SWHP-WAPDA) and Pakistan Meteorological Department (PMD), respectively, in Pakistan, with the earliest record starting in 1960. Eight streamflow gauges and 16 climate

stations along with precipitation gauges at different elevation levels within the range of the Pakistan border are presented in Fig. 2.1 and Table 2.1.

The daily streamflows of the Jhelum River are usually measured by the Directorate of Mangla Dam at Mangla Station (Fig. 2.1). The inflow data of Mangla Dam has been collected from 1995 to 2010 (~15 years) and also at other gauging stations installed by SWHP-WAPDA, as illustrated in Fig. 2.1 and Table 2.1, from 1971 to 2009 (~38 years). The Pakistan Meteorological Department (PMD) is responsible for the measurements of precipitation, temperature, wind speed and humidity. Most of these stations have rather long historic data records starting from 1961, but at some stations data is missing due to disastrous events (earthquakes and floods).

The stations installed by the PMD are generally situated in low-altitude areas of the sub-basins. The Astore station is installed just outside the Mangla catchment in the Upper Indus Basin (UIB). The data at this station has been used by several researchers for the sub-basin of the Neelum River (Kishanganga). Climate data are available from 1961 to 2009 but, as mentioned above, for some years data is missing for some stations. Therefore, this catchment is considered a scarcely gauged catchment for the two reasons that, firstly, no climate stations are available at elevations greater than 3000 m, and secondly, data gathering for the part of the catchment situated in India is very difficult, which makes hydrological analysis slightly problematic. Therefore, the remote sensing data is more helpful to compensate for the data scarcity in this catchment. The remote sensing data is briefly discussed in the next section 2.2.2.

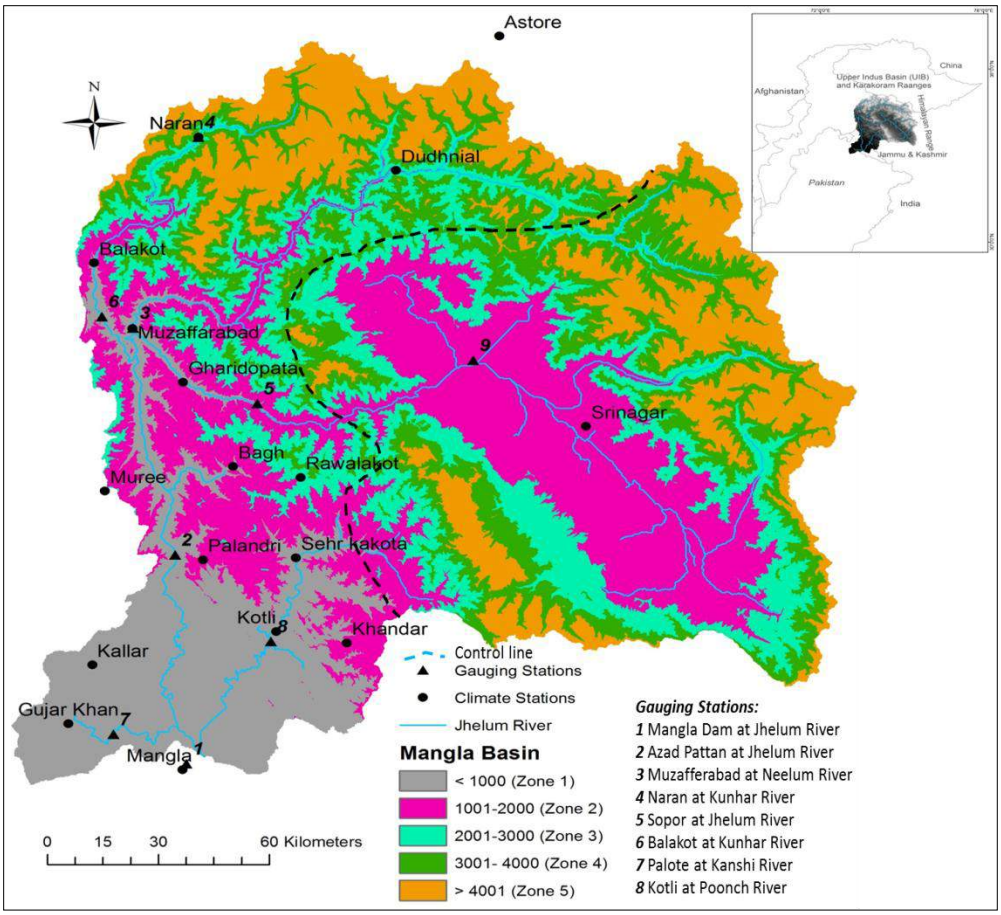

Fig. 2.1: Location of climate and streamflow gauging stations along with zonal distribution of the Mangla catchment.

Table 2.1: Location of gauging and climate stations within and adjoining Mangla Basin.

Station	River	Period of Record	Basin Area (km^2)	Mean Elevation (m)	Mean Flow (m^3/s)
Flow Gauging Stations					
Chinari	Jhelum	1970-1996	13868	2464	341
Domel	Jhelum	1976-2009	14470	2421	385
Muzafferabad	Neelum	1963-2009	7422	3244	369
Naran	Kunhar	1961-2009	1971	3531	56
Gari-Habibullah	Kunhar	1961-1998	2895	3224	109
Azad Pattan	Jhelum	1979-2009	26735	2578	917
Kotli	Poonch	1961-2009	3256	1825	139
Mangla	Jhelum	1995-2009	33,867	-	911
Climate Stations					**Annual Rainfall (mm)**
Astore		1961-2009		2454	485
Naran		1961-2009		2421	1778
Dudhnial		1993-2009		1816	1341
Balakot		1961-2003		980	1479
Muzafferabad		1962-2009		686	1488
Domel		1962-2009		686	1361
G.Dopatta		1971-2009		813	1499
Murree		1971-2009		2206	1760
Rawalakot		1971-2009		1677	1434
Palanderi		1961-2009		1402	1420
Khandar		1971-2009		1067	1336
Kaller		1981-2009		433	843
Gujjar Khan		1971-2009		421	837
Sehr Kokata		1971-2001		1215	1351
Saif-ul-Malok		1981-2009		2932	1247
Bagh		1961-1992		1321	1279
Kotli		1971-2009		1027	1283

2.2.2 Satellite Data

A. ASTER GDEM

The catchment is delineated using the Advanced Spaceborne Thermal Emission and Reflection Radiometer (ASTER) Global Digital Elevation

Model (GDEM) offered by NASA and Japan's Ministry of Economy, Trade and Industry (METI) to the worldwide public on June 29, 2009. This is accessible for the high-altitude and steep hilly areas which are normally not covered by the Shuttle Radar Topography Mission (SRTM3). SRTM-acquired elevation data, on a near-global scale, comprises a particularly improved radar system to produce the most comprehensive high-resolution digital topographic database of the earth. The horizontal grid resolution of the SRTM3 DEM (digital elevation model) is 90×90 m and the absolute vertical precision is slightly better than 9 m (Farr et al. 2007).

The tiles of the ASTER GDEM were downloaded from the (http://reverb.echo.nasa.gov/reverb/) web page for the Jhelum River basin. The downloaded ASTER GDEM tiles were mosaicked by the integration with ArcGIS for the delineation of the study catchment. The layers of gauging and climate stations along with other essential feature layers were superimposed on the extracted study area with the objective of providing locations (Fig. 2.1). For detailed analysis of the cryosphere distribution over the study area, five different elevation zones were extracted from the GDEM. The characteristics of these zones are given in Table 2.1 and the extracted zones are presented in Fig. 2.2.

B. MODIS Snow Cover

The Moderate Resolution Imaging Spectroradiometer (MODIS) snow cover product was used to estimate the snow cover proportion in the study area. Several previous studies used the MODIS snow cover data in hydrological models to simulate the snowmelt-runoff (Bookhagen and Burbank 2010; Immerzeel et al. 2009; Prasad and Roy 2005). The MODIS/Terra Snow Cover 8-Day L3 Global 500 m Grid (MOD10A2) selected for this study comprises of data fields for snow cover extent over an

8-day repeated period with approximately 500 m spatial resolution entirely covering the Jhelum River basin. MOD10A2 consists of snow cover configuration periods and snow fall chronology observations and corresponding metadata over 8-day in HDF-EOS (Earth Observation System) format. It is constructed on a snow mapping algorithm that uses an index namely Normalized Difference Snow Index (NDSI) and other standard assessments and further snow cover percentage explained by pixel values (Hall et al. 2002). The snow mapping algorithm discriminate pixels as land, cloud, snow, ice lakes, water bodies or other, and snow is a crucial or important parameter in this data product. An available processed image data set of MOD10A2 (V005) was downloaded from http://nsidc.org/cgi-bin/snowi/search.pl during March 2000 to December 2010 and then mosaicked and projected by the integration of ArcGIS (Global Information System) with the WGS 1984 UTM ZONE 43N projection system. The study area was then extracted from the processed image to estimate the percentage of SCA in the catchment. The Mangla Basin area was then extracted from the mosaicked image to assess the percentage of snow and ice cover (cryosphere) in the study area. When the cloud cover percentage exceeded 20% on a specific date, the data was removed and then the average snow cover was computed on this date by the linear interpolation of the previous and next available cloud-free images. Furthermore, the zonal snow cover area is estimated for the three and five altitudinal zones used for further analysis. The 8-day snow cover data were converted to daily basis values by the linear interpolation of previous and the next available data. The zonal SCA was estimated for the five altitudinal zones (Figure 2) to be used for snowmelt-runoff modeling.

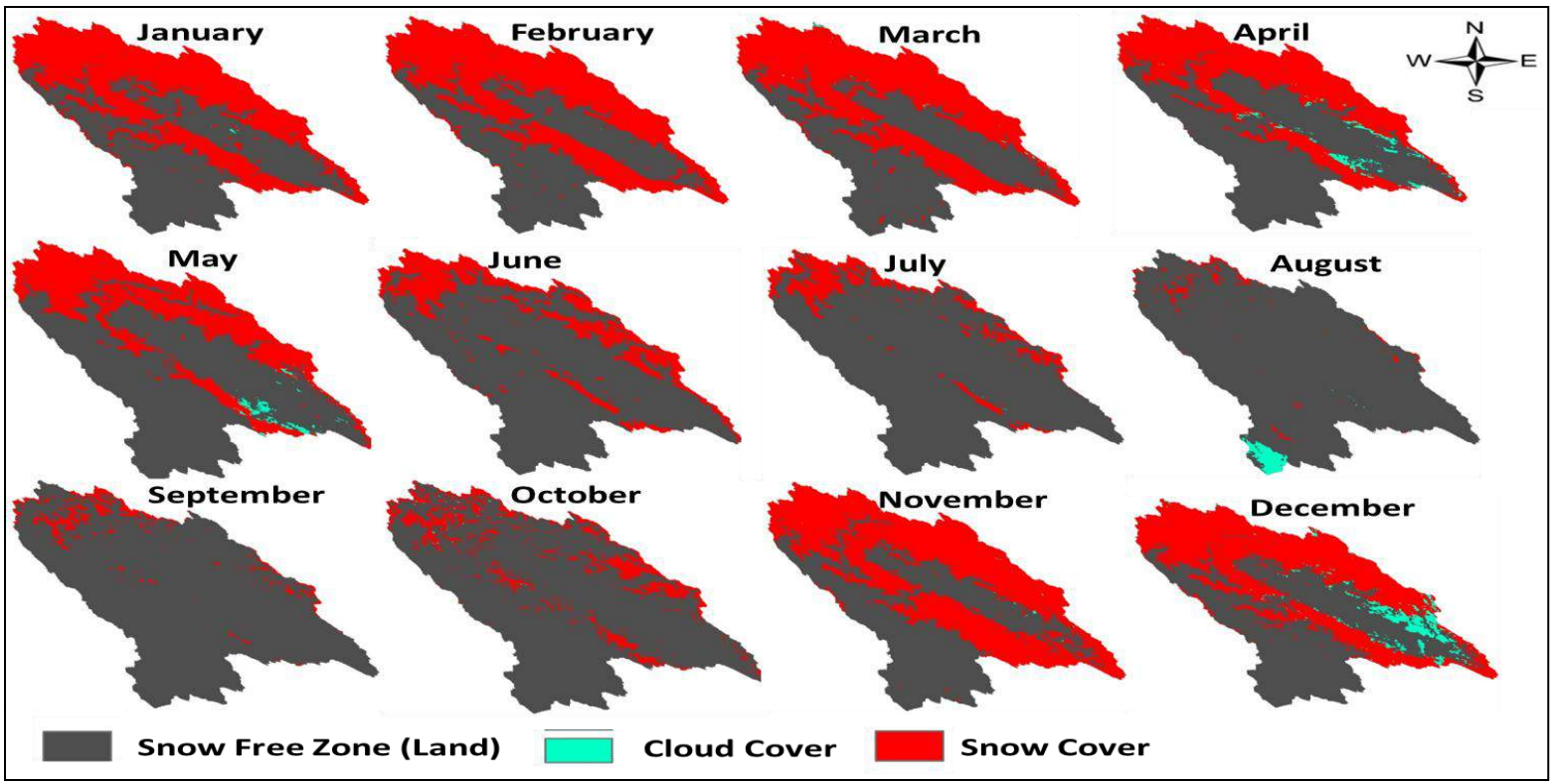

Fig. 2.2: MODIS (MOD10A2) satellite images presenting the average snow cover area for each month in the Mangla Basin in the year 2009.

C. TRMM Precipitation

The Tropical Rainfall Measuring Mission (TRMM) offers precipitation approximations at fine spatial scales using a calibration-based consecutive pattern and data from multiple satellites as well as gauge analysis. In the current investigation, the 3B42 rainfall product is used. This is a daily product with 0.25×0.25° spatial gridded resolution. The initial processing is processed for 3-hr time periods. First, a number of passive microwave sensors aboard TRMM and other satellites are converted to a precipitation estimate. Secondly, an infrared (IR) estimate is generated using the calibrated microwave estimate. Thirdly, the microwave and IR estimates are combined to provide the best estimate at each grid box at each 3-hr period. The final step in generating 3B42 is the inclusion of rain gauge data. It is highly advantageous to include rain gauge data in combination data sets. All the 3-hourly combined microwave and IR estimates are then summed up to create a daily multi-satellite product. The data product was downloaded from the NASA web page (http://mirador.gsfc.nasa.gov/) for the years from 1998 to 2009 at different altitude points within the sub-basin and then the average of all point precipitations was taken. Comparisons were made between the average TRMM precipitation data and the observed data on a monthly basis before being used for further analysis over four selected stations (Kotli, Muzafferabad, Gharidopata and Murree) located within the catchment in Pakistan (Fig. 2.3). The application of TRMM is justified with a least R squares value equal to 0.66 at Murree station. It is observed that the TRMM tends to overestimate light rainfall events but underestimate moderate to heavy rainfall on both types of terrain (high and low elevation levels), as confirmed by Chen et al. (2012). Therefore, the low efficiency of TRMM at Murree station may be associated with the high altitude of this station. The TRMM precipitation product has been successfully used in some studies of

the Himalayan region (Bookhagen and Burbank 2010). This remote sensing data was also calibrated by (Cheema and Bastiaanssen 2012) for Pakistani catchments (the Indus Basin).

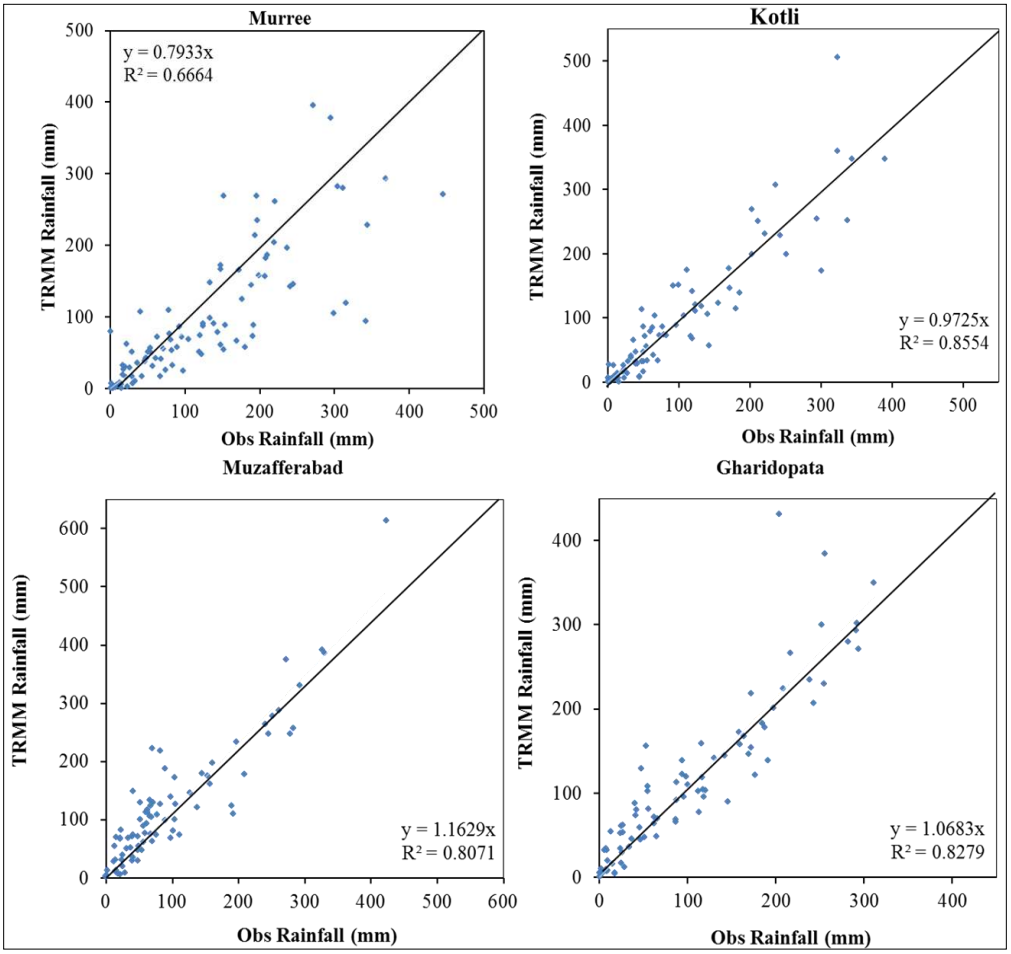

Fig. 2.3: Comparison of observed precipitation data with TRMM data product on a monthly basis at four selected stations.

D. APHRODITE Precipitation Data

A gridded daily precipitation database, developed by the Asian Precipitation – Highly-Resolved Observational Data Integration Towards Evaluation of the Water Resources (APHRODITE Water Resources) project, was used in

this investigation to downscale the precipitation data for the future climate scenario projection, by means of integrating the National Center for Atmospheric Research (NCEP) reanalysis data product with the Statistical Downscaling Model (SDSM) over the ungauged part of the catchment. This data was selected because it is the only daily gridded precipitation product that is available for long-term (1951 onwards) continental-scale daily product that contains a dense network of daily rain-gauge data for Asia, including the Himalayas.

The grid boxes of daily precipitation are defined by the interpolation of rain-gauge observations derived from hydrological and meteorological stations over the region (Yatagai et al. 2009). The data were downloaded from the web page (http://www.chikyu.ac.jp/precip/) of the APHRODITE Water Resources project. The downloaded (from 1961 to 2000) product version Monsoon Asia (APHRO_MA_V0902) comprises of 0.25×0.25° spatial resolution. The APHRODITE data grid has a coarse resolution (30×30 km^2) and it supposed that the precipitation in specified grid to be constant at any altitude point. Several researchers have applied this data product for the simulation of streamflows worldwide. Tahir et al. (2011) successfully used this precipitation data integrated with the snowmelt runoff model (SRM) in the Hunza River Basin, Pakistan.

2.3 Preliminary Analysis

2.3.1 Time series analysis

The time series analysis of the climate data at different stations is performed to understand the climate behaviour of the Mangla Basin.

A. Precipitation Analysis

The comparative analysis of monthly change in precipitation between the climate stations situated in different sub-catchments of the Mangla Basin is presented in Fig. 2.4. These stations are located in an elevation range of 300–2500 m. The highest stations are Astore (2454 m) and Naran (2421 m). The elevations of other climate stations are given in Table 2.1. The total annual precipitation received at the climate stations varies considerably due to the effect of elevation. The mean total annual precipitation is 485 mm at Astore, by contrast with 1778 mm at Naran according to the 10-year data record (1999–2008) of WAPDA. The remarkable difference between the amounts of precipitation at these two stations is quite peculiar because both stations are at the same elevation. This may be because the pattern of monsoon precipitation does not affect the Astore station due to the barrier formed by the high altitude mountains. The Mangla Basin is mainly influenced by the monsoon rainfall pattern. As mentioned earlier, the rainfall pattern in Mangla Basin is slightly odd due to its dual nature, as confirmed by Archer and Fowler (2008). A significant difference exists between the catchments situated in India and in Pakistan, as presented in Fig. 2.4 and 2.5. The low elevation part of the catchment situated in Pakistan is largely dominated by rainfall, as illustrated in Table 2.1. Fig. 2.4 and 2.5 depict how the stations situated in Pakistan receive more precipitation than those in India, which shows that the stations located in Pakistan are mainly affected by monsoon conditions.

However, the current precipitation data records are not a real representation of the Jhelum River flows (Mangla Basin) at Mangla Dam for two main reasons. First is the lack of climate stations installed in the high altitude sub-catchments which are the main active part of the basin due to the runoff

contribution in the form of snowmelt during the spring and summer seasons, particularly from the Kunhar and Neelum Basins (Kishanganga). Second is that underestimation of the average annual precipitation values can be a problem, as explained by some researchers (Hewitt 2005, 2007; Winiger et al. 2005) from the field experience or as derived by modelling techniques in neighbouring catchments of the Upper Indus Basin (UIB). Furthermore, the well-known precipitation gauging errors distort the real data of high-altitude climate stations because most of the precipitation spread outside of the gauges and can catch only 20 to 30% of the total due to of strong wind speed, as explained by Sevruk (1989) and FØrland (1996). This may explain the low precipitation values recorded at the Astore climate station.

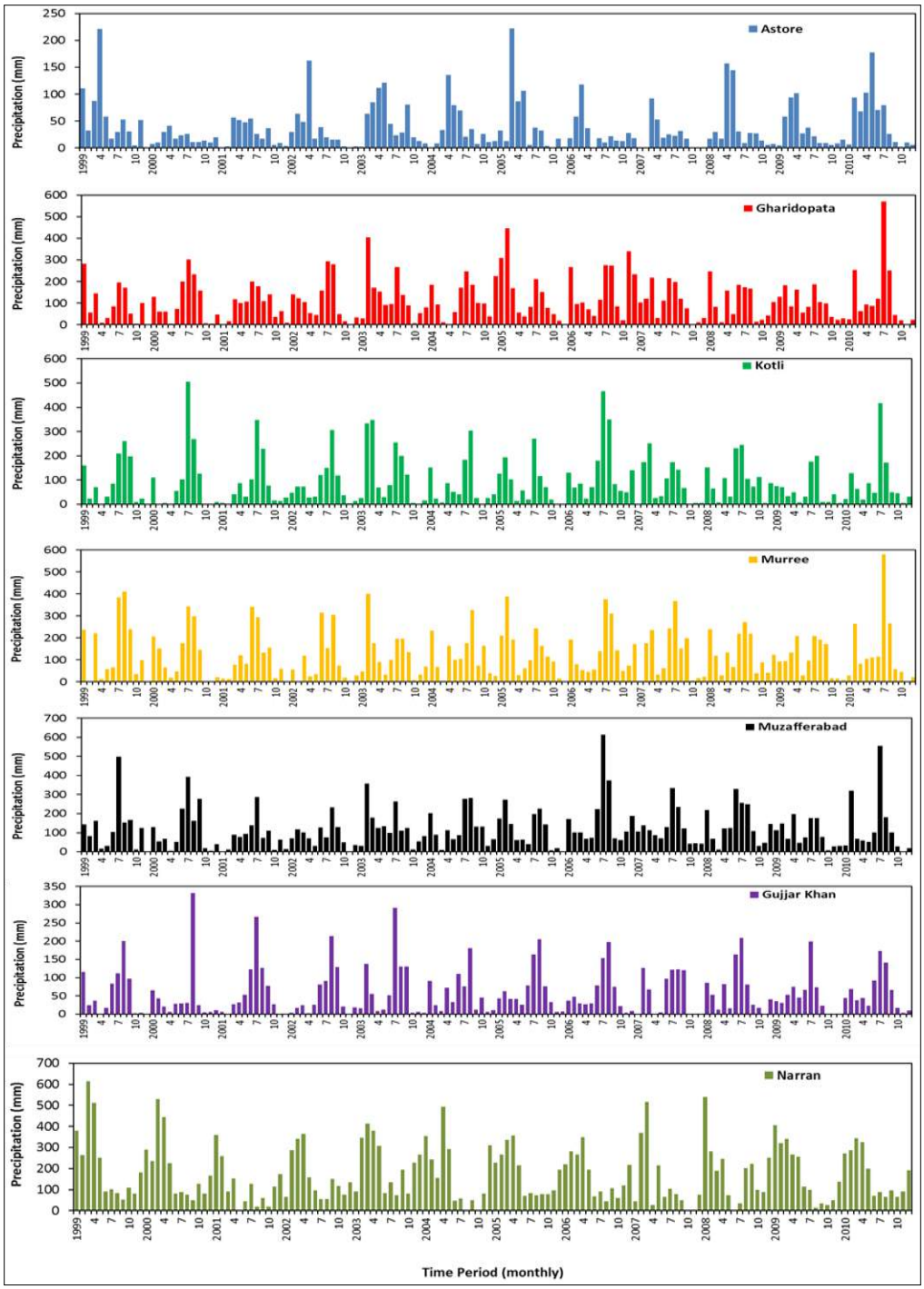

Fig. 2.4: Monthly variations of precipitation at the climate stations within the Mangla Basin installed by PMD and WAPDA.

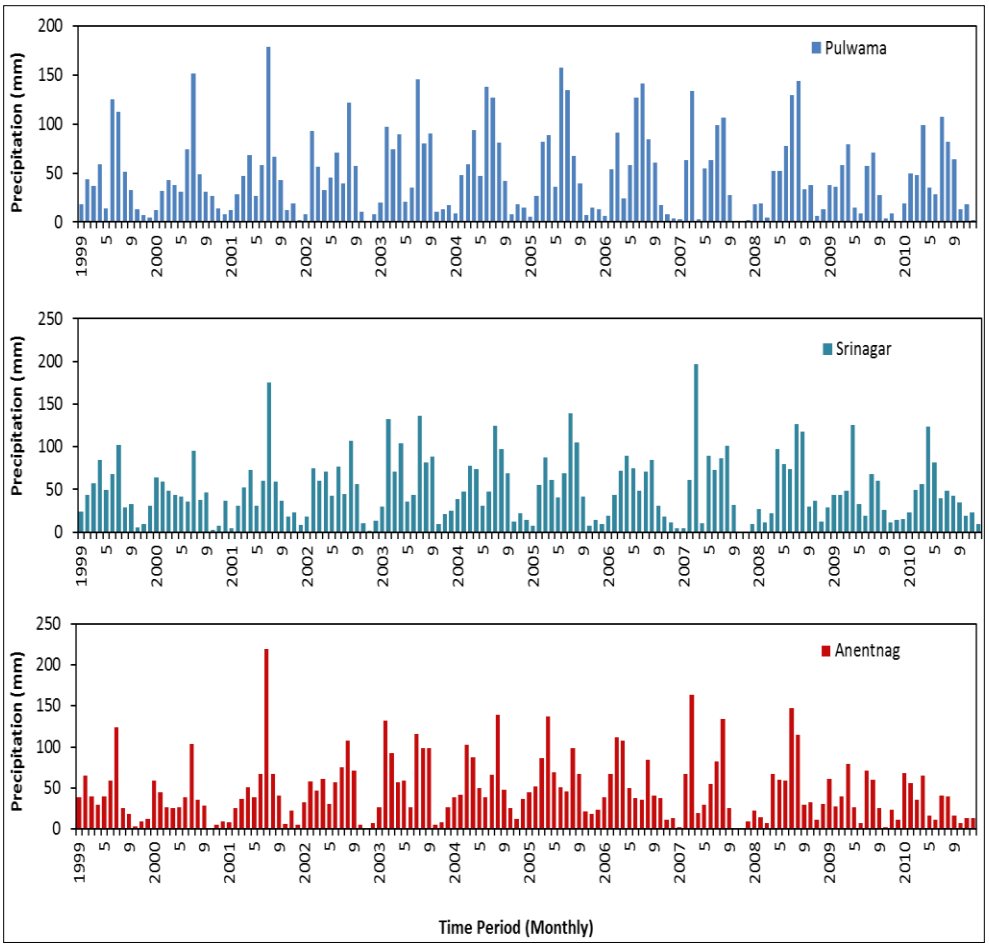

Fig. 2.5: Monthly variations of precipitation data taken from TRMM satellite at the points of ungauged sub-basins situated in India.

Trend analysis of total annual, winter and summer precipitation is carried out (Fig. 2.6) using Kendall's tau (τ) trend test at five selected climate stations (one from each sub-basin) of the Mangla Basin. The Kendall's tau (τ) coefficient value shows a slight increasing trend at all stations except Gujjar Khan, where a very slight decreasing trend is observed. At Naran station, a significant increase with 0.23 and 0.39 Kendall's coefficient value during the annual and summer season is observed but during winter it decreases.

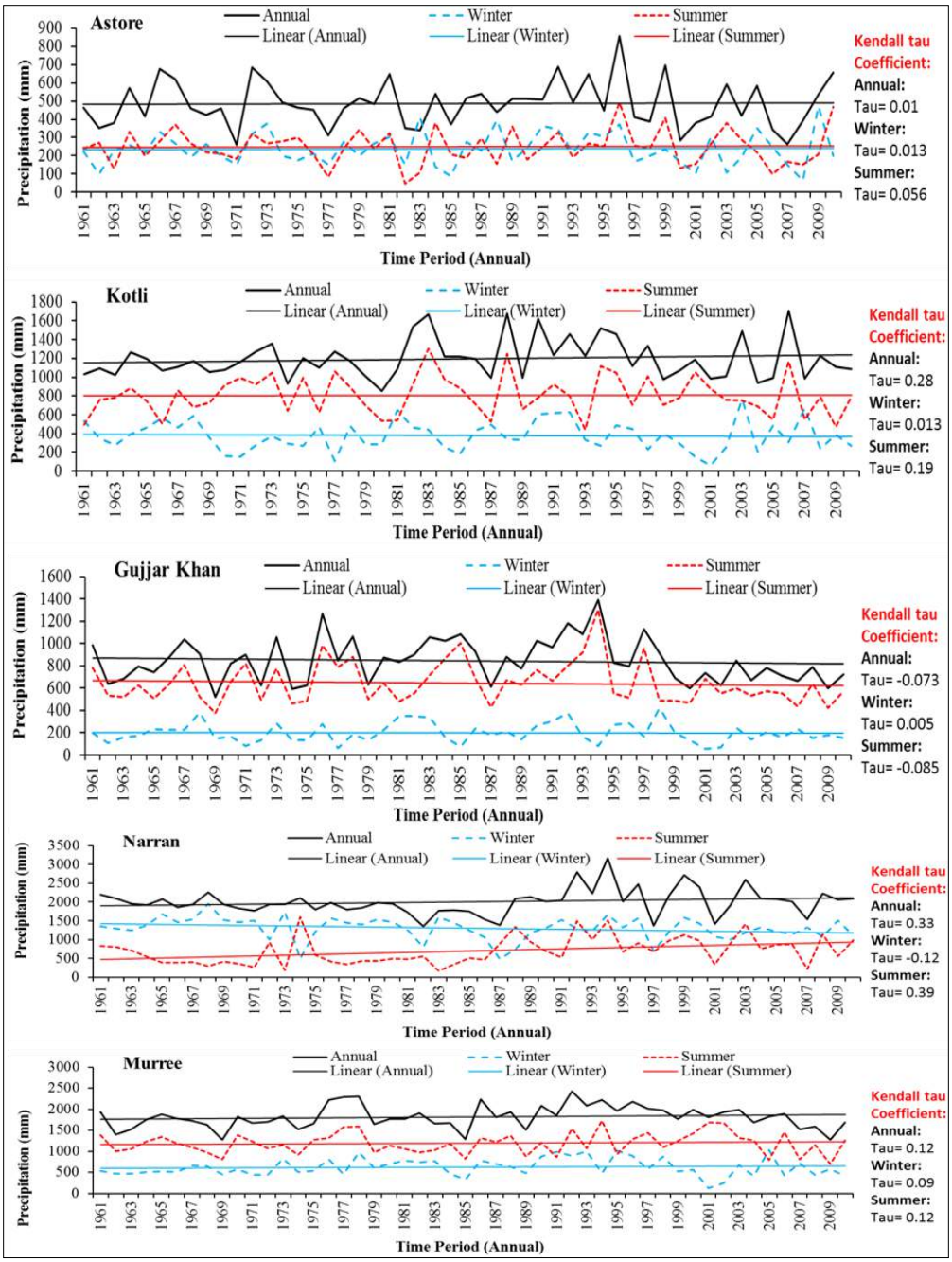

Fig. 2.6: Total annual precipitation trend over 50-year period (1961–2010) for the selected climate stations in the Mangla Basin. Kendall's tau (**τ**) coefficient values are presented for the trend analysis of linear regression line with $p<0.05$.

B. Temperature Analysis

The variations in the magnitude of the observed mean monthly temperature at five selected climate stations (one from each sub-catchment) are shown in Fig. 2.7. A non-parametric Kendall tau trend test was used to analyse temperature variations from 1999 to 2010. The Kendall's tau (τ) coefficient value indicates no significant trend at all the climate stations over the period from 1999 to 2010 in Mangla catchment. However, a slight increase in temperature over all the stations is observed. The temperature variations at two prominent stations, Astore and Naran, indicate that the runoff of these two sub-basins is controlled by temperature seasonality and largely fed by seasonal snow that melts due to increase in temperatures during summer, as confirmed by Archer and Fowler (2008).

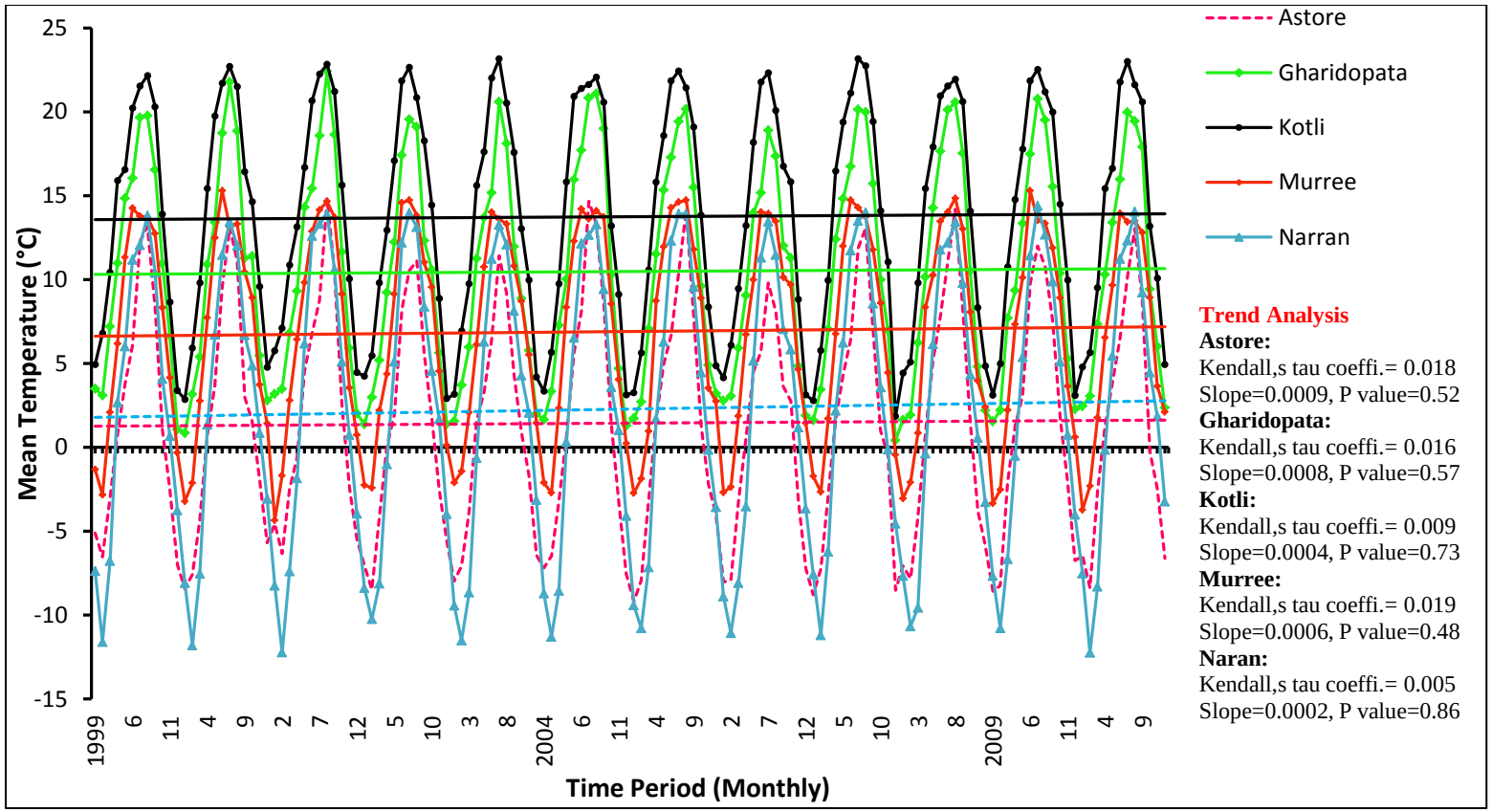

Fig. 2.7: Mean monthly temperature variation at selected climate stations over 12-year period (1999–2010). Kendall's tau (**τ**) coefficient values are presented for the trend analysis of linear regression line with $p<0.05$.

2.3.2 Flow Duration Curve Analysis

The flow duration curve (FDC) analysis was performed at 8 gauging stations to understand the hydrological behaviour of different tributaries within the catchment. FDC analysis consists of viable records of daily streamflow time series within the basin (flow records with less than 10-year time series were excluded from the analysis). Only at Mangla Dam the record available was from 1995 to 2009. The FDCs are separated according to their discharge range and location. As discussed in section 1.4, a maximum 1386 m^3/s discharge is required at Mangla Dam for full capacity hydropower generation, while for the lowest power generation nearly 138.6 m^3/s of outflow of the dam through the power tunnel is required to run at least one turbine which can generate 100 MW. The operational management of the Mangla Dam largely depends upon the discharge received at the Azad Pattan, Muzafferabad, Domel and Mangla stations. Therefore, an understanding of the inflows behaviour at these stations is essential for better management of water resources. Fig. 2.8 shows that the inflows behaviour over each year differs greatly between stations. The discharge at Mangla Dam is aggregated over all Jhelum River tributaries with an approximate catchment area of 33,867 km^2. The mean annual discharge at Mangla Dam is nearly 795 m^3/s, (1995–2009) with minimum and maximum inflows of 70 and 13,161 m^3/s, respectively. On a mean annual basis, on approximately 55 days or 15% of the year, the Mangla Dam receives inflows equal to or greater than (Q_{15}) 1386 m^3/s.

The discharge at Azad Pattan station (basin area of about 26,773 km^2) collects water from the Kunhar and Neelum rivers and the Jhelum Basin. The average annual flow at this station is approximately 775 m^3/s (1979–2009), while the maximum and minimum discharge is 10,822 and 25.4 m^3 /s,

respectively. Furthermore, the Azad Pattan discharge levels are increased as a result of the contribution of some additional water from the Kanshi and Poonch rivers at Mangla Dam.

Furthermore, the Domel station is located near Muzafferabad at the main stream of Jhelum River. (The locations and characteristics of all stations are presented in Table 2.1 and Fig. 2.1. This station is a representation of the inflows contributed by Jhelum River catchment just before joining the Neelum and Kunhar Rivers. The catchment area of the station is approximately 14,470 km^2. The mean annual flow of this station is 331 m^3/s (1980–2009), while the minimum and maximum flow values are 31 and 3,533 m^3/s, respectively.

Similarly, Muzafferabad station represents the inflows of Neelum River (Kishanganga), without considering Kunhar and Jhelum River discharge. The catchment area of this station is about 7,422 km^2 and most of the basin area is covered by snow and glaciers. The inflows at this station depend mostly upon snowmelt runoff from the western Himalayas. The values of the minimum and maximum inflows are 20 and 3,766 m^3/s, respectively, and approximately 323 m^3/s mean annual discharge is observed at this station.

The FDC of Chinari, Naran, Gharidopata and Kotli are presented in Fig. 2.9. Chinari station represents the inflows received by Jhelum River from the catchment area situated in India, as this station is located very close to the Indian border. The catchment area of this station is about 13,868 km^2 and receives mean annual inflows of nearly 328 m^3/s, with minimum and maximum inflows of 25 and 1,876 m^3/s, respectively. Chinari station receives maximum inflows from Jammu and Kashmir and an equal proportion of runoff generated by rainfall and snowmelt contributes at this

station. Furthermore, Naran and Gharihabibullah are both stations located on the Kunhar River, which contributes about 11% of the total Mangla inflows. Gharihabibullah station is located at the point where the Kunhar River joins the Jhelum River and the catchment area of this station is nearly 2895 m^3/s. Overall, the flows are very low at this station, ranging from minimum to maximum discharge values of 7.6 to 1626 m^3/s, respectively. The average annual inflows at this station are 104.6 m^3/s. The largest part of this catchment is covered by snow and glaciers during the winter season. Moreover, the Kotli station is located on the Poonch River near Mangla Dam. The catchment area of this station is about 3,256 km^2, but this catchment is largely dominated by rainfall-runoff. A slight part of the inflows is contributed by the southern slopes of the Pir Panjal range in the form of snowmelt runoff. The discharge at this station varies from 6 (minimum) to 6,561 m^3/s (maximum). The average annual inflows are 126.23 m^3/s at Kotli station.

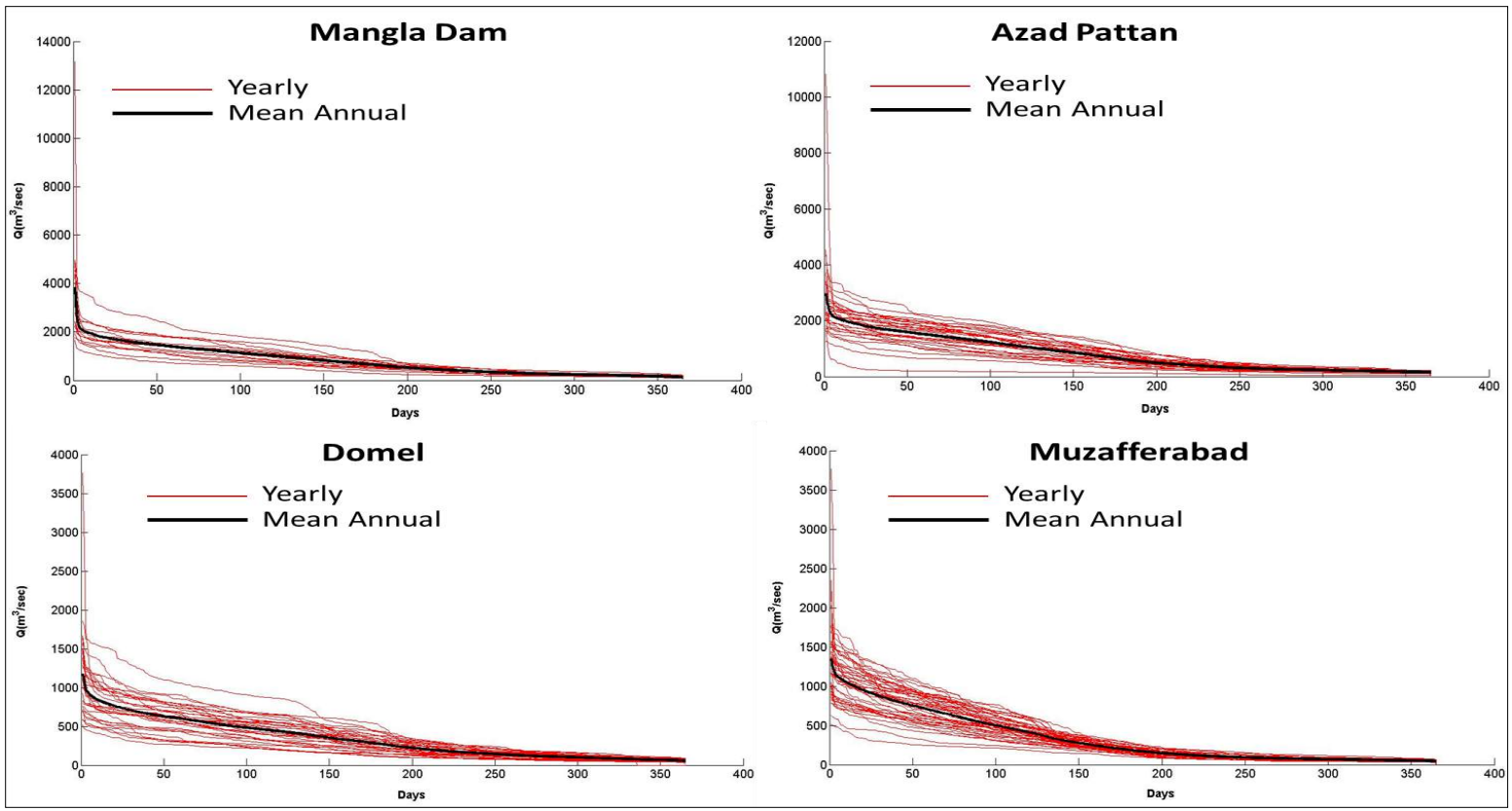

Fig. 2.8: Flow duration curves of selected streamflow gauges (Mangla Dam, Azad Pattan, Domel and Muzafferabad) indicate the average annual and yearly discharges.

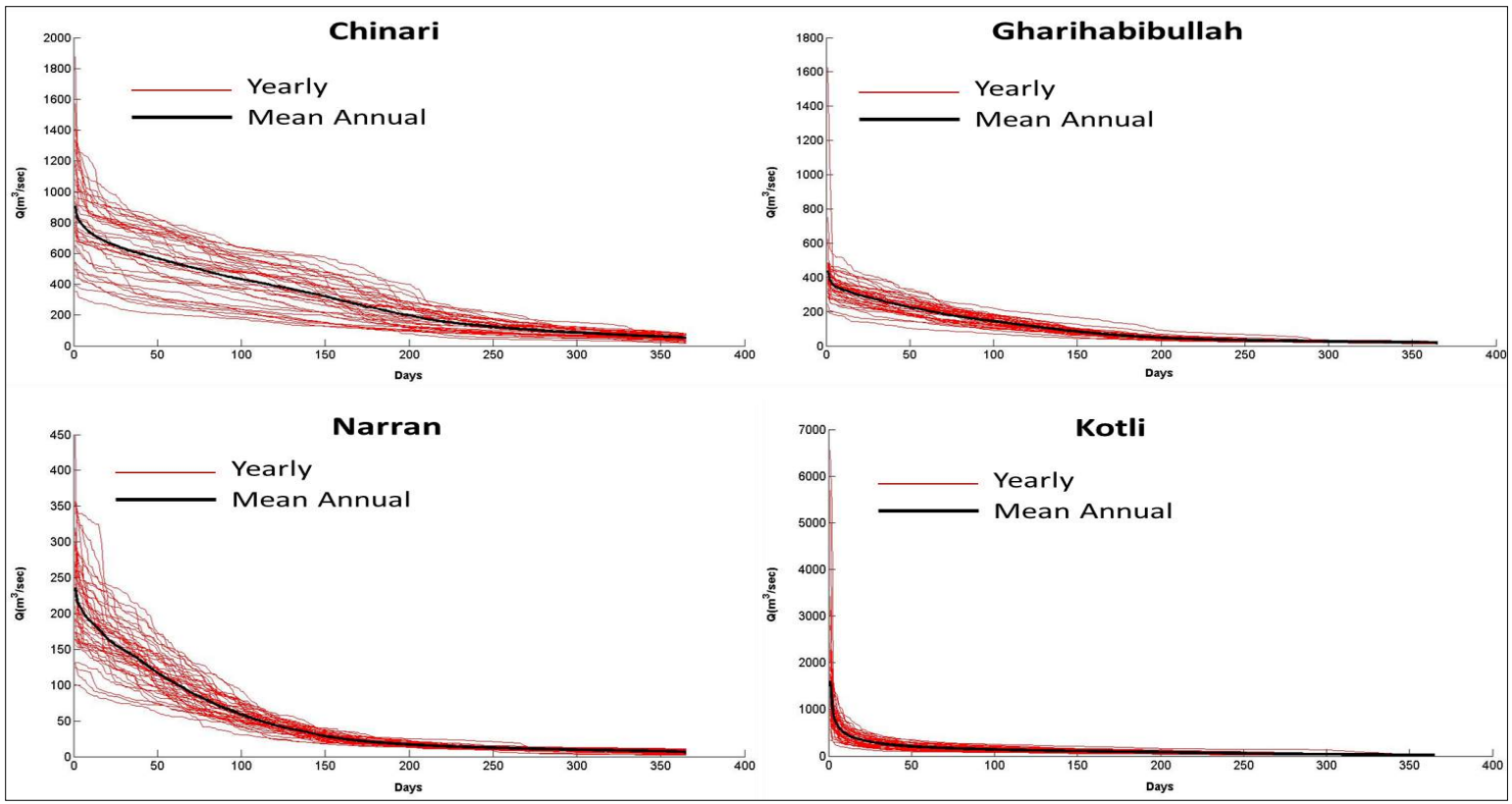

Fig. 2.9: Flow duration curves of selected streamflow gauges (Chinari, Naran, Gharihabibullah and Kotli) indicate the average annual and yearly discharges.

2.4 Analysis of Snow Cover Dynamics and Hydrological Regime of the Mangla Basin

It is interesting to investigate the impact of cryosphere (snow and ice) dynamics for better understanding of the hydrological behaviour in this catchment. In this section a detailed correlation analysis is carried out between climate variables (precipitation and temperature), discharge (at the Mangla Dam) and cryosphere dynamics based on remotely sensed MODIS snow cover data (MOD10A2) over a period of 10 years in the Mangla Basin. The following analysis is performed in this section:

a) The climate variations at different climate stations within the Mangla Basin (Jhelum River basin).
b) The hydrological behaviour affected by the climate variables (precipitation and temperature).
c) Spatial and temporal variations in snow cover dynamics of the Mangla Basin.
d) The climate change impact on the cryosphere dynamics and the correlation analysis between snow cover, mean temperatures and stream flows on annual and seasonal basis in Mangla Basin.

2.4.1 Analysis

Three elevation zones were extracted from the study area for the further detailed analysis of snow cover dynamics by the integration of GDEM with the ArcGIS tool. The characteristics of the elevation zones are illustrated in Table 2.2 and Fig. 1.2.

Table 2.2: Characteristics (extracted from the DEM) and SCA of the three elevation zones (extracted from the remotely sensed MODIS (MOD10A2) snow cover data) of the Mangla Basin.

Zones	Elevation Range (m)	Mean Elevation (m)	Area (%)	Area (km^2)	Snow Cover area (%)	
					Winter (05 Jan)	Summer (09 Aug)
A	< 2000	1118	46.25	15,66	2.26	0.103
B	2001–4000	3076	38.77	1313	80.20	0.442
C	> 4001	4367	14.98	5074	99.92	6.139

The daily streamflow data at Mangla Dam was obtained during 1995 to 2010 from SWHP-WAPDA. As discussed in the previous section, the precipitation and temperature records of 16 climate stations were taken from WAPDA and Pakistan Metrological Department (PMD) from 1961 to 2010 but some data was missing, particularly over 2005 and 2006 at some stations (due to the disastrous earthquake). Correlation analysis of climate data (precipitation and temperature) was performed at selected stations within the Mangla Basin where complete data was available and at Astore climate station (just outside the Mangla Basin in the Upper Indus Basin), to investigate the correlations between these stations. Regression analysis was also accomplished between annual and seasonal (winter and summer) daily inflows data at Mangla Dam and climate data from the Mangla Basin climate stations and Astore station to categorize the stations that were the most representative of inflows at Mangla Dam. Furthermore, this analysis was also accomplished to identify the main factors affecting the Jhelum River flow at Mangla Dam. The Pearson and Kendall rank correlation tests were used to analyse the relationship between hydrological and climate variables of all the gauging stations in Mangla Basin. The MODIS snow products were used to estimate the snow cover area. The cryosphere (snow and ice) percentage was

extracted for the Mangla Basin for 10-year time period. Images with cloud cover greater than 20% were removed and the SCA for those dates was estimated by the interpolation of the previous and next images. The zonal snow cover area was also estimated for the zonewise trend analysis of snow cover dynamics over the period from 2000 to 2009. A non-parametric Mann-Kendall trend test has been applied by several researchers (Hirsch and Slack 1984; Hirsch et al. 1982) for the seasonal/periodic data to identify trends; Kendall's tau coefficient (τ) represents the trend test value.

2.4.2 Climatological Variation Analysis

The correlation coefficients for the monthly temperature and precipitation trends between the Jhelum Basin climate stations and Astore station are given in Table 2.3 and 2.4. The Pearson and Kendall rank correlation coefficients were used to estimate the relationship among the aforementioned variables, at the P = 5% significance level. As mentioned in section 2, the absolute precipitation values are underestimated and cannot be the real representation of precipitation for the exploitation of hydrological behaviour in the catchment. However, the hypothesis is made that the observations for the same precipitation gauge are able to provide us with the relative trend from one month to the next. Therefore, the correlation analysis is carried out on a monthly basis. The correlation results for monthly precipitation data show that there is a strong correlation between most of the Mangla watershed climate stations. However, a significant inverse correlation between some northern stations, particularly at Naran, Astore and Saif-ul-Malok, was found with respect to low elevation climate stations. It is remarkable that the correlation of these three high altitude climate stations is negative with all the other low elevation stations with the exception of Srinagar, even though this is also located at a low elevation. The reason for this correlation with the

stations other than Srinagar may be associated with the locations of the stations, since the correlation analysis was carried out on a monthly basis and the peak rainfall pattern over the year is very different in the southern and north-eastern parts of the basin, as confirmed by Archer and Fowler (2008). These negative correlation values may also be due to the large differences in the annual rainfall of different stations like Srinagar (686 mm), Astore (485 mm) and Muzafferabad (1488 mm), as shown in Table 2.1. The rapid altitude variation and uneven rainfall distribution over Mangla Basin could explain the low correlation between most of the stations. Stations situated at higher elevations (greater than 2000 m, e.g. Naran, Saif-ul-Malok, Astore and Muree) receive more snow than rainfall.

A significant correlation was found for the minimum, maximum and mean temperature between most of the climate stations and at the neighbouring Astor station. The highest correlation value was 0.98 in each case. At some of the stations, the correlation coefficient value was not very high but still significant, with at least 0.50 in each case (Table 2.4).

Table 2.3: Precipitation correlation coefficients between Jhelum River catchment climate stations up to Mangla Dam.

Stations	G.Dopata	Kotli	Muree	M.abad	Srinagar	Khandar	Mangla	Naran	Palandri	Saif-ul-Malok
Astore	(0.075) 0.03	**(-0.24) -0.18**	**(-0.67) -0.24**	**(-0.63) -0.30**	**(0.85) 0.81**	**(-0.23) -0.11**	**(-0.27) -0.12**	**(0.92) 0.67**	(0.05) 0.03	**(0.96) 0.71**
G.Dopata	-	**(0.94) 0.89**	**(0.97) 0.89**	**(0.97) 0.96**	**(0.46) 0.41**	**(0.96) 0.89**	**(0.90) 0.78**	**(0.16) 0.11**	**(0.99) 0.96**	**(0.25) 0.18**
Kotli	-	-	**(0.98) 0.84**	**(0.96) 0.92**	**(0.34) 0.21**	**(0.99) 0.92**	**(0.99) 0.89**	**(-0.14) -0.12**	**(0.95) 0.92**	**(-0.19) -0.11**
Muree	-	-	-	**(0.97) 0.92**	**(0.32) 0.24**	**(0.99) 0.89**	**(0.96) 0.89**	**(-0.22) -0.12**	**(0.98) 0.92**	**(-0.29) -0.15**
M.abad	-	-	-	-	**(0.41) 0.31**	**(0.96) 0.92**	**(0.93) 0.81**	(0.011) 0.01	**(0.97) 0.87**	(0.05) 0.01
Srinagar	-	-	-	-	-	**(0.34) 0.28**	**(0.23) 0.12**	**(0.88) 0.63**	**(0.44) 0.41**	**(0.84) 0.57**
Khandar	-	-	-	-	-	-	**(0.97) 0.89**	**(-0.71) -0.42**	**(0.97) 0.92**	**(-0.69) -0.42**
Mangla	-	-	-	-	-	-	-	**(-0.24) -0.18**	**(0.92) 0.81**	**(-0.34) -0.25**
Naran	-	-	-	-	-	-	-	-	**(0.15) 0.12**	**(0.95) 0.74**
Palandri									-	**(0.21) 0.15**

Values within and outside () are Pearson and Kendall correlation coefficient values, respectively. Bold values are different from 0 with $p = 0.05$.

Table 2.4: Temperature correlations between Jhelum River catchment climate stations up to Mangla Dam.

T_{min}	G.Dopata	Kotli	Muree	M.abad	Naran	Palandri	Rawalakot	Khandar	Saif-ul-Malok
Astore	(0.89) 0.81	(0.87) 0.76	(0.84) 0.71	(0.89) 0.81	(0.76) 0.61	(0.87) 0.77	(0.78) 0.67	(0.87) 0.77	(0.88) 0.78
G.Dopata	-	(0.95) 0.80	(0.88) 0.69	(0.98) 0.87	(0.76) 0.56	(0.95) 0.80	(0.84) 0.67	(0.95) 0.82	(0.61) 0.55
Kotli	-	-	(0.89) 0.70	(0.97) 0.84	(0.73) 0.54	(0.95) 0.82	(0.84) 0.66	(0.96) 0.83	(0.59) 0.49
Muree	-	-	-	(0.90) 0.72	(0.77) 0.58	(0.91) 0.73	(0.79) 0.60	(0.86) 0.66	(0.68) 0.49
M.abad	-	-	-	-	(0.77) 0.57	(0.96) 0.83	(0.85) 0.67	(0.95) 0.82	(0.61) 0.45
Naran	-	-	-	-	-	(0.76) 0.57	(0.72) 0.54	(0.72) 0.52	(0.83) 0.66
Palandri	-	-	-	-	-	-	(0.84) 0.67	(0.93) 0.79	(0.61) 0.54
Rawalakot	-	-	-	-	-	-	-	(0.86) 0.69	(0.63) 0.56
Khandar	-	-	-	-	-	-	-	-	(0.69) 0.51
T_{max}	G.Dopata	Kotli	Muree	M.abad	Naran	Palandri	Rawalakot	Khandar	Saif-ul-Malok
Astore	(0.89) 0.71	(0.84) 0.63	(0.86) 0.68	(0.88) 0.71	(0.84) 0.66	(0.86) 0.65	(0.84) 0.64	(0.88) 0.70	(0.85) 0.67
G.Dopata	-	(0.92) 0.75	(0.94) 0.79	(0.97) 0.86	(0.92) 0.77	(0.84) 0.64	(0.91) 0.74	(0.85) 0.66	(0.65) 0.50
Kotli	-	-	(0.93) 0.78	(0.94) 0.77	(0.93) 0.81	(0.83) 0.63	(0.94) 0.79	(0.80) 0.59	(0.64) 0.47
Muree	-	-	-	(0.95) 0.81	(0.95) 0.83	(0.82) 0.63	(0.92) 0.76	(0.83) 0.62	(0.74) 0.59
M.abad	-	-	-	-	(0.93) 0.80	(0.83) 0.63	(0.92) 0.75	(0.85) 0.65	(0.64) 0.58
Naran	-	-	-	-	-	(0.80) 0.62	(0.92) 0.78	(0.81) 0.61	(0.72) 0.67
Palandri	-	-	-	-	-	-	(0.83) 0.64	(0.82) 0.61	(0.82) 0.65
Rawalakot	-	-	-	-	-	-	-	(0.8) 0.59	(0.61) 0.45
Khandar	-	-	-	-	-	-	-	-	(0.65) 0.49
T_{avg}	G.Dopata	Kotli	Muree	M.abad	Naran	Palandri	Rawalakot	Khandar	Saif-ul-Malok
Astore	(0.94) 0.71	(0.90) 0.63	(0.92) 0.68	(0.94) 0.71	(0.91) 0.66	(0.91) 0.65	(0.91) 0.64	(0.91) 0.70	(0.92) 0.67
G.Dopata	-	(0.96) 0.75	(0.94) 0.79	(0.98) 0.86	(0.96) 0.77	(0.88) 0.64	(0.96) 0.71	(0.91) 0.66	(0.54) 0.40
Kotli	-	-	(0.94) 0.78	(0.97) 0.77	(0.98) 0.81	(0.84) 0.63	(0.97) 0.79	(0.88) 0.59	(0.53) 0.47
Muree	-	-	-	(0.95) 0.81	(0.95) 0.83	(0.86) 0.63	(0.94) 0.76	(0.88) 0.62	(0.50) 0.49

Table 2.4 (Continued)

M.abad	-	-	-	-	**(0.96) 0.80**	**(0.87) 0.63**	**(0.97) 0.73**	**(0.91) 0.65**	**(0.53) 0.48**
Naran	-	-	-	-	-	**(0.85) 0.62**	**(0.97) 0.78**	**(0.88) 0.61**	**(0.93) 0.67**
Palandri	-	-	-	-	-	-	**(0.86) 0.64**	**(0.90) 0.63**	**(0.55) 0.45**
Rawalakot	-	-	-	-	-	-	-	**(0.89) 0.59**	**(0.53) 0.47**
Khandar	-	-	-	-	-	-	-	-	**(0.62) 0.49**

Values within and outside () are Pearson and Kendall correlation coefficient values, respectively. Bold values are different from 0 with $p = 0.05$.

2.4.3 Hydrological behaviour of Jhelum River Basin

The correlation coefficient values between the climate variables of the Mangla Basin and inflows of the Jhelum River at Mangla Dam over an annual and seasonal basis for the Pearson and Kendall rank tests are given in Table 2.5. Significant correlations were found between annual based climate parameters (precipitation and temperature) and streamflows. Although the correlations were found to be significant, for most of the stations the correlation was not strong. The correlation between summer precipitation and streamflow was significant in each case (Table 2.5). A significant inverse correlation was found between winter precipitation at high altitude stations and streamflow at Mangla, which may be because most of the rainfall occurs in solid form as snow. These stations may provide a better representation of precipitation and snowmelt in the Himalayan range, which is the main source of runoff (Archer and Fowler 2008).

Table 2.5 shows that the correlation between annual temperature and streamflow at Mangla Dam was found to be significant, which indicate that the Mangla annual inflows are partially driven by seasonal snowmelt due to increase in the mean temperature. Archer (2003) explained this fact for the Karakoram region (the neighbouring catchment of the Himalayan range), finding that the peak seasonal (summer) and daily stream flows are caused by the heat energy which melts the snow pack and stored water in the form of snow and ice. The highest (r = 0.55) and lowest (r = 0.35) correlation coefficient was observed for annual temperature and streamflow at Kotli and Palandri, respectively.

A significant correlation between seasonal temperature and streamflows for most of the stations was found, with the highest correlation between two

stations and the Jhelum River flows (Naran, Saif-ul-Malok: r = 0.63, r = 0.57, respectively). This positive correlation is associated with the fact that flows generated from these sub-basins are driven by snowmelt due to increment in the mean temperature. This fact is confirmed by Archer (2003) in the neighbouring glacier-fed Karakorum region, where the summer flows are the result of heat energy that melts the snow and ice. The positive correlation suggests that the Naran, Astore and Saif-ul-Malok stations are located in the most active hydrological parts of the catchment, which contribute largely in the form of snowmelt. The correlation between winter mean temperature and discharge at Mangla Dam was not significant for those catchments where rainfall is the dominant factor for runoff generation. However, a positive correlation was found for some high altitude stations. This may be associated with the fact that the snow/ice melt is driven by the long-wave and short-wave energy balance at the surface over early spring and summer (Sicart et al. 2005, 2006) and a higher temperature is only one of the consequences of this balance.

This suggests that the Jhelum River flow is partially contributed by the seasonal snow and glacier melt. In contrast, a strong correlation between temperature and streamflow is a characteristic of the high elevation glacierized sub-basins of the Upper Indus Basins such as Hunza and Shyok (Archer 2003) and this is also confirmed by Tahir et al. (2011). However, a negative correlation was also found for Palandri station over the winter and spring seasons, which may be related to delayed runoff generation because of precipitation occurring in the form of snow. Schär et al. (2004) confirmed the aforementioned fact and stated that the streamflows may also be sensitive to variation in mean monthly temperature, which determines whether

precipitation is in liquid or solid form, which can in turn determine whether the runoff is instantaneous or delayed.

An analysis of Table 2.5 shows that the zone B (specifically corresponding to the Naran, Astore and Saif-ul-Malok climate stations) is the most active zone for Jhelum River flows. The correlation coefficients for both climate variables (temperature and precipitation) at Naran and Saif-ul-Malok with respect to inflow at Mangla Dam were found to be more significant than other stations for annual and seasonal analysis. Approximately 43.44% of the area of Mangla Basin is situated in zone B and the major portion of this zone is covered by snow, which can largely alter the Jhelum River flow due to the variation in temperature and precipitation.

Table 2.5: Annual and seasonal correlation coefficients between discharge data at Mangla Dam (2000–2009) and climate data (daily basis) of Jhelum River catchment stations

Climate data	Discharges of Jhelum River at Mangla Dam		
Correlations	**Annual (Jan-Dec)**	**Winter and Spring (Oct-Mar)**	**Summer (Apr-Sep)**
Precipitation			
Astore	**(0.35) 0.27**	**(-0.60) -0.40**	**(0.39) 0.27**
G.Dopata	**(0.30) 0.24**	(-0.07) -0.02	**(0.40) 0.20**
Kotli	**(0.36) 0.39**	**(-0.33) -0.28**	**(0.70) 0.73**
Muree	**(0.38) 0.33**	**(-0.47) -0.29**	**(0.48) 0.40**
M.abad	**(0.43) 0.30**	**(-0.33) -0.16**	**(0.54) 0.33**
Srinagar	**(0.42) 0.33**	**(0.66) 0.33**	**(0.83) 0.61**
Khandar	**(0.38) 0.33**	**(-0.47) -0.31**	**(0.64) 0.60**
Naran	**(0.46) 0.33**	**(-0.45) -0.33**	**(0.43) 0.37**
Palandri	**(0.35) 0.30**	**(0.41) 0.33**	**(0.49) 0.47**
Rawalakot	**(0.45) 0.33**	**(0.37) 0.29**	**(0.74) 0.47**
Saif-ul-Malok	**(0.46) 0.39**	**(-0.42) -0.32**	**(0.32) 0.19**
Daily Mean Temperature			
Astore	**(0.42) 0.34**	**(0.40) 0.31**	**(0.43) 0.37**
G.Dopata	**(0.49) 0.40**	(0.11) 0.03	**(0.26) 0.22**
Kotli	**(0.55) 0.45**	**(0.15) 0.10**	**(-0.12)** -0.09
Muree	**(0.45) 0.38**	**(0.26) 0.18**	**(0.34) 0.27**
M.abad	**(0.48) 0.39**	(0.08) 0.03	**(0.17) 0.12**
Naran	**(0.52) 0.42**	**(0.37) 0.32**	**(0.57) 0.45**
Palandri	**(0.35) 0.27**	**(-0.19) -0.12**	(0.02) 0.01
Rawalakot	**(0.51) 0.42**	(0.06) 0.01	(0.05) 0.01
Khandar	**(0.48) 0.38**	**(0.14)** 0.05	(-0.09) -0.08
Saif-ul-Malok	**(0.58) 0.46**	**(0.39) 0.27**	**(0.63) 0.48**

Values within and outside () are Pearson and Kendall correlation coefficient values, respectively. Bold values are different from 0 with $p = 0.05$.

2.4.4 Cryosphere Dynamics in the Jhelum River Basin

An analysis of cryosphere dynamics over the 10-year period using MODIS snow cover images suggests that the basin-wide (BW) SCA in Mangla Basin has an increasing tendency and trends are not statistically significant (Fig. 2.10). Meanwhile, on the basis of the zonal distribution of SCA, it reveals that zone C has a decreasing tendency (Fig. 2.11). The Kendall's tau (τ) coefficient value indicates a downward trend in zone C, over an altitude of 4000 m. This downward tendency is slightly stronger in the maximum snow

cover period from October to March (τ = -0.034). A very slight increasing tendency was found in zones A and B. The snow cover shrinkage tendency in high elevation areas of the Himalayan range was confirmed by Berthier et al. (2007) and also by Ageta and Kadota (1992). Scherler et al. (2011) also reported the shrinkage of glaciers in the eastern Himalayas and Tibetan Plateau, in contrast to the Karakoram region (influenced by westerlies), where 50% of the glaciers are expanding or constant. This shrinkage and expansion of snow cover may be due to the increase in temperature and precipitation in all zones, even if the tendency is very low. Change in both climate variables (temperature and precipitation) continuously feeding zones A and B results in the expansion of snow cover during winter. Fig. 2.11 shows that zones A, B and C have average SCA equal to 3%, 40% and 70%, respectively. The SCA in zone C also approaches 100% for some winter months, but was less than 5% over the summer season, while the concurrent SCA in zone B also varies significantly from approximately zero to 90%. This SCA variation in all zones of the catchment explains the large seasonal (winter to summer) change in climatic variables (minimum and maximum temperature) in Mangla Basin.

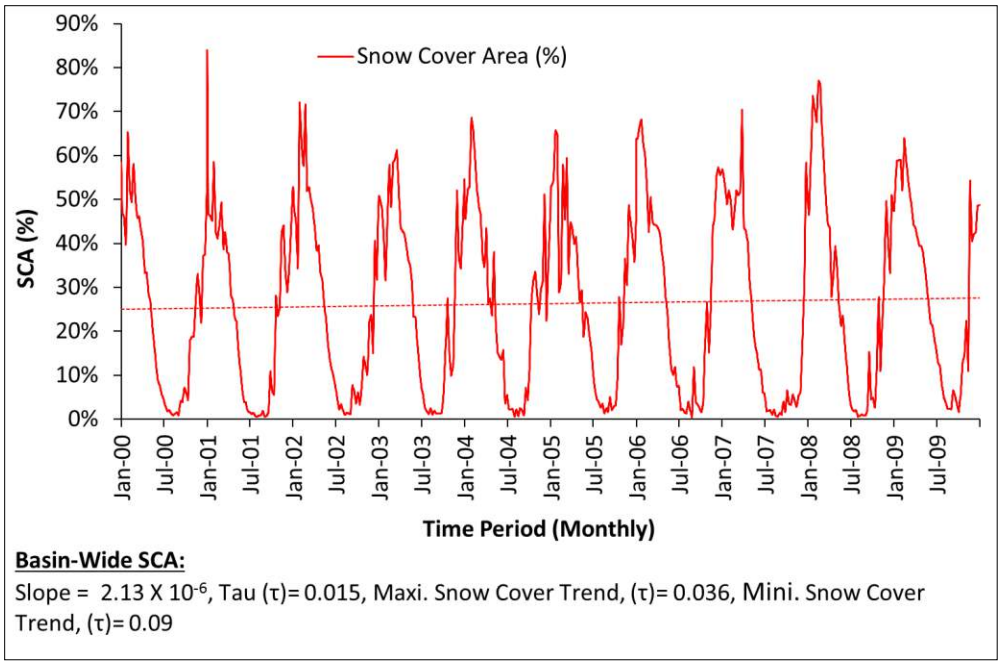

Fig. 2.10: Basin-wide snow cover area (SCA) in Mangla Basin (2000–2009).

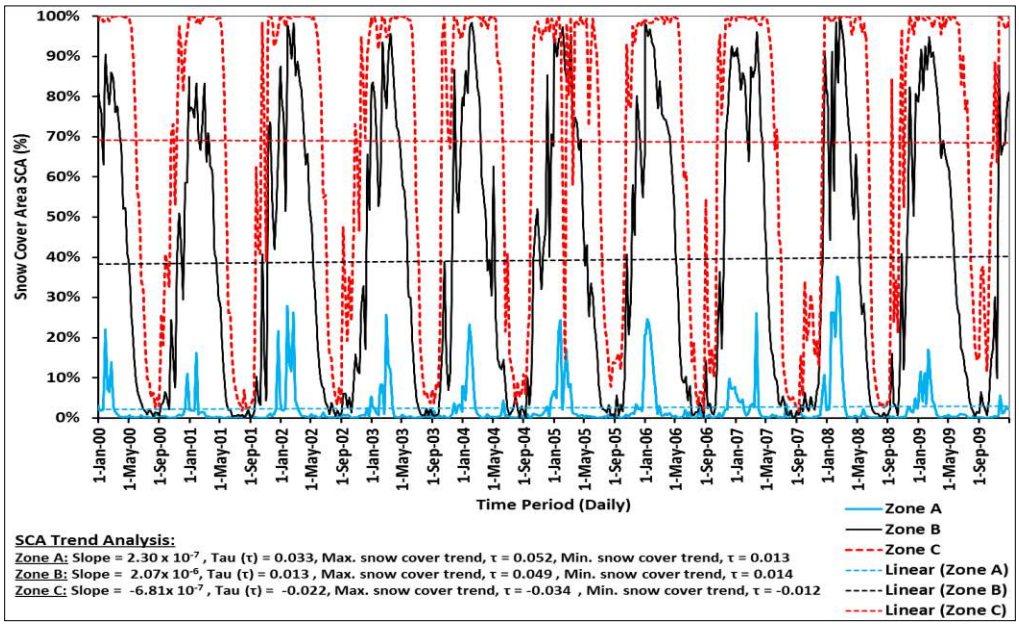

Fig. 2.11: Snow cover distribution trend in three altitude zones of the Mangla Basin from 2000–2009.

2.4.5 Correlation between Change in Cryosphere Climate Variables and Stream Flow in the Mangla Basin

The basin-wide cryosphere area varies from approximately 5 to 60% over the summer (April to Sep) to winter (Oct to March) seasons, respectively, as shown in Fig. 2.12. This snow cover variation has a significant inverse correlation with temperature and discharge in Mangla Basin, as presented in Table 2.6. The correlation was developed among the standardised values of four different variables, including mean temperature, precipitation, snow cover change and stream discharge, as shown in Fig. 2.13. A continuous depletion of the snow cover area is observed as the mean temperature of the basin increases during the summer, which is the main source of the advancement of stream discharges. The correlation between the monthly change in Mangla inflows and the snow cover area is inversely correlated with the Pearson and Kendall correlation coefficient values, equalling -0.54 and -0.42, respectively (Fig. 2.14), which indicates that the variation in Mangla Dam inflows also depends upon the change in the snow cover area.

The Pearson and Kendall rank correlation coefficient at 5% significance level was used to evaluate the relationship of the change in cryosphere dynamics with the climate variables (precipitation and temperature) and stream flows of Jhelum River at Mangla Dam (Table 2.6). There are some other variables which can influence the river discharge, like sublimation, evapotranspiration, debris-free glaciers and melting permafrost, but these factors were not considered in this study. These variables would be more important for theoretical application of a mountainous hydro-climatic model. There is no significant correlation present between snow cover and precipitation in Mangla Basin. This fact may be associated with the well-known “under-sampled” precipitation error in high elevation gauged

catchments, as reported by FØrland (1996). Such errors are unable to give a real representation of snow cover change in high elevation areas. The inverse significant correlation between mean temperature and snow cover change was found in Mangla Basin. In the summer season, a higher correlation between mean temperature and snow cover change was found compared to winter. This correlation suggests that the Jhelum River discharge strongly depends upon the snow cover dynamics and temperature. This was confirmed by De Scally (1994), who stated that a strong correlation was found between snowpack and discharge of Jhelum River.

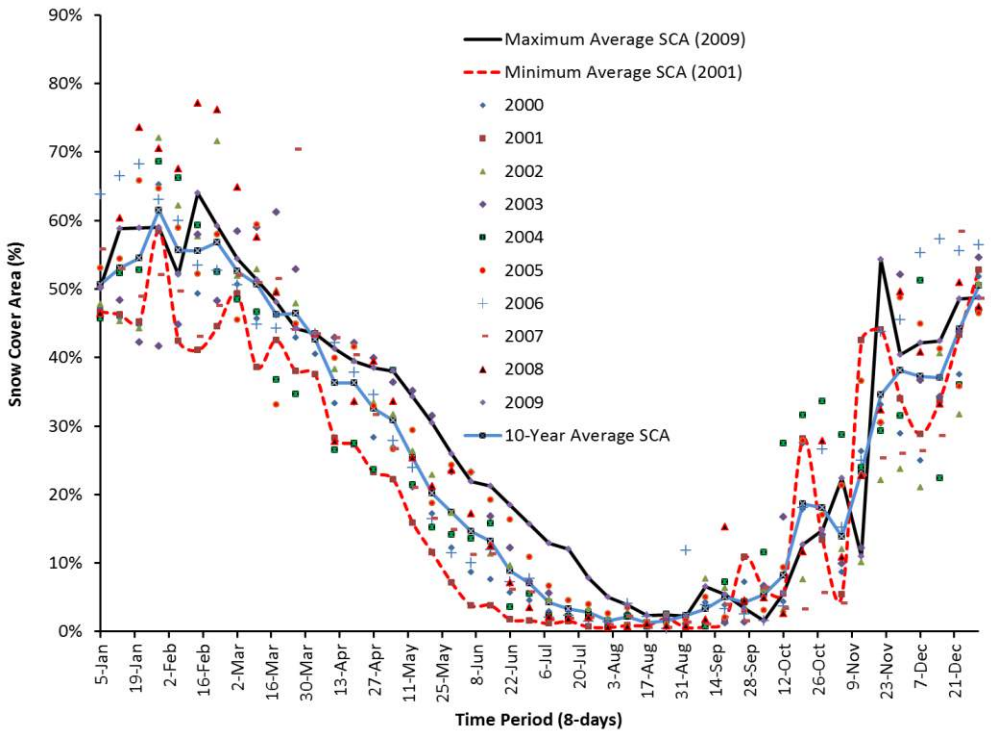

Fig. 2.12: Basin-wide Snow Cover Area (SCA) percentage in the Jhelum River Basin up to Mangla Dam estimated by using MODIS (MOD10A2) images.

Table 2.6: Annual and seasonal correlation coefficients between snow cover change, Jhelum River Basin daily climate variables (precipitation and temperature) and daily stream flow data at Mangla Dam (2001–2009).

(a) Climate data	**Cryosphere Change in Mangla Basin**		
Correlations	**Annual**	**Winter and Spring (Oct-Mar)**	**Summer (Apr-Sep)**
Precipitation			
Astore	**(0.29) 0.21**	**(0.26) 0.18**	**(0.31) 0.25**
G.Dopata	(-0.08) -0.05	(-0.08) -0.01	**(0.12) 0.10**
Kotli	**(-0.13)** -0.07	**(-0.13) -0.10**	**(0.11) 0.10**
Muree	**(-0.14)** -0.09	**(-0.14) -0.10**	**(0.10)** 0.09
M.abad	**(-0.13)** -0.05	**(-0.14) -0.13**	**(0.14) 0.11**
Srinagar	(-0.08) -0.03	(-0.08) 0.08	**(0.12)** 0.08
Khandar	(-0.09) -0.04	(-0.09) 0.07	(0.07) 0.09
Naran	**(0.33) 0.201**	**(0.30) 0.20**	**(0.36) 0.25**
Palandri	**(-0.12)** -0.05	**(-0.12)** -0.09	(0.09) 0.03
Rawalakot	(0.01) -0.06	(-0.12) -0.06	**(0.14) 0.12**
Saif-ul-Malok	**(0.35) 0.24**	**(0.26) 0.18**	**(0.28) 0.21**
Mean			
Astore	**(-0.83) -0.62**	**(-0.51) -0.35**	**(-0.71) -0.62**
G.Dopata	**(-0.76) -0.54**	**(-0.49) -0.27**	**(-0.59) -0.54**
Kotli	**(-0.71) -0.67**	**(-0.45) -0.23**	**(-0.70) -0.59**
Muree	**(-0.74) -0.51**	**(-0.42) -0.20**	**(-0.62) -0.51**
M.abad	**(-0.75) -0.53**	**(-0.39) -0.17**	**(-0.59) -0.53**
Naran	**(-0.71) -0.49**	**(-0.38) -0.18**	**(-0.58) -0.48**
Palandri	**(-0.84) -0.62**	**(-0.37) -0.23**	**(-0.77) -0.62**
Rawalakot	**(-0.72) -0.49**	**(-0.40) -0.29**	**(-0.60) -0.49**
Khandar	**(-0.77) -0.55**	**(-0.38) -0.24**	**(-0.58) -0.50**
Saif-ul-Malok	**(-0.72) -0.53**	**(-0.33) -0.15**	**(-0.53) -0.45**
(b) Streamflow	**(-0.34) -0.22**	**(-0.26) -0.16**	**(-0.48) -0.38**

Values within and outside () are Pearson and Kendall correlation coefficient values, respectively. Bold values are different from 0 with $p = 0.05$.

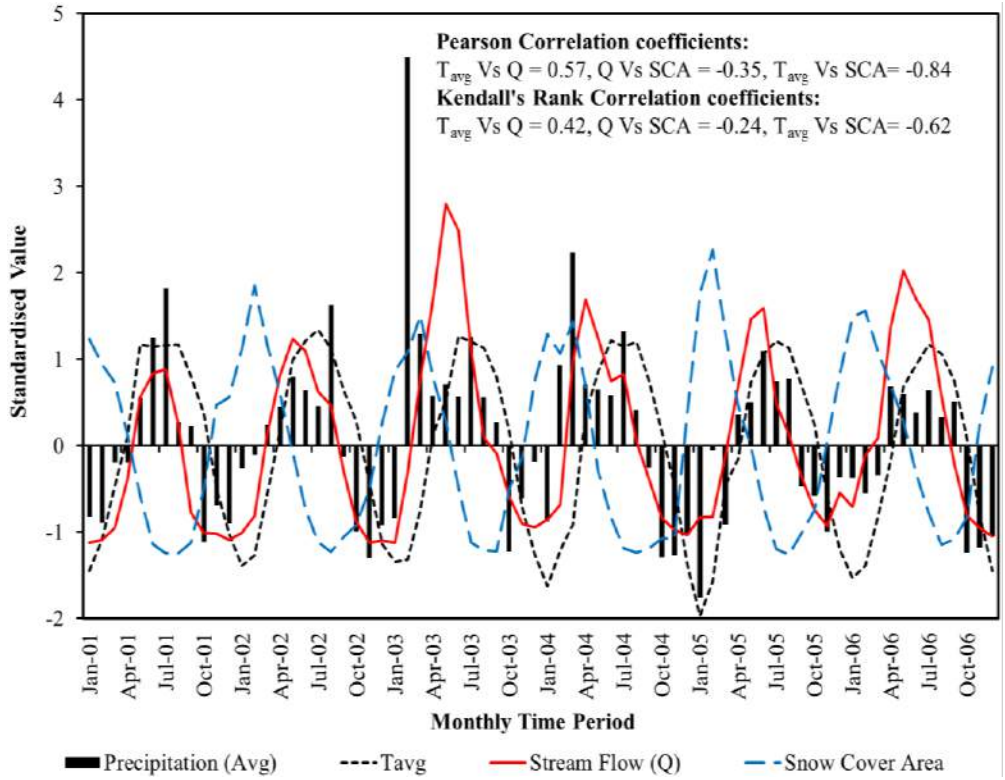

Fig. 2.13: Correlation ($p<0.05$) between standardised precipitation, temperature, snow cover and discharge (at Mangla Dam) in Jhelum River Basin (monthly basis).

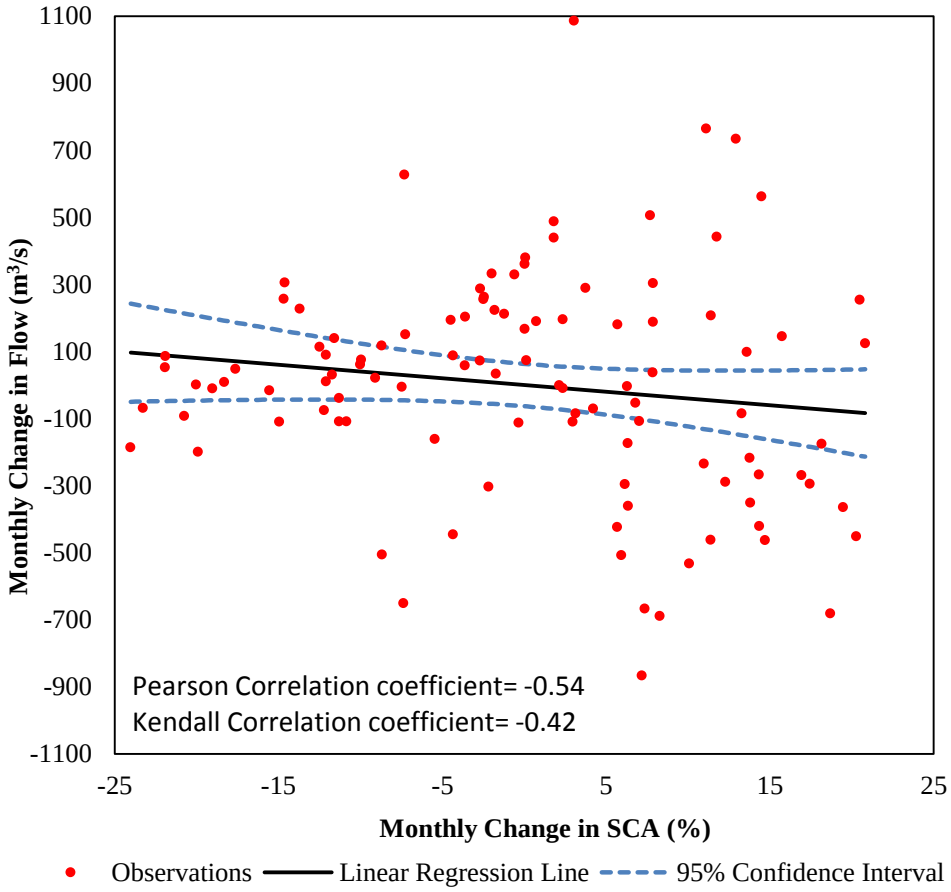

Fig. 2.14: Correlation ($p< 0.05$) between monthly difference in SCA and discharge at Mangla Dam in Jhelum River Basin.

2.5 Conclusion

The Jhelum River is a major tributary of the Indus River which contributes to the Indus Basin Irrigation System through Mangla Dam. The stream flows of the Jhelum River depend upon monsoon rainfall and snowmelt from the high altitude eastern Himalayas and Pir Panjal range. The snowmelt process at high altitude regions largely depends upon energy input indirectly associated with temperature. The following conclusions can be drawn from the results obtained in this study:

1 The inflows at Mangla Dam are mainly influenced by winter precipitation in the form of snow and glaciers at high altitudes, and by summer precipitation in the form of monsoon rainfall at low altitudes in the study basin.

2 Mean seasonal (winter and summer) temperatures play a significant positive role in deriving the hydrological and cryosphere regime of the basin. Changes in the temperature variables (minimum and maximum) have a large significant effect specifically on high-altitude regions of the basin, where they shift the hydrological regime of winter precipitation into summer runoff by deriving the snow accumulation and melt processes.

3 The part of the basin situated in high elevation (>2000 m) zones is the most active hydrological regime of the Mangla Dam. The 100% availability of snow cover area (SCA) in zone C (comprising 15% of the total basin area with the highest elevation) during winter that falls to 6% during the summer season clearly indicates the large contribution of high-altitude regions in the form of snowmelt runoff.

4 An analysis of changes in the annual and seasonal snow cover, hydrological regime and climate variables demonstrated a negative correlation, which means that the streamflow at Mangla Dam is strongly affected by changes in snow cover during the summer season. This was the reason for the recent mega floods in Pakistan due to the climate changes in recent years (2010 onwards).

5 The area above 2000 m elevation is the most active layer of the catchment because this layer shifts winter rainfall into summer runoff. The snow cover trend of zone C is negative, which explains the shrinkage of the Himalayan range cryosphere due to climate change

specifically in high-altitude areas. Meanwhile, the expansion of snow cover in zones A and B explains the difference in air temperature range between the high and low altitude zones of Mangla catchment is decreasing, with the temperature of zone C increasing and the temperature of zones A and B decreasing.

Although, the findings of this study present an important current scenario of temporal variations in snow cover trends, further study is required at sub-catchment level using longer time series of the MODIS snow cover dataset for developing future scenarios. Moreover, the use of Global Land Data Assimilation System (GLDAS) data products in future studies could efficiently address the gauging errors in meteorological data from the climate stations.

The streamflows of Jhelum River basin at Mangla Dam were analysed by using the available climate data for different climate stations within the catchment. However, the results suggest that the meteorological data collection techniques should be enhanced at the high elevation areas. Also, modern meteorological data collectors should be installed in high elevation glacierized catchments where gathering data on the most important factors for streamflow prediction, such as precipitation, temperature and snow data is very difficult when using ordinary instruments and their accuracy is also doubtful.

Chapter 3

Application of Hydrological Models

Foreword: This chapter is mainly concerned with the application of hydrological models and the computation of water resources availability in Mangla Basin. In order to select an appropriate hydrological model, a comparative study of two different hydrological models (HEC-HMS; a standard rainfall runoff model and SRM; widely used for snowmelt runoff simulations worldwide) is carried out, as presented in section 3.5. Furthermore, the calibration was carried out over each time window to optimize the parameters for the assessment of spatial and temporal variations between calibrated parameters for each time window as presented in section 3.6 and then used these parameters to examine the impact of climate change by using HEC-HMS. Subsequently, the water resources availability estimation at Mangla Dam is given in section 3.6 of this chapter.

3.1 Brief Introduction and Background

The Mangla Basin comprises low and high altitude mountains of the Pir Panjal and Himalayan ranges. In this region, total winter snow accumulation is an important control on the amount of runoff available for filling Mangla Reservoir. Snow accumulation is one of the most poorly understood aspects of the hydrological cycle in the Himalayas, despite the importance of snowmelt in many river basins (Kattelmann 1987). For example, the snow and glacier melt contribution is approximately 85% of the annual flow of the River Indus at the point where it emerges from the Himalaya/Karakoram Mountains onto the moisture-deficient lowlands (Tahir et al. 2011). On an

annual basis, the rainfall-generated runoff and snowmelt runoff contribution are similar for the Jhelum River flow.

There are several hydrological models available for rainfall and snowmelt runoff predictions. The selection of an appropriate model is tremendously important for the hydrological analysis in such peculiar hydrological behavioural catchments. Nevertheless, most of the hydrological models are less efficient for daily streamflow forecasting due to the snowmelt in high elevation catchments (Martinec et al. 2007). The selection of the model in a study depends on the basin characteristics, the type of data available and the objective of the simulation in a catchment (Hunukumbura et al. 2012), i.e. whether it is a snowmelt or rainfall-based runoff simulation.

The snowmelt runoff simulation process is complex and comprises mass and energy balances and heat and mass transport by vapour diffusion, conduction and meltwater drainage (Tarboton and Luce 1996). The complex nature of the snowmelt runoff process has motivated hydrologists to develop simple hydrological models to incorporate the snowmelt contribution (ŞENSOY 2005). Different hydrological models with the aim of snowmelt runoff modelling (Şorman et al. 2009; Verdhen and Prasad 1993; WMO 1986) have been used to simulate the daily streamflows in snow-fed basins.

In general, each model is reliable in the regions for which it was developed while for application in other catchments it requires extensive calibration. The evaluation is of two different models; one is based on the snow cover area and is specially designed for snowmelt runoff simulation, and the second is a standard rainfall-runoff model which is based on rainfall data. Due to the complex hydrological behaviour of Mangla Basin, both models are calibrated in this catchment to select the one that is more suitable for the estimation of water availability. Both models comprise a snowmelt

generation algorithm, but their input data requirements are different. Since Mangla Basin is a transboundary river catchment, the climate data of one part of the catchment is not available, so remote sensing data are used for calibration, and by comparison it is also easy to select on the basis of suitable data. In this study, two well-known hydrological models, the snowmelt runoff model (SRM) and hydrological modelling system (HEC-HMS) are selected for daily streamflow simulation. Both models employ the temperature index method also known as the degree–day method for the snowmelt runoff simulation.

3.2 Description of Hydrological Modelling System (HEC-HMS)

The HEC-HMS (Hydrologic Engineering Center Hydrologic Modeling System) model was developed by the US Army Corps of Engineers. The HEC-HMS is a distributed model designed to simulate the rainfall-runoff of dendritic watershed systems. This model can also be used to investigate flood frequency, urban flooding, flood warning system planning, reservoir spillway capacity, stream restoration, etc. (US Army Corps of Engineers, 2008). The propagation of personal computers (PC) and the improvement in the HEC-1 model of the US Army Corps of Engineers in 1998 to a GUI (graphical user interface) based on the user-friendly HEC-HMS model, available in the public domain, have come as further useful tools for field hydrologists. Unfortunately, the HEC-HMS model has not found many users due to the ambiguity involved in the optimization of model parameters, as with several other watershed models. But, at least optimization of the parameters at regional scale may be likely to shift over to watershed models like HEC-HMS rather than worksheet exercises (Kalita 2008).

The HEC-HMS comprises four major components: 1) an analytical model to estimate overland flow runoff as well as channel routing (basin models). This

component includes physical characteristics of the basin like the watershed area and methods for calculating the loss, transfer and baseflow of the watershed and channel. 2) A progressive graphical user interface demonstrating hydrologic system constituents with interactive structures (meteorological models), which incorporates the precipitation gauge weights, snowmelt and evapotranspiration method. 3) A structure for keeping and handling the data, particularly large, time-variable datasets (control specifications and time series data), and 4) a means for displaying and reporting model outputs (Bajwa and Tim 2002). The predictability of the rainfall-runoff model is improved using locally available gauge streamflow data through calibration of the model according to the local watershed conditions. The HEC-HMS provides different loss methods, some of which are mainly designed for event-based simulation, whereas others are proposed for continuous simulation. Gridded Loss Methods and Soil Moisture Accounting Loss Methods are required for a high number of input parameters. The "Deficit and Constant Loss" method is quite simple and useful because it involves only four input parameters, namely the initial deficit (mm), maximum deficit (mm), impervious area (%) and constant rate (mm/h). Halwatura and Najim (2013) applied HEC-HMS and tested different transfer and loss methods to check the reliability of the methods in HEC-HMS for Attanagalu Oya River, Sri Lanka and suggested that the deficit and constant loss method is more reliable than the CN method. There are seven different transformation methods available in HEC-HMS. Some of these methods are complex because of the high requirements for input parameters which are not accessible for most of the ungauged or scarcely gauged catchments. Some methods like the SCS unit hydrograph, Snyder unit hydrograph (Fang et al. 2005; Hunukumbura et al. 2012; Yilma 2007) and Clark unit hydrograph (Banitt 2010; Cunderlik and Simonovic 2007; Straub

et al. 2000) methods have been used successfully for the simulation of daily streamflows.

3.3 Description of Snowmelt Runoff Model (SRM)

The Snowmelt Runoff Model (SRM) is a conceptual, deterministic degree–day (temperature index method) model used to simulate and forecast daily rainfall and snowmelt runoff in mountainous regions. It can be usefully applied for the estimation of the consequences of climate change on snow cover and runoff from the alteration of the percentage of snow cover and temperature. SRM was designed by Martinec (1975) for small basins in Europe. The availability of remote sensing snow cover data provides flexibility to apply this model in large basins. The SRM has been applied in the Ganges River Basin, which has an area of 917,444 km^2 and elevations up to 8,840 m (Martinec et al. 2007). This model has been used successfully in more than a hundred catchments located in different regions of the world.

SRM was effectively tested by the World Meteorological Organization (WMO) for daily streamflows simulation (WMO 1986) and moderately to simulate the circumstances of real-time runoff predictions (WMO 1992). Initially, the user must provide a known or gauge streamflow value as the initial condition, and then it can be run according to the length of input data set variables, such as precipitation, temperature, and snow-covered area (SCA). Furthermore, the model requires a number of basin physical characteristics such as the basin area, zone area (in the case of zone-wise application) and the hypsometric (area–elevation) curve. The main Equation (3.1), on which the algorithm of the model is based, computes the water generated from rainfall and snowmelt, overlaid on the computed recession flow and converts this into daily streamflow from the catchment.

$$Q_{n+1} = \left[C_{s_n}.a_n(T_n + \Delta T_n)S_n + C_{r_n}P_n\right]\frac{A.10000}{86400}(1 - k_{n+1}) + Q_n k_{n+1} \quad (3.1)$$

where

Q = average daily discharge (m^3/s);

C = runoff coefficient, with C_s referring to snowmelt and C_r to rain;

a = degree–day factor, DDF (cm. °C^{-1} d^{-1}), *T* = number of degree–days (°C.d);

S = ratio of the snow covered area (SCA) to the total area;

n = sequence of days;

P = precipitation contributing to runoff;

A = area of the basin or zone;

k = recession coefficient (X_c and Y_c).

A detailed description of the variables and parameters used in this equation is given by Martinec et al. (2007).

3.4 Model Accuracy Criteria

The precision standards used for the assessment of SRM and HEC-HMS, the Nash-Sutcliffe coefficient (NS) and the percent difference of volume (DV), Root Mean Square Error (RMSE) and Mean Absolute Error (MAE) are defined as in Equations (3.2), (3.3), (3.4) and (3.5) as follows:

$$NS = 1 - \frac{\sum_{i=1}^{n}(Q_i - Q_i')^2}{\sum_{i=1}^{n}(Q_i - Q_{Avg})^2} \quad (3.2)$$

where

NS = Nash-Sutcliffe coefficient (a measure of model efficiency);

Q_{avg} = average daily discharge for the simulation year or simulation season;

Q_i = measured daily discharge;

n = number of daily discharge values;

Q'_i = simulated daily discharge.

$$D_v(\%) = \frac{(V - V')}{V} * 100 \quad (3.3)$$

where

D_V = difference between the total measured and simulated runoff;

$V^{'}$ = simulated runoff volume;

V = measured runoff volume.

$$RMSE = \sqrt{\frac{\sum_{i=1}^{n}(X_{obs,i}-X_{model,i})^2}{n}} \quad (3.4)$$

where

X_{obs} = observed values;

X_{model} = modelled values at time/place *i*.

$$MAE = \frac{\sum_{i=1}^{N}(S_i-O_i)}{N} \quad (3.5)$$

where

N = number of observations in the time series;

S_i = simulated values;

O_i = observed values.

Furthermore, the Kendall rank correlation and Pearson correlation coefficient (Lee Rodgers and Nicewander 1988) and the (Kendall and Gibbons 1990) tests were applied (significance level, 5%) to estimate the correlation between the simulated and measured daily streamflows.

3.5 Comparison of Hydrological Models

3.5.1 Application of HEC-HMS

The model was applied in Jhelum River Basin at Mangla Dam on a semi-distributed basis over single, 3- and 6-year time windows from 2001 to 2009. Since the Pooch River joins Mangla Reservoir directly, the simulation was

carried out separately at the Pooch River Basin and the main stream of Jhelum River at Mangla Dam (Fig. 3.1). The Mangla Basin was divided into 22 sub-basins. The observed precipitation and temperature data was used in the catchment area situated in Pakistan and TRMM rainfall data was used in the part of the catchment situated in India. The temperature data for the sub-basins in India was estimated by extrapolating the mean temperature of the available records by using the lapse rate. The extraction of physical parameters (river length, basin drainage area, slope, etc.) of the sub-basins and preparation of the conceptual model (Fig. 3.1) was performed by the integration of GDEM with ArcGIS and GeoHEC-HMS.

The physical descriptions of the watershed are accomplished through basin components in HEC-HMS. A basin component comprises loss, transfer and baseflow estimations through various methods to compute runoffs. In this investigation, deficit and constant, SCS unit hydrograph, lag time and constant monthly baseflow approaches were used as the loss, transfer, channel routing and baseflow methods, respectively.

Meteorological data was incorporated through the meteorological component of the model. The meteorological model includes the precipitation, evapotranspiration and snowmelt methods. HEC-HMS has two snowmelt approaches, (1) gridded temperature index and (2) temperature index, either of which can be chosen for the snowmelt modelling. The temperature index method was selected for estimation of the melt rate based on recent atmospheric and past snowpack conditions. The temperature index method has been used successfully by several researchers for snowmelt runoff computational analysis (Gyawali and Watkins 2012; Yilmaz et al. 2011). The gauge weight and constant monthly method were applied for precipitation and evapotranspiration, respectively.

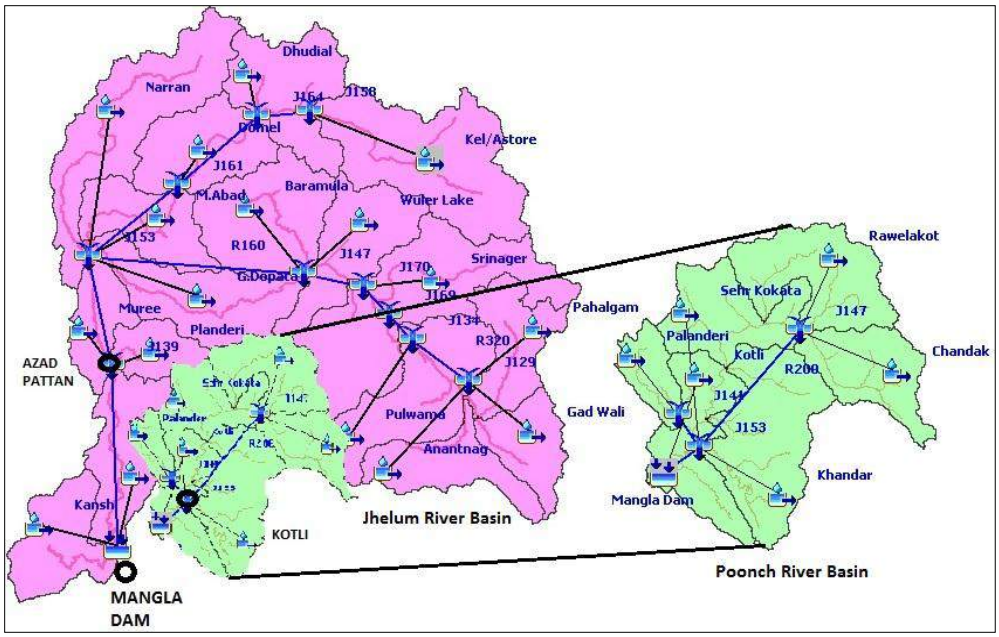

Fig. 3.1: Conceptual model of Mangla watershed prepared by using GeoHEC-HMS for flows simulation at Jhelum (Azad Pattan Station) and Poonch Rivers (Kotli Station).

There are in total 17 parameters in HEC-HMS. These parameters are constant rate, initial deficit, maximum deficit, lag time, standard lag time, impervious area, base temperature, px temperature, rain rate limit, wet melt rate, cold limit, melt rate coefficient, water capacity, cold rate coefficient, lapse rate, degree–day factor and ground melt. In HEC-HMS, px temperature is used to differentiate between precipitation falling as rain or snow. The parameters were computed by using calibration trials. In the temperature index, the degree–day factor and lapse rate are considered as the most important parameters for more efficient estimation of the snowmelt contribution. The lapse rate was calculated by using the available observed temperature data from different installed gauging stations within the Pakistani border, while for the ungauged basins (the Indian part of the basin) either the global lapse rate value was used or they were adopted from the gauged basins on the basis of similar elevation range. The sources of the

initial values and the ranges of some critical parameters of the HEC-HMS to be calibrated for streamflow simulation and the ranges of their input values are presented in Table 3.1.

Table 3.1: Range of parameter values for application of HEC-HMS in Mangla watershed.

Parameters	**Parameter Values Range in Jhelum and Poonch Basins**	**Source of Initial Values**
Initial deficit (mm)	10 to 25	HEC-HMS Trail Optimization
Maximum deficit (mm)	30 to 45	HEC-HMS Trail Optimization
Constant rate (mm/hr)	0.30 to 3.10	HEC-HMS Trail Optimization
Impervious (%)	0 to 26	HEC-HMS Trail Optimization
PX temperature (°C)	2.0 to 3.0	HEC-HMS help (constant for each sub-basin but varies over simulation time window)
Lag time (hrs)	5.82 to 23.73	Equation developed by US Soil Conservation Service for time of concentration (Wanielista et al. 1997)
Lapse rate (°C/100 m)	-0.65 to -0.010	By using observed temperature data (WAPDA)
Degree day factor (mm $°C^{-1}$ d^{-1})	4 to 5.7 for snow 5.7 to 7.4 for ice	Extract from previous studies conducted on Himalayan range (Dey et al. 1989; Immerzeel et al. 2010; Prasad and Roy 2005; Zhang et al. 2006).
Evapotranspiration (mm/month)	3 to 75 (from winter to summer)	By using Hamon method (Hamon 1963).

3.5.2 Model Calibration and Validation (HEC-HMS)

A. Over Single Year

The results obtained by the application of HEC-HMS input parameters (Table 3.2) in Mangla watershed over six individual hydrological years (2001 to 2003, 2007 to 2009) (annual, snowmelt, extreme discharges period) are presented in Table 3.3, for both the Poonch and Jhelum River catchments. The maximum spatial variation in the calibrated parameters was

perceived in the initial deficit, maximum deficit, constant rate, lag time, impervious area, lapse rate and evapotranspiration. The base temperature and px temperature were 0°C and 2.5°C, respectively. In general, the snowmelt contribution was found to be very nominal in Poonch Basin, so the flows were low and consistent over the winter months, but rapid fluctuation with overestimations was observed during the extreme events period (Fig. 3.2). On the other hand, the inflows are gradual in Jhelum Basin, which may be because of the large snowmelt contribution. Moreover, the flow simulation is not substantial over the winter months because of low flow during the snow accumulation period. Fig. 3.4 and 3.5 depicts the overestimation during snowmelt especially in the extreme events period. Some overestimations may be associated with the TRMM rainfall product which can affect the flow simulation over extreme events. So, water management is very closely associated with the discharge contribution over the peak flow months (spring and summer).

The best results were found over the calibration for year 2001 in Poonch Basin with RMSE and MAE values equalling 40 and 6.73, respectively, as expected. Meanwhile, the NS coefficient and Dv values were 0.85 and -3.42%, respectively. The correlation coefficient values were 0.88 and 0.69 for the Pearson and Kendall rank tests, which shows a good correlation between the simulated and observed daily flows.

Table 3.2: Values of parameters used for the simulation of single hydrological year (2001) time window in HEC-HMS application.

Sub-basin of HMS	Initial Deficit (mm)	Maxi Deficit (mm)	Constant Loss (mm/hr)	Imp (%)	Lag Time (hr)	Lapse Rate (deg. °C/100 m)	ET (mm/month) (Winter to Summer)
Chandak	18	34	1.15	12	22.53	-0.65	10 to 47
Khandar	18	36	1.85	0	18.07	-0.17	11 to 58
Kotli	22	38	1.55	0	17.40	-0.31	7 to 41
Rawelakot	14	39	0.65	3	21.53	-0.26	10 to 58
Sehr Kokata	25	30	0.85	0	16.00	-0.20	12 to 49
Naran	18	33	1.85	21	16.03	-0.58	3 to 46
Dudhnial	20	38	2.10	16	23.73	-0.46	8 to 44
Domel	14	37	0.70	9	19.05	-0.16	11 to 70
Astore/Kel	12	39	1.35	14	20.67	-0.43	6 to 41
Baramula	15	36	1.80	11	9.02	-0.65	12 to 60
M.Abad	10	34	1.00	6	19.70	-0.12	12 to 70
G.Dopata	13	38	2.30	17	8.92	-0.38	13 to 68
Srinagar	11	35	0.75	4	14.55	-0.49	8 to 48
Muree	19	35	0.90	11	14.73	-0.41	9 to 43
Palanderi	12	35	0.80	7	12.00	-0.01	11 to 54
Nawan	10	33	2.40	3	15.88	-0.14	5 to 63
Kanshi	23	45	0.75	7	8.00	-0.21	12 to 74
Wuler Lake	14	38	0.70	0	8.80	-0.65	10 to 47
Pulwama	15	30	0.85	6	9.57	-0.65	10 to 52
Anantnag	21	34	1.85	0	11.83	-0.41	10 to 52
Pahalgam	15	39	1.20	0	7.12	-0.65	8 to 46
Gad Wali	24	37	2.75	15	11.63	-0.65	8 to 46

DDF (mm $°C^{-1}$ d^{-1}) = 4.8; Base temperature = 0 °C; Px temperature = 2.5 °C

Imp (%) = Impervious area in percent.

Table 3.3: Application of HEC-HMS in Poonch and Jhelum River Basins over individual hydrological year, annual basis (Jan to Dec), snow melts period (April to August) and extreme flows period basis (June to August).

Hydrological Year (Jan-Dec)	Poonch Basin (Kotli Station)		Jhelum Basin (Azad Pattan Station)	
	Calibration Period (2001)	Validation Period (2002-2003, 2007-2009)	Calibration Period (2001)	Validation Period (2002-2003, 2007-2009)
RMSE	40	72	113	196
MAE	6.73	13.02	12	23.40
NS Coefficient	0.85	0.73	0.87	0.79
Dv (%)	-3.42	6.51	-5.17	-6.89
Pearson Correlation	0.88	0.78	0.91	0.81
Kendall Correlation	0.69	0.63	0.74	0.62
Snowmelt Period (April-August)				
RMSE	60.29	69	83	266
MAE	4.74	9.59	32	42.3
NS Coefficient	0.76	0.68	0.71	0.63
Dv (%)	-3.36	-4.31	-4.87	-11.46
Pearson Correlation	0.86	0.73	0.84	0.78
Kendall Correlation	0.62	0.47	0.66	0.63
Extreme Events Period (June-August)				
RMSE	75.95	82	91	252
MAE	5.10	8.32	53	59.93
NS Coefficient	0.57	0.51	0.49	0.53
Dv (%)	4.15	-5.88	-9.29	-12.16
Pearson Correlation	0.76	0.65	0.74	0.68
Kendall Correlation	0.52	0.47	0.59	0.58

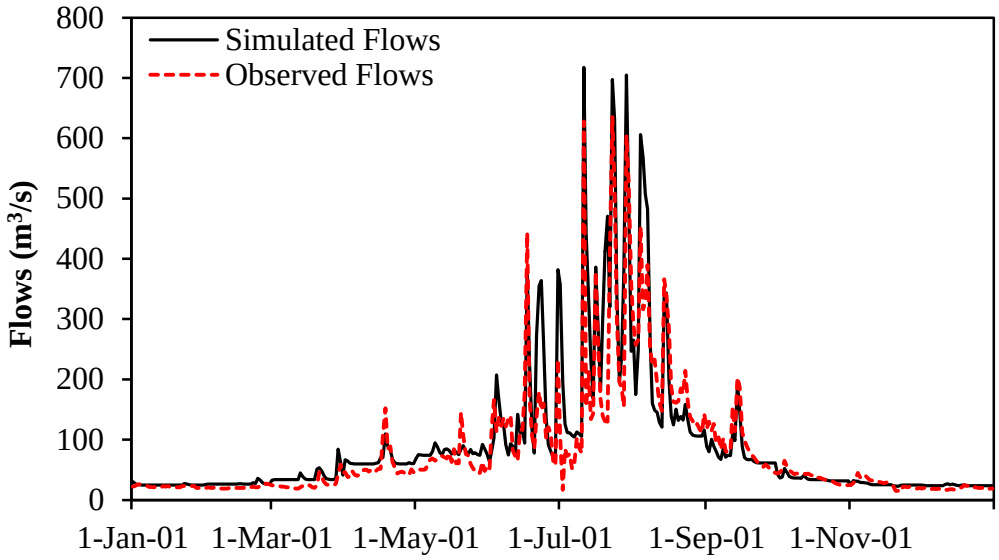

Fig 3.2: HEC-HMS generated graphical presentation of simulated and observed hydrographs of Poonch River flows at Kotli station for single year simulation run over the hydrological year 2001.

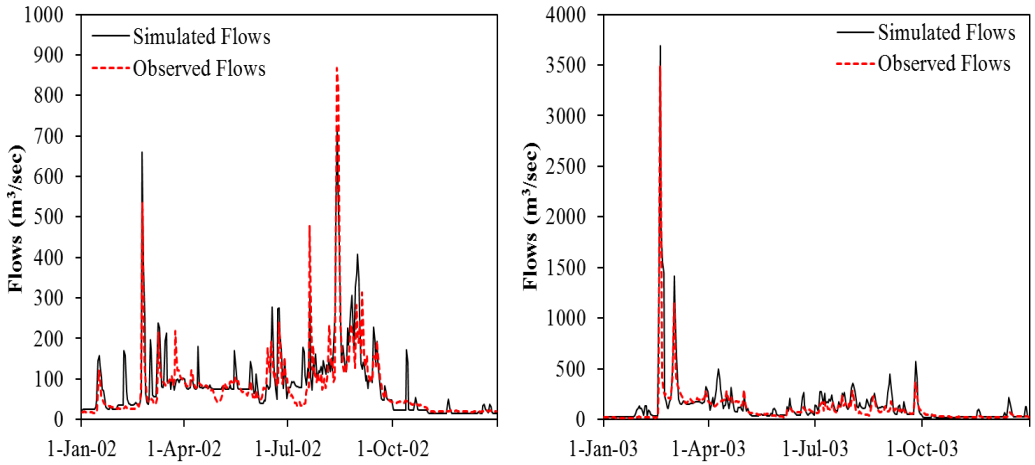

Fig 3.3: Simulated and observed hydrographs of Poonch River flows at Kotli station over single year validation run for 2002 and 2003.

Similarly, in Jhelum Basin the RMSE and MAE values were 113 and 12, respectively, over the calibration period (2001), in which the best model performance was found with correlation coefficients equal to 0.91 and 0.74 for the Pearson and Kendall rank tests, respectively. The NS coefficient was

0.87 and there was a -5.17% difference in volume. The average value of the performance descriptors (NS coefficient and Dv (%)) were computed for entire validation datasets over the single year simulation. The values show the poor model efficiency during the validation compared to the calibration period in both catchments.

The efficiency of the whole data series was clearly affected by snowmelt and the extreme events period, where flows were not modelled as efficiently as for the complete hydrological year, but over the snowmelt period the model performed well compared to the extreme events period. The NS and RMSE values were never less than 0.63 and greater than 266 during entire the snowmelt period analysis, respectively, but the lowest NS coefficient was found to be equal to 0.49 over the extreme events period (Table 3.3). Overall, the efficiency was found to be within an acceptable range, and the model was found to be more efficient in Jhelum (at Azad Pattan) compared to Poonch Basin. This may be associated with the fact that streamflows at Azad Pattan vary gradually due to snowmelt runoff, in contrast to Poonch Basin, where several rapid peaks occur, as presented in Fig. 3.3, which shows that some rapid peaks occurred in 2002 and 2003 (validation windows) at Kotli station.

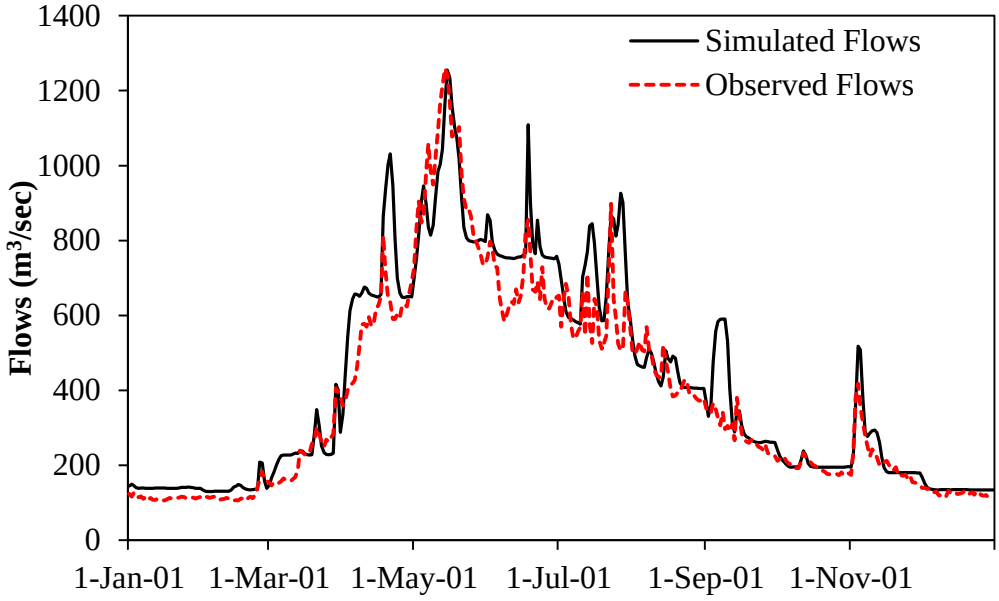

Fig 3.4: HEC-HMS generated graphical presentation of simulated and observed hydrographs of Jhelum River flows at Azad Pattan station for single year simulation run over the hydrological year 2001.

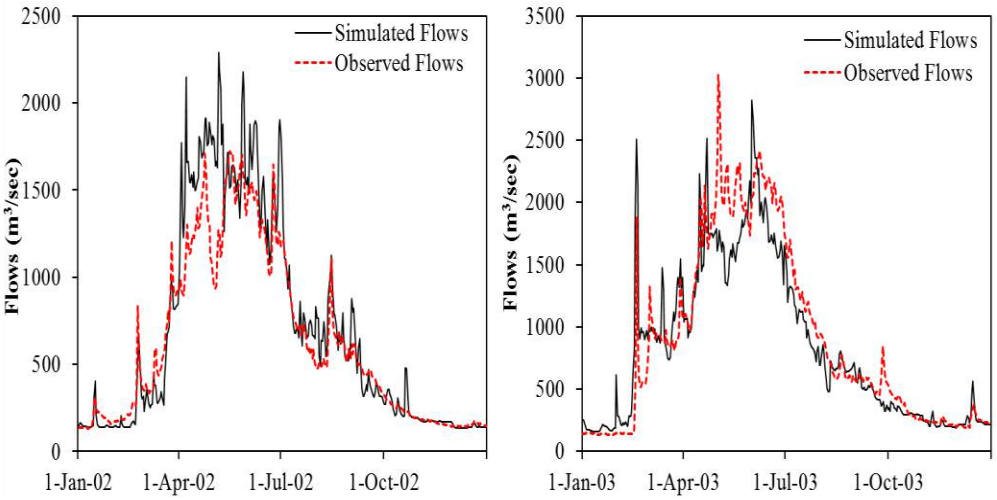

Fig 3.5: Simulated and observed hydrographs of Jhelum River flows at Azad Pattan station over single year validation run for 2002 and 2003.

B. Over Three Years

The results obtained using calibrated parameters (Table 3.4) in HEC-HMS in Mangla watershed for three-year continuous simulations over the annual (January–December), snowmelt (April–August) and extreme flow (June–August) periods are given in Table 3.5, for both the Poonch (at Kotli station) and Jhelum River (at Azad Pattan station) catchments. Similarly to the single year simulation, spatial variation was found in the parameters used for rainfall-runoff simulation, e.g. initial deficit, maximum deficit, constant loss, impervious and lag time, etc. Temporal variation between the single and three-year simulation was also observed. Furthermore, in HEC-HMS, the snowmelt model parameters required for the temperature index method are the same for all sub-basins in the meteorologic model, e.g. wet melt rate (4.8 mm/°C-day), rain rate limit (0.6 mm/day), ATI cold rate coefficient (0.5) and water capacity (5%), while the base and px temperatures were set to 0 and 3°C, respectively.

Table 3.4: Parametric values used for simulation by the application of HEC-HMS in Mangla Basin over 2001–2003.

Sub-basin of HMS	Initial Deficit (mm)	Maxi Deficit (mm)	Constant Loss (mm/hr)	Imp (%)	Lag Time (hrs)	Lapse Rate (deg. °C/100 m)	DDF (mm $°C^{-1}$ d^{-1})	ET (mm/month) Range (Winter to Summer)
Chandak	15	34	1.70	7	5.82	-0.65	5.2	10 to 47
Khandar	18	36	1.85	0	8.23	-0.15	5.2	11 to 58
Kotli	22	38	1.10	6	8.47	-0.26	5.2	7 to 41
Rawelakot	14	39	2.10	0	11.20	-0.28	5.2	10 to 58
Sehr-Kokata	20	30	1.85	0	6.37	-0.23	5.2	12 to 49
Naran	22	33	0.95	12	19.10	-0.62	5.2	3 to 46
Dudhnial	12	38	1.30	0	15.42	-0.38	5.2	8 to 44
Domel	14	37	2.45	0	17.00	-0.16	5.2	11 to 70
Astore/Kel	12	39	0.55	3	20.83	-0.38	5.2	6 to 41
Baramula	15	36	0.80	0	13.67	-0.65	5.2	12 to 60
M.Abad	10	34	1.50	21	12.50	-0.16	5.2	12 to 70
G.Dopata	13	38	3.10	16	17.52	-0.31	5.2	13 to 68
Srinagar	11	35	1.00	14	20.67	-0.65	5.2	8 to 48
Muree	19	35	2.70	11	7.63	-0.46	5.2	9 to 43
Palandri	12	35	3.15	15	10.75	-0.11	5.2	11 to 54
Nawan	10	33	0.65	17	8.17	-0.12	5.2	5 to 63
Kanshi	23	45	1.16	3	10.50	-0.16	5.2	12 to 74
Wuler Lake	14	38	1.10	9	17.92	-0.65	5.2	10 to 47
Pulwama	15	30	0.50	6	18.77	-0.65	5.2	10 to 52
Anantnag	10	34	0.90	4	14.27	-0.46	5.2	10 to 52
Pahalgam	15	39	0.75	11	15.58	-0.65	5.2	8 to 46
Gad Wali	14	37	0.50	7	12.55	-0.65	5.2	8 to 46

Imp (%): Impervious area of watershed in percentage (%).

The computed RMSE, MAE, NS coefficient and Dv (%) for the continuous simulation (Table 3.5) show that the simulations agree reasonably well with the observed flows. Figs 3.6, 3.8 and Table 3.5 depict the ability of HEC-HMS to reproduce both rainfall and snowmelt generated flows. The simulation results in Jhelum Basin are slightly better than in Poonch Basin over the annual, snowmelt and extreme events periods. The model performed less efficiently over the snowmelt and extreme events periods. The simulation for the validation of Poonch Basin produced the lowest NS coefficients of 0.59 and 0.44 for the snowmelt and extreme events periods, respectively. The correlation coefficient values were never less than 0.61 and 0.42 for the Pearson and Kendall rank correlation coefficients, respectively. Figs 3.6 and 3.7 depict the model's ability to reproduce such fluctuations accurately. Moreover, the simulation results show that the model is capable of capturing the seasonal characteristics of streamflow adequately.

In Jhelum Basin, snowmelt is a major runoff contribution source, but runoff from some of the sub-basins still depends on the rainfall. Since the snowmelt is a gradual process, rapid flow fluctuations in Jhelum Basin are typically due to the overlapping of rainfall-runoff with snowmelt runoff (Figs 3.8 and 3.9). In general, the water management is largely associated with the flows in the summer season because of the high inflows and large fluctuations, which need to be reproduced more precisely by the model. In contrast, the simulation and water management over the winter months is not optimal because of the low flows during the snow accumulation period.

In general, the large fluctuations in flow magnitudes were properly simulated by HEC-HMS in both basins, but the model performed slightly better in the Jhelum Basin compared to the Poonch Basin because of the large fluctuations due to the rainfall-generated runoff. Furthermore, the single year

results were slightly better than the three-year simulation, with the lowest NS and Dv (%) values of 0.49 and 4.15 over the extreme events, respectively.

Table 3.5: Evaluation of HEC-HMS application at Kotli (Poonch River Basin), Azad Pattan (Jhelum River Basin) and Mangla Dam station over a three hydrological year time step, on the basis of annual (Jan. to Dec.), snowmelt (April to August) and extreme flow (June to August) periods.

Annual (Jan-Dec)	**Poonch Basin**		**Jhelum Basin**		**WRA at Mangla Dam (2001-03 and 2007-09)**
	Calibration (2001-2003)	**Validation (2007-2009)**	**Calibration(2001-2003)**	**Validation (2007-2009)**	
RMSE (m^3/s)	72.48	91.04	162	198	302
MAE (m^3/s)	14.84	17.85	20.15	49	113
NS Coefficient	0.77	0.71	0.80	0.73	0.71
Dv (%)	5.36	24.91	-3.61	13.64	-21.05
Pearson Correlation	0.79	0.78	0.85	0.81	0.80
Kendall Correlation	0.69	0.65	0.70	0.69	0.65
Snowmelt Period (April-August)					
RMSE (m^3/s)	84.17	68.74	204	268	399
MAE (m^3/s)	8.60	41.47	13.0	181	126
NS Coefficient	0.62	0.59	0.70	0.61	0.51
Dv (%)	7.10	26.30	-3.19	14.51	-20.12
Pearson Correlation	0.67	0.67	0.81	0.77	0.54
Kendall Correlation	0.47	0.43	0.61	0.59	0.42
Extreme Events Period (June-August)					
RMSE (m^3/s)	101.4	71.08	211	189	374
MAE (m^3/s)	4.58	35.77	6.0	113	192
NS Coefficient	0.59	0.44	0.64	0.65	0.47
Dv (%)	-8.40	22.02	6.61	10.22	-17
Pearson Correlation	0.65	0.61	0.72	0.68	0.63
Kendall Correlation	0.42	0.42	0.53	0.49	0.50

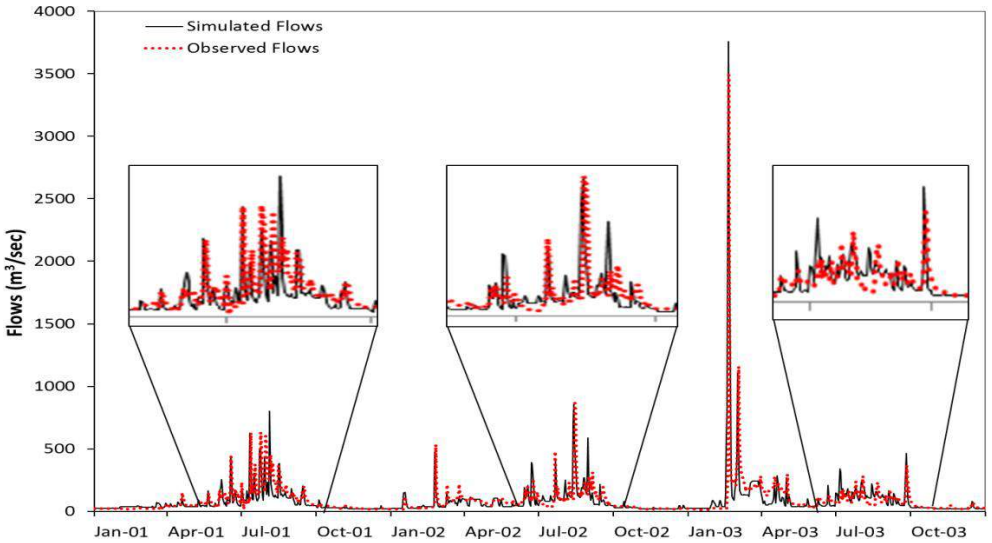

Fig. 3.6: Simulated and observed hydrographs of Poonch River flows at Kotli station over the three-year (2001–2003) calibration run.

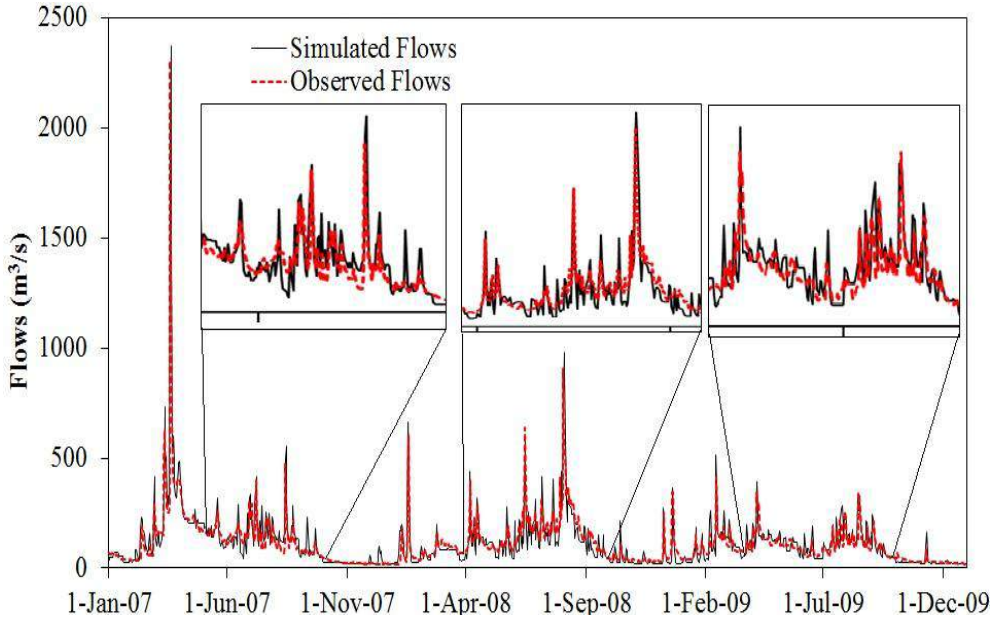

Fig. 3.7: Simulated and observed hydrographs of Poonch River flows at Kotli station over the three-year (2007–2009) validation run.

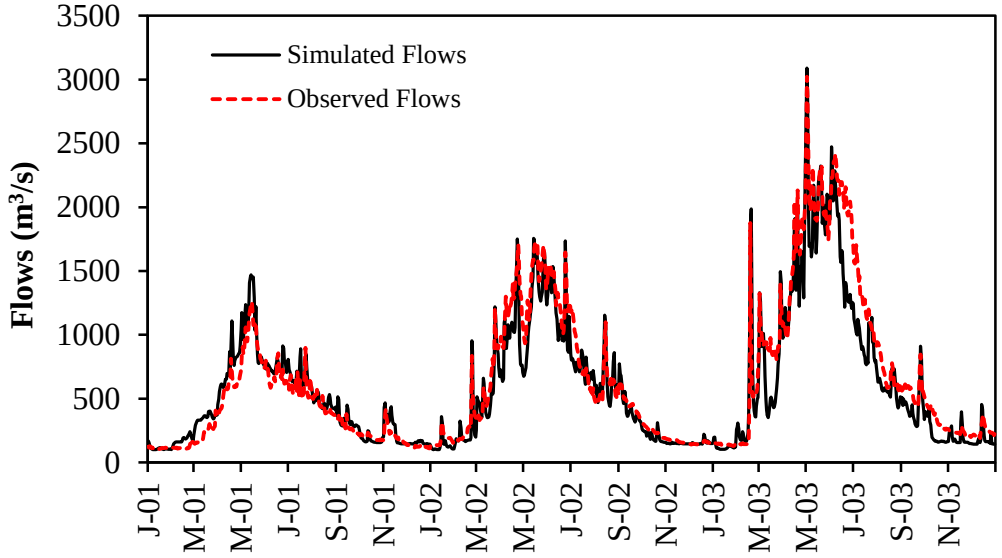

Fig. 3.8: Simulated and observed hydrographs of the Jhelum River flows at the Azad Pattan station over the three-year (2001–2003) calibration run.

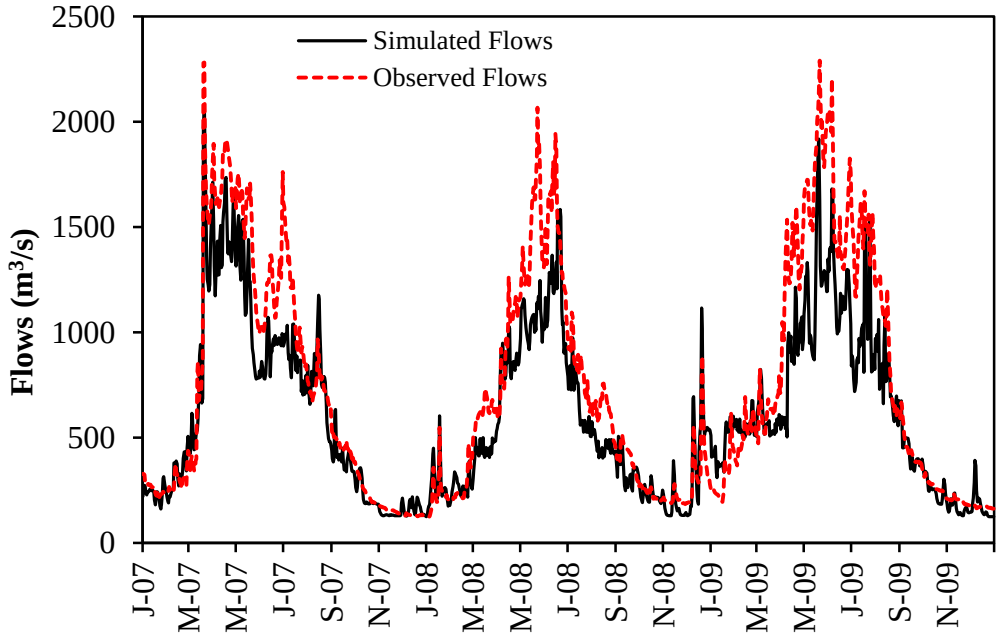

Fig. 3.8: Simulated and observed hydrographs of the Jhelum River flows at the Azad Pattan station over the three-year (2007–2009) validation run.

3.5.3 Application of Snowmelt Runoff Model

The SRM has been applied and tested by several researchers and institutions, with regard to runoff simulation, e.g. Bookhagen and Burbank (2010); Immerzeel et al. (2009); Tahir et al. (2011); WMO (1986). It is based on the degree–day method in which the daily air temperature, precipitation and snow cover area are used as input data. In addition, different physical characteristics of the basin such as the zone area (in zone-wise application), basin area and the hypsometric (area–elevation) curve are also required as input data. The daily streamflows generated from the snowmelt and rainfall are superimposed on the calculated recession flow and transformed into daily discharge from the catchment.

There are in total 10 parameters including the snow cover area, the runoff coefficient C, where Cs refers to snowmelt and Cr refers to rain, a, the degree–day factor, DDF (cm $°C^{-1}$ d^{-1}), T, the number of degree–days (°C d), S, the ratio of the snow covered area (SCA) to the total area, n, the sequence of days, P, the precipitation contributing to runoff, A, the area of the basin or zone, and the recession coefficient k (Xc and Yc). The snowmelt runoff model (SRM) is an SCA-based model which is discussed in detail by Tahir et al. (2011). The Mangla Basin was divided into five altitude zones at 1000 m intervals. The average temperature and precipitation of stations within the each zone of the Mangla watershed were estimated, and the percentage of the daily snow cover area was used as an input variable. The lapse rate was estimated by using daily observed temperature data in each zone. The daily zonal snow cover area was estimated by linear interpolation for each zone from 8-day composite MOD10A2 satellite images (Fig. 3.10). The TRMM rainfall data was used for the sub-basins situated in the Indian part of the basin. The SRM daily streamflow simulation is strongly affected by the percentage of snow cover and less by precipitation (Tahir et al. 2011). The

initial value of the degree day factor (DDF) was extracted from previous studies, e.g. Dey et al. (1989); Zhang et al. (2006) for the Himalayan region. The DDF value in previous studies was 5.7 to 7.4 mm $°C^{-1}$ day^{-1} for ice and 4 to 5 mm $°C^{-1}$ day^{-1} for snow. A zone with elevation higher than 5000 m was considered to be glacier-covered (equal to only 1%) and below 5000 m was considered as snow, as discussed by Tahir et al. (2011). The range of values for most critical parameters is given in Table 3.6.

Table 3.6: Range of SRM calibrated parametric values for flow simulation.

Parameters	**Range of Values (from zones 1 to 5)**
Temperature lapse rate ɣ (°C/100 m)	-0.010 to -0.65
Critical temperature (T_{crit} , °C)	1.0 to 2.0
Degree–day factor (DDF), (mm $°C^{-1}$ day^{-1})	4.2 to 5.5 (winter to summer)
Lag time, *L* (hr)	6 to 21
Runoff coefficient of snow (C_s)	0 to 0.45
Runoff coefficient of rainfall (C_r)	0 to 0.20
Rainfall contribution area (RCA)	0 to 1.0
Recession coefficient (X_c), *k*	0.80 to 1.06
Recession coefficient (Y_c), *k*	0.15 to 0.30

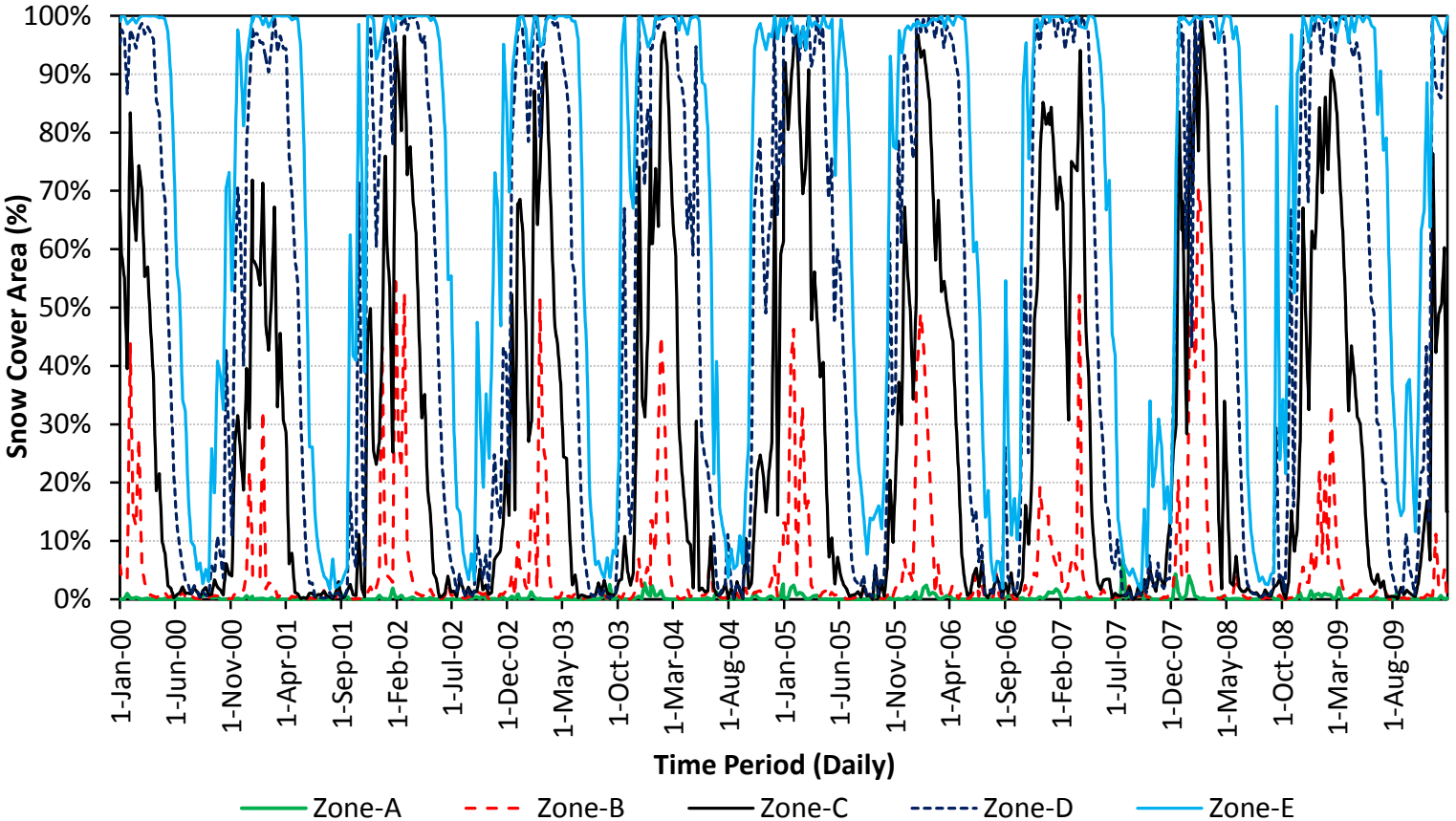

Fig. 3.10: Daily snow cover area (SCA) distribution in five elevation zones (A-E) of Mangla watershed (Jhelum River Basin). Snow cover area is estimated from the remotely sensed MODIS (MOD10A2) snow cover data.

3.5.4 Comparison of SRM with HEC-HMS

The results obtained using calibrated parameters of the SRM (Table 3.7) in Mangla watershed for five years through continuous simulations over the annual (January–December) and snowmelt periods (April–August), are given in Table 3.8. The maximum spatial variation was found in the initial deficit, maximum deficit, constant loss, impervious area, lag time, lapse rate and evapotranspiration in the HEC-HMS application. However, in SRM the maximum spatial variation was found in the lapse rate, degree–day factor, recession coefficients (X_c and Y_c) and runoff coefficients for snow (C_s) and rainfall (C_r). The way the parameters are calibrated in the two models is very different. The SRM provides flexibility to the user to calibrate parameters both spatially and temporally, but in HEC-HMS the spatial change can be performed in parameters (initial deficit, maximum deficit, constant rate, etc.) used for the rainfall-runoff simulation. The calibrated parameters of HEC-HMS are presented in Table 3.4. Furthermore, the SRM parameters were calibrated on a seasonal (winter and summer) and zonal basis (Table 3.7). Different values of DDF were set for snow and ice, as presented in Table 3.7.

Table 3.7: SRM parametric values of zone-wise application in Jhelum River Basin.

Parameters	**Zonal Parametric values (Zones 1 to 5)**				
	1 (< 1000)	**2 (1000-2000)**	**3 (2000-3000)**	**4 (3000-4000)**	**5 (> 4000)**
Lapse rate γ (°C/100 m)	-0.19	-0.32	-0.48	-0.58	-0.65
T_{crit} (°C)	0	0	0	0	0
DDF (mm $°C^{-1}$ day^{-1})	4.0	4.5	5.5	5.5	6.0
Lag time, *L* (hr)	9	12	15	18	21
C_s	0	April-Aug=0.25 Sep-May=0.20	April-Aug=0.35 Sep-May=0.30	April-Aug=0.40 Sep-May=0.35	April-Aug=0.55 Sep-May=0.40
C_r	April-Aug=0.55 Sep-May=0.45	April-Aug=0.50 Sep-May=0.40	April-Aug=0.40 Sep-May=0.30	April-Aug=0.30 Sep-May=0.25	0
RCA	1	1	1	April-Aug=1 Sep-May=0	April-Aug=1 Sep-May=0
X_c	April-Aug=0.80 Sep-May=1.06	April-Aug=0.80 Sep-May=1.06	April-Aug=0.80 Sep-May=1.06	April-Aug=0.80 Sep-May=1.06	April-Aug=0.80 Sep-May=1.06
Y_c	0.03	0.03	0.025	0.02	0.015
June-August	Period of snow, glacier melt and monsoon rainfall				
September-May	Snow accumulation and dry period for most of the sub-basins				
Zone 4 and 5	Almost 100% snow cover during winter months				
Zone 3	Partially snow-covered				
Cs and Cr	Zone 1 and 2 have a small snowmelt runoff contribution and Zones 4 and 5 have a small rainfall runoff contribution				
RCA	Rainfall contribution is very small in zones 4 and 5 because rainfall occurs in solid form during winter				

The results obtained by the application of HEC-HMS and SRM for Jhelum River at Mangla Dam for three-year (2001-2003) simulation over the annual and snowmelt periods are presented in Table 3.8. The results suggest that both models simulated the daily streamflows during the annual (Jan–Dec) and snowmelt periods (April–Aug) efficiently in the Mangla watershed. Simulation efficiency is more closely associated with the snowmelt months due to the rapid peaks and high inflows at Mangla Dam. The best efficiency was observed over three-year simulation, with NS coefficients of 0.75 and 0.73 by the application of HEC-HMS and SRM, respectively. Similarly, the difference in volume was 10.4% for HEC-HMS and 8.82% for the SRM model. The simulation efficiency was found to be slightly less over the snowmelt period than over the complete time series, but still significantly within the acceptable range. Overall, the HEC-HMS simulation results were found to be better than SRM over the annual and snowmelt periods.

Table 3.8: Evaluation of HEC-HMS and SRM application in Mangla Basin (Jhelum River) during the single and three-year hydrological simulation over the complete simulation period, snowmelt period and extreme flows period.

Hydrological Year (Jan-Dec)	**Calibration (2001-2003)**	
	HEC-HMS	**SRM**
NS Coefficient	0.75	0.73
Dv (%)	10.4	8.82
Pearson Correlation Coefficient	0.89	0.91
Kendall Rank Correlation Coefficient	0.79	0.77
Snowmelt Period (April-August)		
NS Coefficient	0.62	0.59
Dv (%)	12.4	1.74
Pearson Correlation	0.74	0.70
Kendall Rank Correlation	0.59	0.62

However, according to the results in Table 3.8, both models were found to be less efficient over the snowmelt months compared to the whole simulation run, particularly the SRM model. This may be due to the occurrence of rapid flow fluctuations because of rainfall during the snowmelt months, especially in July and August. Both models seem to be unable to capture such rapid variations accurately.

Fig. 3.11 depicts the high peak discharges that occurred during the winter months (September to March). The SRM was unable to capture rapid peaks of rainfall-runoff; a poor efficiency was found over rapid fluctuations of peak flows; for example, during February 2003 a peak of more than 4500 m^3/sec was not captured by the SRM. In the case of the HEC-HMS simulation, the model captured some peak flows better than SRM. Overall, the efficiency was reduced due to the peak events simulation in both models, but the HEC-HMS daily flows simulation over snowmelt events was slightly more efficient than SRM, which may be associated with the SRM integration, where the snow cover dynamics and snowmelt runoff were overlapped by the rainfall-runoff peaks, as discussed earlier.

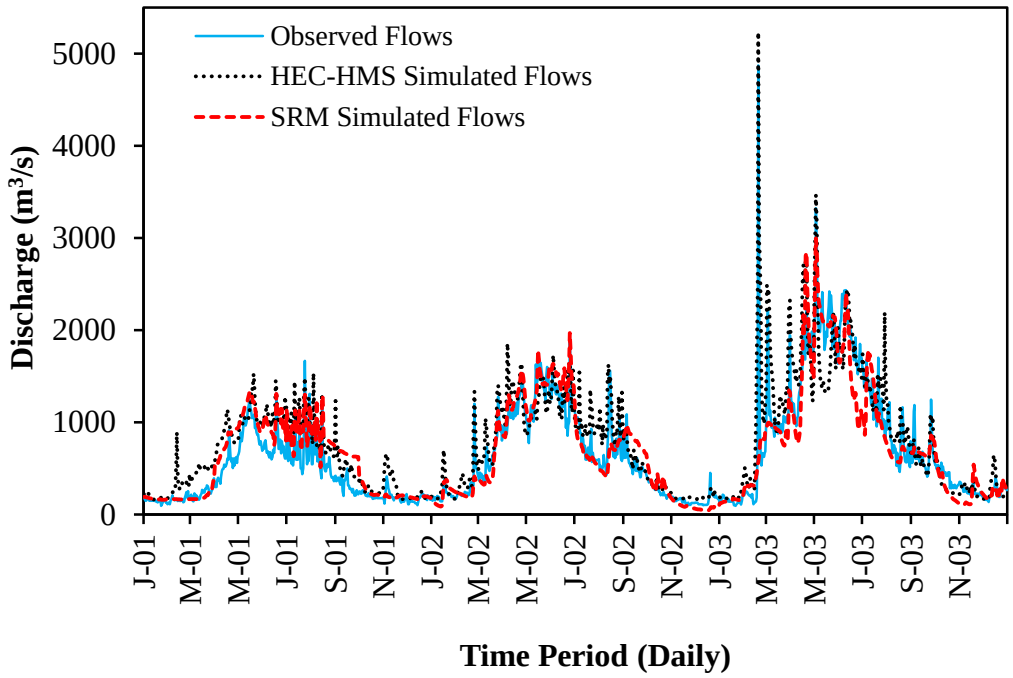

Fig. 3.11: Evaluation of SRM application over the three years 2001–2003 in the Mangla Basin (Jhelum River).

The scatter plot between the simulated and observed inflows was drawn to check the reaction during the peak flows period. The simulated flows were found to have been underestimated by the application of SRM and during the winter peaks (Fig. 3.12). Similarly, the scatter plot of HEC-HMS shows overestimations in contrast to the SRM simulation during the winter peaks (Fig. 3.13).

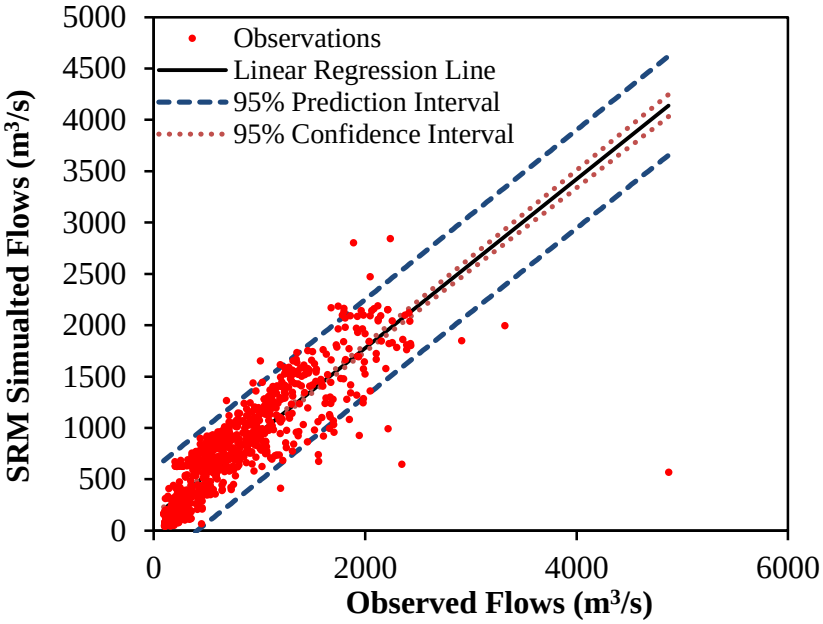

Fig. 3.12: Comparison of SRM modelled and observed flows over three-year (2001–2003) simulation period in Mangla Basin.

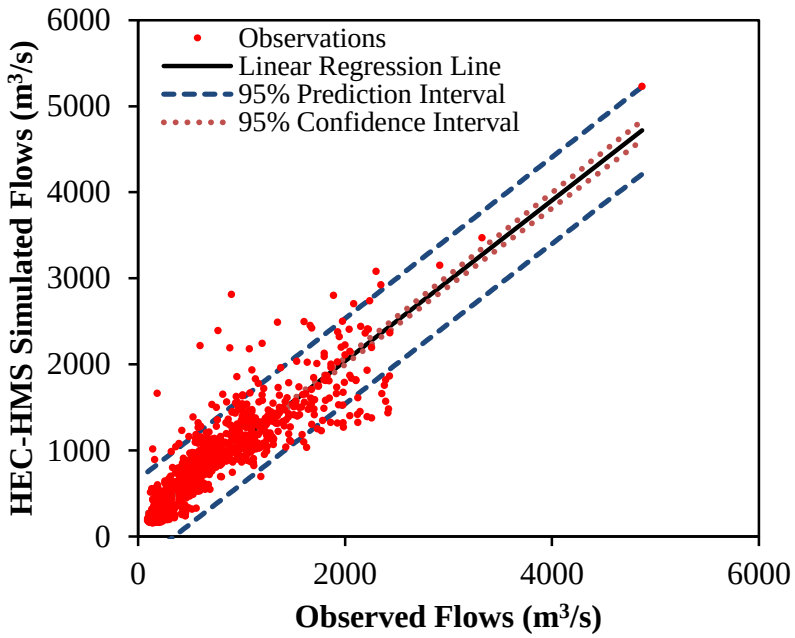

Fig. 3.13: Comparison of HEC-HMS modelled and observed flows over three-year (2001–2003) simulation period in Mangla Basin.

Overall, the results suggested that HEC-HMS performed slightly better than SRM, which may be due to the fact that SRM was developed specifically for snowmelt runoff modelling, and was therefore unable to capture the high rainfall-runoff peaks during the winter months. This may be associated with the fact that the SRM largely depends upon the snow cover dynamics of the study area less on rainfall. Since, the SRM was designed to simulate the daily discharges in high-altitude glacierized regions by considering the well-known precipitation deficit and the scarce measurement errors for high elevation areas. Consequently, the SRM uses the snow-covered area whenever needed to compute the runoff input, thereby compensating for the deficiency of precipitation data measurement. The slight discrepancies between the results obtained by several studies may be due to the different study areas in which SRM was applied; e.g. Tahir et al. (2011) applied basin-wide SRM with APHRODITE satellite rainfall data in the Hunza River Basin (mean elevation 4631 m) and found the NS coefficient and difference in volume (Dv) to be equal to 0.90 and -2.6%, while Immerzeel et al. (2009) applied SRM in a Himalayan river basin along with TRMM rainfall data (approximate mean elevation 5000 m) finding an NS coefficient of 0.78, but the catchment area was 200,677 km^2. On the other hand, HEC-HMS was developed especially for rainfall-runoff simulation and it provides the user with flexibility in the application of temperature and rainfall data on sub-basin scale, which helps the model to categorize rainfall in the form of solid or liquid. In general, the results suggest that both models could be a good choice for the simulation of daily flows in Mangla Basin (Jhelum River). Although SRM simulated the snowmelt contribution slightly better than HEC-HMS, HEC-HMS could be a more feasible choice specifically for the Mangla Basin, as HEC-HMS is a standard rainfall-runoff model. This particular basin is only partially influenced by seasonal snow cover and the

major part of the basin is influenced by the monsoon rainfall-runoff; HEC-HMS can pick up such peak discharges better than SRM, which is normally considered more sensitive for the design of a hydraulic structure.

3.6 Calibration of HEC-HMS over Different Time Windows

The calibration of HEC-HMS was carried out over different time windows. The model was calibrated over single years from 2001 to 2003 and 2007 to 2009 (a total of six time windows), three-year periods from 2001–2003 and 2007–2009 (two time windows) and a six-year period (one time window). This calibration was carried out with the objective of optimizing the parameters for the simulation of climate change impact studies. The results of calibration over all the time windows are illustrated in Table 3.9 given below.

3.6.1 Single Year

Single-year calibrations were carried out over six individual years for the optimization of model parameters in order to analyse spatial and temporal variation in the parametric values of the six calibration windows. There was a remarkable difference in the model efficiency and parametric values between the calibration and validation time windows, as expected. The average NS coefficient value was 0.73 over the validation, which was improved upon by the calibration into 0.84 at Azad Pattan, which shows a significant difference (Table 3.3 and 3.9). Although the difference between the calibration and validation windows was significantly high, very slight differences were observed among each calibration. Furthermore, the average NS coefficient value was 0.71 for the validation run, which changed into 0.80 after the calibration, at Kotli station. Fig. 3.14 shows that the validation results were less efficient because of rapid variations, and the calibrated flows are more consistent, which improves the efficiency at Azad Pattan.

Meanwhile, at Kotli station no remarkable change was found in the calibration and validation runs. Just a slight change is observed and the calibration results were slightly better than the validation, as expected. The simulation efficiency during the snowmelt and extreme events periods was significantly lower than the complete data series. The lowest NS coefficient and highest Dv (%) value were found to be 0.47 and -10.54 respectively at Kotli station during the extreme event months.

Mainly, the rapid variation in streamflow leads to the difference between the calibration and validation over the same time period at Azad Pattan station, even though this station receives a major proportion of runoff from snowmelt (Fig. 3.14). A rapid change in streamflows was observed during validation but this variation was found to be much lower in the calibration, which may be because the parameters were optimized using only the single calibration window of 2001. The rainfall and snowmelt runoff was much lower during 2001 than during later time windows. Furthermore, the rapid variation may also be due to the overlapping of snowmelt runoff with rainfall runoff. Similarly, the rapid variations at Kotli station are the major cause of the low model efficiency even over the calibration window. Moreover, a slight difference is observed between the calibration and validation runs at Kotli station, which may be because this basin is rainfall-dominated and the model is poor at reproducing all the rapid variations generated by rainfall.

The parametric values over the temporal and spatial scale were considerably different. Mainly, the parameters regarding rainfall runoff, e.g. constant loss (mm/hr), impervious area (%), lag time (hr), vary considerably over the calibration window with respect to each other. Furthermore, the HEC_HMS calibrate single value for the parameters used to model snowmelt runoff, e.g. degree–day factor (DDF), base temperature, px temperature, wet melt rate,

rain rate limit, melt rate coefficient, cold rate coefficient, cold limit, water capacity and ground melt. The values of the aforementioned parameters have already been discussed in the previous section. A very slight variation was observed in these parameters during all the single-year calibrations. The lapse rate is also an important parameter which affects the simulation critically, as confirmed by Singh (1991), who stated that a 1°C/km change in the lapse rate can vary the results from 28–37%. As discussed in the previous section, the lapse rate was computed using the observed gauge data for each calibration time window. The variation in lapse rate over different calibration windows depends upon change in temperature during those calibration time windows. The temperature variation from 2001 to 2009 was observed to be very low and therefore the change in lapse rate was also very low. Furthermore, a significant change in constant loss was perceived over all the calibration windows compared to 2001. The negative change (value) describes the increase in the constant loss rate value compared to 2001. The most remarkable change is observed in the Naran, Domel and Astore sub-basins. This may be associated with the fact that these sub-basins received lower precipitation during 2001 than in all the other calibrated years and this low rainfall led to low streamflows. A slightly lesser variation was observed in constant loss when comparing the calibration over 2002 with other calibration windows and amongst each other. Meanwhile, over the other years (2003, 2007, 2008 and 2009) the variations were not so significant between each other, as presented in the Appendix A. Furthermore, the percentage of impervious area significantly varies in the Astore, Kanshi, Srinagar and Anantnag sub-basins, while in some sub-basins a very slight change was found. A remarkable point observed was that the spatial and temporal change in the impervious area of the Poonch River sub-basins was zero, except for Kotli.

Table 3.9: Average values of precision standards for the calibration of HEC-HMS at Kotli (Poonch River Basin) and Azad Pattan (Jhelum River Basin) stations over single-, three- and six-year continuous time steps, on the basis of annual (Jan to Dec), snowmelt (April to August) and extreme flow (June to August) periods.

Annual (Jan-Dec)	**Single-Year Calibration**		**Three-Year Calibration**		**Six-Year Calibration**	
	Azad Pattan	**Kotli**	**Azad Pattan**	**Kotli**	**Azad Pattan**	**Kotli**
RMSE (m^3/s)	121.50	41.38	171.5	70.74	234.81	81.52
MAE (m^3/s)	51.20	7.21	25.5	20.42	45.49	29.38
NS Coefficient	0.84	0.80	0.81	0.78	0.75	0.70
Dv (%)	-7.13	-4.35	-3.61	5.64	-18.29	-10.23
Pearson Correlation	0.94	0.88	0.865	0.84	0.81	0.76
Kendall Correlation	0.83	0.70	0.72	0.725	0.73	0.62
Snowmelt Period (April to August)						
RMSE (m^3/s)	174.83	65.21	209	78.085	259	99.61
MAE (m^3/s)	33.50	7.93	15	9.8	63	15.84
NS Coefficient	0.63	0.59	0.615	0.585	0.57	0.48
Dv (%)	-9.58	-2.60	-4.71	11.22	-9.82	13.41
Pearson Correlation	0.88	0.74	0.84	0.69	0.74	0.65
Kendall Correlation	0.75	0.58	0.68	0.53	0.59	0.54
Extreme Events Period (June to August)						
RMSE (m^3/s)	206.83	74.82	217	82.7	353	84.41
MAE (m^3/s)	41.67	-6.83	10	7.79	106	21.32
NS Coefficient	0.52	0.47	0.56	0.49	0.49	0.41
Dv (%)	-9.02	-10.54	7.68	-15.57	-14.37	10.92
Pearson Correlation	0.69	0.72	0.735	0.715	0.71	0.68
Kendall Correlation	0.54	0.51	0.51	0.505	0.54	0.48

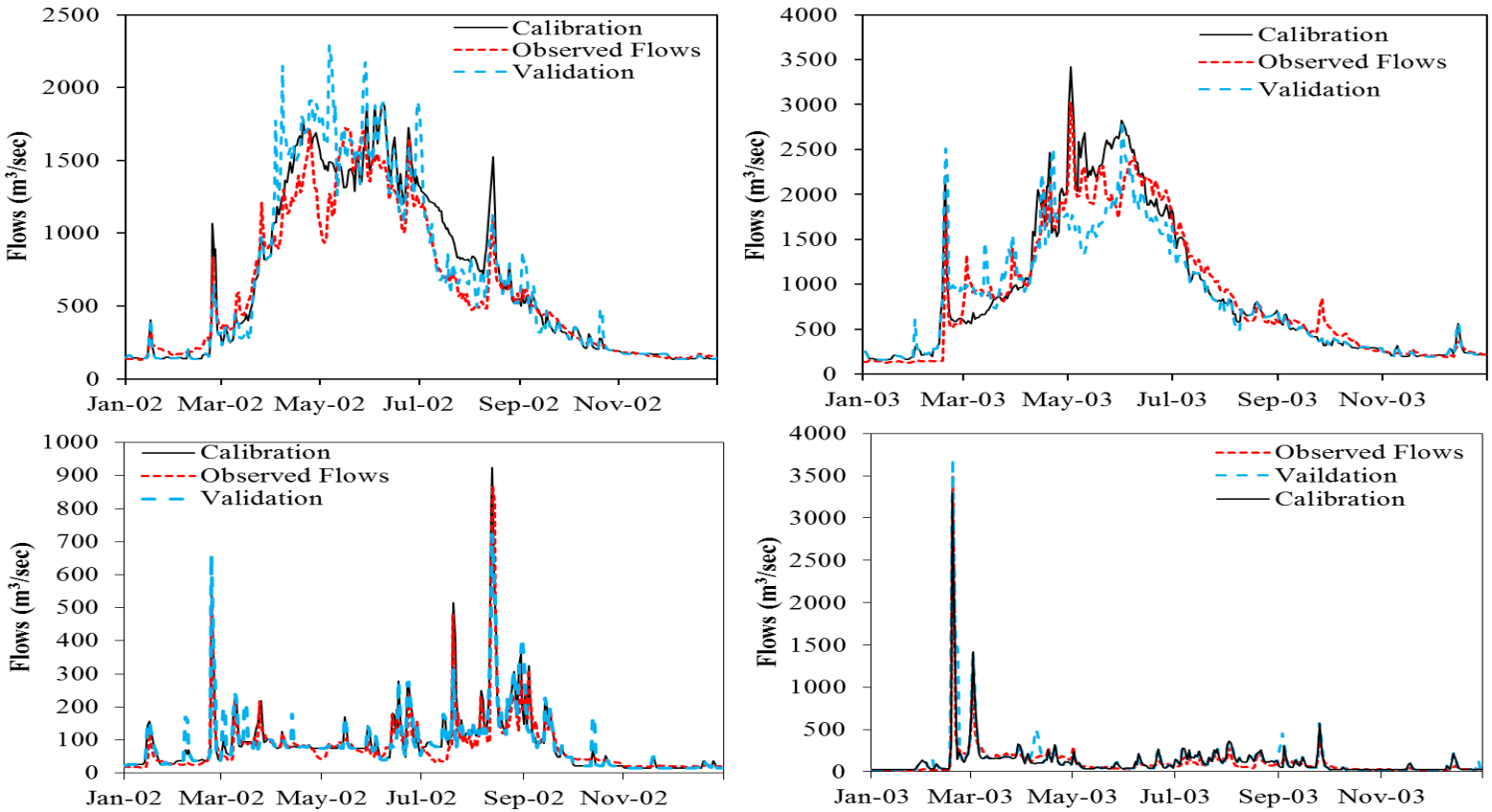

Fig. 3.14: Comparison between calibrated and validated hydrographs for single years of 2002 and 2003 at Azad Pattan (upper) and Kotli stations (lower).

The variation in the impervious area between the calibration windows of 2003, 2007, 2008 and 2009 was not significant compared to 2001 and 2002. This may be due to the similar behaviour of the climatology and streamflow trend over the aforementioned years and because it is quite easy for the model to reproduce similar flow behaviour, especially in catchments having a snowmelt contribution. In contrast to the constant loss and impervious area, the lag time decreased over all five years with respect to 2001. A significant positive change was found which may be due to heavy rainfall occurring after 2003 compared to 2001 and 2002. Because the HEC-HMS is a rainfall-runoff model, the rainfall trend has a large effect on the parametric values of the model related to snowmelt runoff. Similar to the other parameters, the alteration in values with respect to each other for the calibration onward from 2003 was very low. Moreover, the parameters used over 2001 for snowmelt runoff also varied significantly with respect to other calibration windows. The greater concern is with the DDF value, which increased from 4.8 to 5.0 and then 5.3 mm $°C^{-1}$ d^{-1} for 2001, 2002 and then onwards for 2003 to 2009, respectively. The base and px temperatures shifted from 0 to 1°C and from 2.5 to 3°C, respectively. The detail of the parametric values is presented in the Appendix A.

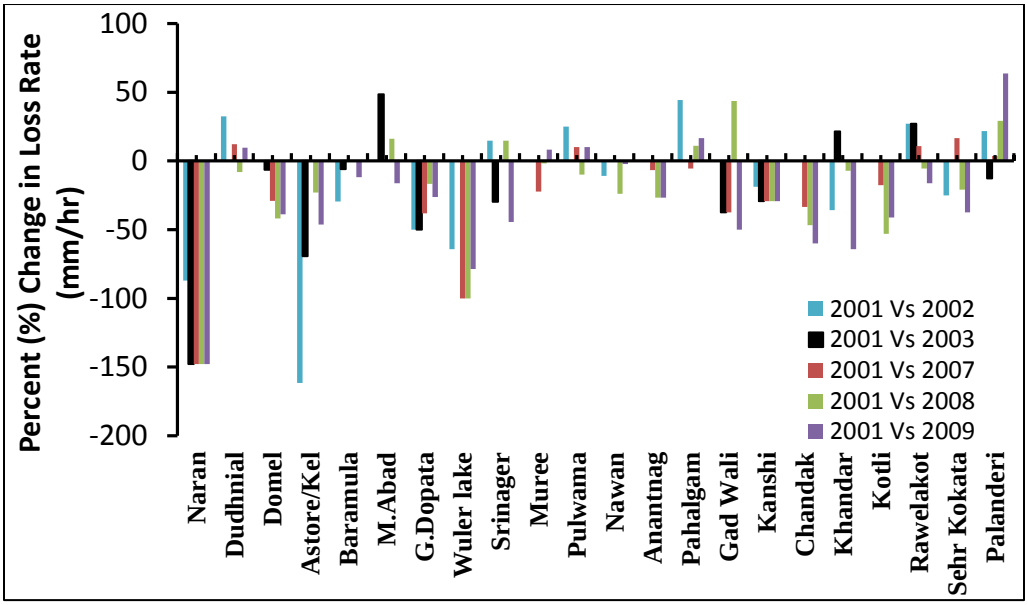

Fig. 3.15: Percent (%) spatial and temporal change in constant loss (mm/hr) in Mangla catchment over single-year calibration (a negative change describes an increase in value).

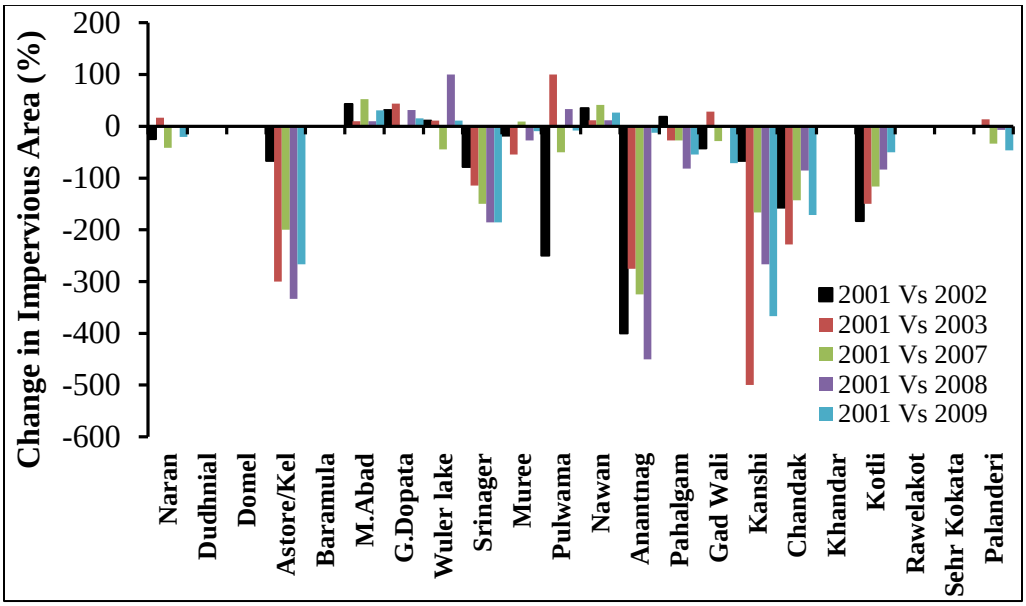

Fig. 3.16: Percent (%) spatial and temporal change in impervious area in Mangla catchment over single-year calibration (a negative change describes an increase in value).

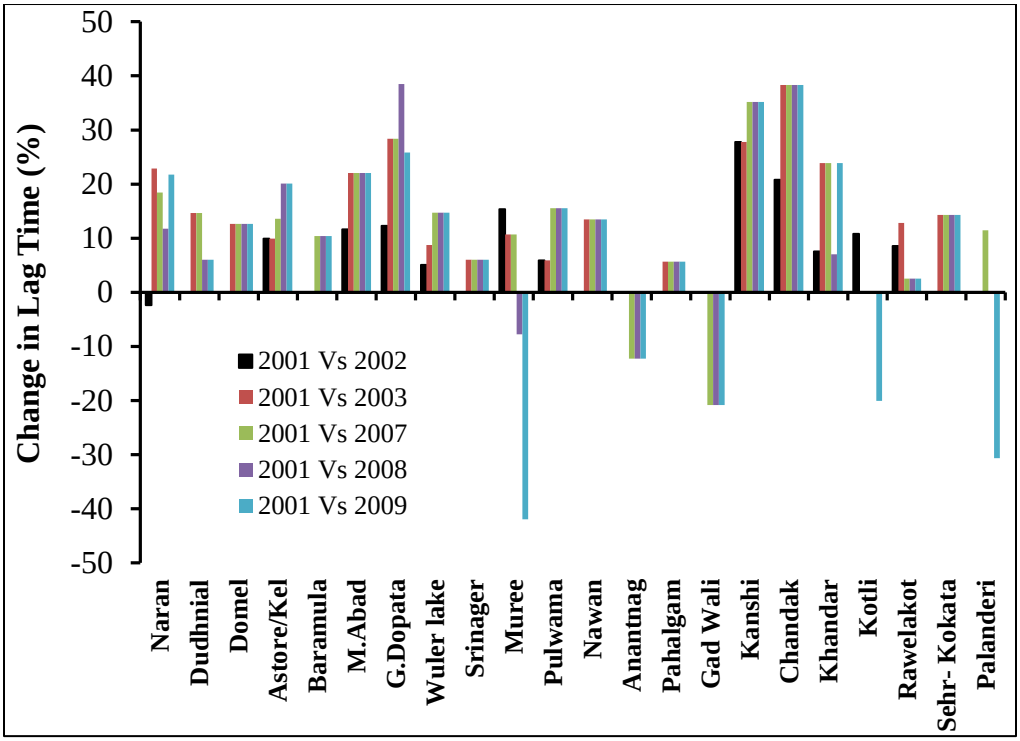

Fig. 3.17: Percent (%) spatial and temporal change in lag time (hr) in Mangla catchment over single-year calibration (a negative change describes an increase in value).

3.6.2 Three Year

The calibration results are significantly improved compared to the validation (discussed in section 3.5.2). After calibration, the average NS coefficient value was improved to 0.81 from 0.73 over 2007–2009. Some underestimation was found during the validation run, but by the calibration of the same time window, the simulation is improved at Azad Pattan station. The underestimations may be due to the low streamflows during the calibration over 2001–2003 compared to later years (2007–2009) due to the low contribution of snowmelt runoff. The optimized values over the calibration of 2001–2003, in particular the degree–day factor (DDF) and some other snowmelt parameters were lower, which could be the reason for the underestimation over the validation, as presented in Fig. 3.18. The

optimized parameters also varied significantly over the three-year calibration. At Kotli station only a very slight change was observed between the calibration and validation of the same window and the optimized parameters as well. Similar to the previous analysis, the efficiency of the simulated streamflows was considerably lower than the complete data series, with the lowest NS coefficient and highest Dv (%) values being 0.49 and -15.47, respectively, at Kotli station during the extreme event months. Furthermore, the change in parameters was not substantial, like the single-year calibration. The calibrated parameters over 2001–2003 differed slightly compared to 2007–2009. A remarkable change, approximately -300%, was observed at Nawan sub-basin. During the 2007–2009 calibration, a significant increment was observed in constant loss for most of the sub-basins, compared to 2001–2003. In the impervious area, overall a slight change was observed, but in Astore sub-basin a significant decrease of approximately -300% occurred. In contrast to the impervious area, a significant decrease (up to 30%) in lag time was observed during the calibration of 2007–2009 (Fig. 3.22). Since there was no considerable change between the calibration and validation results in Poonch Basin, the change in parameters was also minimal. The DDF also increased from 5.2 to 5.3 mm $°C^{-1}$ d^{-1}, which is a slight but very effective change for the improvement of the calibration results. The px and base temperature were unchanged.

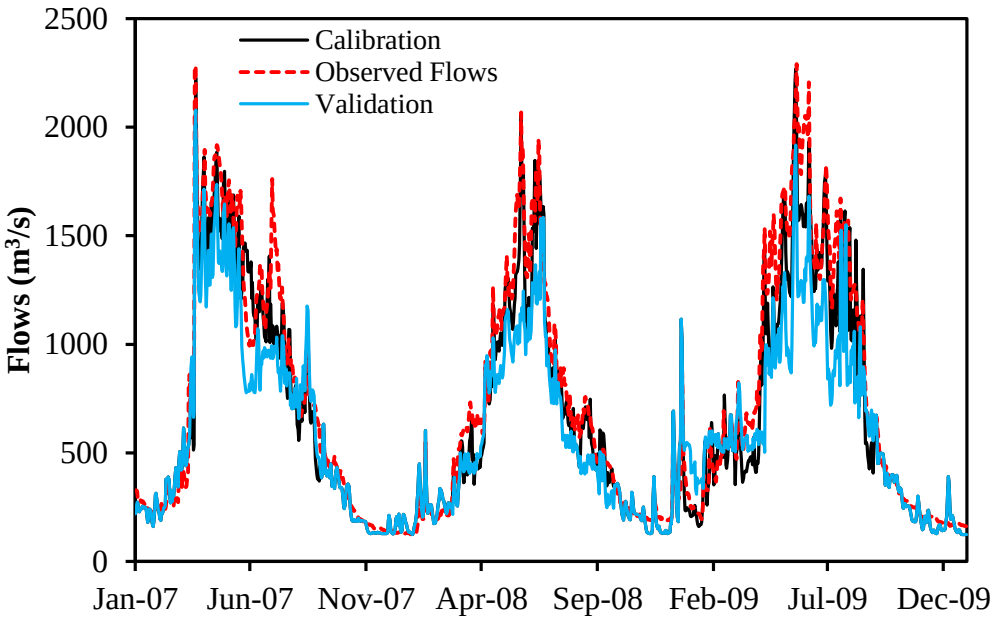

Fig. 3.18: Comparison between calibrated and validated hydrographs for three-year time window of 2007–2009 at Azad Pattan**.**

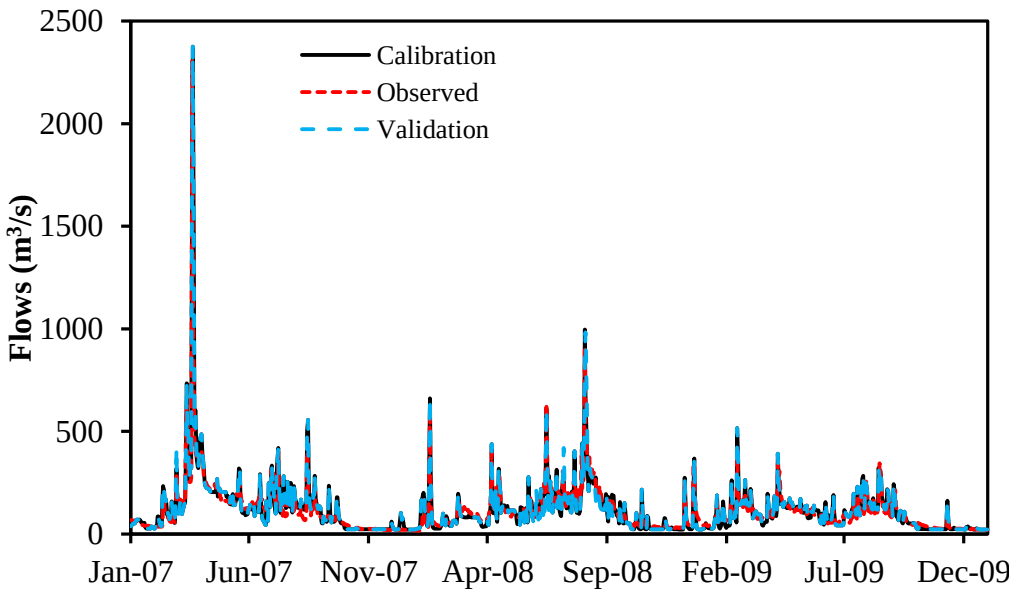

Fig. 3.19: Comparison between calibrated and validated hydrographs for three-year time window of 2007–2009 at Kotli station**.**

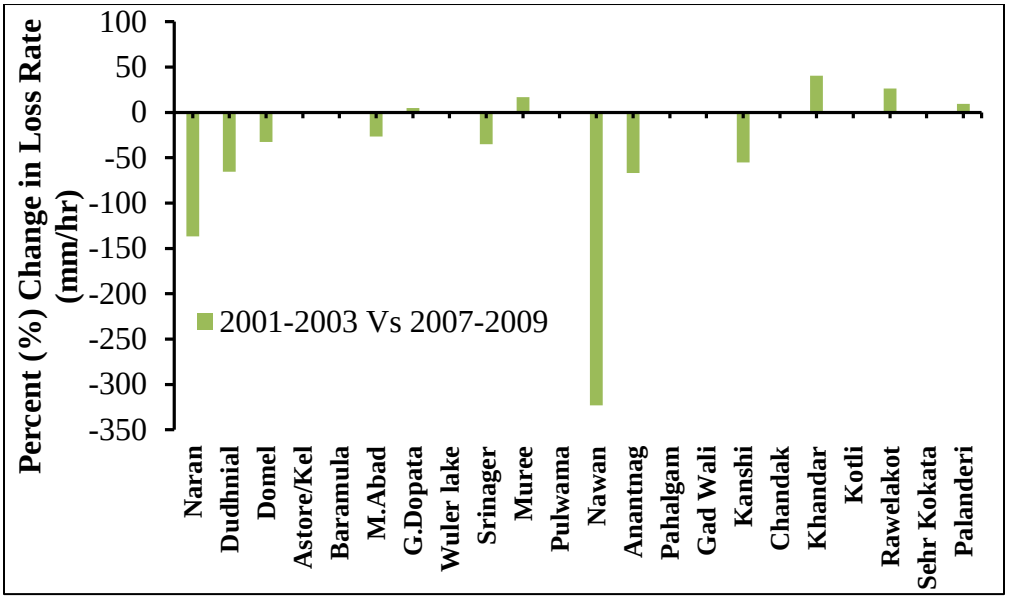

Fig. 3.20: Percent (%) spatial and temporal change in constant loss (mm/hr) in Mangla catchment over three-year calibration (a negative change describes an increase in value).

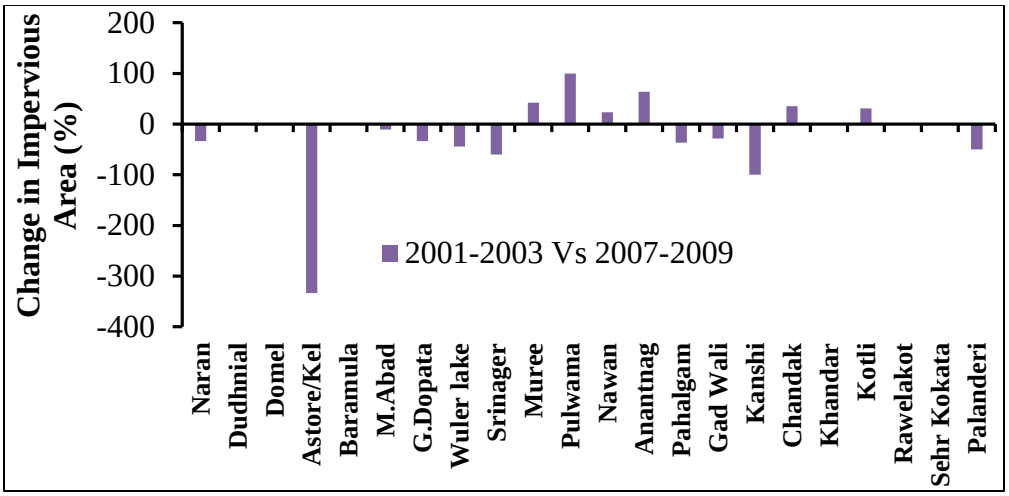

Fig. 3.21: Percent (%) spatial and temporal change in impervious area in Mangla catchment over three-year calibration (a negative change describes an increase in value).

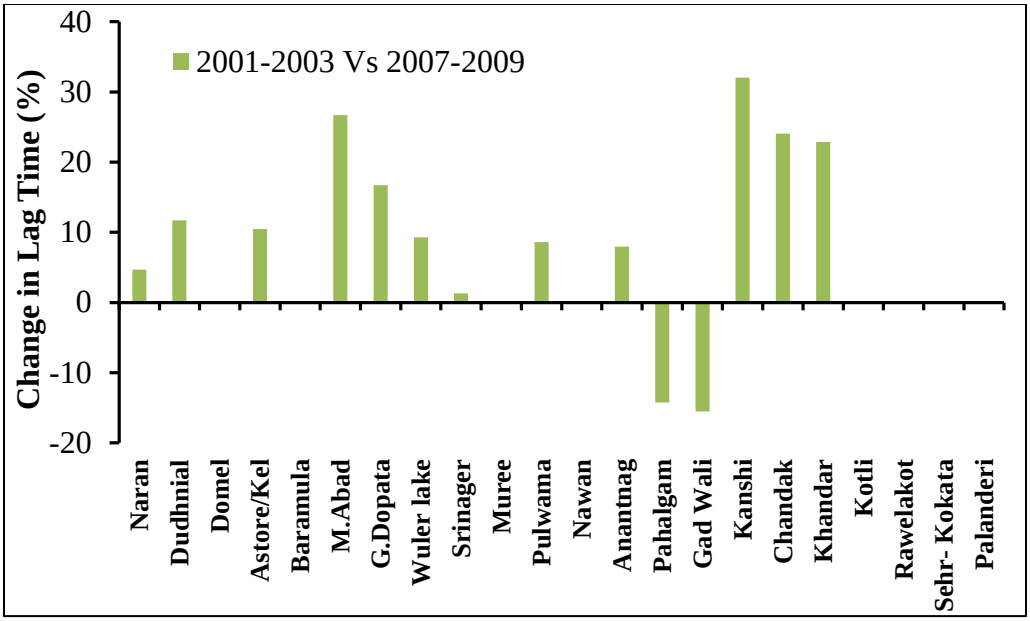

Fig. 3.22: Percent (%) spatial and temporal change in lag time (hr) in Mangla catchment over three-year calibration (a negative change describes an increase in value).

3.6.3 Six Year

The calibration results of six continuous years are given in Table 3.9 at Azad Pattan and Kotli stations. The NS coefficient values are 0.75 and 0.70 at Azad Pattan and Kotli stations, respectively. A strong correlation was found between the calibrated and observed streamflows, with 0.81 and 0.73 coefficient values for the Pearson and Kendall correlation tests at Azad Pattan. The six-year calibration was very similar to the three-year simulation at Kotli station, as presented in the Appendix A. A very slight change occurred between the average NS values of the calibrated parameters for the three- (2001-2003 and 2007-2009) and six-year time windows. Overall, the simulation efficiency of the model for Kotli station is less than for Azad Pattan, which demonstrates that the model reproduces poorly the rapid variations generated by rainfall-runoff (Fig. 3.23). Kotli station receives more rainfall-generated runoff and a very small contribution from snowmelt,

whereas Azad Pattan station receives a significant proportion of the snowmelt runoff from the Himalayan and Pir Panjal ranges. The figure showing the Poonch Basin calibration based on the six-year calibration at Kotli station is presented in the Appendix A.

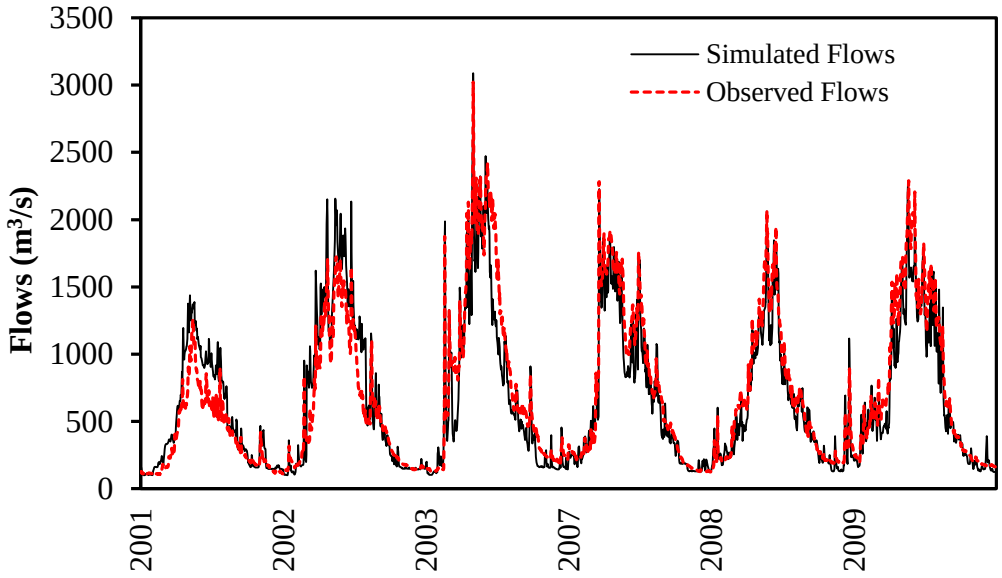

Fig. 3.23: Comparison between calibrated and validated hydrographs for six years from 2001–2003 and 2007–2009 at Azad Pattan station**.**

3.7 Water Resources Availability at Mangla Reservoir

The water resources availability at Mangla Dam was estimated by the application of HEC-HMS, which was found to be slightly more efficient than SRM in the Mangla catchment, as discussed in the previous section.

The daily inflows at Mangla Dam were computed by accumulating simulated flows of the Jhelum and Poonch Basins at Mangla Dam. The model was also run at the points where both rivers (the main streams of the Jhelum River and Poonch River) fall into Mangla Dam, then both simulated flows were accumulated for the estimation of water availability at Mangla Dam and compared with observed streamflows. The model efficiency was slightly

lower in this case (Table 3.5). The NS coefficient and Dv (%) values were found to be 0.71 and -21 at the mouth of Mangla Dam. A significant correlation of 0.80 and 0.65 was found for the Pearson and Kendall rank tests, respectively. The simulated and observed flows at Mangla Dam are also compared in Fig. 3.24. Several large rapid fluctuations were found, due to overlapping of the rainfall-runoff and snowmelt, during the snowmelt and extreme events periods. These fluctuations may be due to rapid inflows occurring in the rainfall-runoff dominated sub-basins (Kanshi and Poonch Basins), and the accumulation of both inflows at Mangla Dam enhanced such fluctuations. Overestimation may also be due to the influence of the monsoon rainfall pattern and snowmelt contribution, as reported by several researchers (Archer and Fowler 2008; De Scally 1994), since the southern and eastern tributaries of the Mangla Basin are significantly affected by monsoon rainfall. A scatter plot was drawn to analyse the reaction of both inflows (observed and simulated) at Mangla Dam (Fig. 3.25).

The average annual observed and simulated inflows (during 2001–2003 and 2007–2009) were found to be 731 and 830 m^3/s, respectively. The results obtained suggest that HEC-HMS is a proper tool to estimate water resource availability on a daily temporal scale in Mangla watershed. The scatter plot between the observed and simulated inflows at Mangla Dam indicates that satisfactory model efficiency was found over the complete simulation and snowmelt periods, while during extreme events the simulation was slightly less efficient (Fig. 3.25). It can be seen easily that discharge greater than 1500 m^3/s is clearly over- or underestimated by the model.

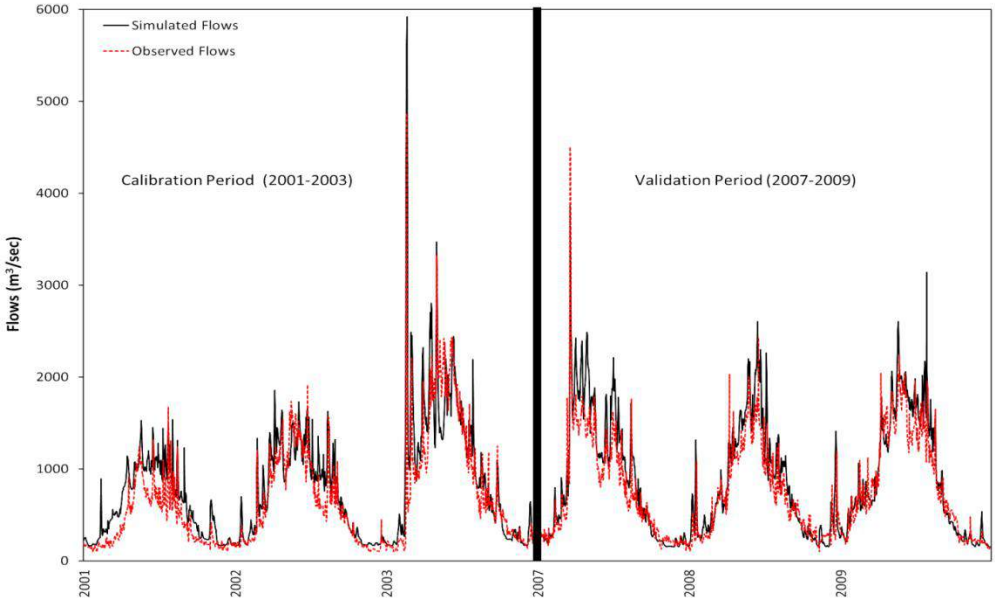

Fig. 3.24: Graphical representation of the simulated and observed hydrographs at Mangla Dam during 2001–2003 and 2007–2009 for estimation of the water resources availability (WRA)

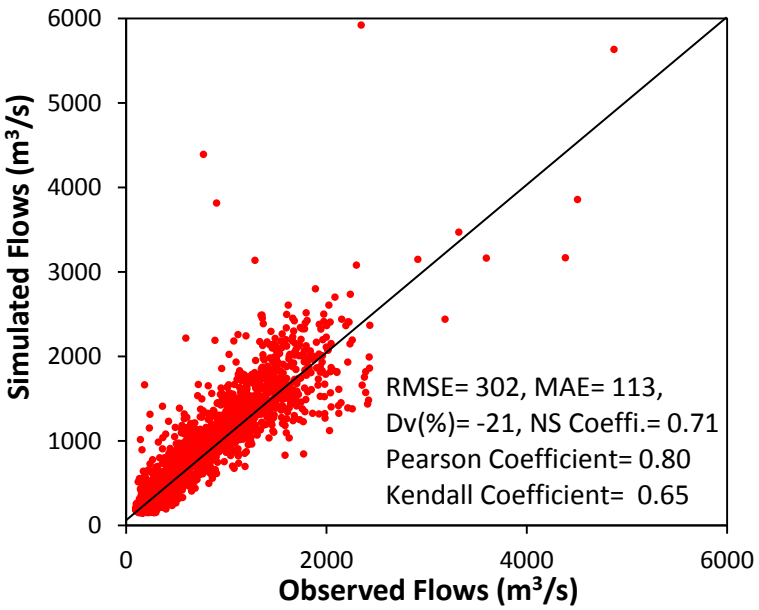

Fig. 3.25: Relationship between daily observed and simulated runoff applying HEC-HMS during 2001– 2003 and 2007–2009.

3.8 Conclusions

This investigation concluded that the HEC-HMS, a standard rainfall-runoff model, can simulate daily streamflow efficiently in high-altitude scarcely gauged catchments of the Jhelum River (Mangla Basin). Despite being a standard rainfall-runoff model, it is a good tool for the seasonal snow-covered watersheds. Rainfall data are the most important input for precise simulation, specifically in scarcely gauged catchments. Therefore, the 0.25×0.25 gridded TRMM rainfall products (3B42) can be successfully integrated with the HEC-HMS in the Himalayan range catchments, where hydrometeorological data are scarce or unavailable. It is also concluded that while the HEC-HMS is a rainfall-runoff model, its efficiency is rather low for the simulation of rapid flow variations, like other watershed models. In contrast, it performs more conveniently over catchments where the streamflow varies gradually.

Furthermore, this investigation concludes that the snowmelt runoff model (SRM) and HEC-HMS based on the temperature index method can efficiently simulate the daily discharges in snow-fed transboundary catchments. The efficiency of both models is based on their input data and the characteristics of the catchment. However, the SRM's efficiency depends on the use of MOD10A2 remotely sensed cryosphere data as input to model the snowmelt runoff, and its efficiency will be high in catchments where snowmelt is a major source of inflows. Therefore, this model is not likely to be affected by the well-known rainfall measurement deficit errors in mountainous regions, where a considerable part of the runoff is in the form of snowmelt. Similarly, as the HEC-HMS is a rainfall-based runoff model, rainfall data is the most important factor for precise simulation. However, both models showed very similar performance for the Mangla Basin. The SRM performed poorly at capturing rainfall runoff over the winter period

compared with HEC-HMS. The SRM allows some flexibility to change the parameters over the temporal scale, i.e. calibrated parametric values can be changed for the winter and summer months and even for individual days, whereas the HEC-HMS user can change some parameters over the spatial scale (along the sub-basins). Moreover, the TRMM satellite rainfall and MODIS snow cover data products were found to be a feasible choice for the ungauged sub-catchments in transboundary high elevation catchments such as the Jhelum River Basin.

A considerable temporal and spatial variation in parameters over the calibration of each time window is observed. Obviously, this change occurs because of the change in datasets over the temporal and spatial scale. This catchment is mainly influenced by monsoon rainfall, so the major change occurs in parameters related to the rainfall-runoff contribution. A slight change is also observed in the snowmelt model parameters, but only for the sub-basins of the Jhelum River catchment at Azad Pattan station. Due to this change in parameters, the efficiency of the model also significantly increased by comparison with the validation.

These results have allowed us to simulate the water availability at Mangla Dam for the planning and management of water resources. Moreover, this model can be applied for further daily flows simulation in neighbouring catchments of the Indus River. This model can also be applied under different scenarios for future predictions, as will be presented in the next chapter.

Chapter 4

Climate Change Analysis and its Impact on Sustainability of Water Resources at Mangla Dam

Foreword: This chapter is included with application of Global Circulation Models (GCMs) to downscale climate variables (precipitation and temperature) and subsequently used hydrological models to compute water resources availability under climate change at the end of this century in Mangla Basin. In order to downscale climate variables two downscaling techniques are used namely Statistical Downscaling Model (SDSM) and smooth support vector machine (SSVM). From the aforementioned techniques, a comparison is made to choose best downscaling results for examining future climate change impact by using hydrological model HEC-HMS, as illustrated in section 4.3 to 4.7. Additionally, SRM is used to exploit the impact of climate change by developing some future scenarios based on change in temperature and SCA in study basin at the end of this century, as presented in section 4.8.

4.1 Brief Introduction and Background

The global temperature is expected to be increased by 1.5 to 4.5 °C, with a 'best estimate' of 2.0°C due to the doubling of CO_2 in next century (IPCC 2007). The global circulation models (GCMs) are the primary source for the estimation of the expected future climate variations due to increase in the concentration of greenhouse gases in the atmosphere (Busuioc et al. 2001; Dibike and Coulibaly 2005). The GCMs spatial resolution is too coarse to compute the impact of climate change on a regional scale, and it is essential

to convert it into a suitable resolution to inform local meteorological analysis. The methods used for the extraction of regional scale climate variables from GCM outputs are known as downscaling techniques. Generally, downscaling techniques can be categorized into four, including regression (empirical) methods (Enke and Spekat 1997; Faucher et al. 1999; Li and Sailor 2001; Raje and Mujumdar 2011; Wilby et al. 2002), weather pattern approaches (Anandhi et al. 2011; Bardossy and Plate 1992; Bárdossy et al. 2002; Wetterhall et al. 2009; Yarnal et al. 2001), stochastic weather generators (Bates et al. 1998; Semenov and Barrow 1997), a regression-based empirical approach (Raje and Mujumdar 2011), and regional climate models (Mearns et al. 2003).

Compared to other downscaling methods (e.g. dynamical downscaling), the statistical method is relatively easy to use and provides station-scale climate information from GCM-scale outputs (Wilby et al. 2002). Thus, statistical downscaling methods are widely used in hydrologic impact studies under climate-change scenarios. Finding the empirical relationships between the global and local scale of climate circulation is the basic requirement of any statistical downscaling method. According to this assumption, correlation of global GCM meteorological variables (predictors) and local meteorological variables such as observed precipitation and temperature (predictands) is the key point of this type of downscaling procedure. The most well-known regression-based downscaling methods are structured for separate estimation of the occurrence and amount of meteorological variables. The merits and demerits of statistical regression-based downscaling approaches have been discussed with detail by Hessami et al. (2008).

Moreover, GCMs do not provide direct hydrological and meteorological responses related to climate change. Therefore, the hydrological models are much needed for the simulation of streamflows under climate change

scenarios. A number of hydrological models are offered to simulate daily streamflows, but mostly models perform less efficiently in high-altitude scarce data catchments, where the proportion of snowmelt runoff is dominant in the water resources (Martinec et al. 2007).

Recently, a number of studies have been carried out to examine the impact of climate change on the hydrological regime of rivers by the application of global emission scenarios. Yimer et al. (2009) and Meenu et al. (2013) successfully applied the Hydrological Modelling System (HEC-HMS) for the streamflow simulation by using downscaled meteorological variables (precipitation and temperature) under different global scenarios for the Beles River in Ethiopia and Tunga-Bhadra River catchment in India, respectively. Furthermore, Chen et al. (2012) provided a comparison of different downscaling models for the evaluation and comparison of different hydrological models by using GCMs. In recent years, several researchers have worked on assessing the impact of climate change on hydropower generation as well.

4.2 Description of Statistical Downscaling

General Circulation Models (GCMs) offers to project expected outcomes under climate change at the global and regional scales as a consequence of increase in greenhouse gases. Unfortunately, GCMs usefulness is restricted to study impact at local scale due to coarse spatial resolution (typically $\geq$50,000 km^2) and also shows inability to overcome vital sub-grid-scale features such as topography and clouds. Consequently, two sets of different approaches have combined in order to compute local scale future climate variables from regional weather predictors (Fig. 4.1). First, the statistical downscaling is equivalent to the "model output statistics" (MOS) and "perfect prog" techniques generally applied for short-range numerical

weather projections. Second, Regional Climate Models (RCMs) used to compute climate variables dynamically by using time-varying atmospheric conditions provided by a GCM bounding a specified domain at grid-scale. A continuous role will be played by the aforementioned techniques to assess the potential impacts of climate change due to increase in the concentration of greenhouse gases in the future.

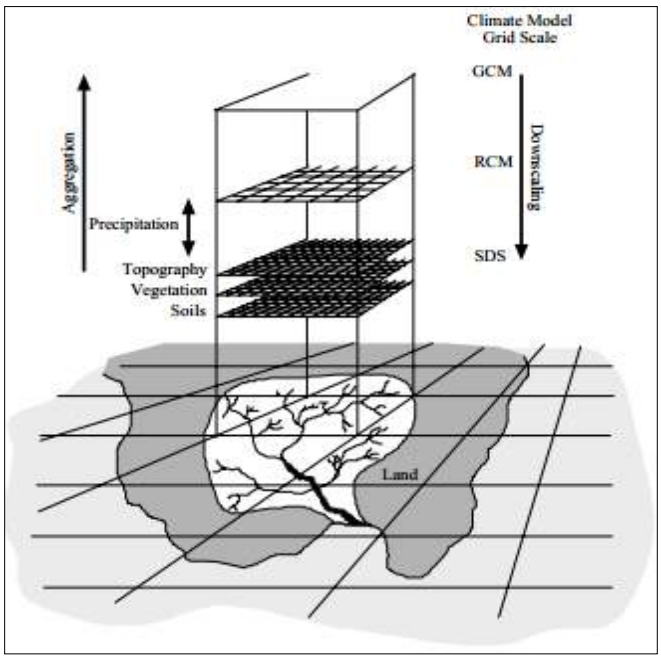

Fig. 4.1: A schematic illustrating the general approach to downscaling.

4.2.1 Overview Downscaling Models

A. SDSM

Statistical Downscaling Model (SDSM) is a decision support tool developed by Wilby et al., (2002) for examining the impact of local climate change. This is a hybrid statistical downscaling model includes scenario, weather generator and provides multiple linear regression methods. The downscaling

of local climate variables (predictands) by using large scale variables (predictors) by using SDSM can achieved in two parts. First, by developing a statistical relationship between local predictands and large scale predictors (given in **Table 2**) and then separate most suitable predictors for the weather generator according to predictands using several functions such as quality control, transformation, screening and calibration function on the basis of results obtained from seasonal and partial correlation analysis and scatter plots. In second part, the model used to predict future climate variable series by using predictors screened in first step, as presented in Fig. 4.2. It is a freely available decision support tool for assessing the local impact of climate change using a robust statistical downscaling technique. SDSM is well documented and has been successfully tested in numerous studies (Nguyen et al. 2005; Wilby and Dawson 2007). Statistical downscaling models have been widely used by several researchers e.g. Meenu et al. (2013); Nasseri et al. (2013); Wilby et al. (2002), for the downscaling of future climate predictions.

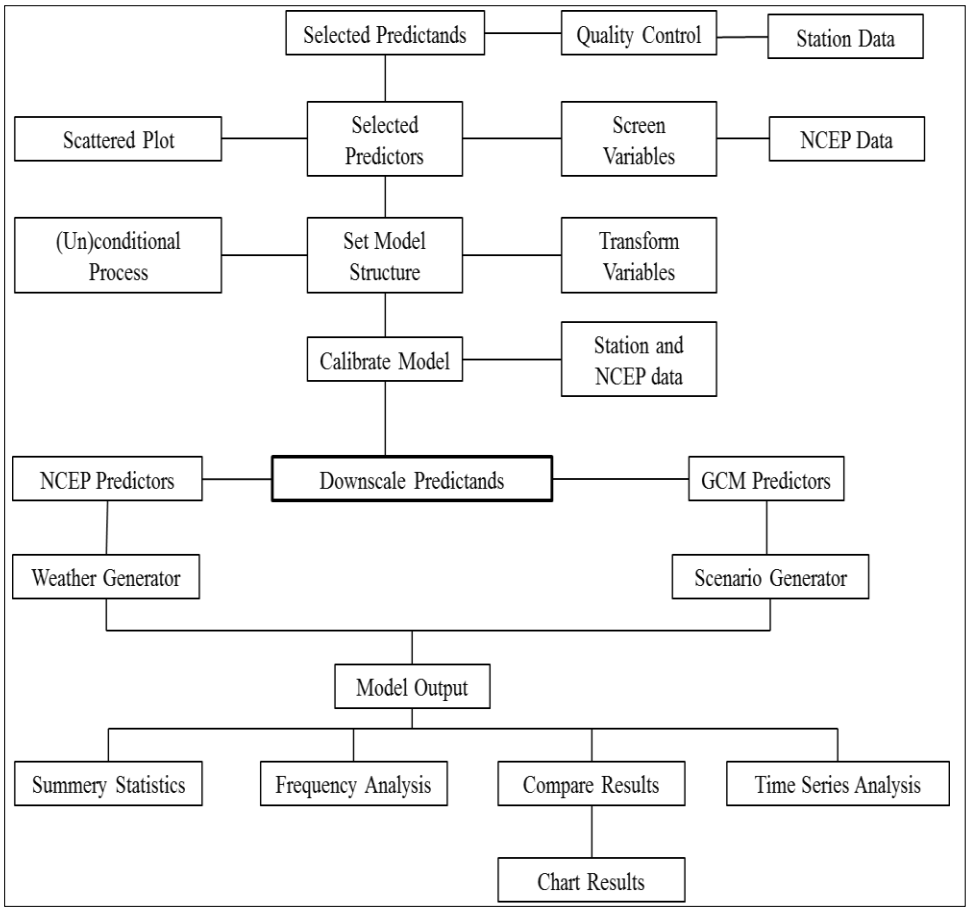

Fig. 4.2: Flow chart for the downscaling of climate variables using SDSM Version 5.1.1 under climate change scenarios.

B. Smooth Support Vector Machine (SSVM)

Recently, Support Vector Machine (SVM) approach proposed by Vapnik (1998) is recognized to pick up nonlinear regression relationships between large scale and local variables for a small sample. By using Vapnik-Chervo-nenkis (VC) and structural risk minimization (SRM) principle it able to overcome several practical issue by establish a best suitable relationship between model complexity and learning ability such as nonlinear, global minimum points and high dimension number (Chen et al. 2012). The scheme diagram of SVM is presented in Fig. 4.3. The SVM is not efficient to deal

large data set as stated by Chen et al. (2012) and Xu (2010). It is therefore, the improved form of SVM namely Smooth Support Vector Machine (SSVM) proposed by Lee and Mangasarian (2001) and Lee et al. (2005) attempts to simplify the SVM. The SSVM is efficient to handle the sample classification and non-linear regression of a large data sample in order to minimize model computational complexity. The SSVM is converted the quadratic constrained optimization problem into convex quadratic unconstrained problem. The literature shows that the SSVM has ability to perform better than that of SVM (Chen et al. 2012).

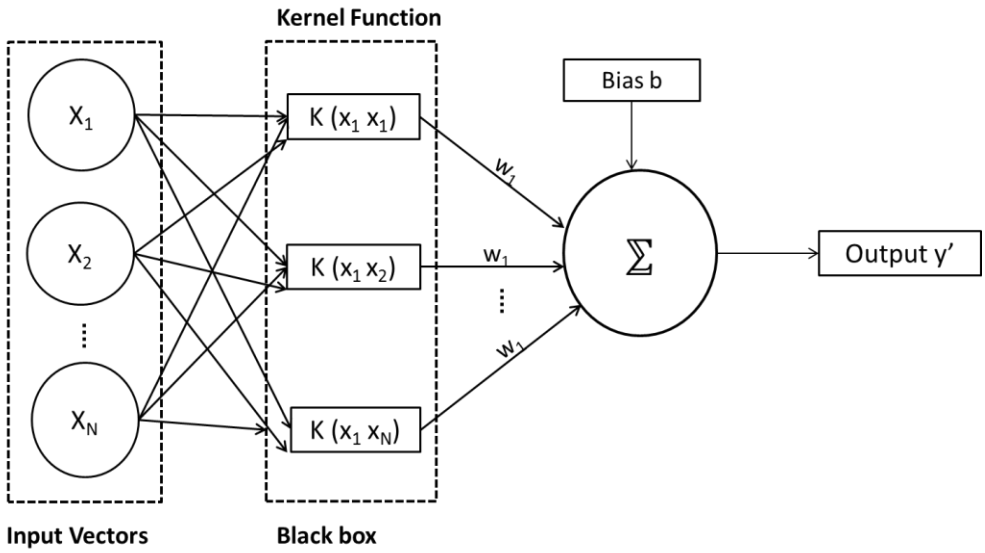

Fig. 4.3: Schematic structure of Support Vector Machine (SVM) based on kernel function.

4.2.2 Predictors Data

In this investigation, National Center for Environmental Protection (NCEP) reanalysis atmospheric data were used for the calibration and validation of the model over the baseline period of 1961–2000.

The outputs of Hadley Centre's GCM (HadCM3) have been utilized for the downscaling of climate variables. The HadCM3 output emission scenarios A2 and B2 are discussed in the special report on emission scenarios (SRES) prepared by the IPCC to produce regional future climate change scenarios thorough the downscaling. The spatial resolution of NCEP/NCAR is 2.5° (long.) × 2.5° (lat.), whereas the grid box dimensions of HadCM3 outputs are 3.75° (long.) × 2.5° (lat.), covering three grids over the Mangla watershed. Selection of the most suitable predictors from the 26 predictors (Table 4.1) must be performed prior to downscaling of the data. The NCEP and HadCM3 predictors used as input for the SDSM model were derived from the Canadian Climate Impacts Scenarios (CCIS) website (www.cics.uvic.ca/scenarios/sdsm/select.cgi).

Table 4.1: Large-scale atmospheric variables from the NCEP reanalysis and HadCM3 simulation output that are used as potential inputs to the multiple linear regression model.

Predictor	Description	Predictor	Description
mslp	men sea level pressure	p_f	geostrophic air flow velocity at the surface
temp	2 meter near surface temperature	p8_f	geostrophic air flow velocity at 850hPa height
t_lag	2 meter near surface temperature lagged 1 day	p5_f	geostrophic air flow velocity at 500hPa height
p500	500hPa geopotential heights	p_z	vorticity at the surface
p850	850hPa geopotential heights	p8_z	vorticity at 850hPa height
shum	near surface specific humidity	p5_z	vorticity at 500hPa height
r500	relative humidity at 500hPa height	p_u	zonal velocity component at the surface
r850	relative humidity at 850hPa height	p8_u	zonal velocity component at 850hPa surface
p_v	meridional velocity component at surface	p5_u	zonal velocity component at 500hPa surface
p5_v	meridional velocity component at 500hPa height	p_zh	divergence at the surface
p8_v	meridional velocity component at 850hPa height	p8_zh	divergence at 850hPa height
		p5_zh	divergence at 500hPa height

4.3 Application of Downscaling Methods (SDSM and SSVM)

In this study, a model developed based on the statistical approach called Statistical Downscaling Model (SDSM) and statistical learning machine theory, SSVM was used for the downscaling of climate variables. the application of SDSM is detailed discussed by Meenu et al. (2013). While the application and algorithm of SSVM is discussed by Chen et al. (2012); Xu (2010) with detail. The baseline period ranges from 1961 to 1990 and 1991 to 2000 for calibration and validation of downscaled climate data set, respectively. The calibration and validation was carried out using SDSM and SSVM by utilizing NCEP reanalysis data and climate variables of selected stations. The best suitable NCEP predictors were screened by using both models and these screened predictors were further used to downscale the data (Table 4.2). The calibration and validation was carried out over 30- and 10-year temporal scales from 1961 to 1990 and 1991 to 2010, respectively. The results obtained were finalized if the explained variance results were found to be satisfactory.

The further future scenarios were generator on a daily basis by using atmospheric predictor variables supplied by the GCM HadCM3. The comparison was made between the baseline and future scenarios of daily maximum and minimum temperatures and precipitation over the 2020s (2015–2045), 2050s (2046–2075) and 2080s (2076–2099) for both models. The comprehensive evaluation was made of SSVM and SDSM using mean values of observed and simulated downscaled data of five selected stations and APHRODITE data points of ungauged catchment.

Table 4.2: Screened predictors used for the downscaling of climate variables at different stations for precipitation, minimum and maximum temperatures

Stations	Screened Predictors Used for Future Climate Scenarios Projection		
	Minimum Temperature	**Maximum Temperature**	**Precipitation**
Astore	t_lag, p850, shum, temp	r500, shum, temp, p8_v	p_f, p5_f, p5_z, p8_z
Gharidopata	p5zh, p8_u, p8_f, shum, p8zh	p8_f, r500, temp	p5_v, p8_f, shum
Gujjar Khan	p500, shum, rhum	Temp, p_zh, p5_v	p_u, p_v, p_z, rhum
Kotli	shum, temp, t_lag	p8_z, p500, rhum	p_u, p5_v, p8_f
Naran	p500, shum,p8_u, p8_f	shum, temp, p850	p5_z, p500, temp
Domel	p500, shum, temp	p5_z, p8_z, r500, temp	p_u, p8_f, p8_u, r500
Muzafferabad	p5_z, p500, shum	p5zh, p8_z, p500, temp	p_zh, p5_f, p5_v,
Murree	p5_z, p500, shum, temp	p500, temp	p_zh, p_z, shum
Palandri	p500, shum, temp	p500, temp	p5_v, p8_u, shum
Rawelakot	p5_z, p500, shum, temp	p5_z, p8_z, shum, temp	p_v, p850
Khandar	-	-	p8_z, p5_v
Sehr Kokata	-	-	p_u, p_zh
Stations of APHRODITE Precipitation Data Used for the Downscaling			
Srinagar	-	-	p8_f, p_v
Baramula	-	-	p_f, p5_z
Anantnag	-	-	p5zh, r500
Wuler Lake	-	-	shum, p8_u
Pulwama	-	-	p5_v, p8_f
Gad Wali	-	-	p8_z, p5_z
Pahalgam	-	-	p8_f, p5_v

As discussed in section 2.2.2 (D), due to the unavailability of gauge data for part of the catchment situated in India, the APHRODITE rainfall data product was used to downscale the rainfall data for those sub-basins. Since the APHRODITE precipitation data is the only remote sensing product available long-term (from 1951 to date), this data was used for the calibration and validation of SSVM and SDSM by using NCEP reanalysis predictors and then future scenarios were generated under the A2 and B2 scenarios at seven different points of the catchment situated in India.

4.4 Statistical Downscaling of Climate Variables (Temperature and Precipitation)

The results obtained by the calibration and validation of SDSM and SSVM for the downscaling of minimum and maximum temperatures and precipitation data are shown in Table 4.3. Furthermore, Table 4.3 shows that the both models are suitable for the downscaling of temperature variables. A comparison was established to study the best downscaling model from SDSM and SSVM. The coefficient of determination (R^2), variance (E) and standard error (SE) is explained capability of SDSM for downscaling of precipitation with minimum variance, R^2 and SE values by 48.69%, 0.31 and 0.24 mm, respectively, in each case of calibration period. The obtained values of variance (E), R^2 and SE by using SDSM are never less than 69.69%, 0.82 and 0.46 (°C), respectively, for maximum temperature. Moreover, the obtained least values are 58.2%, 0.81 and 0.42 for variance (E), R^2 and SE (°C), respectively. Additionally, by using SSVM the obtained value of variance (E), R^2 and SE (°C) for precipitation are never less than 548.69%, 0.59 and 0.36 (°C), respectively. The SSVM is performed very similar to SDSM for downscaling of temperature variables (minimum and maximum) with lowest values 69.27%, 0.83 and 0.44 (°C) of E, R^2 and

SE, respectively for maximum temperature. Similar trend of values is found for minimum temperature by using SSVM. On the other hand, SDSM is found slightly less efficient for the downscaling of daily precipitation but SSVM is found considerably efficient than that of SDSM. Aforementioned parametric values depict that the SSVM is more suitable for the downscaling of climate variables by using GCMs. In contrast to calibration, over the validation period both models are found to be slightly less efficient, as expected. In case of APHRODITE data products such as precipitation and mean temperature, the obtained results show that both models are highly efficient to downscale climate variables at local data series. This data product is helpful to overcome scarce data issues in climate change studies. As, the variance (E), R^2 and standard error (SE) alone are not evaluate the efficiency of both models for downscaling of precipitation during calibration and validation it is therefore, means daily (mm/day), standard deviation (mm/day), percentile (95%), percent wet, maximum dry and wet spell length were also utilized as performance descriptors. The thresh hold for wet condition was set to 1 mm. Table 4.4 explains the difficulty of SDSM for downscaling of local precipitation from regional scale predictors using NCEP data compared with SSVM during calibration and validation. Table 4.4 is used to compare SSVM and SDSM by taking average of all statistics estimated from daily baseline precipitation including observed and APHRODITE and NCEP downscale data in term of bias, that is, difference between baseline and NCEP downscaled values. The maximum number of shaded values are clearly indicates the superiority of SSVM over SDSM for precipitation downscaling in both calibration and validation period.

It can be seen in Fig. 4.4 and 4.5 that there is good agreement between the observed temperature variables (minimum and maximum temperatures) and those driven by using NCEP reanalysis predictors HadCM3 A2 scenario over

the calibration period. It is also easy to find in Fig. 4.6 that the monthly mean precipitation driven by using the HadCM3 scenario A2 is overestimated compared to the observed precipitation, at most of the stations with the exception of Naran, particularly during peak rainfall months as presented in appendix B. Moreover, the agreement between the gauged precipitation and downscaled climate data using SSVM is significantly better than that of SDSM. The results for the downscaling of APHRODITE precipitation for the ungauged part of the catchment situated in India are presented in Fig. 4.7 Similarly, the efficiency of downscaled precipitation using gauge data, the projected precipitation using the APHRODITE product is also found to be less efficient using SDSM while SSVM reproduced precipitation series using NCEP and A2 scenario efficiently, over the calibration period. Whereas, the APHRODITE mean temperature is efficiently downscaled by both models.

Table 4.3: Explained variance (*E*), coefficient of determination (R^2) and SE for the evaluation of SSVM and SDSM during calibration (1961-1990) of downscaled observed and APHRODITE precipitation (mm), temperatures (°C) by using NCEP predictors.

Stations	Models	Precipitation			Max. Temperature			Min. Temperature		
		E (%)	R^2	SE (mm)	E (%)	R^2	SE (°C)	E (%)	R^2	SE (°C)
Astore	SDSM	32.41	0.35	0.30	71.62	0.87	0.49	62.3	0.84	0.46
	SSVM	62.33	0.75	0.41	74.59	0.89	0.47	64.27	0.85	0.51
Naran	SDSM	43.21	0.42	0.31	75.69	0.89	0.51	65.91	0.87	0.47
	SSVM	55.74	0.68	0.39	77.62	0.91	0.53	66.68	0.89	0.53
G.Dopata	SDSM	36.52	0.39	0.29	78.31	0.91	0.55	65.67	0.85	0.49
	SSVM	60.38	0.71	0.44	75.2	0.88	0.48	67.91	0.87	0.54
Kotli	SDSM	39.84	0.31	0.24	70.23	0.86	0.48	62.18	0.83	0.44
	SSVM	52.31	0.66	0.41	73.55	0.84	0.45	64.23	0.86	0.56
Gujjar	SDSM	41.69	0.36	0.25	71.69	0.87	0.48	58.2	0.81	0.43
Khan	*SSVM*	48.69	0.59	0.36	69.71	0.83	0.44	61.51	0.85	0.56
Muree	SDSM	36.22	0.32	0.39	72.36	0.85	0.46	63.37	0.87	0.49
	SSVM	55.29	0.64	0.43	76.12	0.89	0.51	74.51	0.88	0.49
M.abad	SDSM	34.69	0.35	0.31	71.24	0.84	0.47	66.23	0.83	0.42
	SSVM	49.31	0.61	0.37	73.54	0.85	0.49	63.57	0.82	0.40
Domel	SDSM	36.97	0.38	0.41	69.69	0.82	0.47	69.35	0.85	0.48
	SSVM	52.36	0.68	0.45	69.27	0.84	0.45	64.81	0.83	0.46

Ungauged Basin Points		APHRODITE Precipitation			APRIDOIT Mean Temperature		
		E (%)	R^2	SE (mm)	E (%)	R^2	SE (°C)
Baramula	SDSM	26.53	0.32	0.35	68.12	0.81	0.43
	SSVM	53.24	0.68	0.39	71.39	0.83	0.52
Wular	SDSM	23.51	0.26	0.31	66.57	0.83	0.45
Lake	*SSVM*	51.93	0.63	0.36	69.31	0.85	0.55
Srinager	SDSM	32.91	0.33	0.38	66.69	0.83	0.46
	SSVM	57.63	0.72	0.39	68.75	0.88	0.48
Pulwama	SDSM	29.66	0.25	0.31	64.03	0.81	0.41
	SSVM	52.36	0.68	0.37	63.02	0.79	0.45
Anantnag	SDSM	23.57	0.26	0.31	71.61	0.85	0.43
	SSVM	50.15	0.64	0.35	69.84	0.85	0.47
Gad Wali	SDSM	26.39	0.28	0.32	59.36	0.78	0.38
	SSVM	48.37	0.61	0.33	65.55	0.82	0.42
Pahalgam	SDSM	31.96	0.35	0.39	66.92	0.81	0.4
	SSVM	46.87	0.65	0.38	68.48	0.86	0.44

Table 4.4: Explaining Bias in comparative statically analysis for the downscaling calibration and validation period of observed and APHRODITE precipitation on average values at selected stations by using NCEP predictors.

Statistical Indicators for average precipitation of five stations	**Calibration (1961-1990)**														
	Annual (Jan-Dec)					**Winter (Sep.-March)**					**Summer (April-Aug)**				
	SDSM			**SSVM**		**SDSM**			**SSVM**		**SDSM**			**SSVM**	
	OBS	**NCEP**	***Bias***	**NCEP**	***Bias***	**OBS**	**NCEP**	***Bias***	**NCEP**	***Bias***	**OBS**	**NCEP**	***Bias***	**NCEP**	***Bias***
Mean (mm/day)	2.91	3.12	0.20	3.13	0.22	2.36	2.68	0.32	2.3	0.01	3.7	4.14	0.41	4.176	0.45
SD (mm/day)	9.21	9.06	-0.14	8.81	-0.32	7.43	7.45	0.02	7.8	0.44	10.8	10.76	-0.09	10.73	-0.12
Percentile (95%)	17.2	19.42	2.19	18.61	1.37	15.04	17.35	2.30	16.3	1.31	21.3	22.72	1.42	21.28	-0.02
%Wet days	22.7	20.73	-2.06	20.77	-2.02	20.52	19.23	-1.28	21.4	0.92	27.9	25.97	-1.94	28.45	0.53
Maxi dry spell length	102	100	-2	95	-7	79	75	-4	75.8	-3.2	68	61	-7	72	4
Maxi wet spell length	10	9	-1	10	0	9	8	-1	9	0	11	10	-1	12	1
	Validation (1991-2000)														
Mean (mm/day)	3.39	3.71	0.32	3.56	0.17	3.07	3.71	0.63	3.665	0.58	3.80	3.95	0.14	3.78	-0.03
SD (mm/day)	9.22	8.25	-0.97	9.31	0.09	8.07	7.98	-0.08	8.195	0.12	10.1	8.19	-1.95	8.94	-1.19
Percentile (95%)	18.48	21.43	2.95	20.11	1.62	16.78	20.26	3.48	19.59	2.80	21.69	23.54	1.86	22.78	1.1
%Wet days	24.98	21.62	-3.36	25.23	0.24	23.47	22.54	-0.92	24.81	1.33	26.87	24.35	-2.51	26.96	0.09
Maxi dry spell length	64	58	-6	64	0	62	56	-6	61	-1	45	36	-9	43	-1.6
Maxi wet spell length	10	10	0	12	2	10	8	-2	11	1	9	9	0	11	2

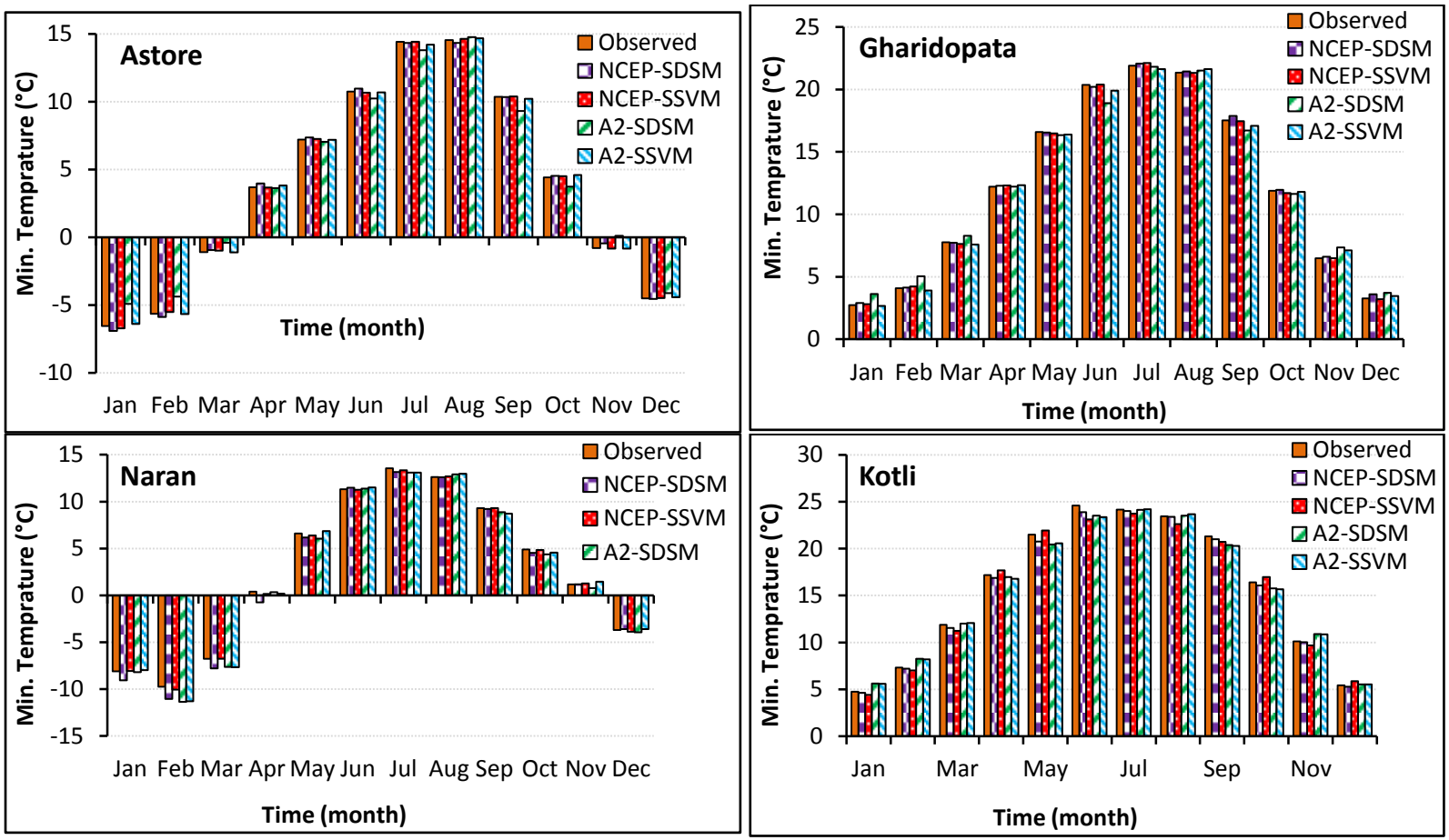

Fig. 4.4: Comparison between observed and downscaled minimum temperature by using SDSM and SSVM under NCEP, HadCM3 A2 scenarios at four selected stations in Mangla watershed over calibration (1961–1990).

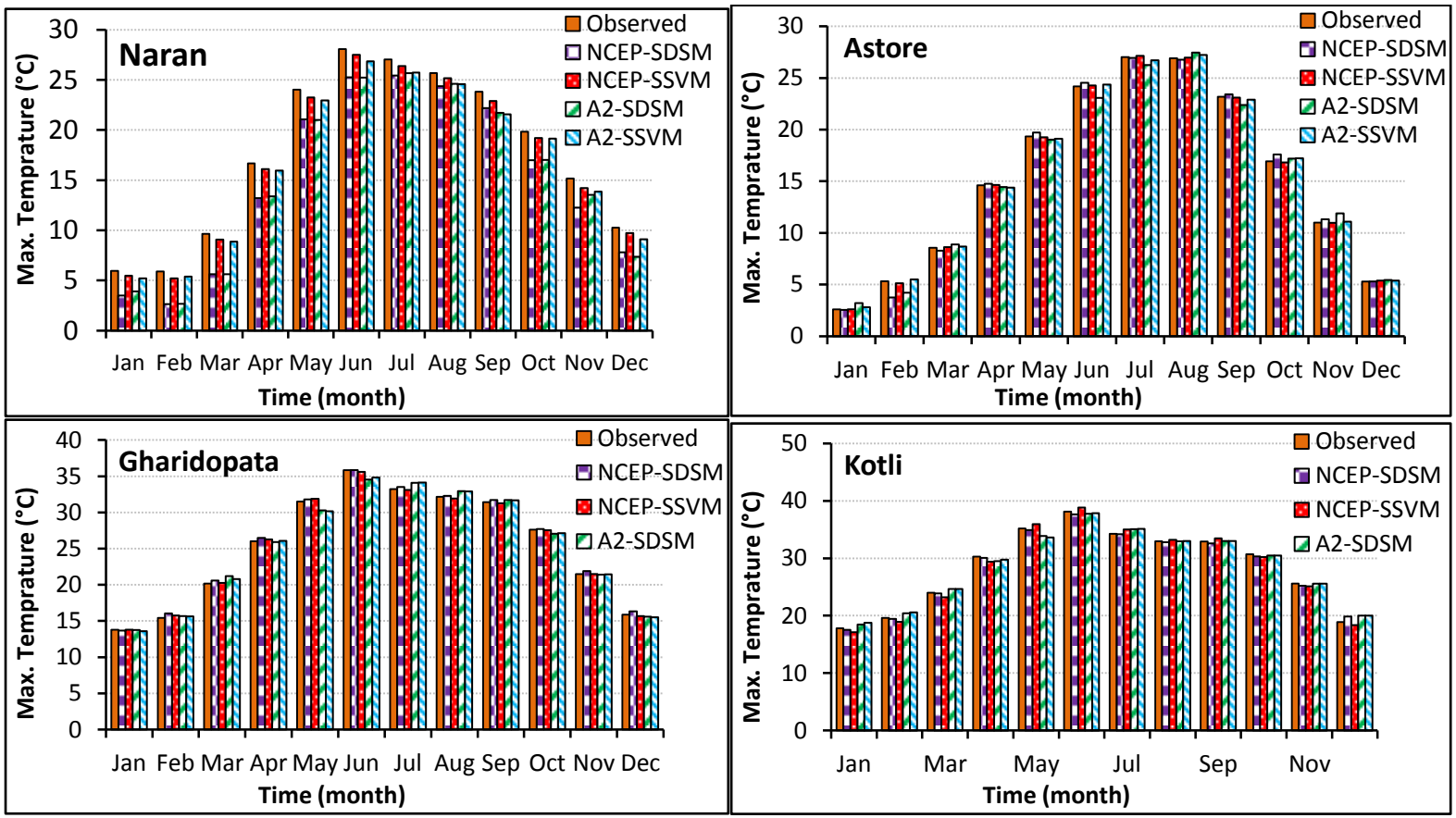

Fig. 4.5: Comparison between observed and downscaled maximum temperature by using SDSM and SSVM under NCEP, HadCM3 A2 scenarios at four selected stations in Mangla watershed over calibration (1961–1990).

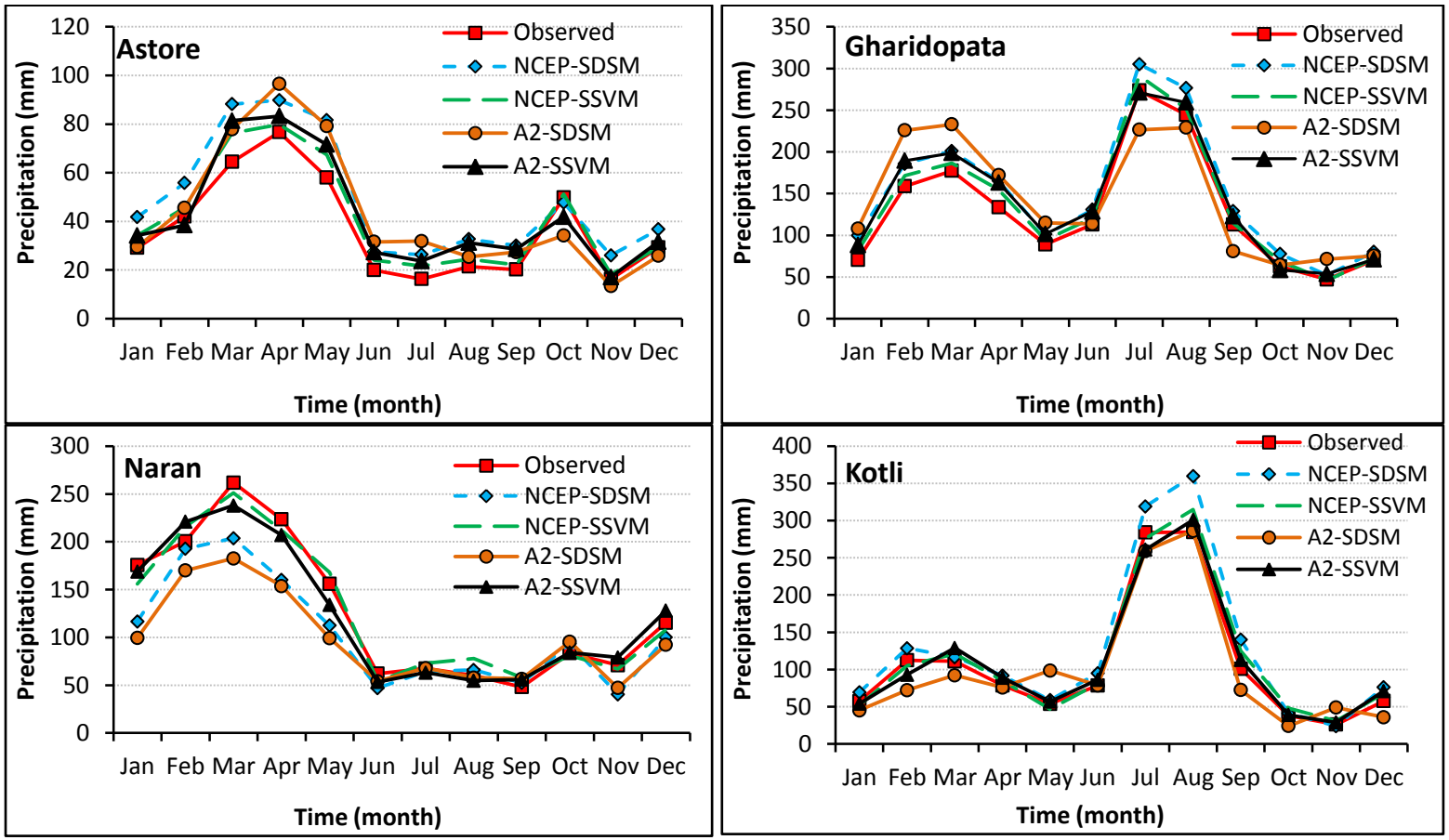

Fig. 4.6: Comparison between calibrated and observed (gauge) precipitation by using SDSM and SSVM under NCEP, HadCM3 A2 scenarios at four selected stations in Mangla watershed from 1961 to 1990.

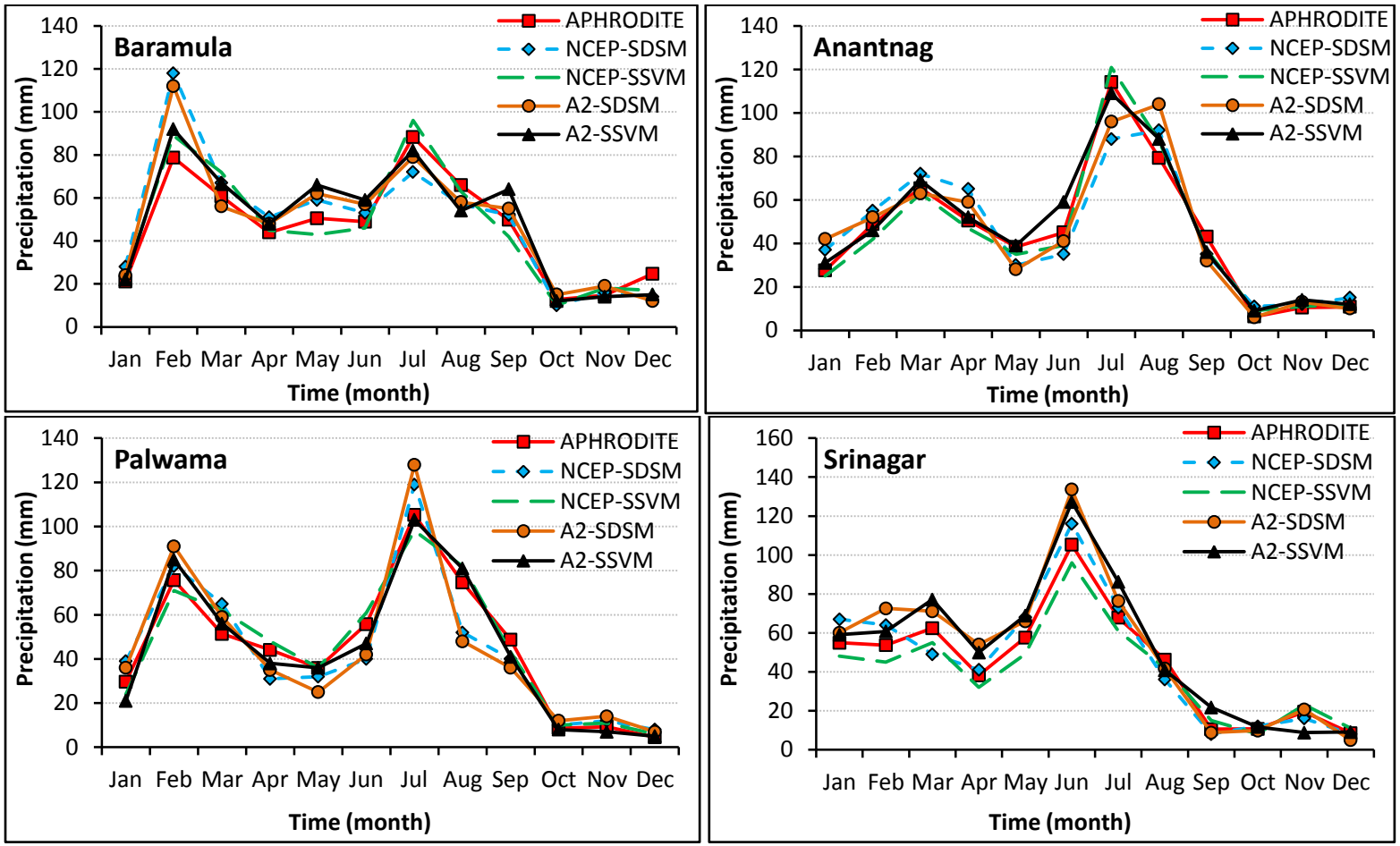

Fig. 4.7: Comparison between APHRODITE and downscaled precipitation under NCEP, HadCM3 A2 scenario using SDSM and SSVM at selected ungauged points in Mangla watershed from 1961 to 1990.

4.5 Future Climate Scenarios

The future climate change scenarios are generated by using SSVM because of its high efficiency particularly for the downscaling of precipitation data series. The results obtained for the projected daily maximum and minimum temperatures under the A2 and B2 scenarios at selected stations are presented in Table 4.5. At most of the stations, both variables are increasing over the 2020s, 2050s and 2080s, but at Naran station the temperature is projected to decrease. Over the 2080s, the minimum and maximum temperatures at Astore station will increase by 2.69°C (during winter) and 3.98°C (during summer) under the A2 scenario. The variation in projected temperature at Naran station behaves differently; the minimum temperature at this station is increasing during the summer but decreasing during the winter season. The decrease in winter temperatures over the 2020s is by -2.59°C under the B2 scenario. In contrast to Naran, it is observed that at most stations the temperature during the winter season is significantly increasing compared to the summer. In contrast, a considerable decrease is observed during the winters. A significant increment is also found at Astore station in both minimum and maximum temperatures. The change in temperature and precipitation under the A2 scenario is slightly greater than B2. Furthermore, Table 4.6 shows that the change in projected and baseline precipitation over the 2020s, 2050s and 2080s is positive at most stations, with the exception of Naran and Kotli. However, a decrease is found at Kotli during the winter season, and a significant increase is observed over the annual time period and during the summer. A negative change in precipitation is perceived at Naran station. The maximum decrease is found during the winter season at Naran by -41.76 mm over the 2020s, as shown in Table 4.5. In contrast, the precipitation is increasing significantly at Gharidopata by 125 mm over the 2080s under the A2 scenario.

Table 4.5: Change in baseline and downscaled temperature variables (minimum and maximum) on seasonal basis (annual, winter and summer) using SSVM under HadCM3 scenarios A2 and B2 (minimum and maximum).

Stations	Seasons	Change in Minimum Temp (°C)						Change in Maximum Temp (°C)					
		H3A2			H3B2			H3A2			H3B2		
		2020s	2050s	2080s	2020s	2050s	2080s	2020s	2050s	2080s	2020s	2050s	2080s
Astore	Annual	0.70	1.42	2.42	0.57	1.31	1.95	0.64	1.55	3.00	0.44	1.41	2.26
	Summer	0.59	1.09	2.49	0.33	0.90	1.86	1.01	1.83	3.98	0.69	1.47	2.90
	Winter	1.32	1.79	2.69	1.21	1.79	2.27	0.98	1.35	2.48	0.75	1.42	1.93
Gharidopata	Annual	0.65	1.17	2.07	0.51	1.02	1.60	0.16	0.88	1.94	0.26	0.81	1.29
	Summer	0.67	0.83	2.16	0.17	0.55	1.46	0.13	0.81	1.85	0.19	0.52	1.11
	Winter	1.70	1.55	2.27	1.13	1.55	1.94	0.58	1.01	2.29	0.53	1.16	1.71
Gujjar Khan	Annual	0.28	0.01	0.38	0.12	0.05	0.17	3.29	4.15	4.97	3.23	4.15	4.95
	Summer	0.07	0.00	0.13	0.00	-0.11	0.05	0.26	0.33	0.34	0.32	0.27	0.30
	Winter	0.31	0.42	0.68	0.22	0.51	0.55	0.69	0.78	1.15	0.76	0.87	0.94
Kotli	Annual	0.60	1.13	1.99	0.59	1.07	1.54	1.08	1.08	2.01	1.02	1.02	1.44
	Summer	0.40	0.84	1.94	0.34	0.72	1.30	-0.13	0.52	1.06	0.04	0.25	0.55
	Winter	1.13	1.42	2.04	1.06	1.44	1.77	1.22	1.62	2.95	1.24	1.80	2.33
Naran	Annual	-0.16	-0.19	0.10	-0.24	-0.23	-0.03	-2.21	-1.95	-1.52	-2.37	-2.05	-1.77
	Summer	0.23	0.11	0.52	0.14	0.10	0.24	-1.79	-1.65	-1.08	-1.92	-1.78	-1.46
	Winter	-0.49	-0.47	-0.34	-0.49	-0.52	-0.30	-2.36	-2.22	-1.96	-2.59	-2.28	-2.08

Table 4.6: Change in baseline and projected precipitation by using SSVM at selected stations.

Stations	Seasons	Change in Precipitation (mm)					
		H3A2			H3B2		
		2020s	2050s	2080s	2020s	2050s	2080s
Astore	Annual	8.08	12.48	13.43	7.57	10.83	11.08
	Summer	14.00	18.17	21.93	12.80	17.08	20.92
	Winter	3.90	5.50	8.37	3.01	4.59	5.21
G.Dopata	Annual	89.5	108.6	125.5	82.9	103.9	121.6
	Summer	69.45	83.67	98.22	63.89	85.66	91.54
	Winter	37.21	53.26	58.18	32.99	47.99	53.42
Gujjar Khan	Annual	26.27	28.24	38.14	23.23	25.04	34.37
	Summer	13.81	8.81	50.81	17.81	13.81	58.81
	Winter	21.47	33.47	26.47	31.47	22.47	35.47
Kotli	Annual	68.01	98.96	114.37	64.82	92.42	104
	Summer	93.91	129.07	132.34	90.97	124.90	126
	Winter	-36.75	-46.25	-58.30	-42.18	-56.14	-46.0
Naran	Annual	-23.61	-24.54	-24.96	-26.94	-28.98	-22.92
	Summer	-14.09	-20.13	-18.58	-16.87	-23.98	-21.44
	Winter	-28.11	-29.68	-25.35	-41.76	-35.36	-28.47
APHRODITE Precipitation Data Used for the Downscaling							
Srinagar	Annual	15.23	19.39	25.64	18.67	24.39	31.64
	Summer	13.71	12.97	16.17	12.45	12.37	12.73
	Winter	8.69	10.45	15.29	11.19	13.65	16.59
Baramula	Annual	25.39	34.97	47.55	37.23	39.47	55.28
	Summer	19.87	24.26	36.84	22.41	28.18	38.57
	Winter	11.67	13.69	17.60	15.49	15.63	18.91
Anantnag	Annual	32.74	39.58	52.39	38.69	45.87	56.33
	Summer	20.23	24.36	35.80	29.92	31.95	39.68
	Winter	12.36	15.66	20.45	14.39	18.47	24.61
Palwama	Annual	29.66	42.81	59.32	36.29	56.38	66.49
	Summer	43.61	52.36	69.49	48.42	71.36	68.62
	Winter	-15.91	-16.32	-25.69	-21.77	-29.56	-15.78

The changes in precipitation where APHRODITE data were used are also found to be positive at most of the locations, with the exception of Palwama, where a decreasing trend of precipitation is found during the winter season.

As discussed earlier, a peculiar behaviour was found at Naran station for the minimum and maximum temperatures. It can be seen from Figs 4.8 and 4.9 that, over the future climate scenarios, the maximum temperature is decreasing over the 2020s, 2050s and 2080s from December to July, while from October to November a gradual increment is found from the 2020s to 2050s. Overall, an increment in both temperature variables is observed at most of the stations. Furthermore, the projected precipitation increases over the 2020s, 2050s and 2080s at most of the stations, but at Naran station the projected precipitation decreases compared to the baseline over all three future scenarios. At Gharidopata and Kotli stations, a significant increment in precipitation is found during the summer months, particularly over the 2080s (Fig. 4.10).

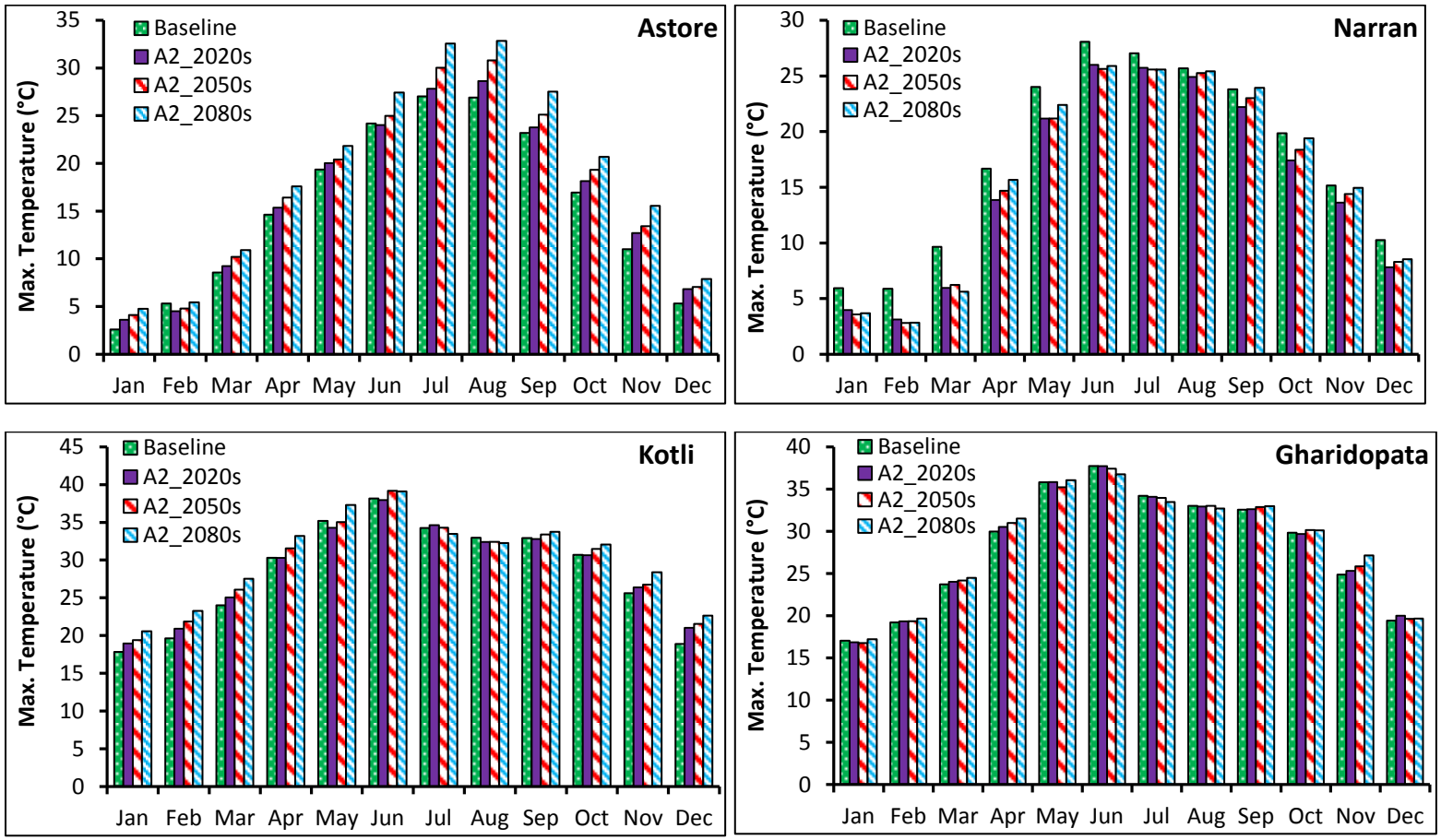

Fig. 4.8: Comparison between baseline and downscaled future maximum temperature (T_{max}) during 2020s, 2050s and 2080s on monthly basis at selected stations within the Mangla catchment under A2 scenario by using SSVM.

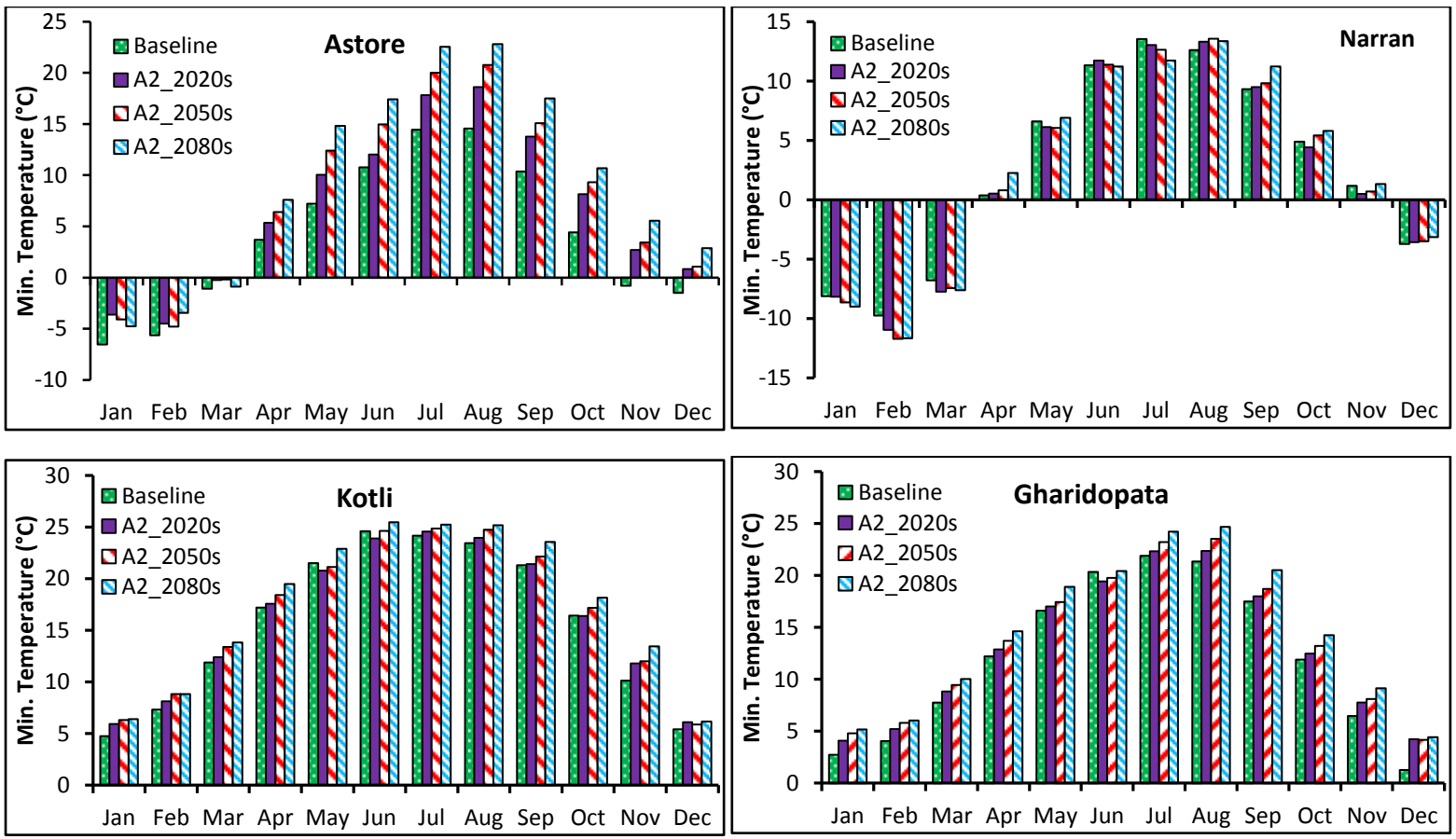

Fig. 4.9: Comparison between baseline and downscaled future minimum temperature (T_{min}) during 2020s, 2050s and 2080s on monthly basis at selected stations within the Mangla catchment under A2 scenario by using SSVM.

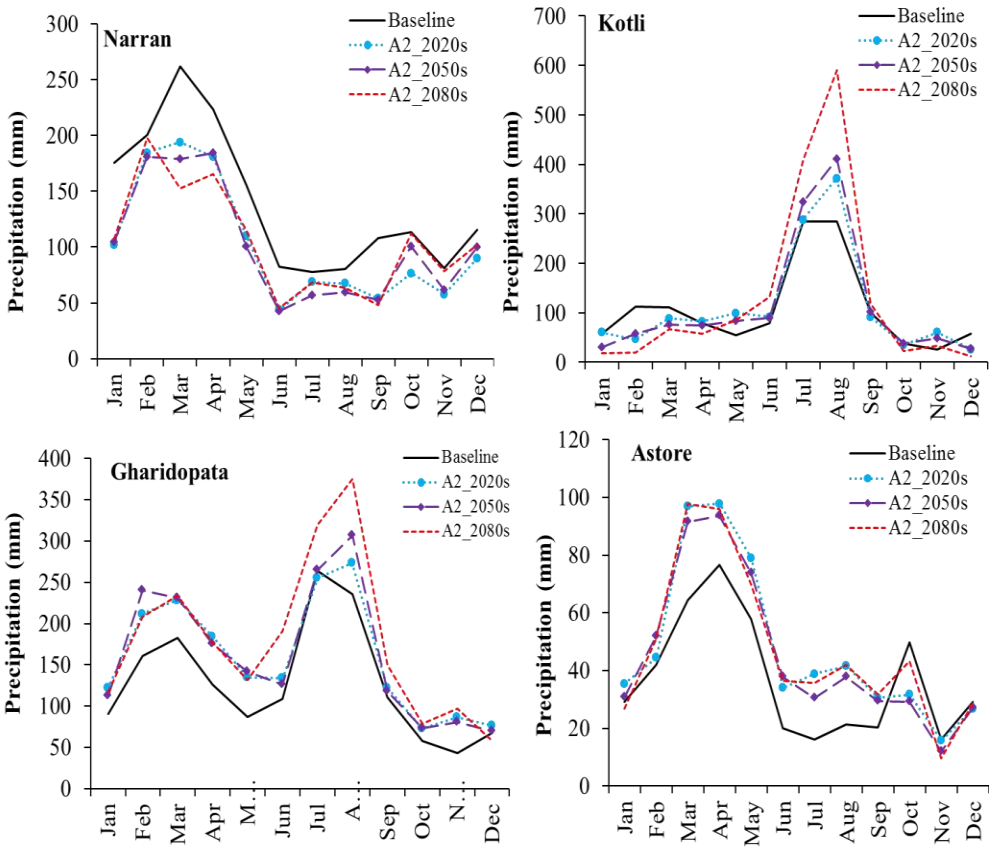

Fig. 4.10: Comparison between baseline and downscaled future precipitation during 2020s, 2050s and 2080s on monthly basis at selected stations within the Mangla catchment under A2 scenario by using SSVM.

4.6 Hydrological Model Calibration and Validation

As discussed in chapter 3, HEC-HMS model calibration was carried out over single (2001, 2002, 2003, 2007, 2008 and 2009), three- (2001–2003 and 2007–2009) and six-year (2001 to 2003, 2007 to 2009) time windows for the optimization of model parameters for future climate scenarios, on a daily basis. The model parameters were also calibrated over the aforementioned time windows by using downscaled climate variables (precipitation and temperature). The model was run by replacing daily observed precipitation and temperature data with the downscaled data to optimize the finer parameters for the climate change impact studies. The average values of the

optimized parameters over single, three- and six-year simulation runs were used for the simulation of streamflows by using downscaled climate variables over the calibration (2001–2003) and validation (2007–2009) windows. On the contrary, a significant variation was found between the average optimized parameters over the simulation driven by using observed data and those driven by HadCM3 scenarios, as presented in Fig. 4.11. The optimized model parameters for the simulation under the A2 scenario are presented in Table 4.9. Furthermore, a very slight change was found in the parameters used for the snowmelt runoff modelling. This change may be due to small changes between the observed and downscaled mean temperature, as discussed earlier. A significant difference between the parameters of the two simulation windows may be due to the low SDSM efficiency at downscaling precipitation data. It was also found that the precipitation downscaled by using SDSM was overestimated, which could be the main reason for significant change particularly in the parameters used to manage rainfall-runoff.

Table 4.8: Parametric values used for simulation under A2 scenario by the application of HEC-HMS in Mangla Basin over 2001–2003.

Sub-basin of HMS	Initial Deficit (mm)	Maxi Deficit (mm)	Constant Loss (mm/hr)	Imp (%)	Lag Time (hrs)	Lapse Rate (deg. °C/100 m)	DDF (mm °C^{-1} d^{-1})	ET (mm/month) Range (Winter to Summer)
Chandak	25	48	2.25	17	10.82	-0.68	5.2	10 to 47
Khandar	38	56	2.15	10	8.833	-0.17	5.2	11 to 58
Kotli	42	58	1.75	15	11.77	-0.31	5.2	7 to 41
Rawelakot	24	59	2.10	18	13.61	-0.25	5.2	10 to 58
Sehr-K	32	50	1.85	10	9.37	-0.28	5.2	12 to 49
Naran	28	53	0.50	6	21.38	-0.67	5.2	3 to 46
Dudhnial	22	48	1.75	22	17.42	-0.34	5.2	8 to 44
Domel	26	47	2.75	12	20	-0.12	5.2	11 to 70
Astore/Ke	24	49	1.90	0	23.13	-0.31	5.2	6 to 41
Baramula	32	46	1.25	0	17.67	-0.69	5.2	12 to 60
M.Abad	20	44	2.50	15	10.5	-0.2	5.2	12 to 70
G.Dopata	23	48	3.55	25	15.67	-0.26	5.2	13 to 68
Srinagar	22	45	0.75	0	23.67	-0.71	5.2	8 to 48
Muree	38	53	1.80	30	10.33	-0.51	5.2	9 to 43
Palandri	24	45	2.55	25	10.75	-0.17	5.2	11 to 54
Nawan	20	43	3.15	0	8.17	-0.19	5.2	5 to 63
Kanshi	35	55	1.65	15	15.5	-0.11	5.2	12 to 74
Wuler	34	58	1.10	9	15.69	-0.57	5.2	10 to 47
Pulwama	27	60	0.75	6	18.77	-0.69	5.2	10 to 52
Anantnag	20	54	0.45	4	14.27	-0.41	5.2	10 to 52
Pahalgam	35	59	0.50	11	15.58	-0.65	5.2	8 to 46
Gad Wali	34	57	0.50	7	12.55	-0.65	5.2	8 to 46

Imp (%): Impervious area of watershed in percentage (%).

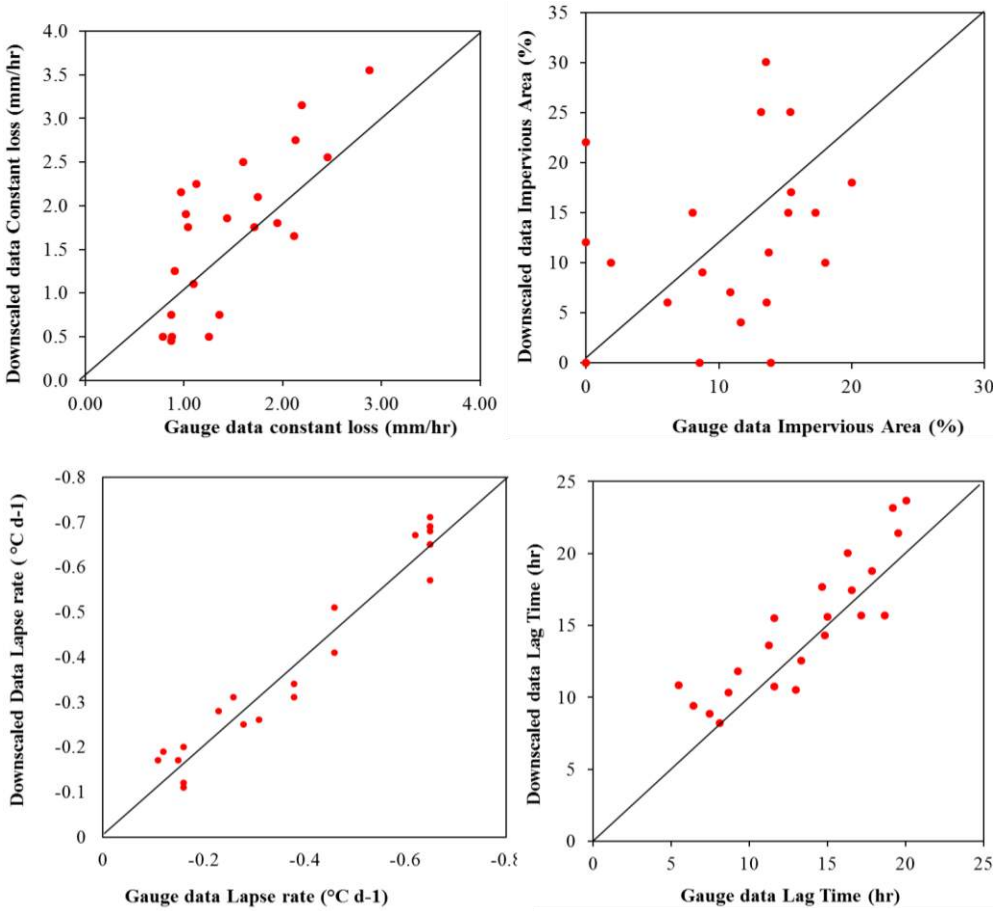

Fig. 4.11: Comparison of calibrated parametric values of constant loss (mm/hr), lag time (hr), lapse rate (°C d^{-1}) and impervious area (%) for the simulation of streamflows by using observed and downscaled climate data.

The results obtained from HEC-HMS by using downscaled meteorological data under the A2 and B2 scenarios are presented in Table 4.9. The simulation efficiency of HEC-HMS by the application of SDSM downscaled data was found to be slightly less efficient compared to calibration by using observed data, with the lowest NS coefficient value of 0.63 over the validation run. The correlation coefficient values were never less than 0.65 and 0.59 for the Pearson and Kendall rank correlation tests, respectively.

Furthermore, Fig. 4.12 depicts the capability of HEC-HMS to reproduce daily streamflows by using downscaled climate variables under the A2 and B2 emission scenarios. Several overestimations were found over the simulated streamflows, particularly during the summer months (April to August), which may be associated with the slightly less efficiency of downscaled precipitation data.

Table 4.9: Evaluation of HEC-HMS at Mangla Dam by using downscaled data with HadCM3 under A2 and B2 scenarios over three-year simulation time window.

Performance Descriptors	**Mangla Dam Station**			
	H3A2		**H3B2**	
	Calibration (2001-2003)	**Validation (2007-2009)**	**Calibration (2001-2003)**	**Validation (2007-2009)**
RMSE (m^3/s)	227.21	311.04	234.2	314.8
MAE (m^3/s)	44.74	57.15	60.34	74.29
NS Coefficient	0.69	0.63	0.67	0.59
Dv (%)	15.61	24.27	-18.25	27.74
Pearson Correlation	0.73	0.65	0.76	0.69
Kendall Correlation	0.65	0.59	0.62	0.54

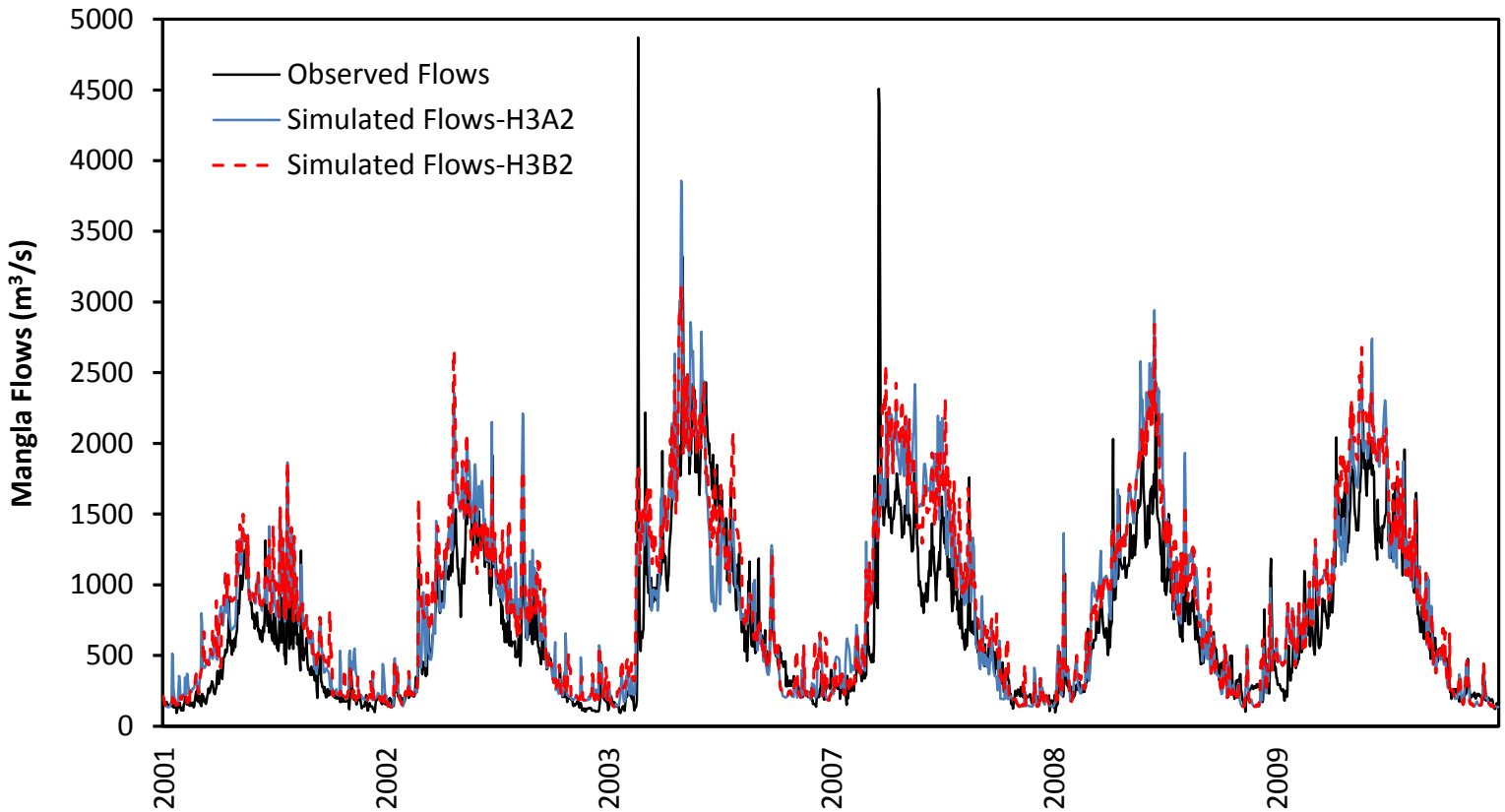

Fig. 4.12: Observed and simulated flows by using downscaled data derived from HadCM3 under A2 and B2 scenarios at Mangla Dam.

4.7 Future Water Availability

The statistics of the simulation obtained using observed and downscaled data over the current scenario (CS) and future projections are illustrated in Table 4.10. A significant increase is found in streamflows under future scenarios of the 2020s, 2050s and 2080s. It is evident that the simulated discharges over the baseline time window by using downscaled data under the A2 and B2 scenarios are overestimated.

A high percentage of rainfall contribution in the form of direct runoff is found during the 2020s, 2050s and 2080s by using the downscaled climatological data under the A2 and B2 emission scenarios at Mangla Dam. The runoff contribution decreased to -15.25% and -22.71% under the A2 and B2 scenarios, respectively, during the month of April over the 2020s (Table 4.11). In contrast, a significant increase in runoff is observed. The maximum percent change in projected inflows is found during the winter months compared to the summer. Fig. 4.13 shows that several rapid runoff peaks are likely to occur over the winter seasons of the 2020s, 2050s and 2080s under the A2 scenario. This may be associated with the minimum and maximum temperature changes during the winter months. As mentioned in the previous section, the temperature is expected to increase over future scenarios at most of the stations. The solid or liquid form of precipitation is discriminated by using the px temperature in the model. If the air temperature value is greater than the px temperature, the model incorporates precipitation as liquid. Therefore, it may be possible that the snowfall regime shifts into liquid water due to increase in the air temperature in future scenarios, and this change in temperature may explain the generation of high direct runoff peaks during the winter. The magnitude of the runoff is observed to be slightly higher under A2 than B2. The increase in average annual streamflows compared to the baseline (simulated by using downscaled data) is 19.53%, 31.10% and

39.31% over the 2020s, 2050s and 2080s, respectively, under the A2 scenario. Figs 4.14 and 4.15 show more clearly on a monthly basis that the streamflows are increasing very extensively over the 2020s, 2050s and 2080s under the A2 scenario. A significant increment is found during the winter months particularly over the 2080s, possibly due to the increase in mean temperature. An extensive increase in the summer months is also found, and may be associated with rapid snowmelt due to temperature increase. Overall, the climate change scenarios will lead to an increase in available water resources, which will require large storage reservoirs to be managed.

Table 4.10: Statistics of observed (gauge) and projected streamflow data simulated by using downscaled climate variables under A2 and B2 scenarios.

Flows Statistics (m^3/s)	**Mean**	**SD**	**Min**	**Max**	**Change in mean inflows (%)**
Baseline Data	731	558	93	4870	-
Baseline A2	857	651	134	4106	-
Baseline B2	851	650	133	4477	-
2020s (2035-2037)	913	626	143	3846	19.93
2050s (2065-2067)	1015	772	159	4580	31.10
2080s (2095-2097)	1089	721	137	5184	39.31

Table 4.11: Change (%) in future monthly streamflows at Mangla Dam under scenarios A2 and B2.

Months	**A2**			**B2**		
	2020s (%)	**2050s (%)**	**2080s (%)**	**2020s (%)**	**2050s (%)**	**2080s (%)**
Jan	27.57	34.59	38.42	25.17	31.02	34.98
Feb	33.25	35.46	44.96	25.34	27.26	41.79
March	11.00	14.94	36.95	9.71	12.14	39.75
April	-15.25	14.86	31.11	-22.71	18.12	29.64
May	5.49	15.26	23.04	5.22	13.48	17.17
June	36.71	23.54	26.29	39.93	21.91	24.05
July	13.47	29.62	25.64	14.77	27.85	24.39
August	18.48	35.36	41.58	18.14	31.42	44.35
Sep	7.50	9.28	12.75	10.24	12.22	15.34
Oct	18.69	18.96	54.51	16.55	22.35	51.29
Nov	15.58	19.67	29.06	13.41	16.03	26.94
Dec	23.69	22.93	20.06	27.28	27.47	27.75
Annual	**15.85**	**24.54**	**35.20**	**14.50**	**22.94**	**33.95**

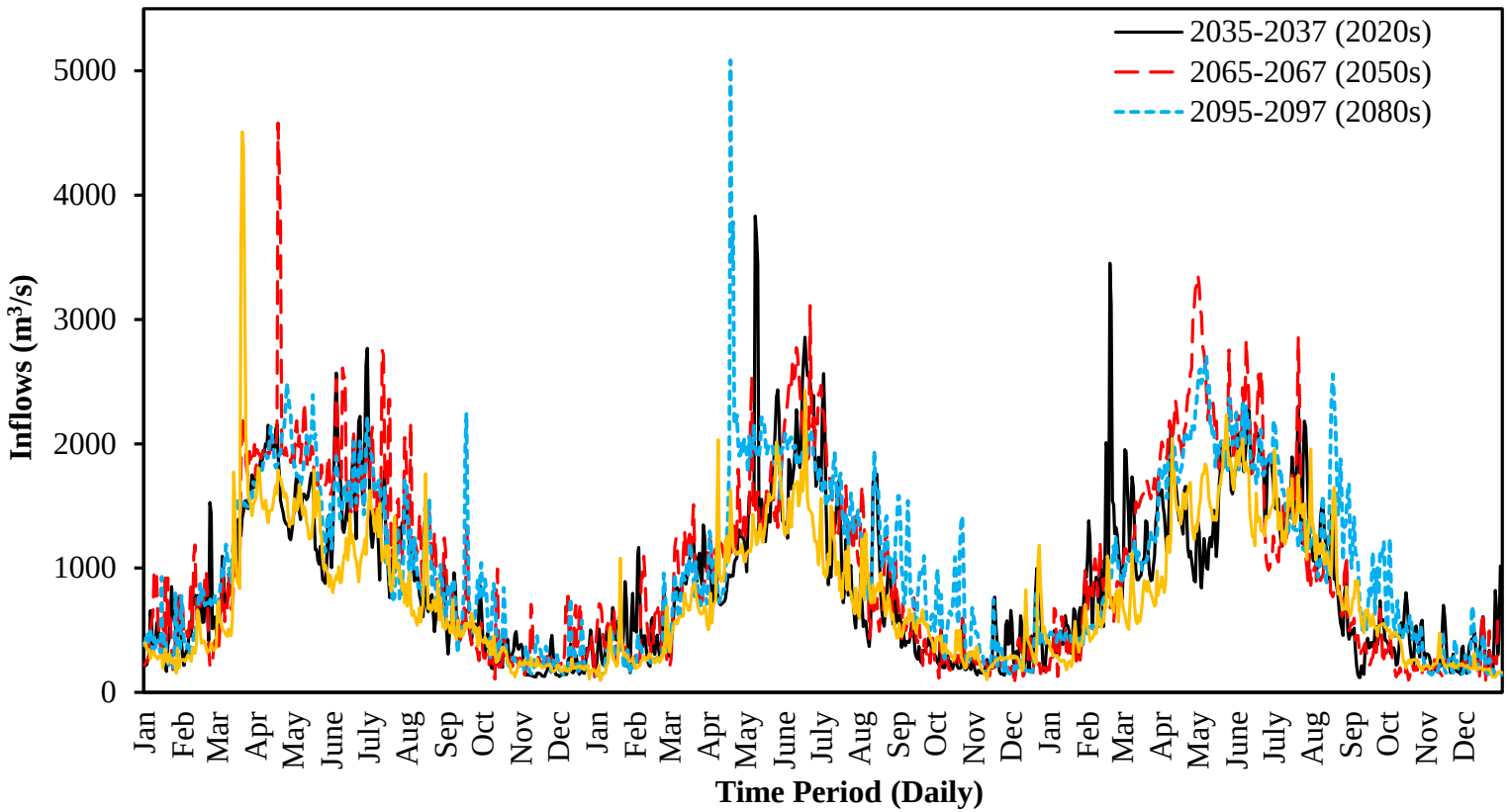

Fig. 4.13: Projection of streamflows over the 2020s, 2050s and 2080s under future scenarios.

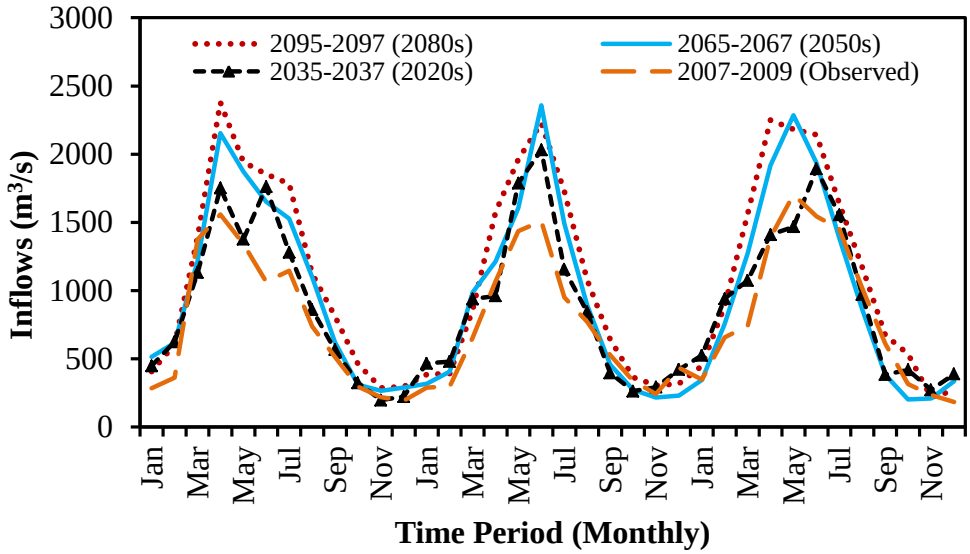

Fig. 4.14: Future simulated flows for 2035–2037 (2020s), 2065–2067 (2050s) and 2095–2097 (2080s) on a monthly basis by using downscaled data under A2 scenario at Mangla Dam.

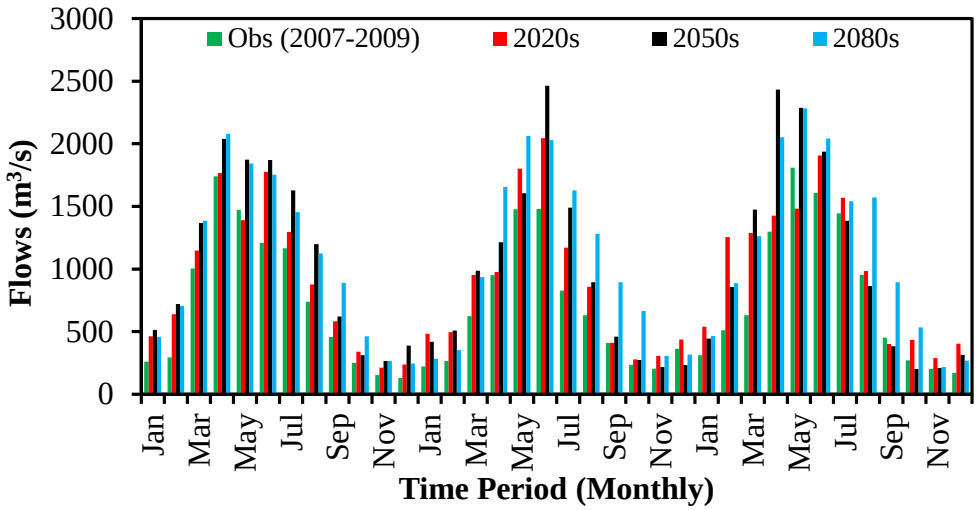

Fig. 4.15: Presentation of monthly streamflows in bar chart under scenario (A2) at Mangla Dam.

The exceedance probability curve is plotted to analyse the characteristics of discharge at Mangla Dam under future climate change scenarios. The flow exceedance probability curve is found for streamflow over the 2020s (2035–

2037), 2050s (2065–2067) and 2080s (2095–2097) to analyse the behaviour of the streamflow compared to the current scenario (2007–2009). The comparison was made at three probability levels of 20% (Q_{20}), 50% (Q_{50}) and 80% (Q_{80}) of the total time. The flow duration curves (FDCs) reflect the percentage of time that the streamflow is likely to be equal to or greater than a value of interest. For example, in the flow duration analysis using the annual flow exceedance curve, the daily average flow in Fig. 4.16 is at least 1200 m^3/s 20% of the time, 650 m^3/s 50% of the time, and 200 m^3/s 80% of the time during the current scenario. Furthermore, using the flow exceedance curve for the 2020s, the daily average flow is at least 1500 m^3/s 20% of the time, 850 m^3/s 50% of the time, and 300 m^3/s 80% of the time. Similarly, the flow exceedance curve for the 2050s shows that the daily average flow is about 1800 m^3/s 20% of the time, and almost 900 m^3/s 50% of the time, which is very close to the 2020s, and Q_{80} was nearly 250 m^3/s, which is less than the 2020s flow. In the case of the 2080s, it is clearly seen that the Q_{20} is 1900 m^3/s, whereas Q_{50} is 1000 m^3/s and the flow at 80% probability of exceedance is very close to the 2020s value (Fig. 4.16). Moreover, at 60% probability, it is observed that the streamflows for the 2020s just exceed the flows of the 2050s and then join the streamflow line of the 2080s at 80%. Furthermore, until the 12% probability of exceedance, the streamflows over the 2050s are greater than the 2080s, but after that the discharge over the 2080s is greater than the 2050s. The streamflows in all four scenarios after 80% probability are very close to each other. Furthermore, on an average annual basis, it is revealed that approximately 37.72, 58.76 and 74.04 million m^3 of water may be available over the 2020s, 2050s and 2080s, respectively, exceeding the current available volume at Mangla Dam.

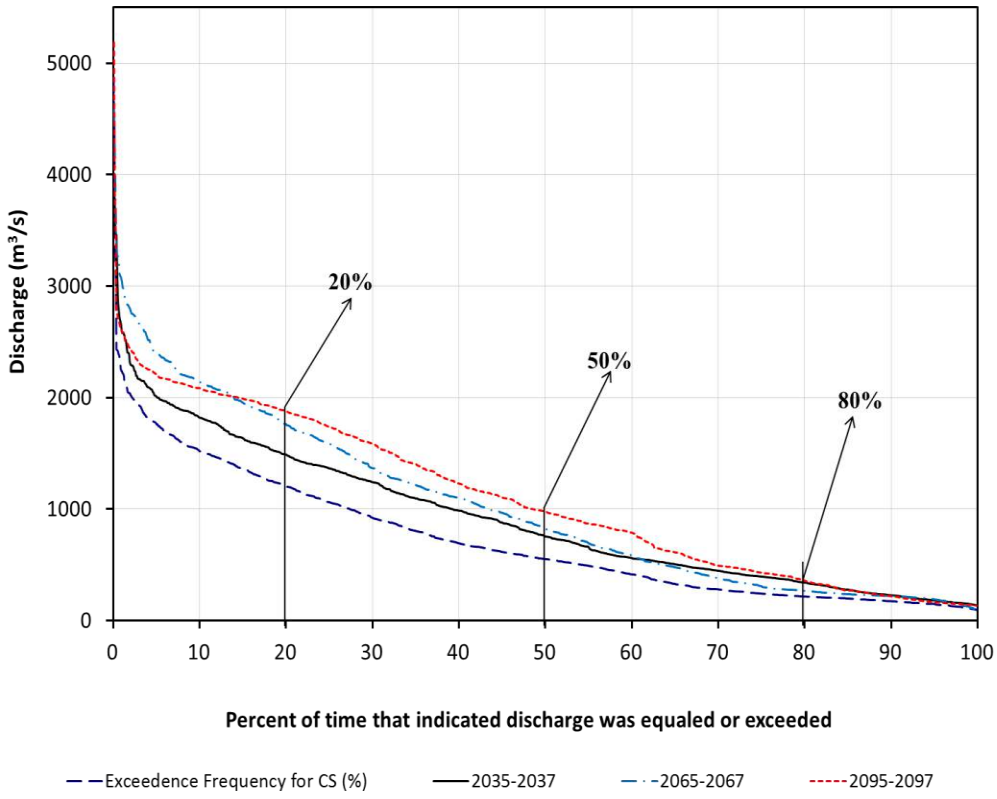

Fig. 4.16: Annual flow exceedance probability curve using mean daily discharge data identifying 20%, 50% and 80% probability points.

The frequency distribution analyses are carried out to understand the number of days when discharge was within a specified interval (Fig. 4.17). It can be seen from Fig. 4.17 that there was no significant change until the 8th class boundary (1401–1600 m^3/s) except for the 2^{nd} class boundary. Meanwhile, a significant increase and decrease over the CS and future scenarios is observed, in the number of days after the 8^{th} class boundary, which ranges from 1601–1800 m^3/s discharge. Overall, a remarkable number of days will receive discharge greater than 1800 m^3/s under all future scenarios. This shows that a considerable increase in peak flows is expected in future.

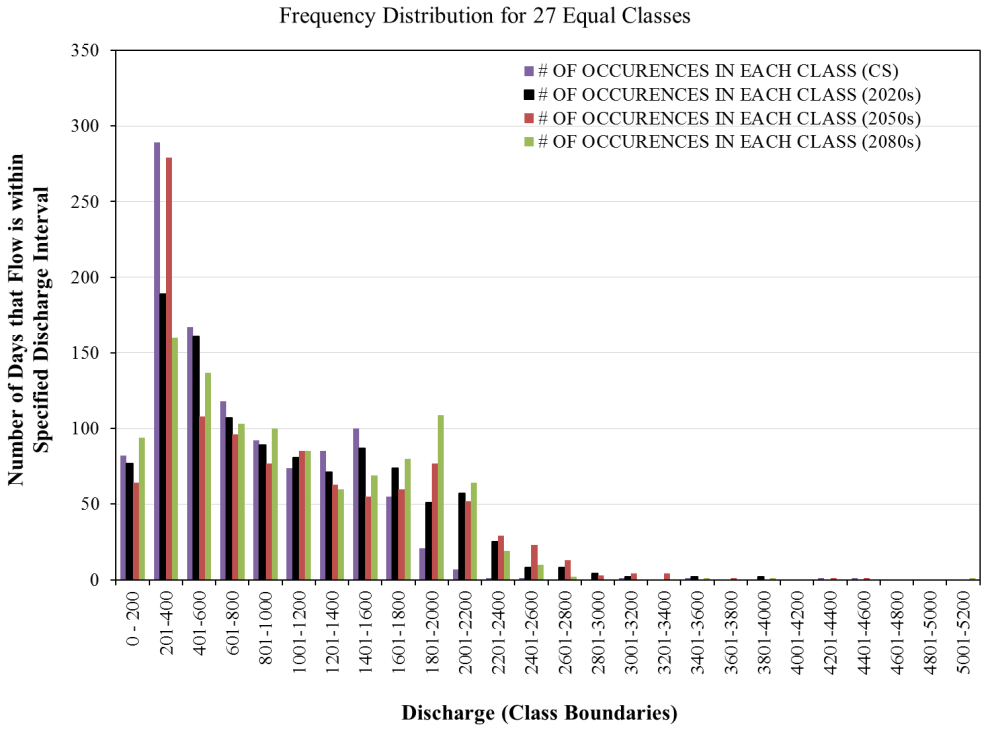

Fig. 4.17: Plot of the total number of occurrences in each class versus discharge providing the frequency distribution.

Fig. 4.18 shows that there is a large difference between the current and future scenarios, which vary from almost the 3rd to the 12th discharge class. Meanwhile, over the current scenario (CS), the cumulative days are observed to be equal to almost the 7th discharge class boundary. Moreover, a flow duration curve of 27 equal classes is plotted to understand the future projected streamflows behaviour over different discharge classes (Fig. 4.19). A large difference between the current and future scenarios is found, but all three future scenarios seem close to each other.

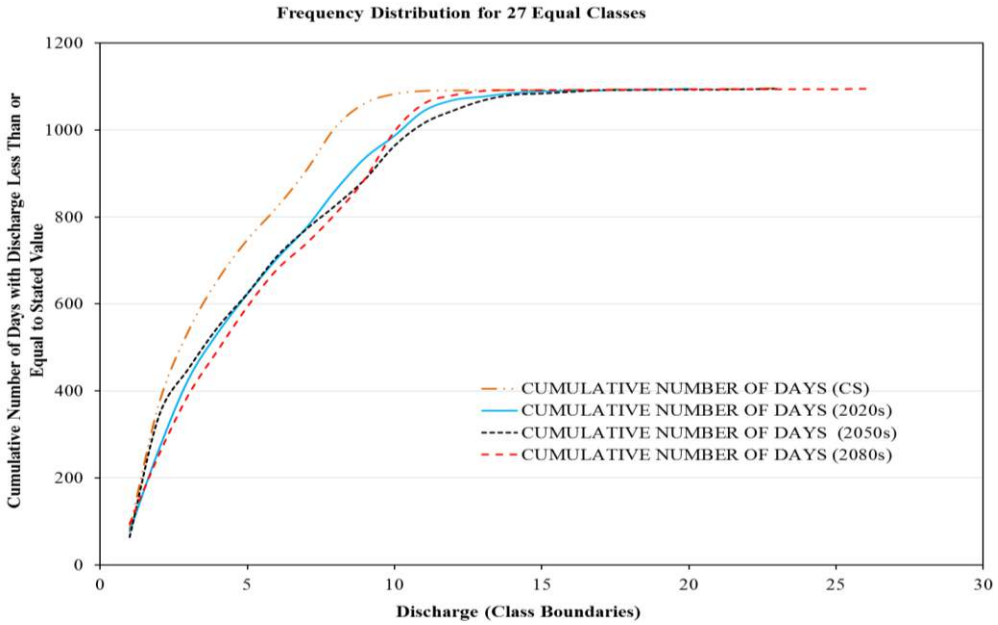

Fig. 4.18: Plot of cumulative number of occurrences over 27 equal classes versus discharge gives a frequency distribution.

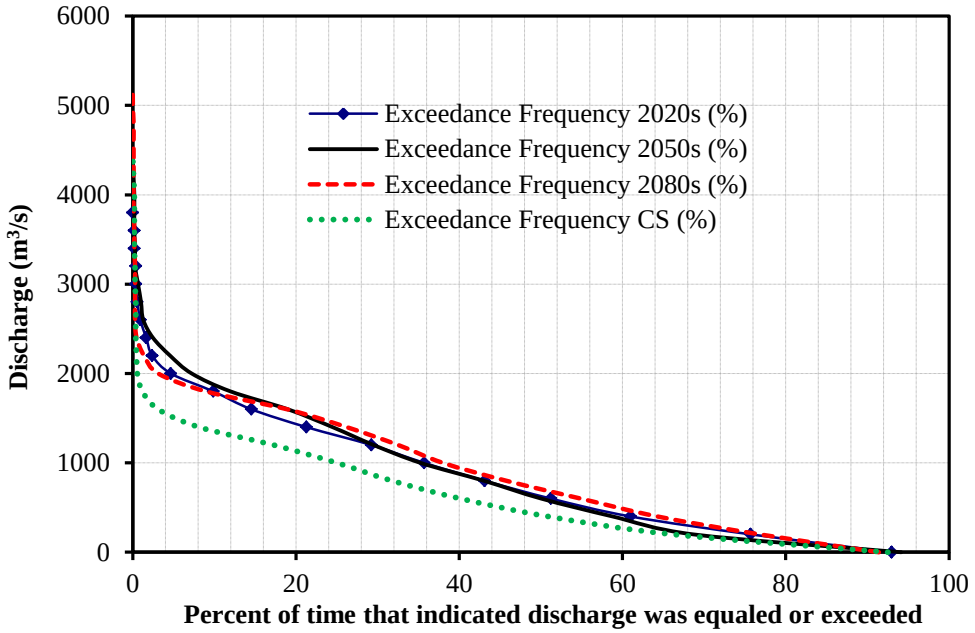

Fig. 4.19: Flow duration curve for the 27 equal discharge boundary classes over current and future scenarios.

4.8 Some Additional Climate Change Analysis by Using SRM

The impact of climate change on Mangla Dam inflows was also analysed by the application of SRM under different future climate scenarios. As discussed in chapter 3, the water management over the winter months is not optimal because of low streamflows, while the water management at Mangla Dam relies more on the summer discharge. Therefore, it is essential to simulate the impact of climate change over the summer months. The calibration period (2007–2009) was taken into account as the baseline for the current scenario (CS). For the future climate scenarios, the precipitation, mean temperature and snow cover area were used to calculate the future streamflows. The climate change scenarios were considered by making certain assumptions on the basis of previous studies in this region.

It is assumed that the cryosphere area will increase until 2050, 2075 and 2095 by up to 10% and 20% and 30% respectively, due to the increasing trend of precipitation in this region, if the temperature remains constant, as stated by Akhtar et al. (2008). Furthermore, several studies, e.g. by Hewitt (2005); Immerzeel et al. (2009)**,** have stated that an increase in the cryosphere area was observed in the neighbouring catchments of the Karakoram region. An increase in mean temperature was also observed by Akhtar et al. (2008); IPCC (2007), equal to 3 and 4°C by 2050 and 2075, respectively. By considering the aforementioned scenarios, a 2–4°C increase in mean temperature is assumed according to the elevation zones of the catchment area. A 4°C increase in mean temperature is taken in zones 1 and 2; 3°C in zones 3 and 4; 2°C in zone 5. Moreover, a 20% increase in SCA until 2075 is assumed for the climate change scenarios.

The simulated discharges under different extents of snow cover are illustrated in Fig. 4.20. An assumption was made to increase the snow cover

area by 10%, 20% and 30% by 2050, 2075 and 2095 due to increase in precipitation, while the mean temperature was kept constant. The impact on the discharge from Mangla Dam was also analysed by the decrease of 10% in the SCA. Fig. 4.20 shows that the discharge at Mangla Dam was decreased by 4.05% (41.43 m^3/s) due to decrease of 10% in the SCA. Furthermore, as a result of increases of 10%, 20% and 30% in the SCA, the mean summer (April–September) discharge at Mangla Dam was found to increase by 4.76% (53.29 m^3/s), 9.94% (117.25 m^3/s) and 15.25% (191.23 m^3/s), respectively, of the present discharge level. The aforementioned results suggest that the 1% increase in SCA in Mangla catchment can lead to an increase by 4.14 m^3/s (0.4%) in the inflows at Mangla Dam.

Moreover, an increase in the mean temperature of the catchment was assumed up to 2°C, 3°C and 4°C by 2050, 2075 and 2095, respectively, by keeping the other variables constant (precipitation and SCA). The monthly simulated discharge indicated that the 2°C rise in temperature will possibly cause an increase of almost 20% (261.19 m^3/s) in the mean summer discharge and a 3°C rise will generate 28.97% (434.92 m^3/s) extra mean summer discharge at Mangla Dam (Fig. 4.21). A 4°C increase in the mean temperature will cause an increase of 38.49% (666.84 m^3/s) in the mean summer discharge. Furthermore, a decrease of 2°C mean temperature will increase the discharge at Mangla Dam by almost 15% (139.72 m^3/s). These results indicate that, if there is a continuous rise in temperature over the Himalayan range at the rate estimated by IPCC (2007), i.e. 3.7°C at the end of the 21st century, then larger capacity reservoirs will be needed to manage the water resources and avoid flooding. It can be seen clearly in Fig. 4.21 that the hydrological regime is shifted by one month (from April to March) due to this scenario. As stated by Null et al. (2010); Young et al. (2009), the

high-altitude catchments in the south-central regions of the Sierra Nevada are most susceptible to shifts in runoff timings. Furthermore, Cannone et al. (2008) showed that several small glaciers may disappear in the next decades under current climate change scenarios. This change may affect the hydrology of high altitude catchments on a long term basis.

The simulated discharge obtained by an increase of 20% in SCA and a 2 to 4°C rise in mean temperature is presented in Fig. 4.21, which indicates that an increase of 37% (626 m^3/s) in the mean summer discharge is expected by the end of this century. This suggests that the Mangla catchment discharge is partially influenced by the snow and glacier melt. Furthermore, as discussed in chapter 3, almost 65% of the catchment is covered by seasonal snow at the end of winter and this part of the catchment will contribute largely in the climate change scenario.

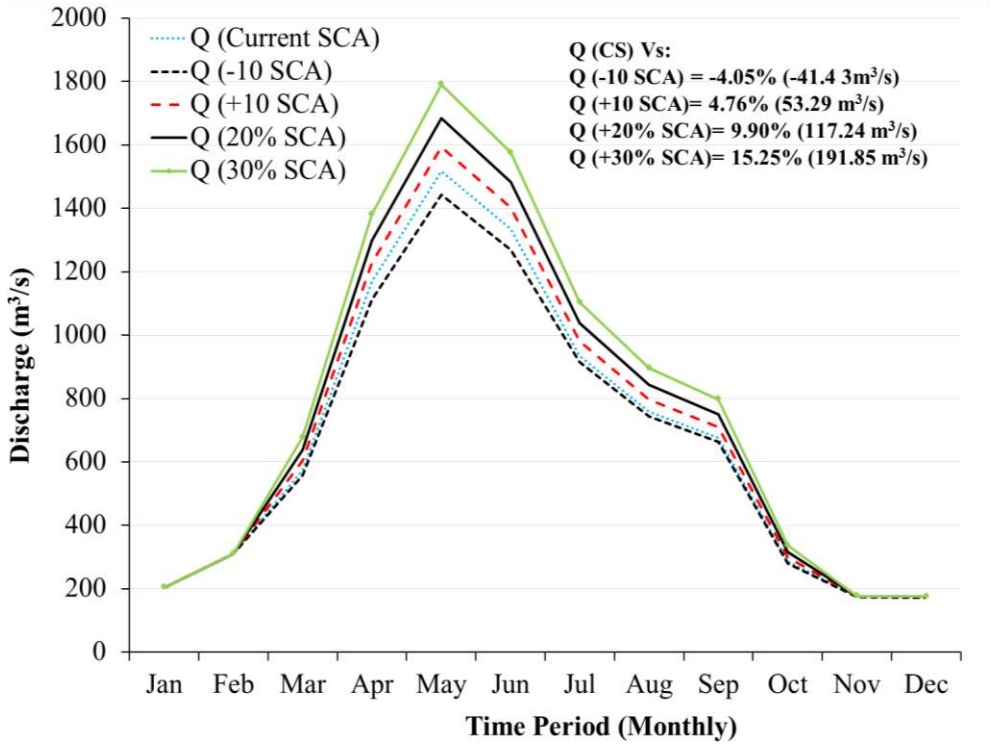

Fig. 4.20: Modelled monthly streamflow at Mangla Dam from 2001 to 2005 ($Q_{baseline}$) and for four climate change scenarios with different snow cover extents (-10%, +10%, +20% and +30%).

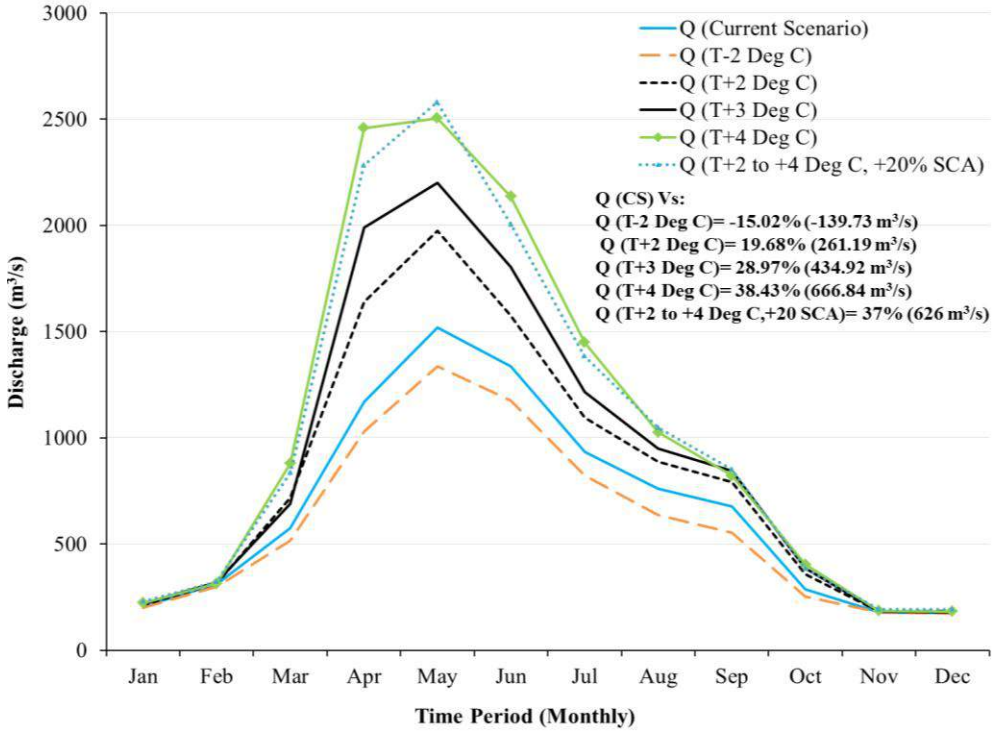

Fig. 4.21: Modelled monthly streamflow at Mangla Dam from 2001 to 2005 ($Q_{baseline}$) and for five climate change scenarios with different temperature extents.

4.9 Conclusion

In this chapter, the investigation aims to downscale climate data and simulate streamflows by using a hydrological model (HEC-HMS) under climate change scenarios to assess the impact of climate change on the hydrological regime of Jhelum River (at Mangla Dam). The SDSM model performed efficiently in downscaling the temperature variables but the precipitation downscaling was slightly less efficient. The low NS coefficient values explained the difficulty of the SDSM in projecting daily precipitation from global to regional scale predictor variables. The results obtained concluded that the SDSM is a good choice for the downscaling of climate variables for future climate analysis in Mangla watershed. Overall, the projected

temperatures indicate an increasing trend in minimum and maximum temperatures and precipitation at most of the stations, compared to the baseline data. Furthermore, the results obtained suggest that the HEC-HMS is a sophisticated option for hydrological analysis under the current and future scenarios. HEC-HMS performed efficiently over the current scenario (baseline window) by using gauge and SDSM downscaled climate variables. Over the summer months, the simulated streamflows were overestimated by the integration of downscaled data with HEC-HMS. This may be associated with some errors in the downscaled climate variables and also due to the inability of the hydrological model to represent extreme events.

The downscaled data results are slightly better under A2 than the B2 scenario. The precipitation increment is slightly higher under the A2 scenario, which may be the reason for the high runoff generation under A2 compared to the B2 scenario. The increase in runoff generation over future periods may have a major effect on Mangla hydropower generation. A large expected change in streamflows at Mangla Dam may be a viable way to overcome the deficit in power generation due to low inflows and storage.

The possible projected climate and streamflow variations provide useful information for efficient water resources management at Mangla Dam. The study proposed to provide the research on climate change impact studies in developing countries by using remote sensing and freely available data in the application of less data-intensive models. This investigation helps to increase awareness of the projected impact of climate change, which can affect the water resources at the local scale and require modifications of the existing water storage infrastructure for the sustainability of water resources against possible climate variations in the future.

Chapter 5

Reservoir Operations and Hydropower Generation: Under Current and Future Scenarios

5.1 Brief Introduction and Background

Hydrological prediction is also strictly connected with operational patterns and hydropower generation. The change in the quantity and timing of river runoff directly affects hydroelectric power production. Hydropower production on a large scale is very beneficial for the economy of a country. Most researchers have discussed the impact of water resources and climate change on hydropower production at dams and reservoir level. Gaudard et al. (2013) analysed hydrological effects on hydropower production by referring to an interdisciplinary approach integrating hydrology, economy and hydropower management using an interdependent quantitative model.

Previous studies have either investigated the impact of hydrological variation (climate change) on hydropower production (Finger et al. 2012; Hänggi and Weingartner 2012) or focused on the effect of global warming on the power market (Ahmed et al. 2012; Christenson et al. 2006; Golombek et al. 2012). "Most hydrological studies have analysed variation in natural runoff quantities in isolation; their results do not often address problems of water management", as reported by Hänggi and Weingartner (2012).

Moreover, some studies have analysed only micro-hydropower generation at the canal level, without considering the hydrological behaviour of upstream catchments and control structures. To our knowledge, no investigation has so

far considered the impacts of basin runoff on mini-hydropower at irrigation canal level. This research is an attempt to fill this gap by linking hydrological modelling approaches with operational management of hydraulic structures and downstream irrigation canal systems.

5.2 Reservoir Operation and Available Power Calculations

The Upper Jhelum Canal discharge depends on the dam outflows; therefore, the Mangla Reservoir inflow–outflow pattern has a considerable impact on mini-hydropower computations. Reservoir storage was computed by using daily inflow–outflow data by resorting to a reservoir water balance model:

$$S_i = S_{i-1} + \Delta t(I_i - O_i), \quad (5.1)$$

where S_i = dam storage at time i (m^3); Δt = time step (seconds); O_i = observed dam outflow (m^3/s); I_i = observed dam inflow (m^3/s).

The required (hydraulic and flow) data were obtained from the Punjab Irrigation and Power Department (PIPD).

There are two types of outflow from Mangla Reservoir: the regular flow is through the power house (Bong Canal) while floods are evacuated through the spillway (flood relief). The total outflow and Bong Canal discharge were obtained from the Water Resources Management Directorate (WRMD) of the Mangla Dam. The spillway outflow was estimated by using the following relationship:

$$Q_{i(f)} = O_i - Q_{i\,(BC)}, \quad (5.2)$$

where $Q_{i\ (f)}$ = spillway outflow at time i (m^3/s); $Q_{i\ (BC)}$ = Bong canal discharge used for power generation (m^3/s); i = daily time step.

At node 1 (a node is defined as the point where a distributary or branch canal diverts from the main canal (UJC) (Fig. 2)), the Bong Canal discharge splits into two parts: one goes to Jhelum River to satisfy the water requirement at Rasul Barrage and the remaining water goes to the Upper Jhelum Canal (see Fig. 2). The Bong Canal discharge into Jhelum River ($Q_{i\ (R)}$) was estimated as:

$$Q_{i,(R)} = Q_{i,(BC)} - Q_{i,1\ (UJC),} \qquad (5.3)$$

where $Q_{i,1(UJC)}$ = Upper Jhelum Canal discharge at the first node.

Along the UJC, there are 25 nodes (n=25) where the small distributaries take off from main UJC. As a consequence, the following continuity equation was used to estimate the UJC discharge at a particular node:

$$Q_{i,j(UJC)} = Q_{i,j-1(UJC)} - Q_{i,j(Dist)} - Q_{seepage}, \qquad (5.4)$$

where $Q_{i,\ j-1\ (UJC)}$ = UJC discharge at time step i and node j-1 (m^3/s); $Q_{i,\ j\ (Dist)}$ = discharge of distributary taking off from the main UJC (m^3/s); $Q_{seepage}$ = seepage losses of the reach (m^3/s), obtained from PIPD.

The potential energy can be obtained by using the elevation head difference:

$$P_{i,j} = \gamma\ Q_{i,j(UJC)}\ \Delta H_j; \qquad (5.5)$$

where $P_{i,\ j}$ = power at time step (i) and node (j) in kW; γ = specific weight of water (kN/m^3); $Q_{i,\ j\ (UJC)}$ = discharge of UJC (m^3/s); $\Delta H_j = H_j - H_{j-1}$, head difference between two nodes (m), estimated by using GDEM with integration of ArcGIS. The efficiency was considered equal to 1.

Furthermore, the kinetic energy was also obtained by using the velocity of water:

$$\text{kinetic power} = \frac{1}{2}(\rho * A * V^3); \quad (5.6)$$

$\rho = \text{density of water}$ (kg/m^3); A = area of the channel cross-section (m^2); V= velocity (m/sec).

The power was estimated by using both equations at the points called nodes for both the design and sanctioned discharge in the form of energy (MWh). Nodes were defined as the location of a point just before off-taking of branch canals from the main canal (UJC). The seepage losses and off-taking discharges were deducted (estimated by Punjab Irrigation and Power Department) from the discharge of the main canal.

The total kinetic and potential energy (Joules) can be estimated along the Upper Jhelum Canal by using:

$$E_{total} = \sum_{i=1}^{365}\left\{\sum_{j=1}^{n}\left(P_{i,j} \,.\, 8640\right)\right\}, \quad (5.7)$$

where E_{total}= total energy along the UJC (kWh).

The potential and kinetic energy was estimated at n=25 locations along the entire length (140 km) of the UJC by using Eqs (5.5) and (5.6). The total available energy was computed by using Eq. (5.7) for both the design and actual discharge.

5.3 Impact of Water Resources on Dam Management

As discussed in chapter 1, Mangla Dam has a strategic role in the irrigation of the downstream agricultural lands. The impact of the water resources availability (WRA) on mini-hydropower generation at Upper Jhelum Canal (UJC) was studied by using Eqs (5.5) and (5.6). The inflow–outflow and storage pattern of the reservoir have a large effect on the discharge of the downstream canal system and the mini-hydropower production since it is

directly proportional to canal discharge. The maximum inflow, outflow (through the power house and flood relief) and storage were observed during the summer and spring months. The dam's operational pattern indicates that the reservoir storage starts from March (start of spring) and the dam is completely full in September (end of summer) for the winter water regulations. The reservoir storage volume varies from approximately 0.70 to 7.25 km^3. The command area of Mangla Reservoir is approximately 6 million hectares (Archer and Fowler 2008), which provides irrigation through the linked canal system (Figs 1.6 and 5.7). The major crops of this area are rice and wheat during the Kharif (wet period: June to Sep.) and Rabi (dry period: Oct. to Feb.) seasons (Hussain 2005). Since the crop water requirement (irrigation depth) of rice is much higher than that of wheat, the Bong Canal discharge during most of the summer season was found to be much higher than in the winter (Fig. 5.1 A and B). In contrast, large outflow variability was found in the winter months, in some of which the outflow is as large as 1000 m^3/s because of the high storage volume availability. During some of the winter months, the outflows were very low or zero because of the low storage volume available. A rapid variation in the dam outflows pattern through the power house was observed throughout the data series. It can be seen clearly from Fig. 5.1 that the outflows from the dam depend upon the inflows. Meanwhile, the UJC discharge does not vary rapidly in time, which indicates that the reservoir operation depends primarily upon storage volume and secondly on the downstream agriculture requirements (Fig. 5.1 (B)). Therefore, the UJC discharge is much less than the design capacity. As discussed in the General Introduction section, Pakistan's major agricultural lands are located in the eastern part of the country (Punjab) while the major water resources (rivers) rise in the northern part. Therefore the stored water of the dams is then delivered to the eastern part of the country

through a major irrigation and linked canal network as shown in Fig. 2 (see the General Introduction). The overall water resources of the country were equally divided in 1991 according to the water requirements of the provinces, to overcome water conflicts between provinces, in the "Pakistan Water Apportionment Accord" (IUCN 2010; Sharif 2010). This may be the main reason why the actual discharge of the UJC is less than the design and a large part of Bong Canal discharge is released towards Jhelum River to satisfy the specified water requirements of other canals such as Lower Jhelum Canal (LJC) and the Rasool-Qadirabad Link Canal (QBLC) (see Fig. 1.6 and 2). These water deficits in UJC can be overcome to some extent by enhancing the reservoir's storage capacity, through which water losses in the form of flood relief can be utilized efficiently.

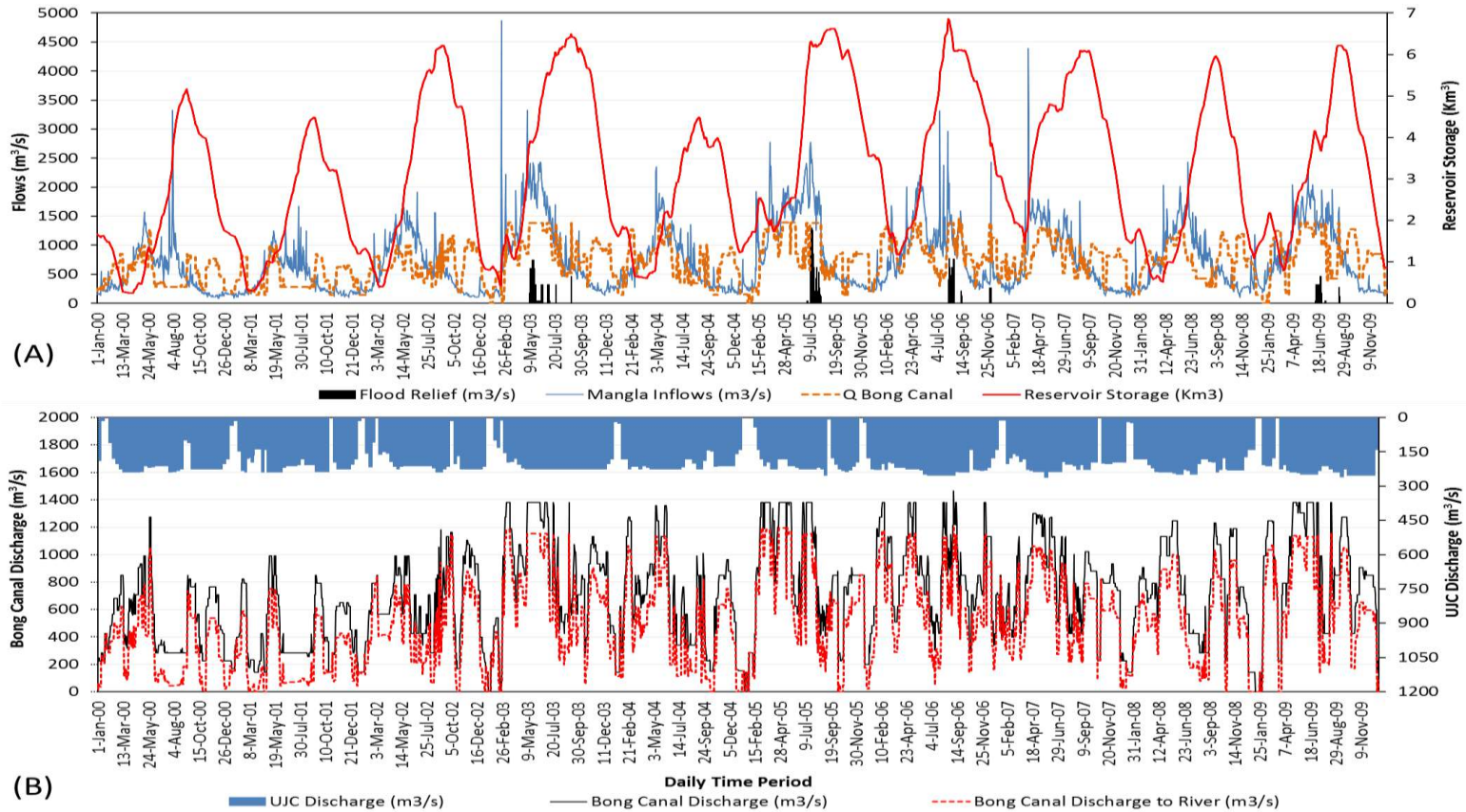

Fig. 5.1: (A) Comparison of daily inflow, outflow (through flood relief and power house) and reservoir storage pattern and (B) discharge pattern of Bong and Upper Jhelum Canal (UJC) from 2000 to 2009.

5.4 Impact of Water Resources on Micro-hydropower Production

Micro-hydropower potential was estimated at 25 different nodes (see Fig. 1.6) along the Upper Jhelum Canal (Fig. 5.2). The total potential energy for the average annual (216 m^3/s) and design discharge (358 m^3/s) was found to be 221 and 407 GWh, which is 2.52% and 4.64% of Mangla's energy generation capacity, respectively. Similarly, the gross theoretical kinetic potential was found to be 27 and 50 GWh for the sanctioned and design discharges respectively. The difference was significantly high in the theoretical potential and kinetic potential, which may be due to a difference in the equation approach. The energy level at nodes 4 to 10 was found to be high due to the high elevation head.

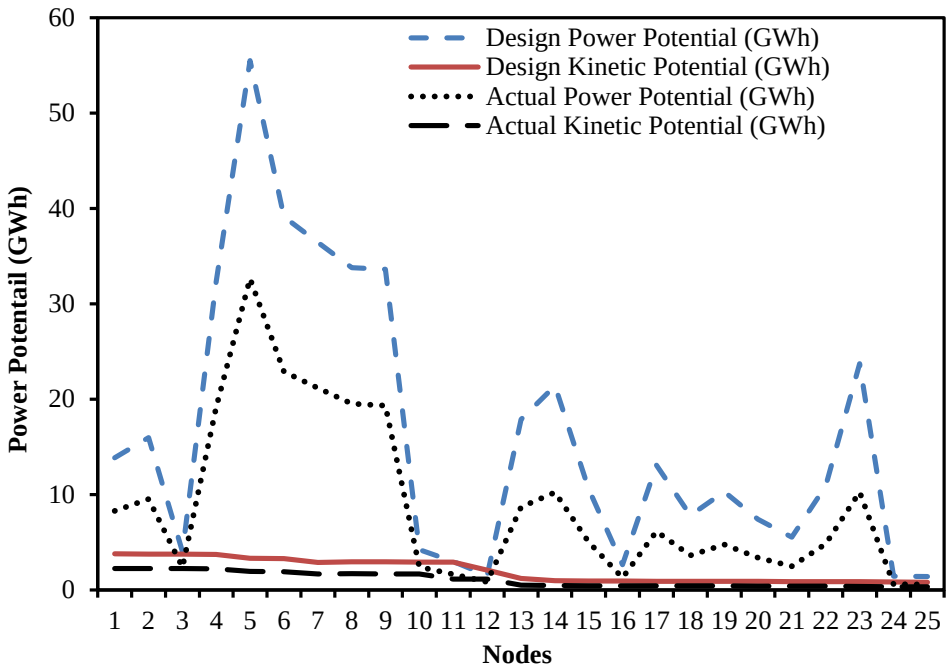

Fig. 5.2: Available micro-hydropower production along the Upper Jhelum Canal at different nodes for design and actual discharge.

5.5 Operational Pattern of Mangla Dam under Climate Change Scenarios

The operational pattern of inflow–outflow of Mangla Dam will also change due to changes in water availability under future scenarios (Figs 5.3, 5.4 and 5.5). The expected outflows were estimated by using a linear model. This linear relationship between inflow and outflow was developed by using previous available records for each month. It can be seen clearly in Figs 5.3, 5.4 and 5.5 that the outflows depend upon the inflow pattern. As the dam receives high inflows, the outflow also approaches the maximum level. The storage level of the dam is expected to increase even higher than the recent full capacity of the dam (7.25 km^3). The maximum water storage according to the inflows and outflows of the dam is expected in the 2050s and 2080s. Moreover, due to increase in inflows, several flood relief events are also expected in future. As discussed in chapter 4, in the future scenarios the time span of high inflow is likely to increase compared to the current scenario. Therefore, the maximum outflows level (1386 m^3/s) time span through the power house is also expected due to the increase in inflows, which can help to increase hydropower generation at Mangla Dam. Moreover, with the increase in the storage capacity of Mangla Dam, the excess amount of water can be stored for beneficial use during low inflow months. A considerable amount of water is expected through the spillway in the future scenarios, particularly in the 2050s. Since UJC is taking a specified amount of discharge from Bong Canal, considering not the Bong Canal discharge (high or low) (Fig. 5.1) but the water deficit at the downstream agricultural lands of UJC (Hussain 2005), the excess water/ storage availability in future will help to increase the discharge.

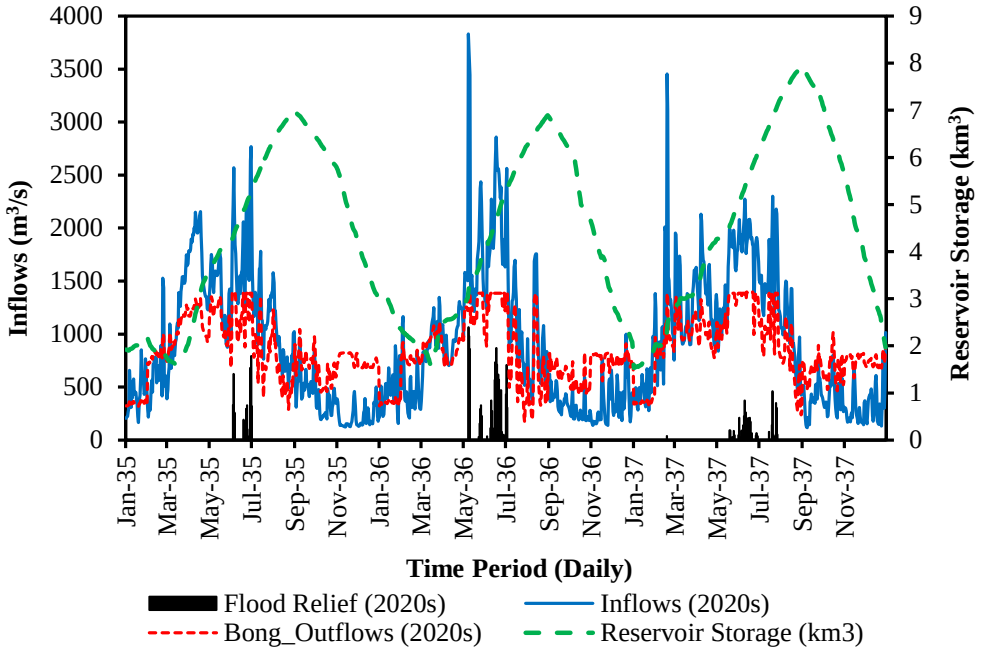

Fig. 5.3: Comparison of projected daily inflow, storage volume of the dam and Bong Canal outflow (through flood relief and power house) over the 2020s.

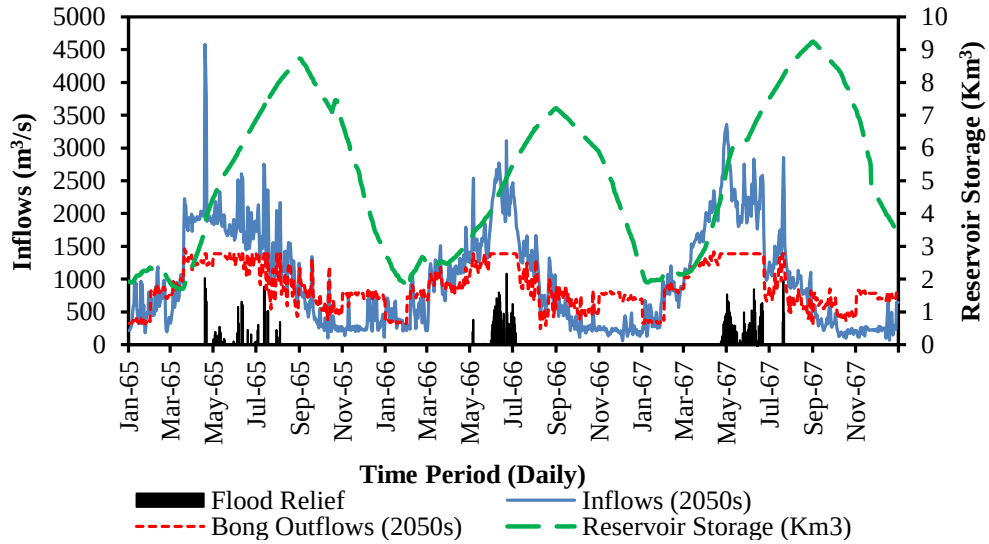

Fig. 5.4: Comparison of projected daily inflow, storage volume of the dam and Bong Canal outflow (through flood relief and power house) over the 2050s.

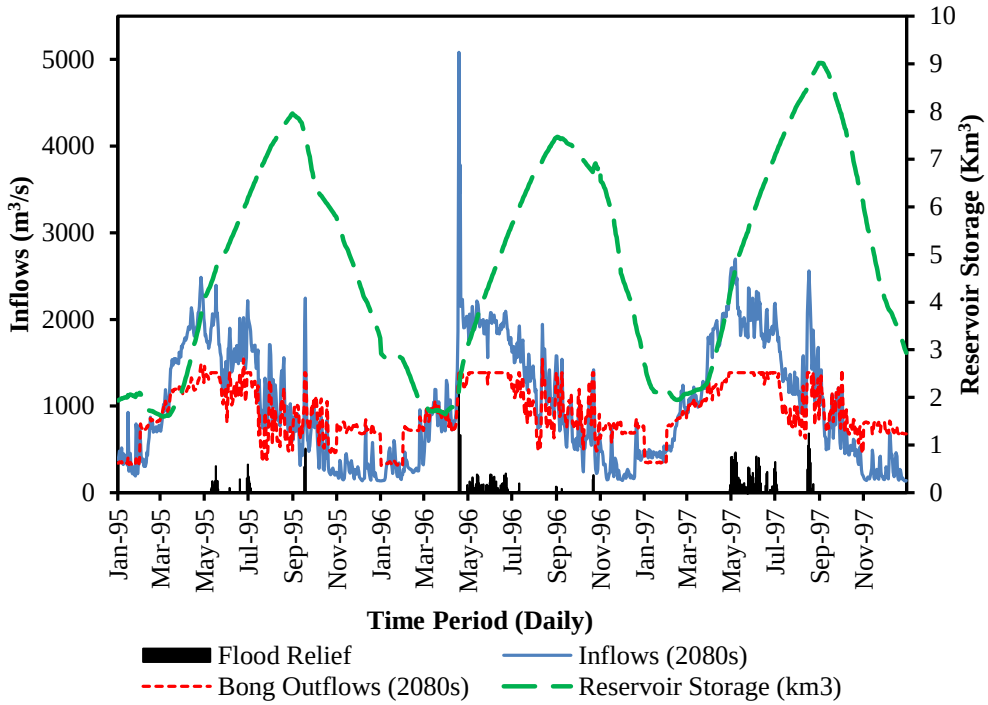

Fig. 5.5: Comparison of projected daily inflow, storage volume of the dam and Bong Canal outflow (through flood relief and power house) over the 2080s.

5.6 Impact of Climate Change on Hydropower Generation

As mentioned in the study area section, the maximum outflow capacity through the power house of Mangla Dam is 1386 m^3/s. Due to low inflows during the current scenario (CS) and low reservoir storage, the hydropower generation at full capacity level is not possible at Mangla Dam. The flow duration curve of the observed and simulated inflows was plotted for comparison of the discharges. Fig. 5.6 shows that approximately 15% of the total inflows of Jhelum River at Mangla Dam were found to be equal to or greater than the outflows required for full capacity hydropower generation in the current scenario. On the other hand, over the projected scenarios the

inflows approximately 21.5, 28.5 and 35.5% of the total time (365 days) were equal to or greater than 1386 m^3/s in the 2020s, 2050s and 2080s, respectively. This indicates that if the projected inflows percentage is 6.5, 13.5 and 20.5% greater than the current values over the aforementioned scenarios, then the same percentage of hydropower can also be increased, which can recover the power generation deficit during low inflows or storage at Mangla Dam to some extent. Furthermore, the additional quantity and percentage of hydropower generation at Mangla Dam in future scenarios was estimated by using the power equation (Table 5.1). The hydropower was computed at 15% streamflow (Q_{15}), 35% (Q_{35}) and 50% (Q_{50}) of the total time under the current and climate change scenarios. The Q_{15} particularly was selected because this level of streamflow is equal to 1386 m^3/s over the current scenario, which is needed for hydropower generation at full capacity. Approximately 15.03, 30.38 and 31.45% increases in hydropower generation would be possible under the climate change scenarios, compared to the current generation (Table 5.1), by raising Mangla Dam. As discussed in section 4.7, on an average annual basis approximately 37.72, 58.76 and 74.04 million m^3 volume of water can be increased in the 2020s, 2050s and 2080s, respectively, compared with the currently available volume at Mangla Dam. This additional amount of water could also help to reduce the country's energy and irrigation water deficit.

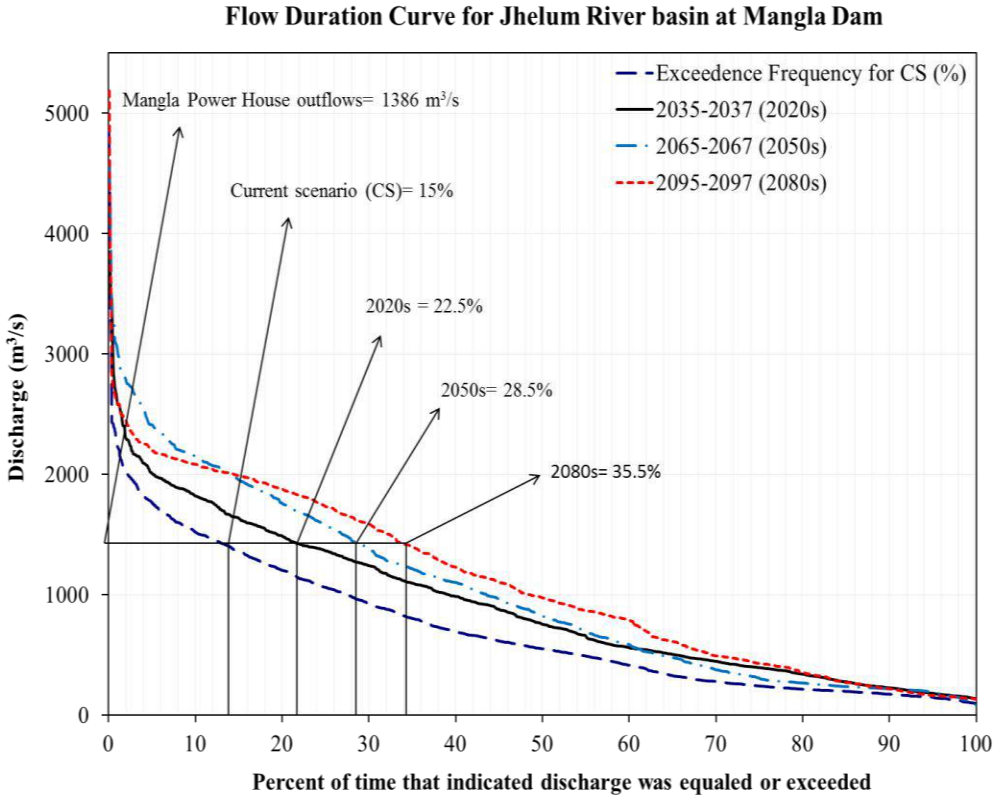

Fig. 5.6: Comparison between flow duration curves for the observed stream flows (current scenario (CS)) and future scenarios over 2035–2037 (2020s), 2065–2067 (2050s) and 2095–2097 (2080s).

Table 5.1: Expected hydropower generated under future climate change scenarios at different discharge levels.

Scenarios	Q (m^3/s)	Head (m)	P (kW)	P (MW) at 100% Efficiency	P (MW) at 82% Efficiency	Energy (MWh)	Percent (%) increase in Power
Discharge that is equalled or exceeded 15% of the time							
CS	1386	89.93	1221501	1222	1002	8774287	-
2020s	1632	89.93	1350173	1350	1117	9698563	15.03
2050s	1991	89.93	1737070	1737	1434	12477720	30.38
2080s	2022	89.93	1782017	1782	1461	12800584	31.45
Discharge that is equalled or exceeded 35% of the time							
CS	822	89.93	724440	724	594	5203798	-
2020s	1116	89.93	983546	984	807	7065011	26.34
2050s	1239	89.93	1091948	1092	895	7843681	33.65
2080s	1418	89.93	1249703	1250	1025	8976868	42.03
Discharge that is equalled or exceeded 50% of the time							
CS	562	89.93	495298	495	406	3557828	-
2020s	838	89.93	738541	739	606	5305089	32.93
2050s	856	89.93	754405	754	619	5419040	34.34
2080s	990	89.93	872501	873	715	6267348	43.23

5.7 Hydropower Production from Future Outflows of the Bong Canal

The Bong Canal is used as a power canal which receives water from the Mangla power house. Therefore, changes in the outflows of the Bong Canal under future climate change scenarios significantly affect the energy generation. Since the power (1000 MW) is already being generated at Mangla Dam by using 1386 m^3/s outflow discharge, which is the maximum power generation capacity of the dam, the expected outflows as presented in Figs 5.3, 5.4 and 5.5 for the 2020s, 2050s and 2080s, respectively, are greater than the current outflows. In particular, the temporal scale of outflows required for full capacity energy generation is increased due to increase in the inflows and storage. The average annual power generation under the expected outflows is 753, 810 and 839 MW in the 2020s, 2050s and 2080s, respectively. These power generations are 7.36% (2020s), 13.91% (2050s) and 16.88% (2080s) more than the current (697 MW). The detailed power/energy generation capacities under different scenarios are presented in Table 5.2.

Table 5.2: Expected hydropower/energy generation under future climate change scenarios at Bong Canal outflows.

Scenarios	Average power generation (MW)	Average annual energy generation (GWh)	% increase under future scenarios
CS	697	2035.60	-
2020s	753	2197.53	7.36
2050s	810	2364.40	13.91
2080s	839	2448.78	16.88

5.8 Micro-hydropower Production at UJC under Climate Change Scenarios

The UJC discharge is almost constant throughout the data record; therefore, the linear relationship between the Bong Canal and UJC discharge was not

devolved. Therefore, it is assumed that discharge of UJC will increase by 10 and 20% due to increase in Mangla Dam inflows. Due to increase in UJC discharge by 10 and 20%, the potential energy will increase to 257 and 290 GWh, respectively, compared to 227 GWh in the current scenario. Moreover, by using the kinetic energy relationship, with 10 and 20% increases of water availability in UJC, the energy generation will increase to 29 and 32 GWh, respectively, compared to 27 GWh in the current scenario. This additional energy generation will help to overcome the energy crisis in Pakistan.

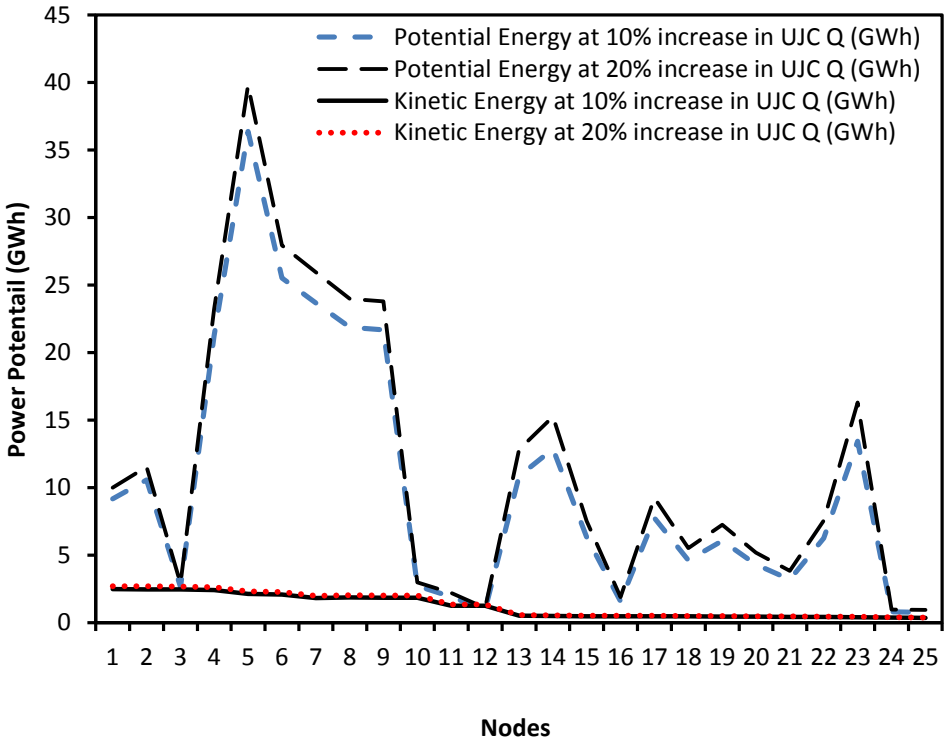

Fig. 5.7: Micro-hydropower generation at UJC considering 10% and 20% excess water availability in future scenarios.

5.9 Future Water Supply and Demand: Post Mangla Raising

The government of Pakistan announced in 2003, to raise the Mangla Dam by 9.14 meters (http://wapda.gov.pk/htmls/ongoing-index.html). The purpose of raising it is to regain storage capacity that has been reduced due to sedimentation, in order to store the summer flow (flood relief) to meet the need for supplementary irrigation supplies in the downstream regions during the winter low-flow period, increasing the power generation, and improve flood control and water supply (for domestic and industrial use). The proposed dam will have a maximum height of 379 m and its gross storage capacity will be increased from 7.25 (initially at the time of construction) to 9.12 km^3 (Fig. 5.8) (source: WAPDA). Overall, the gross storage capacity of about 3.57 km^3 will be increased because the storage has been reduced about 22.84% from the original level (7.25 km^3) (Table 5.3).

Table 5.3: Some salient features of un-raised and raised Mangla Dam (*source: WAPDA*).

Salient Features of Mangla Dam	**Un-raised**	**Raised**
Water surface area at conservation level (km^2)	259	324
Catastrophic flood level (m)	375	384
Maximum conservation level (m)	367	379
Minimum operation level (m)	317	317
Gross storage (km^3)	7.25	9.12
Live storage (km^3)	6.58	8.51
Mean annual flow (km^3)	28.61	28.61
Maximum height (m)	139	148
Power generation (MW)	1000	1120
Bong Canal capacity (m^3/sec)	1387	1387
Bong Escape capacity (m^3/sec)	1219	1219

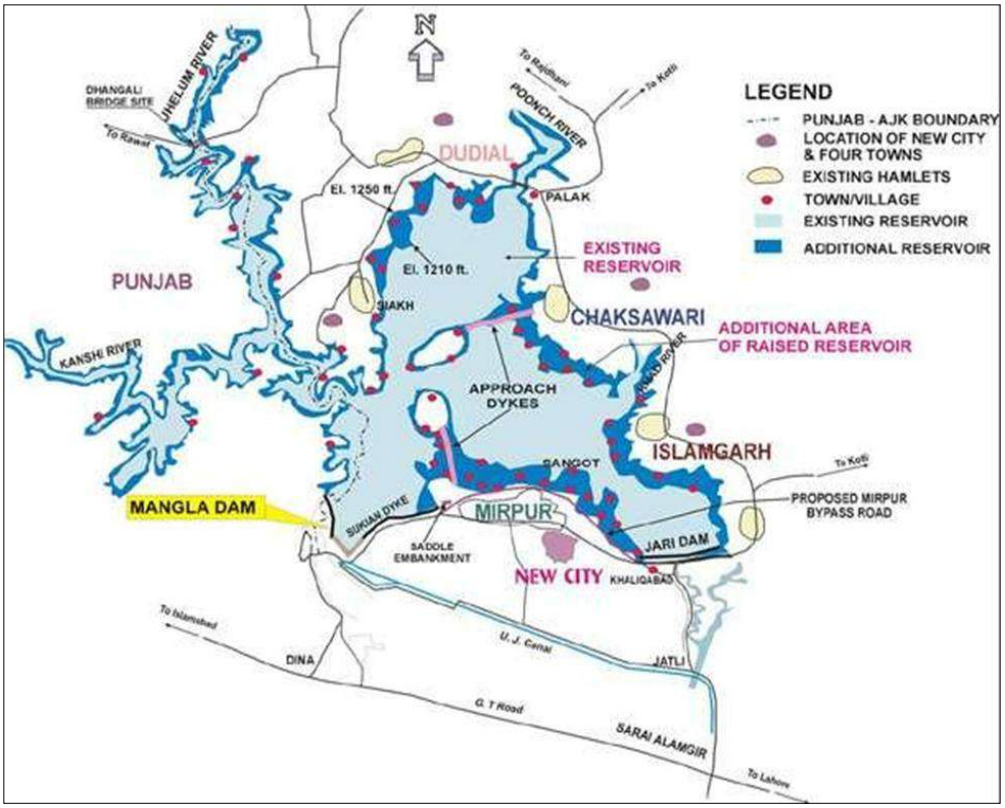

Fig. 5.8: Mangla Reservoir before and after raising project (*source: WAPDA*).

The historic data analysis of available inflow and outflow suggested that, in the case of increase in irrigation and domestic demand, the raising of Mangla Dam would be very constructive. Approximately 29.06 km^3 average annual water is available at Mangla, and if dam will able to store complete amount of water, then, according to the current water demand, almost 2.82 km^3 (75% of the raised volume of 3.57 km^3) of extra water will be available at the end of the year (Fig. 5.9 and Table 5.4). Moreover, if the demand is increased by 5% and 10%, then approximately 42.2% and 6% of the raised volume will be available. Furthermore, Fig. 5.10 shows that the capacity of the reservoir will increase after raising, but with time it will be reduced again due to

sedimentation. This situation suggests that new large reservoirs will be needed to manage and fulfill the future water demands of the country.

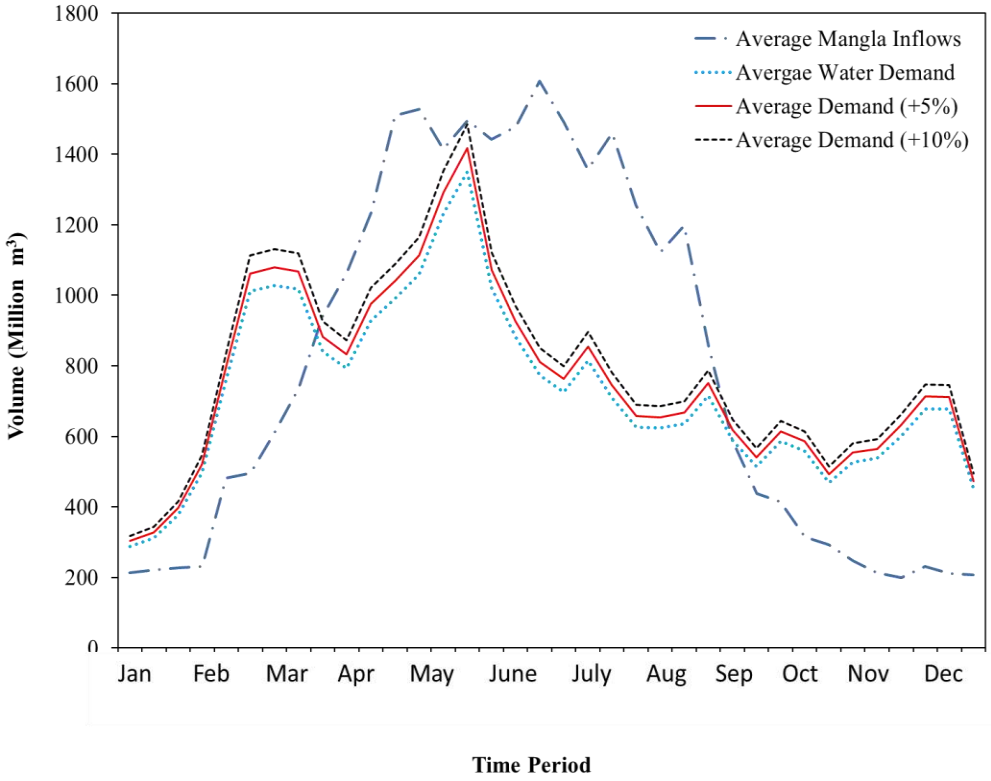

Fig. 5.9: Average monthly Mangla inflow and water demand under current, 5% and 10% at downstream scenarios (1967–2010).

Table 5.4: Effect of different levels of demand on average annual available volume (1967–2009) at Mangla Dam.

Scenarios	**Volume (km^3)**	**Volume Difference (km^3)**	**(%) Volume of expected after Mangla raising (3.57 km^3)**
Average annual available volume	29.06	-	-
Current demand	26.20	2.82	79.0%
At 5% additional demand	27.52	1.51	42.2%
At 10% additional demand	28.83	0.20	6.00%

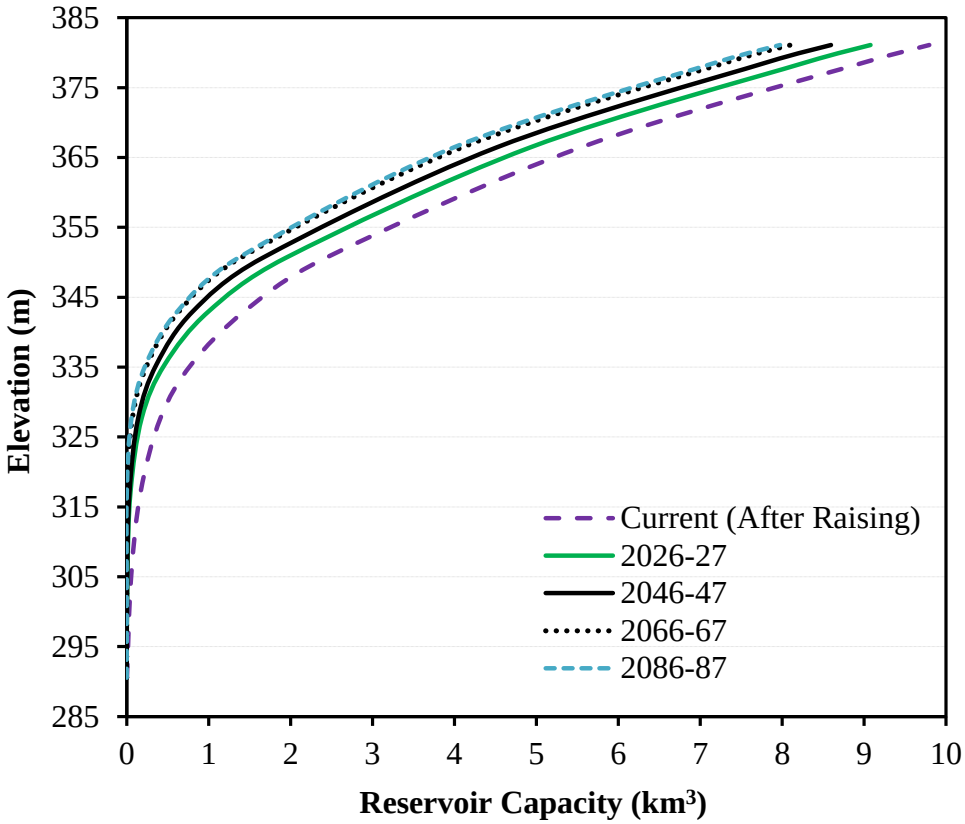

Fig. 5.10: Capacity curve of the Mangla Reservoir for current situation (after raising project) and up to 2086–87.

5.10 Conclusion

This investigation presented the impact of the catchment hydrology on hydropower generation at Mangla Dam and micro-hydropower along the downstream canal system, under current and future climate scenarios. The study suggests that the Mangla Reservoir's operational pattern has a large effect on hydropower generation at Mangla Dam and along the Upper Jhelum Canal. An operational analysis of the Mangla Dam was also performed, indicating that the reservoir storage and outflow pattern depend on summer inflows.

The impact of climate change on hydropower generation at Mangla Dam can significantly overcome the energy deficit by the utilization of additional water in future. Furthermore, the micro-hydropower largely depends on the available canal discharge, which depends on the inflow–outflow, storage volume of the reservoir and irrigation requirement. The micro-hydropower plants could be helpful in minimizing the energy deficit of the Mangla Dam to some extent because the UJC discharge is not significantly influenced by the reduction in the Bong Canal discharge.

Any change in the available water resources of Mangla Basin resulting from climate variability or socio-economic factors will have a serious impact on both food security and power generation. The water demand for urban and agricultural use is expected to increase in the future due to a rapid increase in the population. Although the discharges from all of the Jhelum River (Mangla Dam) tributaries tend to increase under the climate change scenarios, the present water storage is not capable of conserving this in future due to the rapid increase in the population. This will become more challenging with mismanagement of the water resources, environmental degradation (degradation of the river basin, etc.) and an accelerated reduction in the present storage capability due to sedimentation. Therefore, it is of the utmost importance to closely study the building of at least 2 or 3 large capacity multi-purpose dams e.g. Diamer Basha Dam, Rohtas and Kalabagh Dam on the Indus and Jhelum Rivers. Furthermore, the raising of large dams (Tarbela and Mangla Dam) will be very beneficial for the storage and management of available water resources in the country.

Chapter 6

Testing of Kinetic Turbine

6.1 Brief Introduction

In chapter 5, the energy generation was estimated on a theoretical basis by using the kinetic and potential energy relationship and considering the 100% efficiency of the system. Energy generation estimation using theoretical equations normally overestimates the results as compared to the actual situation. The hydropower generation computation analyses are strongly connected with the type and efficiency of the turbine and dimensions of the system. Therefore, it is important to understand the efficiency of the system which needs to be installed for the hydropower generation at the canal system. In this chapter, experiments were conducted in the laboratory using a kinetic turbine to compute the turbine efficiency at different discharge and velocity levels. These experimental data were further applied on the Upper Jhelum Canal (UJC) to estimate the energy by using the kinetic energy equation (Eqs (5.6) and (5.7)).

6.2 Experimental Work for Micro-hydropower Generation

Development and design of a vertical axis turbine: Experimental results on a laboratory prototype

A. The Experimental Work

In this phase of the project, an experiment was carried out in the laboratory by using a kinetic turbine in order to study the similarity in the behaviour of fluid dynamics and then to understand how these results can be related to the

theoretical calculations at UJC using turbine dimensions and efficiency. The turbine used for the experiment is presented in Fig. 6.1.

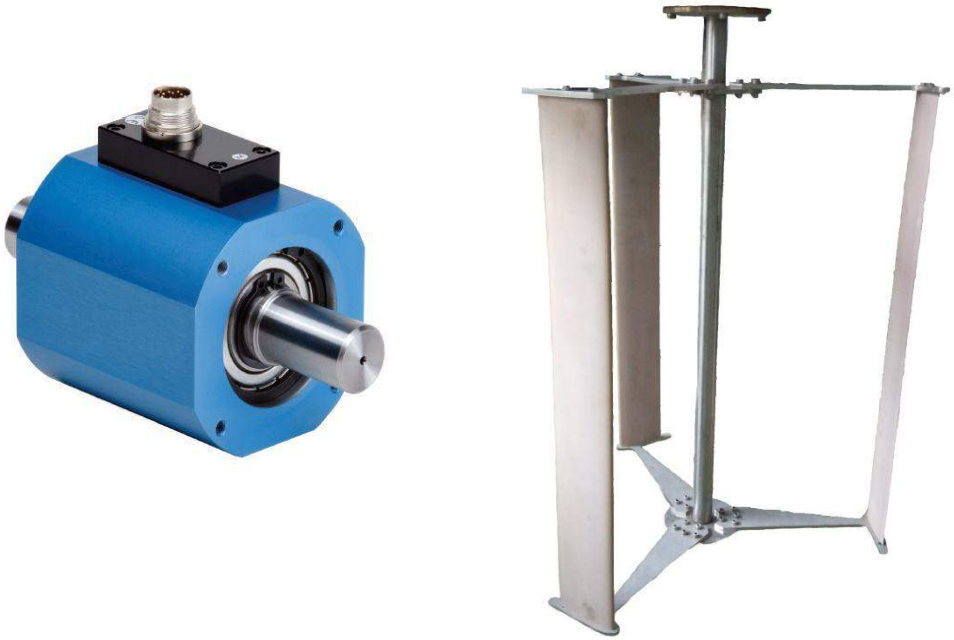

Fig. 6.1: Kinetic turbine

B. Experimental System

Laboratory experiments were carried out in an open channel 15 m in length and 0.88 m wide. The flow rates at which the turbine was tested range from 0.26 to 0.345 m^3/s (260 l/s-346 l/s), which is equivalent to an average speed of flow in the turbine of between 0.38 and 0.51 m/s.

The control and measurements were carried out using a generator controlled in speed (or torque) and a torque transducer inserted between the latter and the turbine, capable of measuring the torque and speed of rotation on the axis.

An ultrasonic sensor allowed the measurement of the level downstream of the turbine and thus the extent of the losses of hydraulic load. Data were acquired and saved to a multifunction data acquisition card from National Instruments.

The control driver of the motor/generator allows control of the current intensity (therefore torque) or speed. The speed control is performed with feedback loops that detected a certain weakness in maintaining the rotation speed equal to that set. As a consequence, its variability continues over a single lap, due to the characteristic behaviour of this type of turbine, where the coefficients of lift and friction constantly change depending on the angle of the blade to the flow lines. It was therefore chosen for the control of the turbine torque, which favours in fact the speed changes on the lap, but allows direct control of the intensity of the motor current.

Figs 6.2 and 6.3 show the experimental system. The turbine has been positioned on a support that is supported and fixed to the side-walls of the channel. On one side of the channel the system data acquisition and control have been set up, while the ultrasonic sensor is positioned downstream of the turbine. The complete system used for control and data acquisition is presented in Fig. 6.4.

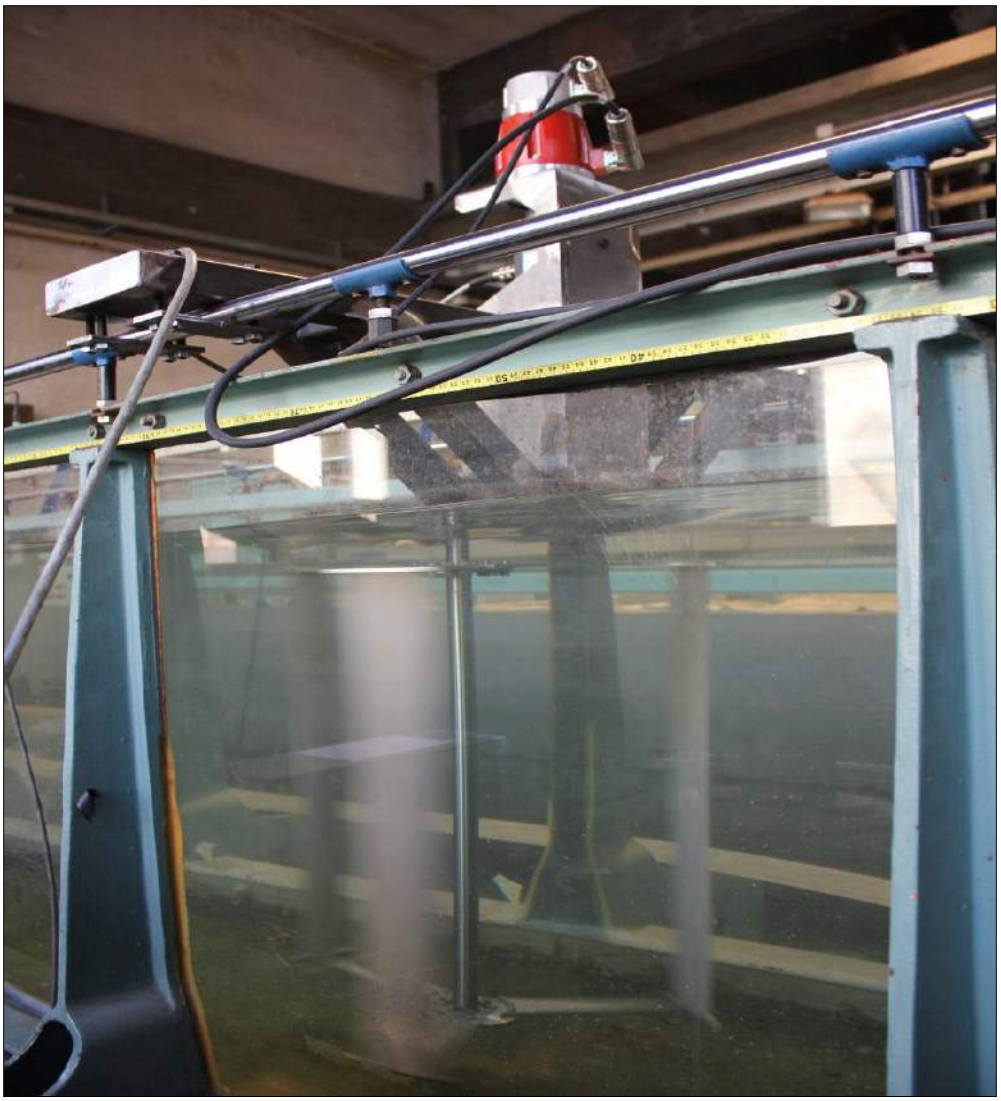

Fig. 6.2: Experimental system - turbine and motor control

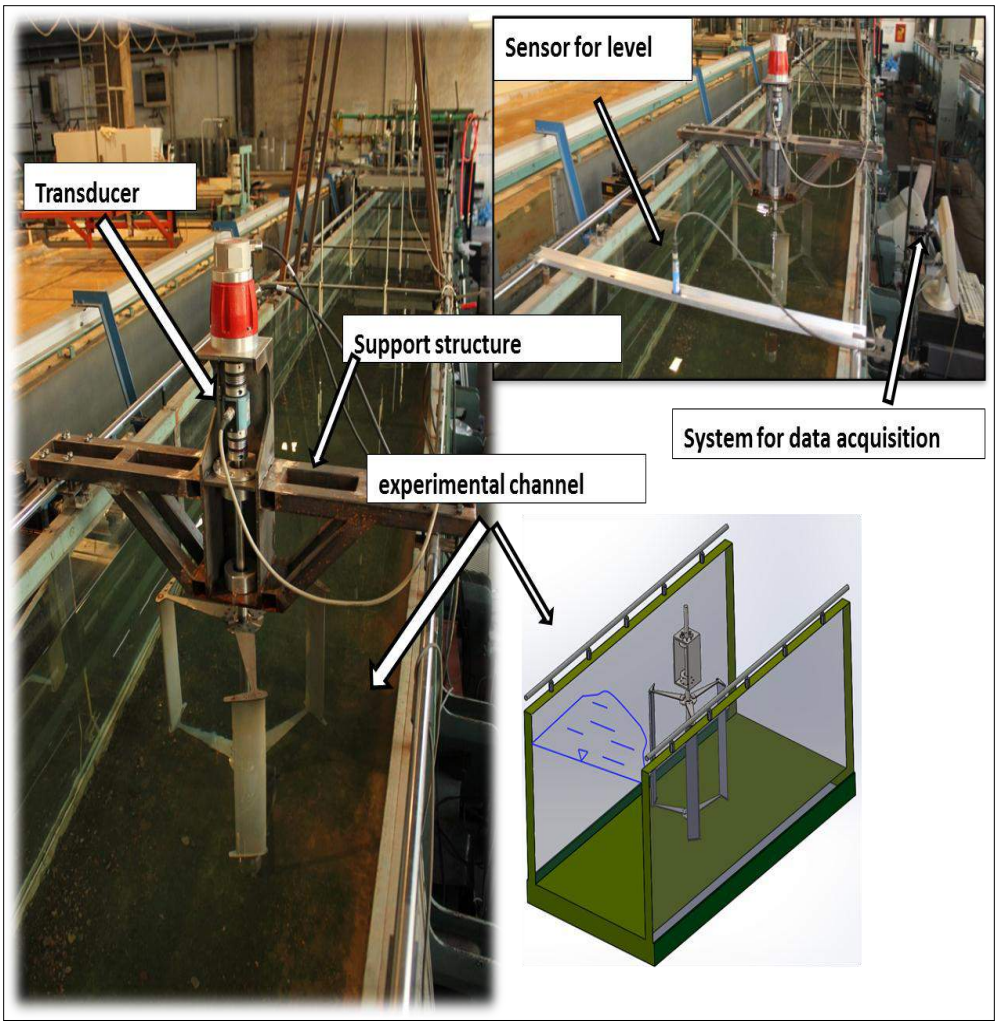

Fig. 6.3: Experimental system - channel, the turbine and the support structure

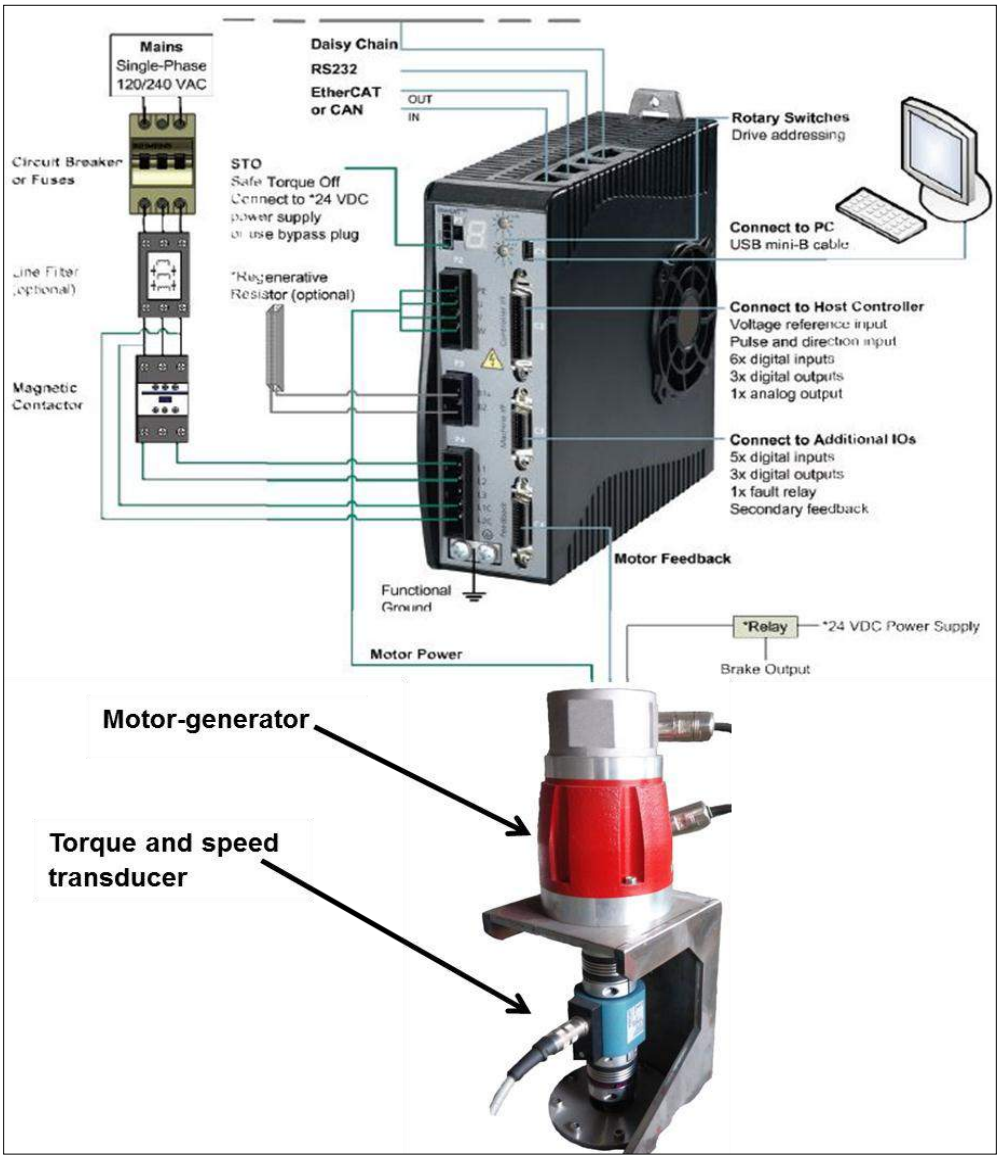

Fig. 6.4: Complete turbine control system.

6.3 Results

A. Experiment Results

The experiments were carried out by maintaining a constant water level upstream of the turbine (0.77 m), such that the turbine was completely

immersed, in order to vary the flow in the channel. The figure below shows the resulting graphs from the data acquired with the torque, the driver of the generator and the ultrasonic sensor. The mechanical power is the product of the torque on the axis of the turbine and speed of rotation. The data were acquired at various discharge (l/s) and velocities (m/s) of the water. Fig. 6.5 shows that the power (W) is directly proportional to the discharge, velocity and intensity. The power generation increases as the discharge and velocity of the water increase. However, as the intensity (torque on motor) increases, the power generation also increases, but at a critical point for a particular discharge level the power generation decreases with further increase in intensity. The maximum power is found to be approximately 7 W when using 346 l/s discharge and 0.51 m/s velocity.

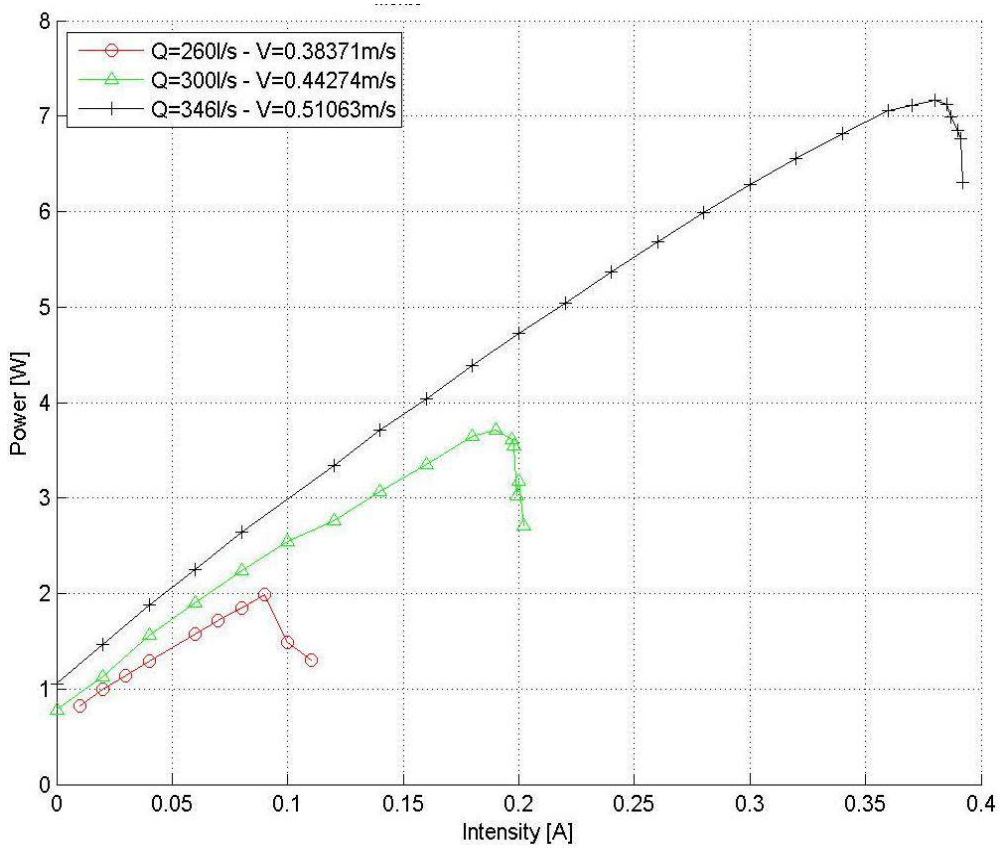

Fig. 6.5: Mechanical power according to the intensity of current in the generator

Fig. 6.6 depicts a linear relationship between torque and intensity. Both are directly proportional to each other and largely depend upon the discharge level of the channel. Both parameters (intensity and torque) are directly proportional to the discharge, as shown in Fig. 6.6.

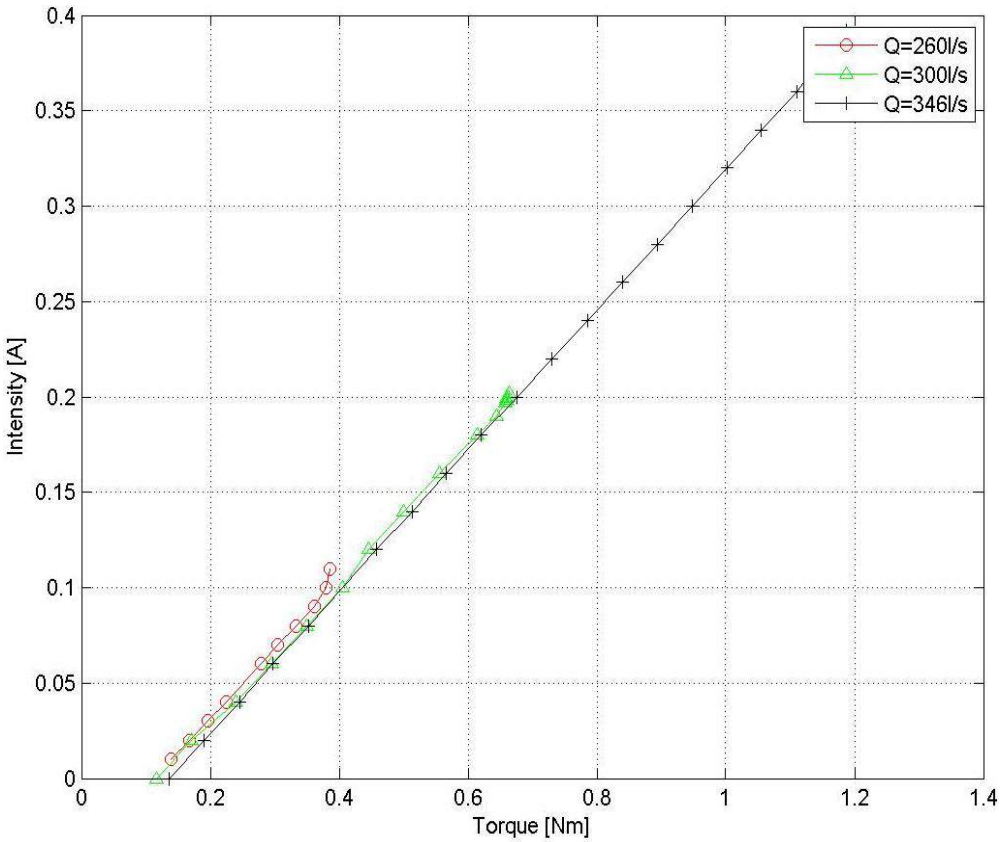

Fig. 6.6: Relation between the intensity of the current in the generator and torque to the generator. Key: flow in the channel l/s.

Figs. 6.7 and 6.8 depict the values of torque and power on the axis as a function of the tip speed ratio (TSR), which not only describes the flow velocity but relates to the peripheral speed of the turbine. The TSR is a dimensionless factor defined in Eq. 6.1:

$$\text{TSR} = \lambda = \frac{\text{speed of rotor tip}}{\text{wind speed}} = \frac{v}{V} = \frac{w\,r}{V} \qquad (6.1)$$

V= wind speed [m/sec]

v = rotor tip speed [m/sec]

r= rotor radius [m]

$w = 2\,\pi f$ = angular velocity [rad/sec]

f = rotational frequency [Hz], [sec]

Generally, the value of TSR depends on the type of turbine and number of blades. Fig. 6.7 shows that the value of TSR varies from 1.7 to 3.1. Similarly, the power generated by using the kinetic turbine as a function of TSR is presented in Fig. 6.8. The critical point at which the power generation starts to decrease is found to be different at different discharges. At 346 l/s discharge, the critical point is at the TSR value of approximately 2.4 and at the same TSR value the maximum power is found to be approximately 7 W.

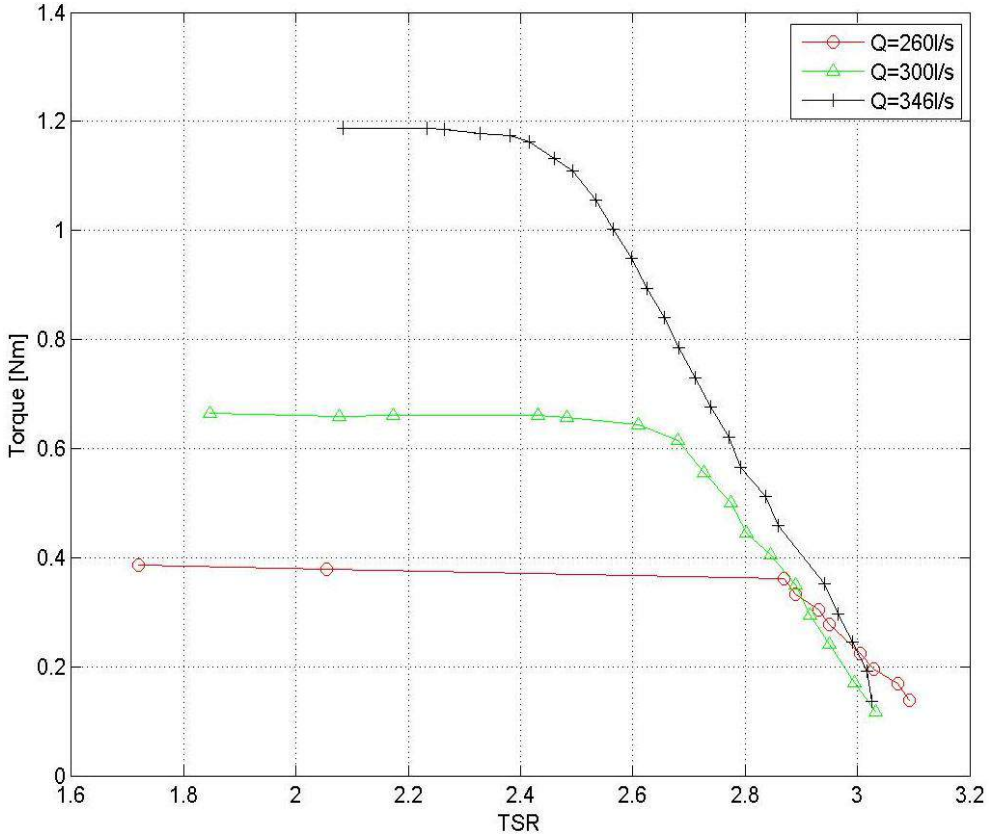

Fig. 6.7: Torque on the shaft of the turbine as a function of TSR. Key: flow in the channel l/s.

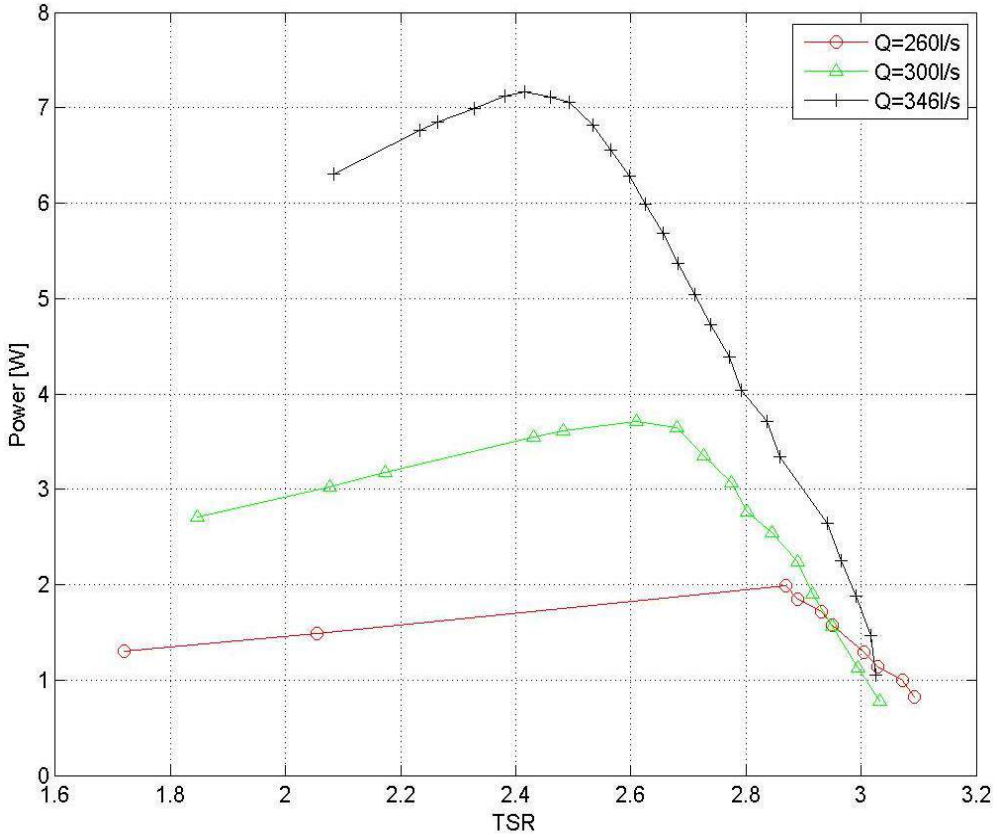

Fig. 6.8: Mechanical power as a function of TSR. Key: flow in the channel l/s.

The turbine efficiency was calculated as the ratio between the mechanical power and the maximum available on the maximum cross-section transverse to the flow of the turbine:

$$P = \frac{1}{2} A \rho V^3 \qquad (6.2)$$

where A is the cross-section to the flow, ρ is the density of water and V the velocity of the flow.

Fig. 6.9 shows the trend of the efficiency as a function of turbine speed. The efficiency of the turbine is reduced as the speed of the turbine increases

beyond a critical point. The critical point at which the efficiency starts to decrease depends on the discharge. The efficiency of the turbine is approximately 37% at 59 rpm when the discharge is 346 l/s.

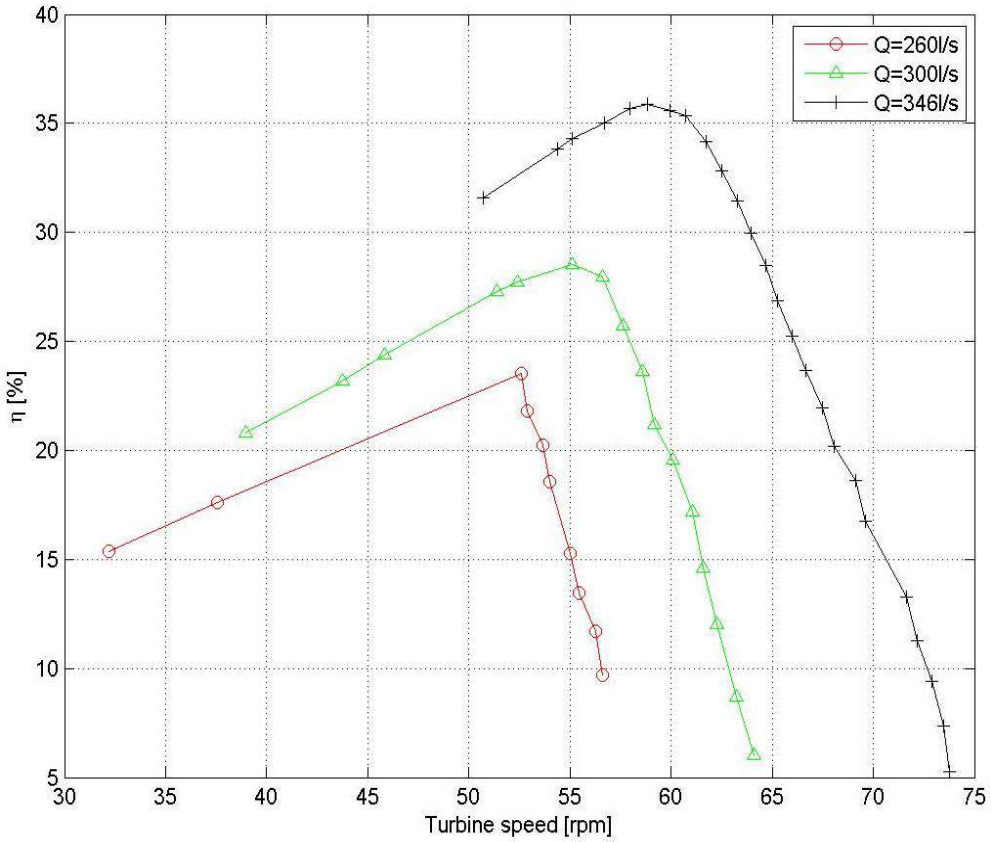

Fig. 6.9: Efficiency of the turbine as a function of its velocity. Legend: flow rate in the channel in l/s.

B. Energy Generation at UJC Canal by Using Experimental Data

The experimental data of the kinetic turbine was used to estimate the number of turbines to be installed, the energy generation per turbine and total energy generation at UJC, according to the efficiency computed from the laboratory experiments. Since the efficiency of the turbine was found to be about 37%

(Fig. 6.11), according to the turbine dimensions, the number of turbines was selected in the transverse direction of the canal. The number of turbines ranges from 72 to 81 according to the width of canal at the 25 nodes along the UJC (discussed in chapter 1). The area of each turbine section is similar to the laboratory channel (0.67 m^2). The minimum head (0.77 m) level of the canal which would be available throughout the year was selected. Similarly, the discharge of each section was estimated by dividing the total discharge by the number of sections and multiplying by the section area. Then, this discharge was used to compute the velocity of the water for that specified section. The total power generation for average discharge (from all of the kinetic turbines) at each node of the UJC varies from 2.83 to 5.87 kW. Similarly, the total power production for the design discharge at each node of the UJC ranges from 7.22 to 9.83 KW. The total energy generation along the UJC at the 25 nodes is 0.992 and 1.99 GWh for the average and design discharge, respectively. This energy generation is much less than that calculated in section 5.5. This discrepancy may be due to the change in calculation methods; i.e. the canal section is divided into a number of sections and turbine installation is on the basis of the dimensions used in the laboratory. Furthermore, the efficiency of the turbine used was 100%, whereas in this section the energy was estimated on the basis of experimental efficiency (37%).

6.4 Conclusions

From the results it is clear that a critical point was not so easily identifiable from the numerical analysis. Also, there are discrepancies due to the difficulty in maintaining a constant speed in a system that in reality has a continuously oscillating speed, when in the numerical model it can be easily kept constant.

The operation of the turbine was carried out at the various speeds of the flow, working in non-critical conditions that were easily definable using the experimental model. Fig. 6.10 shows the lower limit of operation of the turbine. It can be noted that at low speeds the critical point is much more critical than for high speeds, where the power has a more moderate decrease.

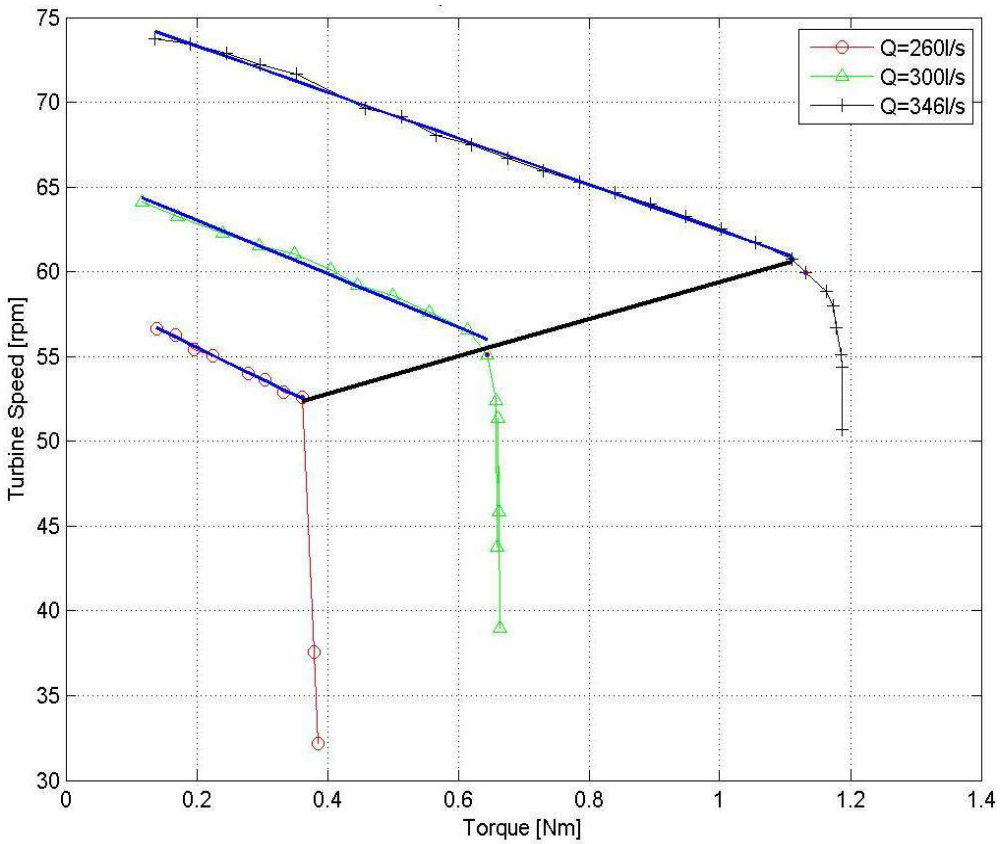

Fig. 6.10: Law of instability of the turbine represented as torsion function of the speed of the turbine. Key: flow rate in the channel in l/s.

Furthermore, in reference to Fig. 6.11, it is possible to observe bending of the blades due to the thrust of the water when they present their entire width to the flow, which can be another factor of discrepancy from the theoretical models.

This experimental work is very useful for the estimation of micro-hydropower along the irrigation canal system. Energy generation at UJC by the installation of kinetic turbines can be very useful to overcome energy crises in Pakistan.

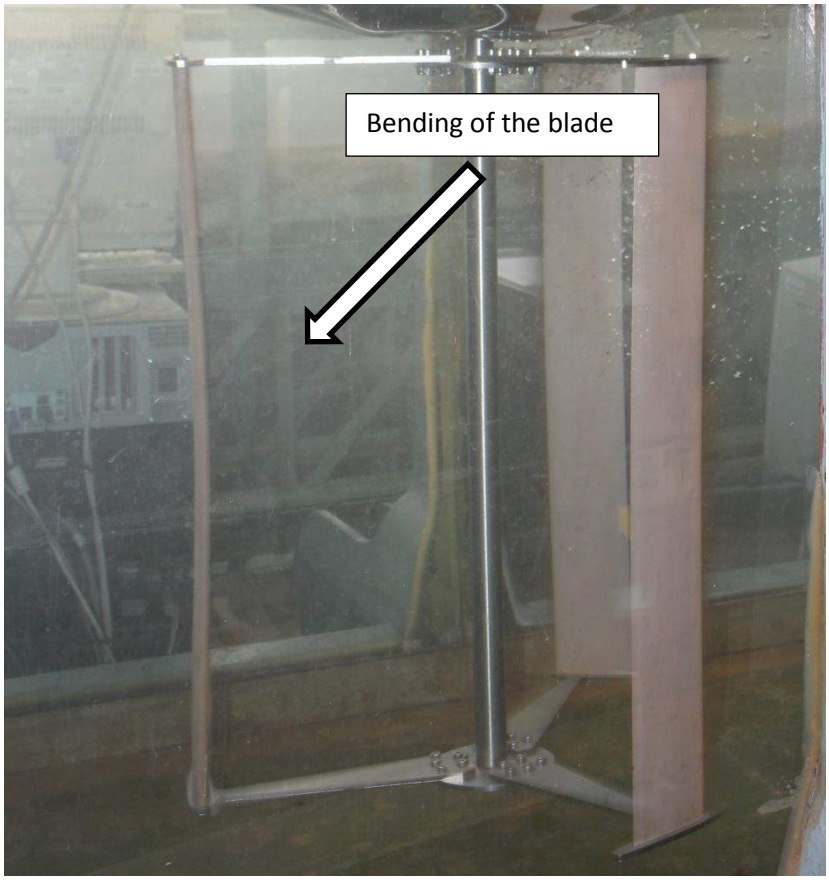

Fig. 6.11: Deflection of the blade in the presence of the flow velocity in the channel of 0.5 m/s.

General Conclusion

The current study was concerned with four important aspects of the Jhelum River Basin (Mangla Basin):

Phase 1: Trend analysis of climate variables and snow cover dynamics and the hydrological regime of the Jhelum River Basin (Mangla Basin)

This investigation began with a trend analysis of climate variables (temperature and precipitation) and the MODIS snow cover product (MOD10A2) to compute the change in snow and the glacierized area in the Jhelum River Basin (Mangla Basin). Available hydrological and climate data were analysed for better understanding of the hydrological regime of the study area.

Phase 2: Water resources availability (application of hydrological models)

The hydrological models, based on the integration of hydro-meteorological (temperature, precipitation and discharge) and MODIS snow cover satellite data are the as basic inputs in the HEC-HMS and snowmelt runoff model (SRM), respectively, were applied to simulate the daily streamflow in Mangla Basin. An evaluation was made to select an appropriate hydrological model for the climate change impact studies by using GCMs.

Phase 3: Climate change analysis and its impact on the sustainability of water resources at Mangla Dam

In this phase, the investigation aimed to simulate a hydrological model and downscale climate data of the Mangla catchment area (Jhelum River Basin) and assess the impact of climate change on the hydrological regime at Mangla Dam. The SDSM model was integrated with GCMs to downscale climate variables under different scenarios.

Phase 4: Operational management of Mangla Dam and its impact on micro-hydropower at the downstream canal system under current and future climate scenarios, then application of laboratory experimental results apply to UJC to calculate micro-hydropower generation

This investigation presented a study of the impact of the catchment hydrology on hydropower generation at Mangla Dam and micro-hydropower along the downstream canal system (UJC) under current and future climate scenarios. Furthermore, the laboratory experimental data was applied to UJC to estimate energy according to the real system efficiency and dimensions.

A conclusion from the results shown in this study is presented in three sections as follows:

1. **Trend analysis of snow cover dynamics and the hydrological regime**

The 10-year analysis of the remotely sensed cryosphere data, an increasing winter precipitation trend, mean temperature and discharge trend in the Jhelum River Basin all suggest that the cryosphere area in Mangla catchment is shrinking slightly, especially at high elevations. On the contrary, the region between altitudes of 2000 and 4000 m is undergoing a slight expansion. The snowmelt process in high altitude regions largely depends upon energy input indirectly associated with temperature. Moreover, the increase in streamflows may also be due to the increasing tendency in monsoon rainfall at most of the stations.

Correlation analysis of the annual and seasonal snow cover suggests that the snow cover area and mean temperature are highly inversely correlated, which results in a high inflow rate during the summer. Therefore, it is vital to estimate the snow accumulation during the winter season at high altitudes in order to predict the summer streamflows and to ultimately allow for better water management at Mangla Reservoir. The Mangla inflows are mainly influenced by the summer and winter temperature and also by the monsoon

rainfall. The discharge is strongly correlated with summer precipitation and the mean temperature of the stations installed at high elevations. Moreover, the region above 3000 m altitude is the most active hydrological zone of the catchment, where maximum snow accumulation occurs. The MODIS snow cover data is a very useful product for the hydrological analysis of the remote regions. It is very easy to process and the snow cover area can be easily extracted by using the MOD10A2 product for the high elevation Himalayan and Karakoram ranges and any other remote regions.

2. Application of hydrological models

This investigation concluded that the HEC-HMS, a standard rainfall-runoff model, can simulate daily streamflows efficiently in high-altitude scarcely gauged catchments of the Jhelum River (Mangla Basin). It is a good tool for the seasonal snow-covered watersheds. Rainfall data are the most important input for precise simulation, especially in scarcely gauged catchments. Therefore, the 0.25×0.25 gridded TRMM rainfall products (3B42) can be successfully integrated with HEC-HMS in the Himalayan range catchments where hydrometeorological data are scarce or unavailable.

Furthermore, this investigation concludes that the snowmelt runoff model (SRM) and HEC-HMS based on the temperature index method can efficiently simulate the daily discharges in snow-fed transboundary catchments. The algorithms of the two models are based on different input data. For example, SRM is based on remotely sensed MODIS snow cover areas. Therefore, this model is not likely to be affected by well-known rainfall measurement deficit errors in mountainous regions where a considerable part of the runoff is in the form of snowmelt. Similarly, as the HEC-HMS is a rainfall-based runoff model, rainfall data is the most important factor for precise simulation. The performance of both models is almost identical, but SRM performed slightly worse at capturing rapid flows

generated by rainfall. Moreover, the HEC-HMS parameters vary significantly over the spatial and temporal scales.

3. Projected water resources availability under climate change scenarios

In this phase, the investigation aimed to downscale climate data and simulate streamflows by using the hydrological model (HEC-HMS) under climate change scenarios to assess the impact of climate change on the hydrological regime of Jhelum River (at Mangla Dam). The climate variables are downscaled by using SDSM with integration of GCMs. The obtained result suggests that the SSVM and SDSM is a good choice to downscale climate data for future climate change predictions. Furthermore, it reveals that the temperature variables are downscaled more efficiently than the precipitation data. The SSVM is more efficient for downscaling of precipitation than that of SDSM. Overall, the projected temperature indicates an increasing trend in the minimum and maximum temperatures compared to the baseline data. A significant change in climate variables is expected in future at most of the stations. The temperature and precipitation is significantly increasing at most of the stations in Mangla Basin, which directly affects the inflow to the Mangla Dam.

The hydrological models (HEC-HMS and SRM) were used to simulate streamflows efficiently under current and future scenarios. In particular, HEC-HMS was used to simulate daily discharge by the application of downscaled climate variables. In both cases, HEC-HMS performed efficiently with gauge and downscale data. Over the summer months the streamflows were overestimated by the hydrological model when using downscaled climate data. This may be associated with some errors in the downscaled precipitation data and also with the inability of the hydrological model to deal with extreme events. Moreover, SRM was also applied for

climate change scenarios by considering the precipitation to be constant. The results obtained suggest that the streamflows will increase with increasing temperature and SCA.

An increase in water availability in future time windows may have a large effect on Mangla hydropower generation. The large expected change in streamflows at Mangla Dam may be viable to help overcome the power and irrigation water deficit arising from low inflows and storage.

4. Operational pattern of Mangla Dam and micro-hydropower generation at UJC

The study suggested that the Mangla Reservoir's operational pattern has a large effect on hydropower generation at Mangla Dam and along the Upper Jhelum Canal. An operational analysis of the Mangla Dam was also performed, indicating that the reservoir storage and outflow pattern depend on summer inflows. The impact of climate change on hydropower generation at Mangla Dam can significantly overcome the energy deficit by the utilization of additional water in future. Furthermore, the micro-hydropower largely depends on the available canal discharge, which depends on the inflow–outflow, the storage volume of the reservoir and the irrigation requirement. The micro-hydropower plants could help to minimize the energy deficit of the Mangla Dam to some extent because the UJC discharge is not significantly influenced by the reduction in the Bong Canal discharge.

Any change in the available water resources of Mangla Basin resulting from climate variability or socio-economic factors will have a serious impact on food security and power generation. The water demand for urban and agricultural use is expected to increase in the future due to a rapid increase in the population. Although the discharges from all of the Jhelum River (Mangla Dam) tributaries tend to increase under the climate change scenarios, the present water storage is not capable of conserving this in

future due to the rapid population increase. This will become more challenging with mismanagement of the water resources, environmental degradation (degradation of river basin, etc.) and an accelerated reduction in the present storage capability due to sedimentation. Therefore, it is of the utmost importance to closely study the building of at least 2 to 3 large capacity multi-purpose dams, e.g. Diamer Basha Dam, Rohtas and Kalabagh Dam on the Indus and Jhelum Rivers. Furthermore, the raising of large dams (Tarbela and Mangla Dams) will be very beneficial for the storage and management of available water resources in the country.

References

Ageta Y, Kadota T (1992) Predictions of changes of glacier mass balance in the Nepal Himalaya and Tibetan Plateau: a case study of air temperature increase for three glaciers. Annals of Glaciology 16:89-94

Ahmed T, Muttaqi K, Agalgaonkar A (2012) Climate change impacts on electricity demand in the State of New South Wales, Australia. Applied Energy 98:376-383

Akhtar M, Ahmad N, Booij M (2008) The impact of climate change on the water resources of Hindukush–Karakorum–Himalaya region under different glacier coverage scenarios. Journal of Hydrology 355:148-163

Anandhi A, Frei A, Pierson DC, Schneiderman EM, Zion MS, Lounsbury D, Matonse AH (2011) Examination of change factor methodologies for climate change impact assessment. Water Resources Research 47

Archer D (2003) Contrasting hydrological regimes in the upper Indus Basin. Journal of Hydrology 274:198-210

Archer D, Fowler H (2008) Using meteorological data to forecast seasonal runoff on the River Jhelum, Pakistan. Journal of Hydrology 361:10-23

Archer DR, Forsythe N, Fowler HJ, Shah SM (2010) Sustainability of water resources management in the Indus Basin under changing climatic and socio economic conditions. Hydrology and Earth System Sciences 14:1669-1680

Bajwa H, Tim U Toward immersive virtual environments for GIS-based Floodplain modeling and Visualization. In: Proceedings of 22nd ESRI User Conference, 2002.

Banitt AMM (2010) Simulating a century of hydrographs e Mark Twain reservoir. Paper presented at the In: 2nd Joint Federal Interagency Conference, Las Vegas, USA,

Bardossy A, Plate EJ (1992) Space-time model for daily rainfall using atmospheric circulation patterns. Water Resources Research 28:1247-1259

Bárdossy A, Stehlík J, Caspary H-J (2002) Automated objective classification of daily circulation patterns for precipitation and temperature downscaling based on optimized fuzzy rules. Climate Research 23:11-22

Bates BC, Charles SP, Hughes JP (1998) Stochastic downscaling of numerical climate model simulations. Environmental Modelling & Software 13:325-331

BBC (2010) '2.5 m people affected' by Pakistan floods. http://www.bbc.co.uk/news/world-south-asia-10834414 (accessed 24 June 2011).

Berthier E, Arnaud Y, Kumar R, Ahmad S, Wagnon P, Chevallier P (2007) Remote sensing estimates of glacier mass balances in the Himachal Pradesh (Western Himalaya, India). Remote Sensing of Environment 108:327-338

Bookhagen B, Burbank DW (2006) Topography, relief, and TRMM-derived rainfall variations along the Himalaya. Geophysical Research Letters 33

Bookhagen B, Burbank DW (2010) Toward a complete Himalayan hydrological budget: Spatiotemporal distribution of snowmelt and rainfall and their impact on river discharge. Journal of Geophysical Research: Earth Surface (2003–2012) 115

Busuioc A, Chen D, Hellström C (2001) Performance of statistical downscaling models in GCM validation and regional climate change estimates: application for Swedish precipitation. International Journal of Climatology 21:557-578

Cannone N, Diolaiuti G, Guglielmin M, Smiraglia C (2008) Accelerating climate change impacts on alpine glacier forefield ecosystems in the European Alps. Ecological Applications 18:637-648

Cheema MJM, Bastiaanssen WG (2012) Local calibration of remotely sensed rainfall from the TRMM satellite for different periods and spatial scales in the Indus Basin. International Journal of Remote Sensing 33:2603-2627

Chen H, Xu C-Y, Guo S (2012) Comparison and evaluation of multiple GCMs, statistical downscaling and hydrological models in the study of climate change impacts on runoff. Journal of hydrology 434:36-45

Christenson M, Manz H, Gyalistras D (2006) Climate warming impact on degree-days and building energy demand in Switzerland. Energy Conversion and Management 47:671-686

Cunderlik JM, Simonovic SP Hydrologic models for inverse climate change impact modeling. In: Proceedings of the 18th Canadian Hydrotechnical Conference, Challenges for Water Resources Engineering in a Changing World Winnipeg, 2007.

De Scally FA (1994) Relative importance of snow accumulation and monsoon rainfall data for estimating annual runoff, Jhelum basin, Pakistan. Hydrological sciences journal 39:199-216

Dey B, Sharma V, Rango A (1989) A test of snowmelt-runoff model for a major river basin in western Himalayas. Nordic Hydrology 20:167-178

Dibike YB, Coulibaly P (2005) Hydrologic impact of climate change in the Saguenay watershed: comparison of downscaling methods and hydrologic models. Journal of hydrology 307:145-163

Enke W, Spekat A (1997) Downscaling climate model outputs into local and regional weather elements by classification and regression. Climate Research 8:195-207

Fang X, Cleveland, T., Garcia, C.A., Thompson, D., Malla, R. (2005) Literature Review on Timing Parameters for Hydrographs., Department of Civil Engineering, Lamar University, Beaumont, Texas,

Farr TG et al. (2007) The shuttle radar topography mission. Reviews of geophysics 45

Faucher M, Burrows WR, Pandolfo L (1999) Empirical-statistical reconstruction of surface marine winds along the western coast of Canada. Climate Research 11:173-190

Finger D, Heinrich G, Gobiet A, Bauder A (2012) Projections of future water resources and their uncertainty in a glacierized catchment in the Swiss Alps and the subsequent effects on hydropower production during the 21st century. Water Resources Research 48

FØrland E (1996) Manual for operational correction of Nordic precipitation data. Norske meteorologiske institutt,

Fowler H, Archer D (2006) Conflicting signals of climatic change in the Upper Indus Basin. Journal of Climate 19:4276-4293

Gaudard L, Gilli M, Romerio F (2013) Climate change impacts on hydropower management. Water resources management 27:5143-5156

Golombek R, Kittelsen SA, Haddeland I (2012) Climate change: impacts on electricity markets in Western Europe. Climatic change 113:357-370

Gyawali R, Watkins DW (2012) Continuous hydrologic modeling of snow-affected watersheds in the Great Lakes basin using HEC-HMS. Journal of Hydrologic Engineering 18:29-39

Hall DK, Riggs GA, Salomonson VV, DiGirolamo NE, Bayr KJ (2002) MODIS snow-cover products. Remote sensing of Environment 83:181-194

Halwatura D, Najim M (2013) Application of the HEC-HMS model for runoff simulation in a tropical catchment. Environmental Modelling & Software 46:155-162

Hamon WR (1963) Computation of direct runoff amounts from storm rainfall. International Association of Scientific Hydrology Publication 63:52-62

Hänggi P, Weingartner R (2012) Variations in discharge volumes for hydropower generation in Switzerland. Water resources management 26:1231-1252

Haq I, Abbas S Sedimentation of Tarbela and Mangla reservoirs. In: Proceedings of the 70th Annual Session of the Pakistan Engineering Congress, 2007.

Hessami M, Gachon P, Ouarda TB, St-Hilaire A (2008) Automated regression-based statistical downscaling tool. Environmental Modelling & Software 23:813-834

Hewitt K (2005) The Karakoram anomaly? Glacier expansion and the'elevation effect,'Karakoram Himalaya. Mountain Research and Development 25:332-340

Hewitt K (2007) Tributary glacier surges: an exceptional concentration at Panmah Glacier, Karakoram Himalaya. Journal of Glaciology 53:181-188

Hirsch RM, Slack JR (1984) A nonparametric trend test for seasonal data with serial dependence. Water Resources Research 20:727-732

Hirsch RM, Slack JR, Smith RA (1982) Techniques of trend analysis for monthly water quality data. Water resources research 18:107-121

Hunukumbura P, Tachikawa Y, Shiiba M (2012) Distributed hydrological model transferability across basins with different hydro-climatic characteristics. Hydrological Processes 26:793-808

Hussain I (2005) Pro-poor intervention strategies in irrigated agriculture in Asia. International Water Management Institute, Colombo, Sri Lanka

Immerzeel W, Droogers P, De Jong S, Bierkens M (2009) Large-scale monitoring of snow cover and runoff simulation in Himalayan river basins using remote sensing. Remote Sensing of Environment 113:40-49

Immerzeel WW, Van Beek LP, Bierkens MF (2010) Climate change will affect the Asian water towers. Science 328:1382-1385

IPCC (2007) AR4 (Intergovernmental Panel on Climate Change Fourth Assessment Report) Climate change and water 2007 IPCC Technical paper VI (htt://www.ipcc.ch/pdf). [Accessed 20 June 2008]

IUCN (2010) Pakistan Water Apportionment Accord for Resolving Inter-provincial Water Conflicts – Policy Issues and Options. IUCN Pakistan, Karachi,

Kalita DN (2008) A study of basin response using HEC-HMS and subzone reports of CWC. Paper presented at the In: Proceedings of the 13th National Symposium on Hydrology, National Institute of Hydrology, Roorkee, New Delhi,

Kattelmann R (1987) Water release from a forested snowpack during rainfall. Forest Hydrology and Watershed Management:265-272

Kendall M, Gibbons JD (1990) Rank correlation methods, fifth ed. Edward Arnold. London.

Lang TJ, Barros AP (2004) Winter storms in the central Himalayas. 気象集誌 第 2 輯 82:829-844

Lee Rodgers J, Nicewander WA (1988) Thirteen ways to look at the correlation coefficient. The American Statistician 42:59-66

Lee Y-J, Hsieh W-F, Huang C-M (2005) ε-SSVR: a smooth support vector machine for ε-insensitive regression. Knowledge and Data Engineering, IEEE Transactions on 17:678-685

Lee Y-J, Mangasarian OL (2001) SSVM: A smooth support vector machine for classification. Computational optimization and Applications 20:5-22

Li X, Sailor D (2001) Application of tree-structured regression for regional precipitation prediction using general circulation model output. Climate Research 16:17-30

Martinec J (1975) Snowmelt-runoff model for stream flow forecasts. Nordic hydrology 6:145-154

Martinec J, Rango, A., Roberts, R. (2007) Snowmelt-Runoff Model (SRM) user's manual. USDA Jornada Experimental Range. New Mexico State University, Las Cruces, NM 88003, USA

Mearns L, Giorgi F, Whetton P, Pabon D, Hulme M, Lal M (2003) Guidelines for use of climate scenarios developed from regional climate model experiments. DDC of IPCC TGCIA, Final Version

Meenu R, Rehana S, Mujumdar P (2013) Assessment of hydrologic impacts of climate change in Tunga–Bhadra river basin, India with HEC-HMS and SDSM. Hydrological Processes 27:1572-1589

Nasseri M, Tavakol-Davani H, Zahraie B (2013) Performance assessment of different data mining methods in statistical downscaling of daily precipitation. Journal of Hydrology 492:1-14

Nguyen VTV, Nguyen, T. D., and Gachon, P. Statistical Downscaling Methods for Climate Change Impact Studies. In: Conference on Adapting to Climate Change in Canada 2005: Understanding Risks and Building Capacity., Le Centre Sheraton Montréal Hotel, Montréal, Québec, May 4-7, 2005. 2005.

NOAA (2010) State of the climate, global analysis, July 2010. National Climate Data Center. http://www.ncdc.noaa.gov/sotc/global/2010/8 (accessed 24 June 2011),

Null SE, Viers JH, Mount JF (2010) Hydrologic response and watershed sensitivity to climate warming in California's Sierra Nevada. PLoS One 5:e9932

Prasad VH, Roy PS (2005) Estimation of snowmelt runoff in Beas Basin, India. Geocarto International 20:41-47

Raje D, Mujumdar P (2011) A comparison of three methods for downscaling daily precipitation in the Punjab region. Hydrological Processes 25:3575-3589

Schär C, Vasilina L, Pertziger F, Dirren S (2004) Seasonal runoff forecasting using model-assimilated precipitation data. Journal of Hydrometeorology 5:959-973

Scherler D, Bookhagen B, Strecker MR (2011) Spatially variable response of Himalayan glaciers to climate change affected by debris cover. Nature Geoscience 4:156-159

Semenov MA, Barrow EM (1997) Use of a stochastic weather generator in the development of climate change scenarios. Climatic change 35:397-414

ŞENSOY A (2005) Physically based point snowmelt modeling and its distribution in Upper Euphrates Basin. Dissertation, MIDDLE EAST TECHNICAL UNIVERSITY

Sevruk B (1989) Reliability of Precipitation Measurement. Paper presented at the International Workshop on Precipitation Measurement, WMO Tech. Document, 13-19.,

Sharif H (2010) Inter Province water distribution conflict in Pakistan. British High Commission, Pakistan, Pakistan

Sicart J-E, Pomeroy J, Essery R, Bewley D (2006) Incoming longwave radiation to melting snow: observations, sensitivity and estimation in northern environments. Hydrological Processes 20:3697-3708

Sicart JE, Wagnon P, Ribstein P (2005) Atmospheric controls of the heat balance of Zongo Glacier (16 S, Bolivia). Journal of Geophysical Research: Atmospheres 110:1984-2012

Singh P (1991) Hydrological Investigations on Chhota Shigri Glacier (H.P.). National Institute of Hydrology, Rookree, India

Şorman AA, Şensoy A, Tekeli A, Şorman A, Akyürek Z (2009) Modelling and forecasting snowmelt runoff process using the HBV model in the eastern part of Turkey. Hydrological processes 23:1031-1040

Straub TD, Melching CS, Kocher KE (2000) Equations for estimating Clark unit-hydrograph parameters for small rural watersheds in Illinois. U.S. GEOLOGICAL SURVEY, 221 North Broadway Avenue Urbana, IL 61801, USA

Tahir AA, Chevallier P, Arnaud Y, Neppel L, Ahmad B (2011) Modeling snowmelt-runoff under climate scenarios in the Hunza River basin, Karakoram Range, Northern Pakistan. Journal of Hydrology 409:104-117

Tarboton DG, Luce CH (1996) Utah energy balance snow accumulation and melt model (UEB). Citeseer,

United Nations (2010) Population division of the department of economic and social affairs, World population prospects, http://esa.un.org/unpd/wpp/Sorting-Tables/tab-sorting-population.htm.

Verdhen A, Prasad T (1993) Snowmelt runoff simulation models and their suitability in Himalayan conditions. IAHS Publications-Publications of the International Association of Hydrological Sciences 218:239-248

Wanielista M, Kersten R, Eaglin R (1997) Hydrology: Water quantity and quality control. John Wiley and Sons,

Wetterhall F, Bárdossy A, Chen D, Halldin S, Xu C-y (2009) Statistical downscaling of daily precipitation over Sweden using GCM output. Theoretical and applied climatology 96:95-103

Wilby R, Dawson C (2007) SDSM 4.2-A decision support tool for the assessment of regional climate change impacts, Version 4.2 User Manual. Lancaster University: Lancaster/Environment Agency of England and Wales

Wilby RL, Dawson CW, Barrow EM (2002) SDSM—a decision support tool for the assessment of regional climate change impacts. Environmental Modelling & Software 17:145-157

Winiger M, Gumpert M, Yamout H (2005) Karakorum–Hindukush–western Himalaya: assessing high-altitude water resources. Hydrological Processes 19:2329-2338

WMO (1986) Intercomparison of models of snowmelt runoff. Geneva, Switzerland.

WMO (1992) Simulated real-time Intercomparison of hydrological models. Geneva, Switzerland.

Xu C-Y (2010) Downscaling GCMs using the Smooth Support Vector Machine method to predict daily precipitation in the Hanjiang Basin. Advances in Atmospheric Sciences 27:274-284

Yarnal B, Comrie AC, Frakes B, Brown DP (2001) Developments and prospects in synoptic climatology. International Journal of Climatology 21:1923-1950

Yatagai A, Arakawa O, Kamiguchi K, Kawamoto H, Nodzu MI, Hamada A (2009) A 44-year daily gridded precipitation dataset for Asia based on a dense network of rain gauges. Sola 5:137-140

Yilma H, Moges, S.A. (2007) Application of semi-distributed conceptual hydrological model for flow forecasting on upland catchments of Blue Nile River Basin, a case study of Gilgel Abbay catchment. Catchment and Lake Research, 200.

Yilmaz AG, Imteaz MA, Ogwuda O (2011) Accuracy of HEC-HMS and LBRM models in simulating snow runoffs in Upper Euphrates Basin. Journal of Hydrologic Engineering 17:342-347

Yimer G, Jonoski A, Van Griensven A (2009) Hydrological response of a catchment to climate change in the Upper Beles River Basin, Upper Blue Nile, Ethiopia. Nile Basin Water Engineering Scientific Magazine 2:49-59

Young CA et al. (2009) Modeling the hydrology of climate change in California's Sierra Nevada for subwatershed scale adaptation. JOURNAL OF THE AMERICAN WATER RESOURCES ASSOCIATION 45:1409-1423

Young G, Hewitt K (1990) Hydrology research in the upper Indus basin, Karakoram Himalaya, Pakistan. Hydrology of Mountainous Areas IAHS Publ 190:139-152

Zawahri NA International rivers and national security: The Euphrates, Ganges–Brahmaputra, Indus, Tigris, and Yarmouk rivers. In: Natural Resources Forum, 2008. vol 4. Wiley Online Library, pp 280-289

Zhang Y, Liu S, Ding Y (2006) Observed degree-day factors and their spatial variation on glaciers in western China. Annals of Glaciology 43:301-306

Appendices

Appendix A

The calibration and comparison between calibrated parameters in chapter 3, are performed for each single, three and six year time window to examine the temporal and spatial variability in calibrated parameters by the application of HEC-HMS.

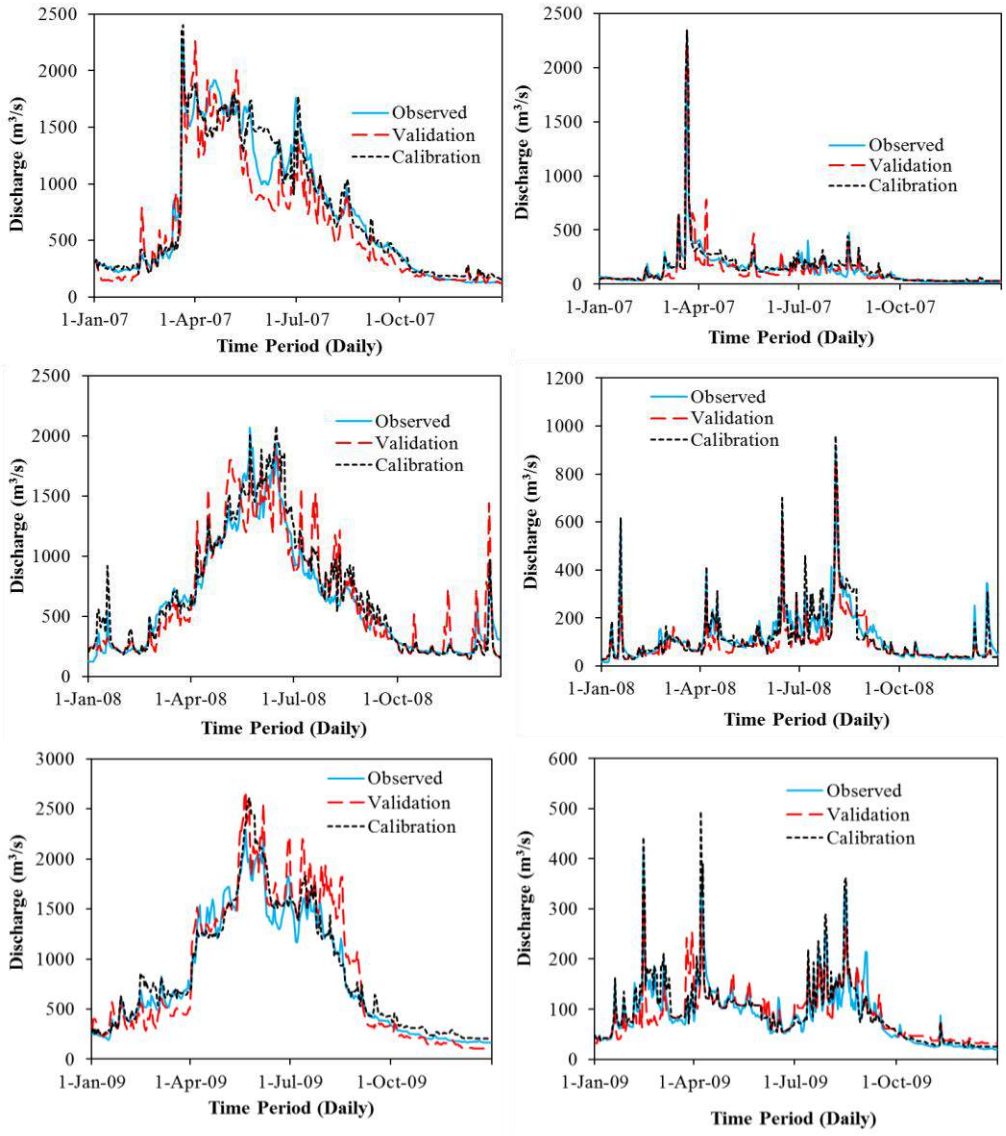

Appendix A01: Calibration of Single year over 2007, 2008 and 2009 by using HEC-HMS.

Appendix A02: Value of parameters used for the simulation of single hydrological year over 2002 in HEC-HMS application.

Sub-Basin of HMS	Initial Deficit (mm)	Maxi Deficit (mm)	Constant Loss (mm/hr)	Imp (%)	Lag Time (Hrs)	Lapse Rate (Deg. °C/100 m)	ET (mm/Month) (Winter to Summer)
Naran	25	34	2.15	15	23.07	-0.58	10 to 47
Dudhnial	23	36	1.25	0	18.07	-0.37	11 to 58
Domel	29	38	1.55	0	17.40	-0.16	7 to 41
Astore/Kel	24	39	1.70	5	19.40	-0.37	10 to 58
Baramula	26	30	1.10	0	16.00	-0.65	12 to 49
M.Abad	26	33	1.85	12	14.17	-0.16	3 to 46
G.Dopata	24	38	3.15	11	20.82	-0.33	8 to 44
Wuler lake	28	37	1.15	8	18.08	-0.65	11 to 70
Srinager	24	39	1.15	25	20.67	-0.37	6 to 41
Muree	30	36	1.80	13	7.63	-0.48	12 to 60
Pulwama	20	34	0.75	21	18.53	-0.65	12 to 70
Nawan	26	38	2.55	11	8.92	-0.11	13 to 68
Anantnag	22	35	0.75	20	14.55	-0.65	8 to 48
Pahalgam	28	35	0.50	9	14.73	-0.65	9 to 43
Gad Wali	24	35	0.80	10	12.00	-0.65	11 to 54
Kanshi	20	33	2.85	5	11.47	-0.19	5 to 63
Chandak	35	45	0.75	18	6.33	-0.65	12 to 74
Khandar	28	38	0.95	2	8.13	-0.19	10 to 47
Kotli	30	30	0.85	17	8.53	-0.31	10 to 52
Rawelakot	20	34	1.35	2	10.82	-0.27	10 to 52
Sehr Kokata	30	39	1.50	0	7.12	0.25	8 to 46
Palanderi	28	37	2.15	15	11.63	-0.06	8 to 46
DDF (mm °C-1 d-1) = 5.5, Px Temperature = 3 °C, Base Temperature = 0 °C							

Appendix A03: Value of parameters used for the simulation of single hydrological year over 2003 in HEC-HMS application.

Sub-Basin of HMS	Initial Deficit (mm)	Maxi Deficit (mm)	Constant Loss (mm/hr)	Imp (%)	Lag Time (Hrs)	Lapse Rate (Deg. °C/100 m)	ET (mm/Month) Range (Winter to Summer)
Naran	25	34	2.85	10	17.38	-0.59	12 to 51
Dudhnial	23	36	1.85	0	15.42	-0.40	14 to 61
Domel	29	38	1.65	0	15.20	-0.19	11 to 44
Astore/Kel	24	39	1.10	12	19.40	-0.40	12 to 51
Baramula	26	30	0.90	0	16.00	-0.65	10 to 46
M.Abad	26	33	0.95	19	12.50	-0.19	5 to 49
G.Dopata	24	38	3.15	9	17.00	-0.33	11 to 44
Wuler	28	37	0.70	8	17.38	-0.65	8 to 60
Srinager	24	39	1.75	30	19.42	-0.40	9 to 46
Muree	30	36	1.80	17	8.05	-0.44	12 to 60
Pulwama	20	34	1.00	0	18.53	-0.65	15 to 80
Nawan	26	38	2.30	15	7.72	-0.13	10 to 61
Anantnag	22	35	0.75	15	14.55	-0.65	10 to 45
Pahalgam	28	35	0.90	14	13.90	-0.65	11 to 40
Gad Wali	24	35	1.10	5	12.00	-0.65	7 to 48
Kanshi	20	33	3.10	18	11.47	-0.03	8 to 60
Chandak	35	45	0.75	23	4.93	-0.65	8 to 62
Khandar	28	38	0.55	8	6.70	-0.17	8 to 41
Kotli	30	30	0.85	15	9.57	-0.27	7 to 48
Rawelakot	20	34	1.35	4	10.32	-0.26	7 to 55
Sehr Kokata	30	39	1.20	0	6.10	-0.12	6 to 40
Palanderi	28	37	3.10	13	11.63	-0.05	8 to 41
DDF (mm °C-1 d-1) = 5.7, Px Temperature = 2 °C, Base Temperature = 0 °C							

Appendix A04: Value of parameters used for the simulation of single hydrological year over 2007 in HEC-HMS application.

Sub-Basin of HMS	Initial Deficit (mm)	Maxi Deficit (mm)	Constant Loss (mm/hr)	Imp (%)	Lag Time (Hrs)	Lapse Rate (Deg. °C/100 m)	ET (mm/Month) (Winter to Summer)
Naran	25	34	2.85	17	18.38	-0.61	8 to 51
Dudhnial	23	36	1.63	0	15.42	-0.41	14 to 51
Domel	29	38	2.00	0	15.20	-0.22	11 to 49
Astore/Kel	24	39	0.65	9	18.60	-0.41	13 to 63
Baramula	26	30	0.85	0	14.33	-0.65	15 to 53
M.Abad	26	33	1.85	10	12.50	-0.22	6 to 51
G.Dopata	24	38	2.90	16	17.00	-0.31	11 to 49
Wuler lake	28	37	1.40	13	16.25	-0.65	8 to 60
Srinager	24	39	1.35	35	19.42	-0.41	9 to 46
Muree	30	36	2.20	10	8.05	-0.44	10 to 53
Pulwama	20	34	0.90	9	16.63	-0.65	9 to 62
Nawan	26	38	2.30	10	7.72	-0.14	10 to 63
Anantnag	22	35	0.80	17	16.33	-0.65	7 to 43
Pahalgam	28	35	0.95	14	13.90	-0.65	9 to 49
Gad Wali	24	35	1.10	9	14.50	-0.65	9 to 51
Kanshi	20	33	3.10	8	10.30	-0.04	7 to 57
Chandak	35	45	1.00	17	4.93	-0.65	9 to 70
Khandar	28	38	0.70	3	6.70	-0.17	13 to 53
Kotli	30	30	1.00	13	9.57	-0.24	10 to 52
Rawelakot	20	34	1.65	2	11.53	-0.26	12 to 48
Sehr Kokata	30	39	1.00	0	6.10	-0.25	8 to 49
Palanderi	28	37	2.65	20	10.30	-0.06	11 to 51
DDF (mm °C-1 d-1) = 5.7, Px Temperature = 2°C, Base Temperature = 0°C							

Appendix A05: Value of parameters used for the simulation of single hydrological year over 2008 in HEC-HMS application.

Sub-Basin of HMS	Initial Deficit (mm)	Maxi Deficit (mm)	Constant Loss (mm/hr)	Imp (%)	Lag Time (Hrs)	Lapse Rate (Deg. °C/100 m)	ET (mm/Month) Range (Winter to Summer)
Naran	25	34	2.85	12	19.88	-0.56	10 to 47
Dudhnial	23	36	2.00	0	16.98	-0.43	11 to 58
Domel	29	38	2.20	0	15.20	-0.16	7 to 41
Astore/Kel	24	39	0.80	13	17.20	-0.43	10 to 58
Baramula	26	30	0.85	0	14.33	-0.65	12 to 49
M.Abad	26	33	1.55	19	12.50	-0.16	3 to 46
G.Dopata	24	38	2.45	11	14.60	-0.35	8 to 44
Wuler lake	28	37	1.40	0	16.25	-0.65	11 to 70
Srinager	24	39	1.15	40	19.42	-0.43	6 to 41
Muree	30	36	1.83	14	9.72	-0.41	12 to 60
Pulwama	20	34	1.10	4	16.63	-0.65	12 to 70
Nawan	26	38	2.85	15	7.72	-0.15	13 to 68
Anantnag	22	35	0.95	22	16.33	-0.65	8 to 48
Pahalgam	28	35	0.80	20	13.90	-0.65	9 to 43
Gad Wali	24	35	0.45	7	14.50	-0.65	11 to 54
Kanshi	20	33	3.10	11	10.30	-0.13	5 to 63
Chandak	35	45	1.10	13	4.93	-0.65	12 to 74
Khandar	28	38	0.75	2	8.18	-0.17	10 to 47
Kotli	30	30	1.30	11	9.57	-0.25	10 to 52
Rawelakot	20	34	1.95	0	11.53	-0.25	10 to 52
Sehr Kokata	30	39	1.45	5	6.10	-0.25	8 to 46
Palanderi	28	37	1.95	16	11.62	-0.01	8 to 46
DDF (mm °C-1 d-1) = 5.4, Px Temperature = 2 °C, Base Temperature = 0 °C							

Appendix A06: Value of parameters used for the simulation of single hydrological year over 2009 in HEC-HMS application.

Sub-Basin of HMS	Initial Deficit (mm)	Maxi Deficit (mm)	Constant Loss (mm/hr)	Imp (%)	Lag Time (Hrs)	Lapse Rate (Deg. °C/100 m)	ET (mm/Month) Range (Winter to Summer)
Naran	25	34	2.85	15	17.63	-0.54	10 to 47
Dudhnial	23	36	1.67	0	16.98	-0.40	11 to 58
Domel	29	38	2.15	0	15.20	-0.14	7 to 41
Astore/Kel	24	39	1.25	11	17.20	-0.40	10 to 58
Baramula	26	30	0.95	0	14.33	-0.65	12 to 49
M.Abad	26	33	2.15	15	12.50	-0.14	3 to 46
G.Dopata	24	38	2.65	14	17.60	-0.36	8 to 44
Wuler lake	28	37	1.25	8	16.25	-0.65	11 to 70
Srinager	24	39	1.95	40	19.42	-0.40	6 to 41
Muree	30	36	1.65	12	12.80	-0.45	12 to 60
Pulwama	20	34	0.90	7	16.63	-0.65	12 to 70
Nawan	26	38	2.35	13	7.72	-0.13	13 to 68
Anantnag	22	35	0.95	5	16.33	-0.65	8 to 48
Pahalgam	28	35	0.75	17	13.90	-0.65	9 to 43
Gad Wali	24	35	1.20	12	14.50	-0.65	11 to 54
Kanshi	20	33	3.10	14	10.30	-0.02	5 to 63
Chandak	35	45	1.20	19	4.93	-0.65	12 to 74
Khandar	28	38	1.15	2	6.70	-0.17	10 to 47
Kotli	30	30	1.20	9	11.48	-0.30	10 to 52
Rawelakot	20	34	2.15	6	11.53	-0.27	10 to 52
Sehr Kokata	30	39	1.65	3	6.10	0.01	8 to 46
Palanderi	28	37	1.00	22	15.20	-0.04	8 to 46
DDF (mm °C-1 d-1) = 5.7, Px Temperature = 2.5°C, Base Temperature = 0 °C							

Appendix A07: Value of parameters used for the simulation of three hydrological years over 2007-2009 in HEC-HMS application.

Sub-Basin of HMS	Initial Deficit (mm)	Maxi Deficit (mm)	Constant Loss (mm/hr)	Imp (%)	Lag Time (Hrs)	Lapse Rate (Deg. °C/100 m)	ET (mm/Month) Range (Winter to Summer)
Naran	25	34	2.25	16	18.37	-0.58	5 to 41
Dudhnial	23	36	2.15	10	15.08	-0.43	8 to 52
Domel	29	38	3.25	8	17.00	-0.19	9 to 45
Astore/Kel	24	39	0.55	13	18.65	-0.43	12 to 62
Baramula	26	30	0.80	7	13.67	-0.65	14 to 53
M.Abad	26	33	1.90	21	10.33	-0.19	6 to 49
G.Dopata	24	38	2.95	16	17.37	-0.31	11 to 49
Wuler lake	28	37	1.10	13	16.25	-0.65	8 to 59
Srinager	24	39	1.35	40	20.40	-0.43	6 to 44
Muree	30	36	2.25	11	7.63	-0.41	8 to 52
Pulwama	20	34	0.50	0	17.15	-0.65	12 to 68
Nawan	26	38	2.75	13	8.17	-0.15	11 to 68
Anantnag	22	35	1.50	4	13.13	-0.65	8 to 48
Pahalgam	28	35	0.75	15	17.80	-0.65	11 to 57
Gad Wali	24	35	0.50	18	14.50	-0.65	13 to 64
Kanshi	20	33	1.80	6	9.40	-0.09	7 to 60
Chandak	35	45	1.70	11	4.42	-0.65	8 to 70
Khandar	28	38	1.10	0	6.35	-0.18	9 to 58
Kotli	30	30	1.10	18	8.47	-0.22	10 to 55
Rawelakot	20	34	1.55	6	11.20	-0.24	8 to 59
Sehr Kokata	30	39	1.85	12	6.37	-0.27	5 to 41
Palanderi	28	37	2.25	15	10.75	-0.01	6 to 40
DDF (mm °C-1 d-1) = 5.5, Px Temperature = 2°C, Base Temperature = 0°C							

Appendix A08: Value of parameters used for the simulation of six hydrological years over 2001-2003 and 2007-2009 in HEC-HMS application.

Sub-Basin of HMS	Initial Deficit (mm)	Maxi Deficit (mm)	Constant Loss (mm/hr)	Imp (%)	Lag Time (Hrs)	Lapse Rate (Deg. °C/100 m)	ET (mm/Month) Range (Winter to Summer)
Naran	25	34	1.6	14	19.32	-0.60	5 to 41
Dudhnial	23	36	1.7	0	16.08	-0.41	8 to 52
Domel	29	38	2.85	0	17.00	-0.18	9 to 45
Astore/Kel	24	39	0.55	8	19.75	-0.41	12 to 62
Baramula	26	30	0.8	0	13.67	-0.65	14 to 53
M.Abad	26	33	1.7	20	12.22	-0.18	6 to 49
G.Dopata	24	38	3.0	14	19.12	-0.31	11 to 49
Wuler lake	28	37	1.1	11	17.08	-0.65	8 to 59
Srinager	24	39	1.175	33	20.53	-0.41	6 to 44
Muree	30	36	2.475	15	7.63	-0.44	8 to 52
Pulwama	20	34	0.5	3	17.97	-0.65	12 to 68
Nawan	26	38	1.7	15	8.17	-0.14	11 to 68
Anantnag	22	35	1.2	7.5	13.70	-0.65	8 to 48
Pahalgam	28	35	0.75	13	16.70	-0.65	11 to 57
Gad Wali	24	35	0.5	16	13.53	-0.65	13 to 64
Kanshi	20	33	1.48	5	11.62	-0.035	7 to 60
Chandak	35	45	1.7	14	5.12	-0.65	8 to 70
Khandar	28	38	1.4	0	7.28	-0.17	9 to 58
Kotli	30	30	1.1	22	8.47	-0.24	10 to 55
Rawelakot	20	34	1.8	0	11.20	-0.26	8 to 59
Sehr Kokata	30	39	1.85	0	6.37	-0.25	5 to 41
Palanderi	28	37	3	13	10.75	-0.06	6 to 40
DDF (mm °C-1 d-1) = 5.5, Px Temperature = 2°C, Base Temperature = 0°C							

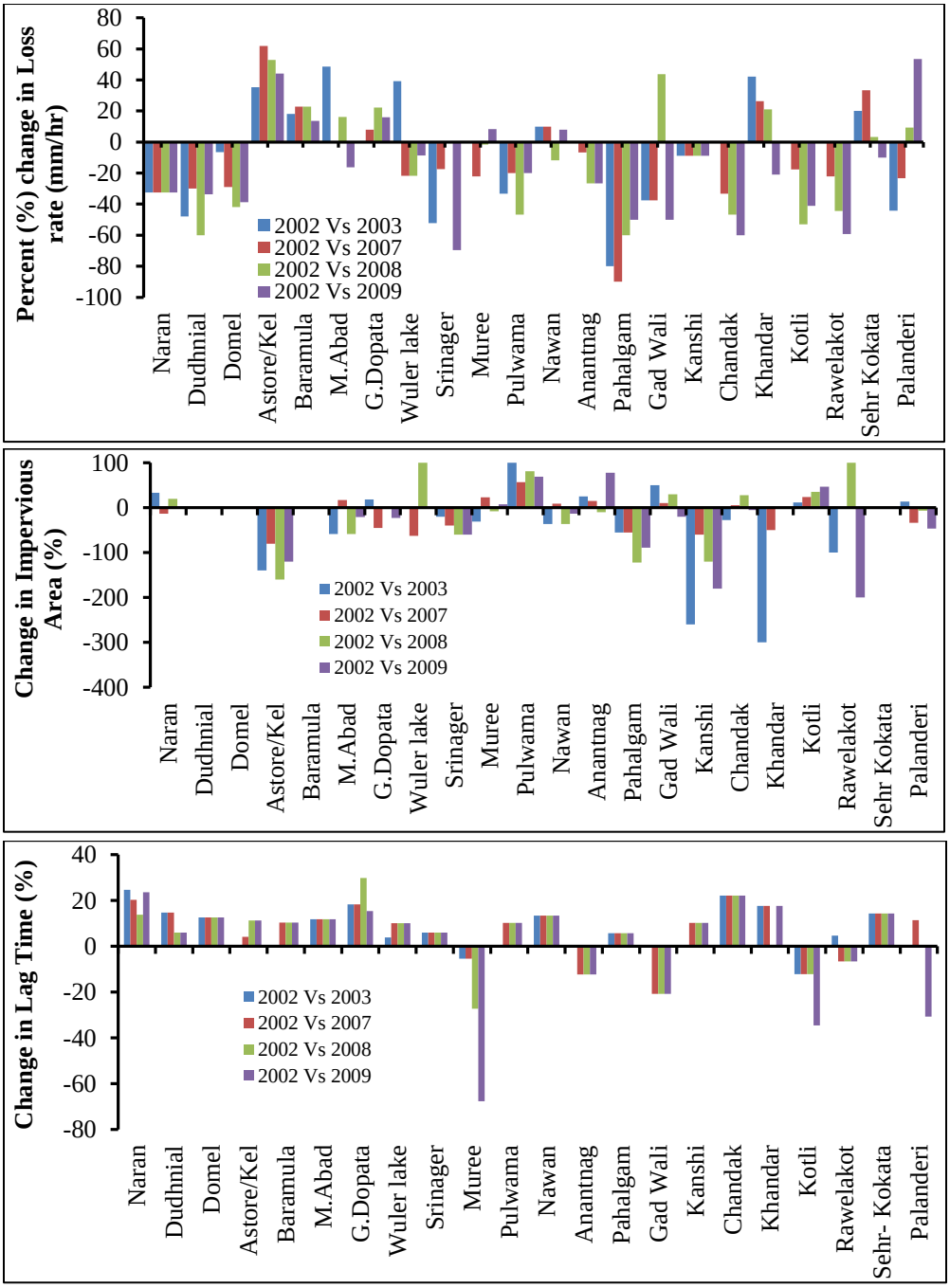

Appendix A09: Percent (%) spatial and temporal change in constant loss (mm/hr), Impervious area (%) and Lag time (hrs) over 2002 with respect to 2003, 2007, 2008 and 2009 calibration (Negative change describes the increase in value).

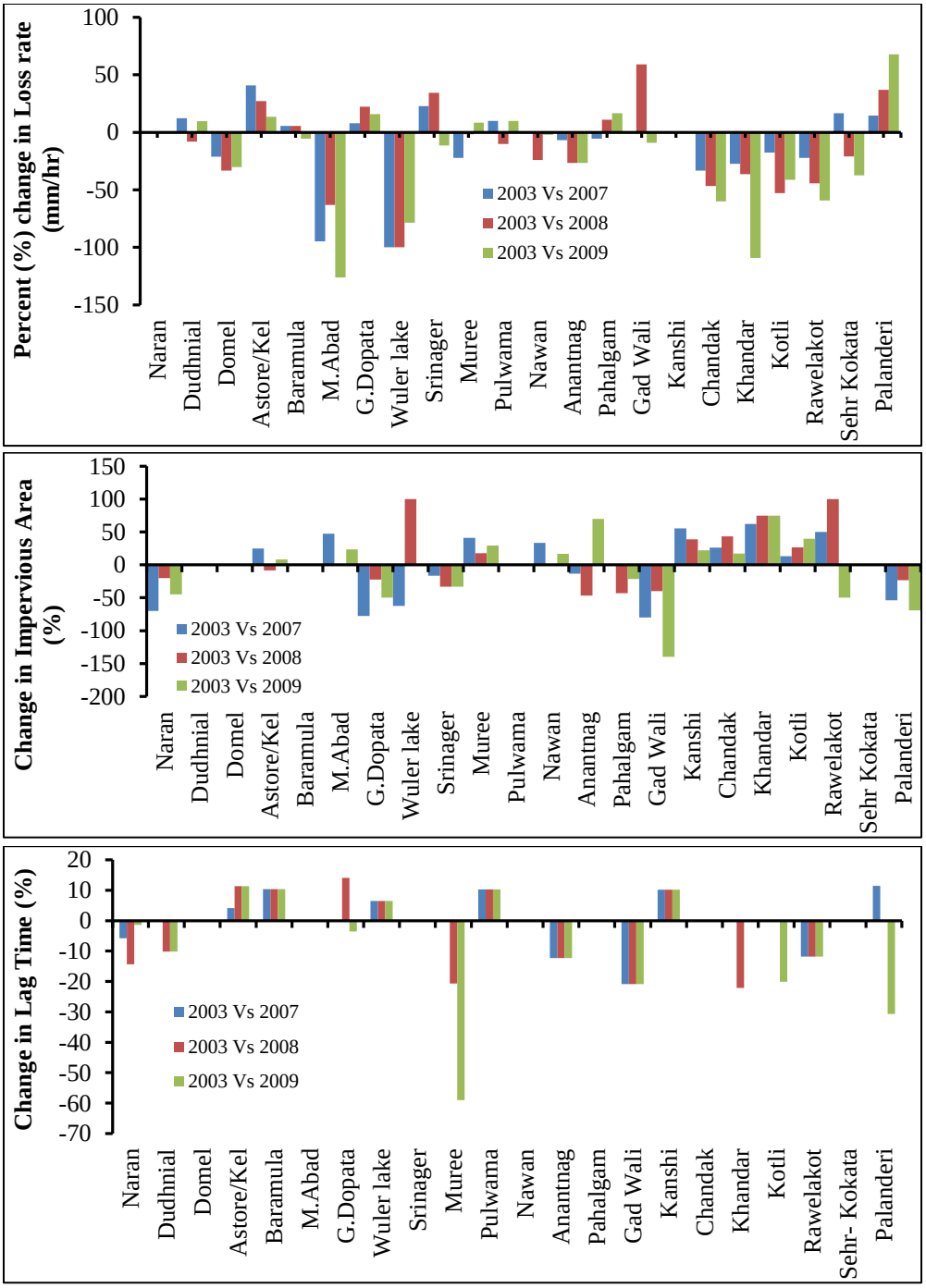

Appendix A10: Percent (%) spatial and temporal change in constant loss (mm/hr), Impervious area (%) and Lag time (hrs) over 2003 with respect to 2007, 2008 and 2009 calibration (Negative change describes the increase in value).

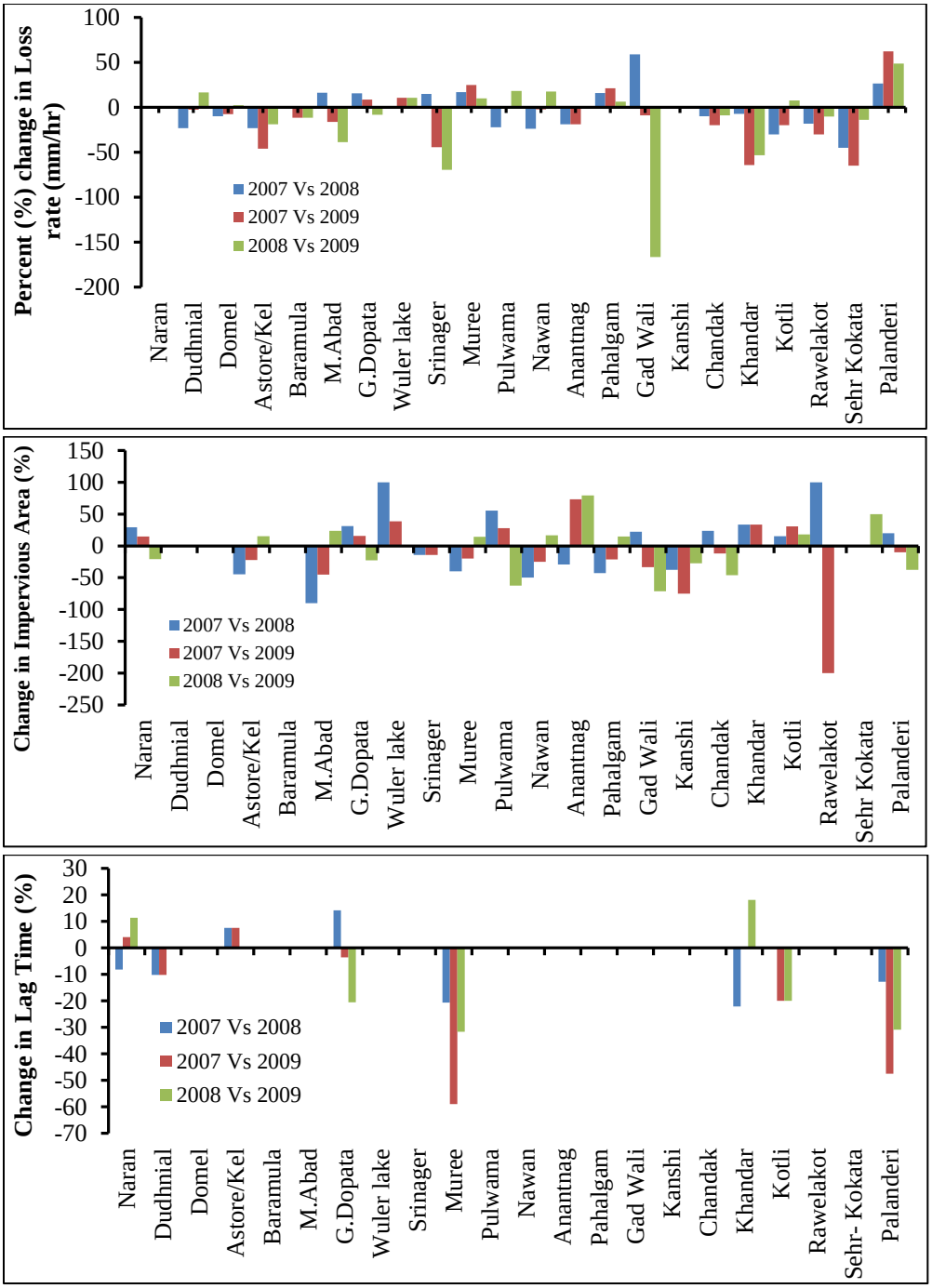

Appendix A11: Percent (%) spatial and temporal change in constant loss (mm/hr), Impervious area (%) and Lag time (hrs) over 2007 with respect to 2008 and 2009 and between 2008 and 2009 calibration (Negative change describes the increase in value).

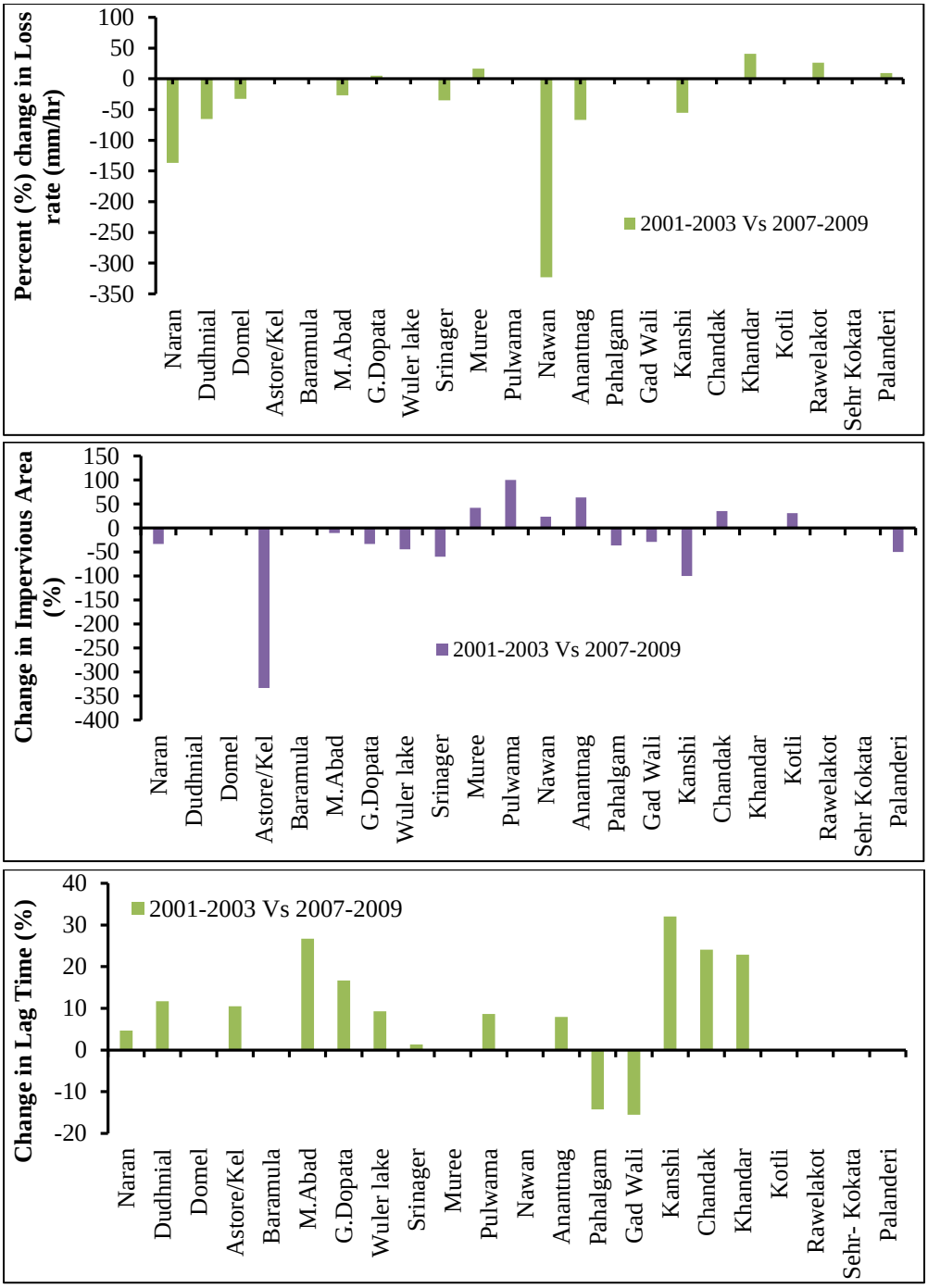

Appendix A12: Percent (%) spatial and temporal change in constant loss (mm/hr), Impervious area (%) and Lag time (hrs) between 2001-2003 and 2007-2009 over three years calibration window.

Appendix B

The comparison between downscaled climate data (precipitation and temperature variables) are performed in chapter 4 to analyse the impact of climate change on water resources at Mangla Dam.

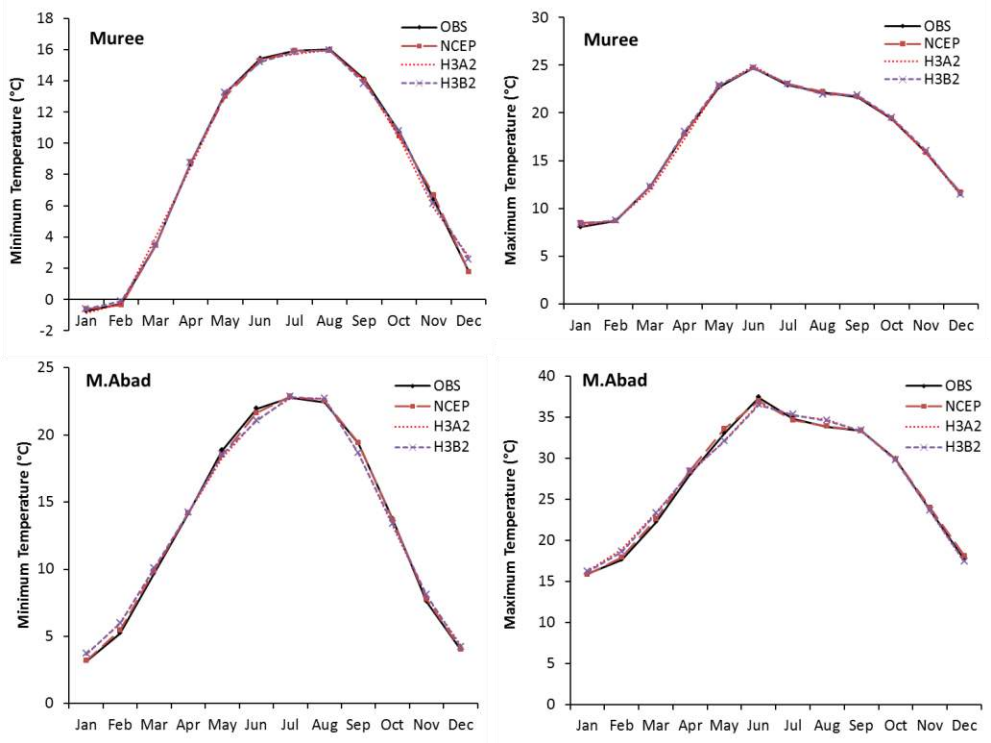

Appendix B01: Comparison between observed and downscaled temperature variables (minimum and maximum) under NCEP, H3A2 and H3B2 scenarios using SDSM at Muree and Muzafferabad stations in Mangla watershed over calibration (1961–1990).

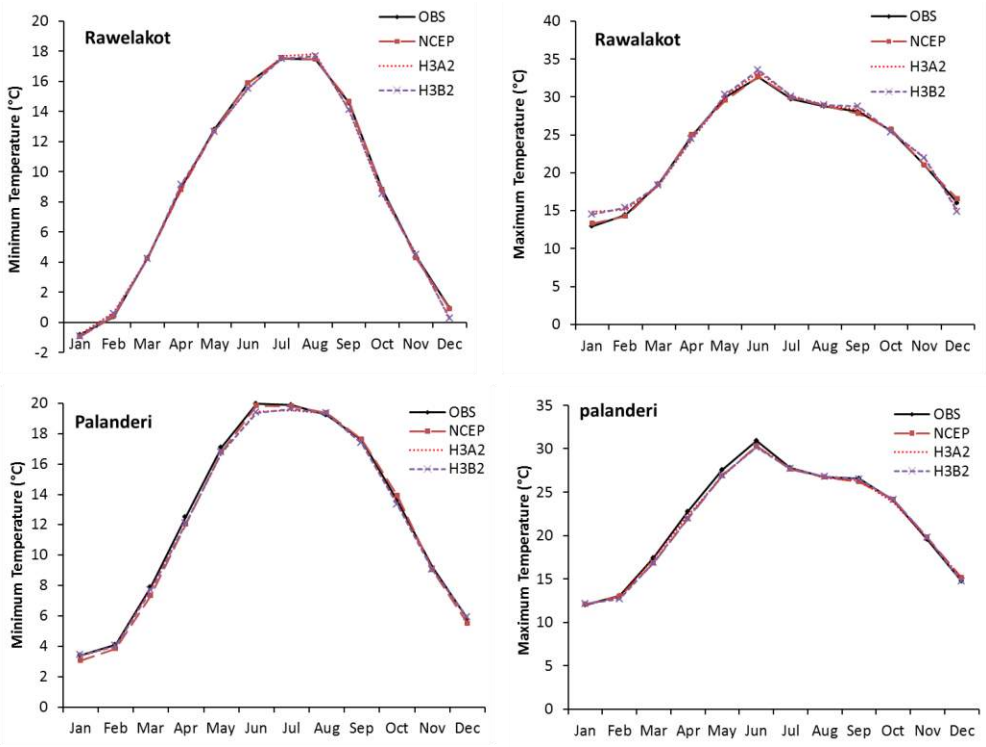

Appendix B02: Comparison between observed and downscaled temperature variables (minimum and maximum) under NCEP, H3A2 and H3B2 scenarios using SDSM at Palanderi and Rawalakot stations in Mangla watershed over calibration (1961–1990).

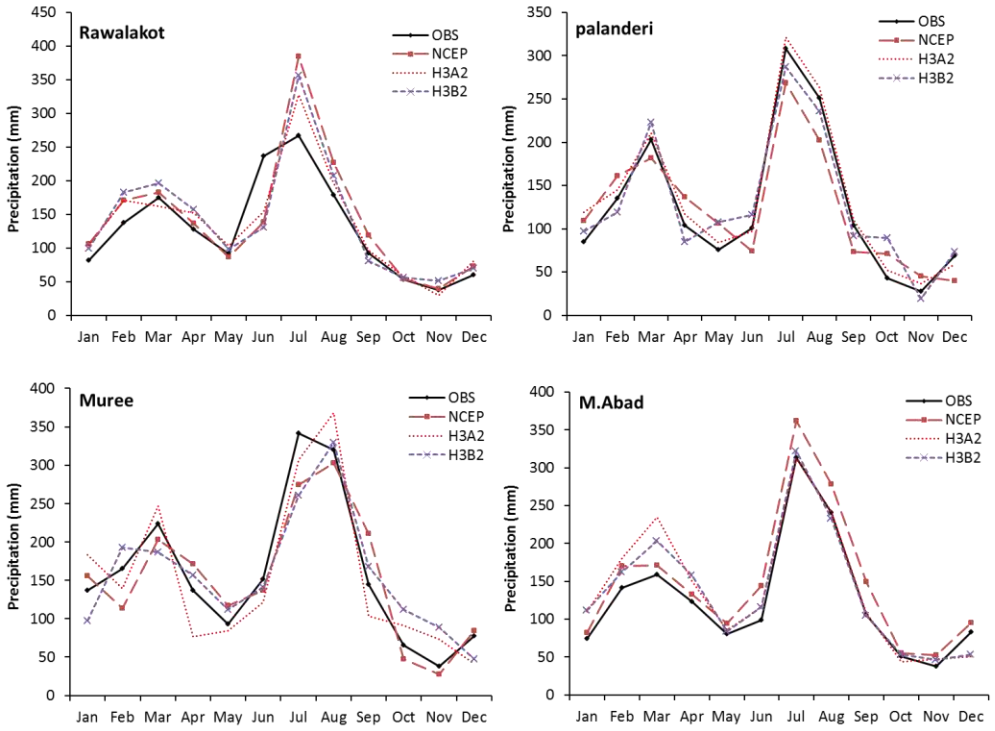

Appendix B02: Comparison between observed and downscaled precipitation under NCEP, H3A2 and H3B2 scenarios using SDSM at Palanderi, Muree, Muzafferabad and Rawalakot stations in Mangla watershed over calibration (1961–1990).